More than just one function -

The multiple roles of selected kinesin-12 class proteins during cell division in *Arabidopsis thaliana*

Dissertation

der Mathematisch-Naturwissenschaftlichen Fakultät

der Eberhard-Karls-Universität Tübingen

zur Erlangung des Grades eines

Doktors der Naturwissenschaften

(Dr. rer. nat.)

vorgelegt von

Arvid Herrmann

aus Lebach

Tübingen

2018

Gedruckt mit Genehmigung der Mathematisch-Naturwissenschaftlichen Fakultät

der Eberhard Karls Universität Tübingen.

Tag der mündlichen Qualifikation:	16.11.2018
Dekan:	Prof. Dr. Wolfgang Rosenstiel
1. Berichterstatter:	Dr. Sabine Müller
2. Berichterstatter:	Prof. Dr. Gerd Jürgens

Danksagung

An dieser Stelle möchte und sollte ich mich bei all jenen bedanken, die zum Gelingen dieser Arbeit ihre Finger nicht bei sich lassen konnten und vieles dadurch erst ermöglichten.

Mein besonderer Dank geht hierbei an Dr. Sabine Müller, meiner Betreuerin, die diese Arbeit förderte, begutachtete, kritisierte, lobte, diskutierte und überhaupt wäre ich wohl ohne sie gar nicht erst im Stande gewesen dies hier zu vollenden. Vielen lieben Dank für eine sehr unvergessliche Zeit.

Weiterhin möchte ich meinen Dank an Herrn Prof. Dr. Gerd. Jürgens entsenden, der sich bereit erklärte das Zweitgutachten dieser Arbeit zu übernehmen.

Nun kommt der inoffizielle Part einer Danksagung, in dem im Normalfall all jenen gedankt wird, die es unter unterschiedlichsten Bedingungen, je nach diversen geistigen Zuständen meinerseits, es die letzten Jahre mit mir und meinen Launen ausgehalten haben. Insbesondere schätze ich mein Labor und all jene Lebensabschnittsverschönerungsgefährten aka Freunde aka Chaoten, die sonst noch so auf diversen Stockwerken oder in Städten ihr Unwesen trieben. Aber ich möchte hier kein Danksagungs-Ranking aufstellen von Namen in einer spezifischen Reihenfolge, nur um in meinem kreativen Chaos am Ende doch die Hälfte zu vergessen. An all jene, die draußen durch die Welt irren und es geschafft haben sich in die tiefe Psyche des Herrn Herrmann über die Jahre einzuschleichen und vor allem einzuarbeiten (Aufmerksamkeitsspanne: Sieh mal ein Eichhörnchen!): mein Dank sei Euch gewiss und ohne Euch wäre wohl Vieles nicht so möglich gewesen, wie es das letztendlich war.

Albert Einstein sagte einmal:

„Wenn ein unordentlicher Schreibtisch einen unordentlichen Geist repräsentiert, was sagt dann ein leerer Schreibtisch über den Menschen, der ihn benutzt aus?“

Denkt immer daran, wenn der größte Chaot auf Erden (C’est moi) es schafft diese Arbeit zu beenden, dann schafft Ihr auch alles, was Ihr euch nur vorstellen könnt. Egal, wie der Schreibtisch aussieht, (meiner unter aller Sau, wen wunderts?!), man muss es nur wirklich wollen!

An meine Familie:

"¡ Agradecimientos especiales a mi familia! Quienes siempre han estado allí para apoyarme. En cada situación de mi vida, incluso en los momentos más dificiles. Muchas Gracias. "

Ach, stimmt. Ihr könnt ja kein Spanisch, macht aber nichts, der Mensch wächst mit seinen Herausforderungen, siehe diese Arbeit. #smiley #kannmanmachenmussmanabernicht #boahbin ichcool. Übrigens, das mit den Hashtags, macht man heute so. Ist trendy und voll dufte.

Memo an mich selbst: Kauf dir eine Hängematte!

Table of contents

1. Summary

Cell division, the physical separation of cellular content, is a fundamental process for all living organisms. As a result of the rigidity of the cellulosic plant cell wall, and contrary to the acto-myosin contractile ring, which constricts the cell surface inwards during cytokinesis in animal cells, vascular plant cells cope with their spatial demands by an inwards-to-outwards directed division mode. The latter is accomplished after the orchestrated and successive assembly of distinct cytoskeletal arrays. Prior to mitosis, a ring of cortical microtubules, the preprophase band (PPB) emerges and prescribes the future division site where the developing cell plate will fuse with the parental cell wall. The PPB disassembles at the end of prophase and simultaneously the nuclear envelope breaks down (NEB). Although the PPB is absent following prophase, the positional information, provided by the PPB, is preserved through mitosis and cytokinesis by a set of highly dynamic components, occupying a zone beneath the PPB established at the cell cortex, named cortical division zone (CDZ). As prophase proceeds a bipolar prospindle is assembled by the reorganization/nucleation of perinuclear microtubules at the surface of the nuclear envelope. After NEB, bundles of microtubules that connect to the kinetochores are formed leading to the generation of a bipolar barrel shaped spindle, which mediates the alignment of the chromosome pairs at the equatorial plane in metaphase. After chromosome segregation in anaphase, the assembly of a newly synthesized cell plate is driven by the rapid centrifugal expansion of a plant specific bipolar cytoskeletal apparatus called phragmoplast. Fusion of the cell plate with the parental cell wall at the CDZ results in the generation of two identical daughter cells at the end of cytokinesis. Although several aspects of this complicated process have been characterized over the years, yet, little is known about the exact molecular interplay of proteins during plant cell division.

Of particular importance during cell division are several proteins that belong to the kinesin-12 class. This class of motor proteins consists of six members in *Arabidopsis* (Kinesin-12A-F). Kinesin-12A/B accumulate at the phragmoplast midzone and together are necessary for proper cell plate formation in the male gametophyte. An additional pair of functionally redundant kinesin-12 members, the PHRAGMOPLAST ORIENTING KINESIN (POK) 1 and 2 (Kinesin-12D/C) preserve the spatial information of the CDZ throughout cytokinesis. Simultaneous mutations in *POK1* and *POK2* cause tilting of phragmoplasts and random cell plate insertions, compromising the usual co-alignment of PPB, phragmoplast and cell plate fusion site. While residing exclusively at the PPB and CDZ, POK1 act as scaffold that retains TAN1 and RanGAP1 from metaphase on at the CDZ supporting its crucial role in CDZ establishment/ maintenance. Little is known regarding the existence of additional proteins that mediate the latter and the dependency on POKs for their function and localization. In the present thesis the identification of two closely related putative Rho-GTPase Activating proteins, namely PH-GAP1 and 2, which are necessary for proper division plane selection during cell division was reported (Stöckle et al., 2016). Briefly, taking advantage of different interaction assays, we were able to show that PHGAPs interact with kinesin-12 POK1 and in addition interact with small ROP GTPases *in vivo*. The GUS reporter gene expression system revealed a similar expression pattern for both genes including the root and leaf meristematic tissue, young leaf epidermal cell as well as the leaf-vascular tissue indicating that they share of a common biological function. Moreover, using fusion proteins and live cell imaging approaches we investigated the intracellular localization pattern of both PHGAP1 and PHGAP2. Interestingly, although PHGAPs decorate the plasma membrane of all cells, in dividing cells both

proteins were restricted to the CDZ in a POK-dependent manner from metaphase onward. However, contrary to *pok1 pok2* double mutants, simultaneous loss of *PHGAP1* and *PHGAP2* results only in mild cell wall positioning defects reflecting and inaccurate positioning of POK1. Collectively, our data shed some light on POK-dependent and small GTPase cell polarity signalling-based mechanisms that control plant cell division in a POK1/2 dependent manner.

The aim of the second project of this thesis was to further characterize the function of POK2. It was found that POK2 exhibits a role in mediating moderate phragmoplast expansion, which explained the reduced phragmoplast expansion rate, monitored in cytokinetic root cells of *pok1 pok2* double mutants (Herrmann et al., 2018). To investigate the latter, we analysed the spatio-temporal localization pattern of a functional POK2 GFP-fusion protein and found that it displays a dual localization pattern throughout cell division, as it is present at the CDZ from prophase onward and at the phragmoplast midzone during cytokinesis. Further dissection of different protein domains revealed that the accumulation of POK2 at the phragmoplast midzone depends on its functional motor-domain, whereas its carboxy-terminal domain is sufficient for CDZ targeting. Intriguingly, the conserved microtubule associated protein MAP65-3/PLE interacts with POK2. Furthermore in collaboration we analysed the mechanistic properties of POK2 motor domain demonstrating that it acts as a weak plus end directed motor *in vitro* as well as *in vivo* (Chugh et al., 2018).

The last project of my thesis focused on the investigation of a plant kinesin-12 with potentially conserved function during spindle assembly, considering that the molecular mechanism of the latter is still poorly understood in plants. For this, aiming to identify the closest relative of kinesin-12 metazoan orthologue HsKIf15 and KLP2, we performed phylogenetic tree analysis based on full length protein sequence of different kinesin-12 homologues in selected plant species. Among those we decided to functionally characterize the closest relative of POK1 and POK2, the Kinesin-12E, which we renamed into PHRAGMOPLAST ORIENTING KINESIN-LIKE (POK-like). Live cell imaging of a functional POK-like GFP-fusion protein uncovered a cell cycle specific and microtubule dependent localization pattern. Using a set of protein deletions, we were able to show that the timely recruitment of POK-like is accomplished by distinct protein domains. POK-like in interphase cells displays a cytoplasmic accumulation whereas it is recruited to the nuclear envelope in prophase and upon NEB localizes to overlapping antiparallel kinetochore microtubule bundles. Finally, POK-like is specifically targeted to the phragmoplast midzone during cytokinesis. As determined by immuno-labeling experiments, dividing meristematic root cells of *pok-like* mutants display significantly reduced spindle length and prolonged duration of the prometaphase/metaphase stage in plants. Furthermore, co-localization analysis with the kinetochore marker RFP-HTR12 combined with the microtubule depolymerizing agent oryzalin recorded an additional accumulation GFP-POK-like close to chromosome-associated structures. In addition, we confirmed RanGAP1 as a novel interaction partner of POK-like *in planta*. Finally, we determined that motor domain activity of POK-like is a prerequisite for its midzone targeting of bipolar microtubule arrays. Collectively, the data presented in this thesis highlight the crucial role of kinesin-12 class motor proteins during plant cell division. We characterized new interactions partners for both POK1 and POK2 and identified a plant kinesin-12 specific function for POK2 during phragmoplast establishment. Furthermore, we investigated the yet uncharacterized protein POK-like, suggesting a functionally conserved activity of kinesin-12 members during spindle assembly throughout the eukaryotic kingdom.

2. Zusammenfassung

Die Zellteilung, also die räumliche Trennung des Zellinhalts, ist einer der fundamentalsten Prozesse aller Organismen. Im Gegensatz zum kontraktilen Actomyosin Ring, welcher die Zellmembran in tierischen Zellen nach innen zieht, haben vaskuläre Pflanzen aufgrund ihrer starren, zellulosehaltigen Zellwand einen von innen nach außen gerichteten Zellteilungsmechanismus entwickelt. Dafür werden spezifische Zytoskelett Strukturen benötigt. Vor der eigentlichen Chromosomentrennung in der Mitose, der sogenannten Prophase, legt das Präprophaseband (PPB), welches aus einem Ring kortikaler Mikrotubuli besteht, die zukünftige Zellteilungsebene fest. Die Zellteilungsebene definiert die Stelle, an welcher die sich entwickelnde Zellplatte mit der parentalen Zellwand fusionieren wird. Am Ende der Prophase löst sich zeitgleich mit dem Zerfall der Zellkernhülle (NEB) auch das PPB auf. Die Positionierung der Zellteilungsebene, welche das PPB zuvor festgelegt, bleibt im weiteren Verlauf des Zellzyklus erhalten. Zuständig für den Erhalt der positionellen Information ist die sogenannte kortikale Teilungsebene (CDZ), eine sich aus verschiedenen, sehr dynamischen Komponenten zusammensetzende Struktur, welche am Zellkortex gebildet wird und sich unterhalb des PPBs befindet. Unterdessen bildet sich durch die Umstrukturierung und Neubildung von sogenannten perinukleären Mikrotubuli eine bipolare Struktur an der Oberfläche der Kernhülle aus, die Prospindel. Mit dem Zerfall der Zellkernhülle bündeln sich die Mikrotubuli der Prospindel und verbinden sich mit den Kinetochoren der Chromosomenpaare. Das Erfassen der Kinetochoren führt zu der Etablierung einer bipolaren, Tönnchen-ähnlichen Struktur, der sogenannten Metaphasenspindel. Deren Aufgabe ist die Ausrichtung der paarweisen angeordneten Chromosomen in der Äquatorialebene zwischen den Spindelpolen und die anschließende räumliche Trennung während der Anaphase. Nach der Chromosomentrennung bildet sich die neu synthetisierte Zellplatte zwischen einer weiteren, Mikrotubuli basierenden, bipolaren Struktur aus, dem Phragmoplasten. Die zentrifugale Expansion des Phragmoplasten und damit einhergehende Synthese der Zellplatte mittels Vesikelfusion führen schlussendlich zum Einbau der neuen Zellplatte an der CDZ der parentalen Zellwand. So entstehen zum Abschluss der Zellteilung zwei identische Tochterzellen. Obwohl über die Jahre viele Aspekte der komplexen Prozesse aufgedeckt worden sind, ist wenig über das exakte molekulare Zusammenspiel der beteiligten Proteine unter- und miteinander bekannt.

Mehrere Motorproteine, sogenannte Kinesine, welche innerhalb der Kinesinfamilie zur Klasse 12 gezählt werden und aus insgesamt sechs Mitgliedern bestehen (Kinesin-12A-F), scheinen während der Zellteilung eine besondere Funktion einzunehmen. Während Kinesin-12A/B beide am Phragmoplastenüberlapp akkumulieren und sind gemeinsam essentiell für die Formierung der Zellplatte im männlichen Gametophyten, bewahren zwei funktionell redundante Kinesine namens PHRAGMOPLAST ORIENTING KINESIN (POK)1 und POK2 (Kinesin-12D/C) die Positionsinformation der CDZ bis zum Ende der Zellteilung. Der zeitgleiche Verlust von *POK1* und *POK2* führt auf Grund der Fehlpositionierung des Phragmoplasten zu einem willkürlichen Einbau der Zellplatte, welche die normalerweise vom PPB festgelegte Fusionsstelle nicht mehr erkennen kann. POK1 lokalisiert ausschließlich am PPB und an der CDZ und verankert die Proteine TAN1 und RanGAP1 ab der Metaphase an der CDZ. Somit wird POK1 vermutlich neben der Phragmoplastenführung auch zur Etablierung und Bewahrung eines molekularen Gedächtnisses benötigt. Ob zuzüglich zu TAN1 und RanGAP1 andere Proteine in Abhängigkeit von POK1 an der CDZ verankert werden und an der CDZ

Etablierung mitwirken, ist bisher nicht bekannt.

Des Weiteren haben wir in unseren Studien die Funktion zweier nah miteinander Verwandte Proteine untersucht, namentlich PHGAP1 und PHGAP2. Diese werden zur Klasse der putativen Rho-GTPase aktivierenden Proteine gezählt, welche für die Selektion der Zellteilungsebene während der Zellteilung in Pflanze eine Rolle zu spielen scheinen (Stöckle et al., 2016). Wir waren durch verschiedene Interaktionsstudien im Stande zu zeigen, dass beide PHGAPs mit dem Kinesin POK1 und den kleinen ROP GTPasen in Pflanze interagieren. Zusätzlich zeigten Analysen mit einem GUS-Reporter-System, dass beide Gene ein ähnliches Expressionsmuster aufweisen (Wurzel- und Blattmeristem, junge Blätter, Leitbündeln), welches auf eine gemeinsame biologische Funktion schließen lässt. Um die intrazelluläre Lokalisation der beiden PHGAPs näher zu untersuchen, erstellten wir transgene Linien mit Fusionsproteinen. Zuzüglich zu ihrer zellweiten Plasmamembranen Lokalisation, befanden sich beide interessanterweise auch ab der Metaphase an der CDZ in sich teilenden Zellen. Diese Lokalisation war POK abhängig. Im Gegensatz jedoch zu der *pok1 pok2* Doppelmutante, zeigte der simultane Verlust beider PHGAP Proteinen nur leichte Zellwandpositionierungsdefekte. Diese Positionierungsdefekte waren jedoch das Resultat der POK1 Mispositionierung während der vorausgehenden Prophase. Insgesamt können wir zeigen, dass es einen Zusammenhang geben muss zwischen POK vermittelter Aktivität und der auf der Signaltransduktion der kleinen GTPasen basierenden Zellpolarität. Das korrekte Zusammenspiel beider Prozesse ist somit von großer Bedeutung für die pflanzliche Zellteilung.

In einer weiteren Studie untersuchten wir die spezifische Funktion des Kinesins POK2. Wir fanden heraus, dass POK2 eine Rolle während der Phragmoplastenexpansion einnimmt. Dies würde im Umkehrschluss auch die reduzierte Expansionsrate der Phragmoplasten in der *pok1 pok2* Doppelmutante erklären (Herrmann et al., 2018). Um das Ganze näher zu charakterisieren bedienten wir uns eines funktionalen POK2 GFP-Fusionsproteins. Erstaunlicherweise besitzt POK2 im Gegensatz zu POK1 ein duales Lokalisationsmuster, welches durch unterschiedliche Domänen vermittelt wird. Während POK2 wie POK1 ab der Prophase in Abhängigkeit seiner Carboxy-terminalen Domäne an der CDZ lokalisiert, akkumuliert POK2 während der Zytokinese zusätzlich noch am Phragmoplastenüberlapp. Hierfür ist eine funktionale Motordomäne von POK2 verantwortlich. Außerdem fanden wir das konservierte Mikrotubuli-assoziierte Protein (MAP) MAP65-3/PLE als Interaktor von POK2. Zusätzlich zu unserer Charakterisierung von POK2, untersuchten wir in Kollaboration die mechanischen Eigenschaften der POK2 Motordomäne sowohl *in vitro* als auch *in vivo* und demonstrierten, dass es sich hierbei um einen schwachen, zum plus Ende gerichteten Motor handelt (Chugh et al., 2018).

In der letzten Studie dieser Arbeit, legten wir unseren Fokus auf die Untersuchung der konservierten Eigenschaft der Kinesin-12 Proteine im Hinblick auf die Entstehung des Spindelapparates in der Pflanze, welcher bis heute nur schlecht verstanden ist. Um einen möglichen Kandidaten für die Etablierung des Spindelapparates in Pflanze innerhalb der Kinesin-12 zu identifizieren, Orthologen aus den Metazoen in der Spindelorganisation eine Rolle spielen (namentlich HsKif15 und KLP2), bedienten wir uns einer phylogenetischen Stammbaumanalyse. Zu diesem Zweck wurden ausgewählte Volllängenproteinsequenzen unterschiedlicher Kinesin-12 Homologen aus Pflanze miteinander verglichen. Innerhalb dieser Analyse stießen wir auf den nächsten Verwandten von POK1 und POK2,

das Kinesin-12E, welches wir umbenannten in PHRAGMOPLAST ORIENTING KINESIN-LIKE (POK-like). Mittels Live-Cell-Imaging eines funktionalen POK-like GFP-Fusionsproteins konnten wir zeigen, dass POK-like sowohl Zellzyklus als auch Mikrotubuli abhängig lokalisiert. Hierfür sind, wie auch schon bei POK2, unterschiedliche Domänen innerhalb von POK-like verantwortlich. Während in der Interphase POK-like zunächst noch im Zytoplasma lokalisiert, wird es am Ende der Prophase zunächst an die Kernhülle rekrutiert und re-lokalisiert nach dem Zerfall der Kernhülle am antiparallelen Überlapp der Kinetochormikrotubuli des Spindelapparates. Im späteren Verlauf der Zellteilung akkumuliert POK-like anschließend am Phragmoplastenüberlapp. Die Untersuchung von sich teilenden Zellen des Wurzelmeristems in der *pok-like* Mutante mittels indirekter Immunlokalisation ergab eine reduzierte Länge des Spindelapparates sowie ein verlängertes Pro-Metaphase/Metaphase Stadium während der Teilung. Außerdem zeigten wir, dass GFP-POK-like höchstwahrscheinlich in der Nähe von Chromosom assoziierten Strukturen lokalisiert. Dazu kombinierten wir Ko-Lokalisationsstudien des Kinetochor-marker RFP-HTR12 mit der Zerstörung von Mikrotubuli durch die de-polymerisierende Chemikalie Oryzalin. Überdies konnten wir eine Interaktion zwischen POK-like und dem schon bekannten RanGAP1 Protein zeigen und im weiteren Verlauf *in planta* charakterisieren. Zu guter Letzt entdeckten wir, dass die Aktivität der Motordomäne von POK-like eine Grundvoraussetzung für die Lokalisation des Proteins an den Überlapp der bipolaren Mikrotubuli Strukturen darstellt. Zusammenfassend konnten wir somit im Rahmen dieser Arbeit die konservierte Rolle der Kinesin-12 Motorproteine während der Zellteilung in den Pflanzen herausarbeiten.

Alles in allem wurde die neuen POK1, POK2 Interaktionspartner PHGAP1 und PHGAP2 charakterisiert und POK2 eine konservierte, pflanzenspezifische Rolle der Kinesin-12 Familie während der Phragmoplastenentwicklung zugewiesen. Des Weiteren entdeckten und charakterisierenten wir das pflanzliche Protein POK-like, welches die konservierte Funktion der Kinesin-12 Familie übernimmt, indem es maßgeblich zur Entstehung des Spindelapparates beiträgt.

3. List of publications

Research articles

Putative RopGAPs impact division plane selection and interact with kinesin-12 POK1.

Dorothe Stöckle, **Arvid Herrmann**, Elisabeth Lipka, Theresa Lauster, Richard Gavidia, Steffi Zimmermann and Sabine Müller

Nature Plants 2, 16120 (2016), DOI: 10.0.38/nplants.2016.120

Dual localized kinesin-12 POK2 plays multiple roles during cell division and interacts with MAP65-3.

Arvid Herrmann, Pantelis Livanos, Elisabeth Lipka, Astrid Gadeyne, Daniel Van Damme, Marie-Theres Hauser and Sabine Müller

EMBO Rep. 2018 e46085. DOI: 10.15252/embr.201846085.

Phragmoplast Orienting Kinesin 2 is a weak motor switching between pro-cessive and diffusive modes.

Mayank Chugh, Maja Reissner, Michael Bugiel, Elisabeth Lipka**, Arvid Herrmann**, Basudev Roy, Sabine Mueller and Erik Schaeffer

Biophysical Journal, 115(2), pp. 375-385.

Manuscript

A conserved kinesin-12 class protein, PHRAGMOPLAST ORIENTING KINESIN-LIKE is necessary for proper spindle assembly in *Arabidopsis thaliana*

Arvid Herrmann, Steffi Zimmermann and Sabine Müller

Review

Mechanisms of plant cell division.

Elisabeth Lipka, **Arvid Herrmann** and Sabine Müller (2015).

WIREs Dev Bio 4, 391-305.

4. Personal contribution

4.1 Putative RopGAPs impact division plane selection and interact with kinesin-12 POK1 (Stoeckle et al., 2016).

For this research article, I cloned all necessary constructs which were used for the Cyto-SUS protein interaction assay and I performed the interaction assay, thus contributed to Figure1. Furthermore, it was shown that PH-GAPs are necessary for accurate division plane selection. For this, I helped with the immunolocalization and the ensuing microscopic analyses (Figure 4). In addition, I participated in cloning (pBIFCt-2in1-NN_POK1$_{1683-2056}$-GAP2) and data collection of the rBiFC experiments (Supplemental Figure S1), along with the generation of the *pok1 pok2 phagap1 phgap2* quadruple mutant (Supplement Figure S3). Moreover, I wrote part of the material and methods section.

4.2 Dual localized kinesin-12 POK2 plays multiple roles during cell division and interacts with MAP65-3 (Herrmann, Livanos et al., 2018).

In this article we characterized the kinesin-12 class POK2. Based on the expansion rate phenotype of the *pok1 pok2* double mutants, we proposed a detailed molecular mechanism for POK2 involvement during phragmoplast expansion in addition to the already known function during cortical division zone maintenance. Therefore, I designed and generated the following entry clones, and respective expression vectors, which were used both *in planta* and in yeast. MAP65x-RFP destination vectors, pENTR:POK2(1-589)^{T281N}, pENTR:POK2(1-189), pENTR:POK2(183-589) and their respective GFP-expression vectors as well yeast vectors, pENTR:MAP65-3/PLE and yeast vector pNX35_Nub-POK2(2083-2771) for yeast expression. Furthermore, I planned and performed the interaction assay (Figure7), together with the transient expression experiments in *tobacco* (Figure 6 and Supplemental Figure 6). In addition, I contributed to the microscopy experiments related to Figure 2, Figure 4 and Figure 5.

4.3 Phragmoplast Orienting Kinesin 2 is a weak motor switching between processive and diffusive mode (Chugh et al., 2018)

In this manuscript we characterized the mechanical properties of the POK2 motor domain *in vitro* and established a theoretical model for cortical division site narrowing. To provide the *in vitro* data, I contributed *in planta* imaging data by expressing the POK2 motor domain (GFP-POK2$_{1-589}$) in *Tobacco* leaf epidermal cells.

4.4 A conserved kinesin-12 class protein, PHRAGMOPLAST ORIENTING KINESIN-LIKE is necessary for proper spindle assembly in *Arabidopsis thaliana* (Herrmann et al., in preparation).

This manuscript illustrates the conserved function of the kinesin-12 class representative POK-like and its involvement during spindle assembly. To uncover the role of POK-like during cytokinesis, I used a set of approaches, including molecular biology techniques, microscopy experiments and genetics. In this study, I performed all experiments, unless otherwise mentioned, and I did most of

the statistical analyses, in cooperation with SM. Figure 1C, the construct pUBN:GFP-POK-likeC in Figure 3C, the BIFC interaction assay in Figure 6A, B were part of either my bachelor or master thesis. In addition, the rescue experiment of the *pok1-2 pok-like-1* double mutant phenotype was performed by Jens Reich as part of his bachelor thesis. Moreover, I generated most of the reported gene constructs, except for pUBN:RFP-HTR12, 35S:RanGAP1-XFP, pUBN:RFP-MBD and pUBN:RFP-EB1b, which were designed and cloned by former members of the lab. The experimental set up were designed together with SM and the initial draft was written by me.

4.5 Mechanisms of plant cell division (Lipka, Herrmann and Müller, 2015).

In this review article I contributed to Figures 2 and 5. Furthermore, I wrote the part “Spindle formation”.

5. Introduction

5.1 Cell division in angiosperms

Cell division, the separation of cellular content, is highly specified in land plants. Due to their rigid cell walls, plants had to develop unique features to fulfil this timely restricted process. As a result, and in contrast to the outward-to-inward membrane separation (acto-myosin contractile ring) during cytokinesis in metazoan, plant cells divide by an inward-to-outward directed division. The biogenesis of a new cell plate, the precursor of the daughter cell wall, is driven by rapid centrifugal expansion of the plant specific cytoskeletal cytokinetic apparatus called phragmoplast. The phragmoplast disassembles upon fusion of the cell plate with the parental cell wall at a pre-selected site at the cell cortex, the cortical division zone (CDZ), giving rise to two identical daughter cells at the end of cytokinesis (Figure 1).

Cell division encompasses various steps (Figure 1), based on specific cellular features, including the presence of different cytoskeletal arrays, the assembly of distinct protein complexes, vesicle/endomembrane fusion events and the activity of certain enzymes. Timely progression and completion of cell division ensures the reliability of plant growth, differentiation and reproduction. During the transition from interphase to preprophase, the cytoskeleton (cortical microtubules, F-actin and their associated proteins) prepares the entrance into cell division by positioning the nucleus into the centre of the cell (Figure 1). A condensed ring of cortical microtubules, the preprophase band (PPB), emerges in preprophase, and demarcates the future cell plate insertion site. At the end of prophase, the PPB disassembles, and the nuclear envelope breaks down. Afterwards the prospindle is transformed into a bipolar barrel shaped cytoskeleton array, the metaphase spindle, which leads to the alignment of the chromosomes at the equatorial plane. The CDZ, underlining the PPB is preserving the future cell plate insertion site. After metaphase, the anaphase spindle segregates the chromosomes and transforms into the phragmoplast at the beginning of cytokinesis. Cell division terminates upon fusion of the cell plate with the parental cell wall in the end of cytokinesis (Figure 1).

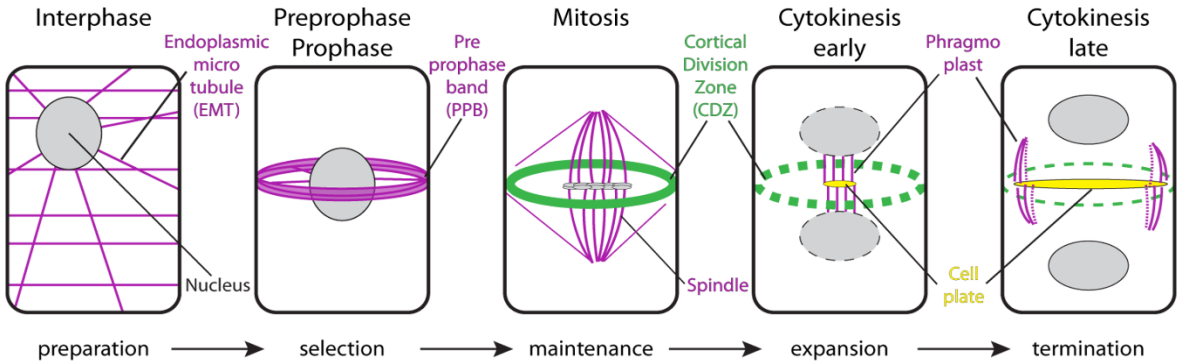

Figure 1:Schematic description of symmetric cell division in higher plants. Endoplasmic microtubules (EMT) are positioning the nucleus into the centre of the cell during the transition from interphase to preprophase. The future cell plate insertion site is selected in preprophase, coincides with the position of the preprophase band (PPB) and remains after PPB disassembly as a polarized region at the cell cortex termed cortical division zone (CDZ), until the end of cytokinesis. Both, meta- and anaphase spindle in mitosis mediate chromosome alignment and segregation, respectively. The phragmoplast is a bipolar cytoskeletal array aiding the targeting of cytokinetic vesicles to the division plane. The phragmoplast and the cell plate expand towards the cell cortex until the cell plate meets and fuses with the parental cell wall. Microtubule arrays are depicted in magenta, CDZ in green, cell plate is shown in yellow, nucleus/chromosomes in grey. Modified from Lipka and Muller (2012)

5.1.1 Formation of a predictive microtubule array – the preprophase band

A plant specific cytoskeletal array termed PPB assembles at the cell cortex during G2 phase, stays at the cell cortex throughout prophase and disappears during prometaphase. It is described as a cortical ring of microtubules, actin filaments and associated cytoskeleton interacting proteins (Smertenko et al., 2017), that delineates the future insertion site of the cell plate. The position of the PPB at the cell cortex is related to the respective position of the nucleus. Moreover these two cellular structures are connected to each other, by microtubules and cytoplasmic strands (Ambrose and Cyr, 2008). Indeed, nuclear localization appears to play a certain role in PPB positioning, since displacement of premitotic nuclei in protonemata of *Adiantum capillus-veneris,* after centrifugation, causes a respective change in PPB orientation (Murata and Wada, 1991). Precise control of the division plane orientation, predicted by the position of the PPB, guarantees proper cell plate insertion, hence ensuring proper plant growth since, alterations in the orientation of the cell division plane often lead to the generation of oblique cell walls and subsequently to misshaped cell and organ anatomy along with dwarfism (Rasmussen et al., 2013). During PPB formation the dynamic properties of microtubules are changing. Upon entering pre-prophase, the microtubules at the cortex at both apical and basal cortical regions become more dynamic and depolymerize, while in the median cortical region microtubule crosslinking and bundle formation results in the generation of the PPB (Vos et al., 2004). Several different protein family members have been identified so far to play a central role in PPB formation by interfering with microtubule stability.

As part of the TTP (TON1-TRM-PP2A) complex, a protein network involved in PPB formation, two closely related proteins namely TONNEAU1a (TON1a) and TON1b play a crucial role in PPB organisation (Azimzadeh et al., 2008, Zhang et al., 2016). These proteins are related to human centrosomal proteins, which are components of the microtubule organizing centres (MTOCs) in metazoan (Drevensek et al., 2012). Simultaneous mutation in these tandem replicated genes completely abolish formation of the PPB in *Arabidopsis thaliana*, supporting a shared function for TON1a and TON1b in microtubule nucleation that leads to PPB establishment. Identified in a visual screen for mutations affecting seedling body organization, similarly to *ton1a/b* mutants, *ton2/fass* mutants fail to form PPBs. In addition to the lack of PPBs and the inability to properly orient division planes (Traas et al., 1995), *fass* mutants display defects in interphase cortical microtubule organization characterized by decrease in the density of cortical microtubules, higher rates of microtubule catastrophe and microtubule nucleation events which are less branched and more parallel (Kirik et al., 2012). TON2/FASS encodes for a phosphatase type 2A (PP2A) B´´ regulatory subunit, suggesting a role in microtubule dynamics via phospho-regulation, during PPB assembly (Torres-Ruiz and Jurgens, 1994, Kirik et al., 2012, Traas et al., 1995, Camilleri et al., 2002). Meanwhile, a recently discovered protein family, consisting of 34 proteins, uncovered a novel mechanism that mediates TON1/TON2 recruitment towards microtubules (Spinner et al., 2013). TON1 RECRUITING MOTIF (TRM) proteins are part of the TTP complex, physically interacting with TON1a/b and TON2/FASS ensuring timely and spatially restricted dephosphorylation events by an indirect targeting of PP2A activity (Drevensek et al., 2012, Spinner et al., 2013). Recent work proposes a reassessment of PPB function in the determination of the cell division plane (Schaefer et al., 2017). Although the *trm678* triple mutants display no PPBs of microtubules in prophase, the mutant develops without major defects. In fact, simply spindle rotations are visible, while the recruitment of a CDZ marker is merely delayed in these mutants. Based on these findings, it has

been suggested that PPBs are not playing a major role in division plane determination, but they are increasing the robustness of cell division through stabilizing the spindle orientation. Whether these findings are sufficient to reassess the necessity of PPB function in terms of cell division plane determination remains to be further validated.

Over the years, in addition to the components of the TTP complex, additional components have been identified interfering with microtubule dynamics as well playing a crucial role in PPB formation via different mechanisms. Most of them are microtubule associated proteins (MAPs) based on their association with microtubules by direct or indirect interactions, the co-localization with microtubules *in vivo* or their homology to already known MAPs (Struk and Dhonukshe, 2014). For instance, a temperature-sensitive *microtubule organization1* (*mor1)* mutant allele, related to the highly conserved MAP215 microtubule polymerase from *Xenopus*, displays an overall decrease in PPB frequency, disorganized interphase microtubules and reduction of microtubules length (Kawamura et al., 2006, Kawamura and Wasteneys, 2008, Brouhard et al., 2008). *In vitro* and *in vivo* analyses suggest a role for MOR1 in microtubule elongation by promoting rapid growth and shrinkage in addition to supressing the pausing of microtubules (Kawamura and Wasteneys, 2008). The control of microtubule elongation via MOR1 might shed some light on the mechanistic aspects of PPB formation, however, it does not elucidate the mechanisms beyond the positioning of the PPB. Members of the MAP65 family have been shown to accumulate at the PPB and other mitotic microtubule arrays (Smertenko et al., 2008, Smertenko, 2014, Li et al., 2017, Sasabe and Machida, 2006, Struk and Dhonukshe, 2014). These MAPs have the ability to bundle microtubules by forming cross bridges between antiparallel overlapping microtubules and therefore might stabilize PPB microtubules via bundling. However, so far reported mutations in single *MAP65* members do not affect PPB formation at all, pointing towards functional redundancies among these nine family members (Fache et al., 2010, Li et al., 2017, Mao et al., 2006, Meng et al., 2010, Sasabe et al., 2011b, Stoppin-Mellet et al., 2013, Van Damme et al., 2004).

CLASP is another MAP mediating the assembly of the PPB and other mitotic structures. *clasp* mutants often display increased microtubule ordering of the cortical microtubule array, together with aberrant PPBs, mitotic spindles and phragmoplasts (Kirik et al., 2007, Ambrose et al., 2011, Ambrose et al., 2007, Ambrose and Wasteneys, 2008). It has been reported that CLASP binds to microtubule plus ends, preventing edge-induced microtubule catastrophe at sharp cell edges (Ambrose et al., 2011). Consequently, microtubules are able to polymerize across cell edges, allowing transverse microtubule arrays, hence, stabilizing the interphase cortical microtubule array. Furthermore, reduced CLASP activity promotes parallel ordering of cortical microtubules, hence, increasing the probability of microtubule bundling and ordering (Ambrose et al., 2007). Intriguingly, the putative transmembrane protein SABRE might direct CLASP activity towards mitotic microtubule arrays (Pietra et al., 2013). The epistatic relationship of *sab* over *clasp* mutants underlines the notion that not only the cortical microtubule array but in addition, the membrane region beneath the PPB is modified, to establish a functional CDZ (Lipka et al., 2015).

The absolute necessity of the PPB in the establishment of the division plane is controversial as plants lacking PPBs often are comparable to wild type plants and certain cell types do not form a PPB at all. Therefore, it seems that the wide presence of the PPB in plants cells might accelerate the establishment of the division site.

5.1.2 Nuclear envelope breakdown and spindle assembly

The assembly/formation of a bipolar spindle, a microtubule-based structure, which mediates chromosome alignment and separation, is one of the most conserved processes among the eukaryotic kingdom. However, different mechanisms evolved between animals and land plants for the latter. Spindle bipolarity is, in general, achieved by the defined antiparallel orientation of higher ordered microtubules at a certain position (Zhang and Dawe, 2011). In animal somatic cells, microtubule minus ends are incorporated in so called centrosomes, microtubule organizing centres (MTOCs) which serve as microtubule nucleation sites (Conduit et al., 2014). During spindle assembly, microtubules radiate from centrosomes and by “search and capture” attach to kinetochores. These multi-protein complexes are assembled at the centromere of chromatids, a particular chromosomal locus, which links both sister chromatids after duplication. (Zhang and Dawe, 2011, Santaguida and Musacchio, 2009, Kirschner and Mitchison, 1986, Cleveland et al., 2003). Notably, many types of animal cells, such as oocytes, lack centrosomes completely, yet, they form functional bipolar spindles (Khodjakov et al., 2003). It was found that *Xenopus* egg extracts *in vitro* self-organize bipolar spindles around DNA-coated vesicles. Based on these findings a model was proposed, in which chromosome-mediated nucleation aided by a chromosome-associated protein is able to promote microtubule nucleation/stabilization that leads to bipolar spindle assembly (Walczak and Heald, 2008, Heald et al., 1996). Further studies revealed that the small GTPase Ran is a key player in this “spindle self-organization” pathway. By maintaining a gradient within a certain threshold at definite positions around the chromosomes, Ran controls the activity of spindle assembly factors (Kalab et al., 2002, Clarke and Zhang, 2008, Zhang and Dawe, 2011). In addition to these two models, a third one proposes that in a microtubule-dependent microtubule nucleation mode critical for spindle assembly, new microtubules are branching from pre-existing microtubules at an angle of 40° (Goshima and Kimura, 2010).

Bipolar spindle organization starts in higher plant cells by the “self-organization” pathway, due to the absence of centrosomes (Zhang and Dawe, 2011). In late prophase, right before PPB disassembly, a prophase bipolar spindle (from now on prospindle) begins to assemble by the reorganization/nucleation of perinuclear microtubules at the surface of the nuclear envelope (Masoud et al., 2013a) (Figure 2). Intriguingly, immunolabeling of tubulin in endosperm cells of the African blood lily *Haemanthus* revealed that microtubules radiating towards the cytoplasm are redistributed into multiple small asters tangential to the nucleus, forming two opposite poles or polar caps encircling the nucleus (Smirnova and Baje, 1998). The redistribution and the subsequent additional microtubule nucleation are promoted by the γ-tubulin ring complexes (γ-TuRCs), components of MTOCs. γ-TuRCs consist of several subunits γ-tubulin and γ-tubulin COMPLEX PROTEINS2 and 3 (GCP2 and GCP3), as well additional factors that enable plus end directed microtubule polymerization (Masoud et al., 2013a, Vinh et al., 2002). Following nuclear envelope breakdown and similarly to animal cells, numerous microtubule bundles emanate from the polar caps/prospindle towards kinetochores, forming kinetochore microtubule bundles (kinetochore fibers; K-fibers) (Smirnova and Baje, 1998). These K-fibers are essential for the alignment of chromosomes in the equatorial plane and for the segregation of chromosomes during anaphase. To guide the attached chromosomes and align in one plane, K-fibers shorten and become wider during prometaphase-metaphase. Consequently, the spindle itself shrinks, resulting in a lateral expansion of the metaphase plate and an arrangement of the chromosomes in one plane (Smirnova

and Bajer, 1992). Synchronously, microtubules nucleate around the chromosomes and branch from existing microtubules (fir trees), leading to a more or less barrel-like structure with an overall bipolar configuration (Yamada and Goshima, 2017). Intriguingly, electron microscopy studies revealed that the majority of microtubules within this array are pointing towards chromosomes with their dynamic plus ends, whereas most microtubule minus ends are facing outwards displaying characteristic broad acentrosomal spindle poles (Euteneuer et al., 1982). Furthermore, interdigitating microtubules, maintain an antiparallel orientation and overlap near the equatorial plane (midzone), forming the spindle midzone, together with the aligned chromosomes in metaphase, (Figure 2). At this midzone, a number of microtubule cross linkers contribute to the integrity of the mitotic apparatus and stabilize the overlap. The spindle midzone becomes even more visible after chromosome segregation in anaphase, when the opposing kinetochore microtubule bundles are pulled towards the poles via minus end directed microtubule disassembly (Yamada and Goshima, 2017, Zhang and Dawe, 2011, Masoud et al., 2013a, Hyman and Karsenti, 1996). Plants lack centrosomes, which are the main microtubule organization centres during spindle assembly in animals, thus contribute to the typical bipolar spindle shape with two defined poles on each spindle half. Therefore, the question arose, how acentrosomal plant cells accomplish a bipolar spindle cap organization in prometaphase as well a barrel shaped bipolar spindle in metaphase and which additional factors contribute to the latter. It has been suggested that, in addition to its primary role in selecting the division site, the PPB might interfere with prospindle organization, and thus contribute, analogously to centrosomes, to the formation of a bipolar array. Mutants without PPBs are often exhibiting delayed prospindle formation, or the prospindles fail to acquire a bipolar organization (Ambrose and Cyr, 2008). Intriguingly, perturbation of microtubule arrays in prophase in BY2 cells can lead to the formation of double PPBs, subsequently followed by the generation of multipolar prometaphase spindles (Yoneda et al., 2005). These findings suggest the existence of a functional link between bipolar prospindle organization and PPB function. In addition, it has been shown that microtubules, radiating outwards from the PPB, get in contact with the nucleus. These microtubules bridge the nucleus with the PPB and subsequently assist the reorganization of the randomly oriented perinuclear microtubules into small asters tangential to the nucleus, resulting in the establishment of polar caps (Ambrose and Cyr, 2008, Lipka et al., 2015).

Even though the PPB contributes to the redistribution of perinuclear microtubules, the nucleation and the establishment of the bipolar and symmetrical organization of the spindles requires opposing forces, that are generated after NEB by a set of unique proteins, such as motor proteins (kinesins) and other MAPs. Most key factors, which are involved in this process, are highly conserved. However, plants developed unique features in order to cope with the lack of the functional modules present in animal cells, centrosomes and dyneins.

A large number of microtubule associated proteins functioning/located in the spindle are affecting its length (i.e. the pole to pole distance), as well as microtubule growth and catastrophe rates, thus mediating the formation of microtubule bundles, and consequently adjust spindle morphology. In both, plants and animals, the spindle length appears to be controlled by microtubule dynamic instability. Mutations in different regulators of microtubule assembly and organization, such as microtubule polymerase MOR1, the microtubule plus end tracking protein END BINDING POTEIN1c (EB1c), CLASP and members of the microtubule cross-linker MAP65 family, cause dramatic decrease in spindle length,

and influence correct chromosome alignment (Kawamura et al., 2006, Komaki et al., 2010, Ambrose et al., 2007, Hussey et al., 2002).

Intriguingly, the TARGETING PROTEIN FOR XKLP2 (TPX2), one of the most conserved MAPs among the eukaryotic kingdom, plays a significant role in microtubule nucleation related to the assembly of a functional prospindle at the end of prophase in plants (Masoud et al., 2013a). Residing in the nucleus in interphase and inhibited by importin β, TPX2 is exported before NEB upon its release from importin β by the small GTPase RAS-RELATED NUCLEAR PROTEIN (Ran) in a GTP dependent manner (Vos et al., 2008). Considering that similarly to animal TPX2, plant TPX2 promotes microtubule asters *in vitro* (Vos et al., 2008), it has been assumed that the accumulation of TPX2 into polar caps is necessary for proper prospindle assembly. Along these lines, inhibition of TPX2 activity after injection of anti-TPX2 antibodies in prophase, delayed or arrested cell cycle progression while impairment of TPX2 function during later cell cycle stages had no effect. These results collectively demonstrate, that TPX2 is specifically required for prospindle assembly (Vos et al., 2008). Moreover, overexpression of TPX2 leads to the formation of aster-like perinuclear and nuclear microtubules and a remarkable reduction of Ran and importin β signal in the nucleus, pointing towards a Ran dependent regulation of TPX2, which in turns drives microtubule nucleation (Petrovská et al., 2013). Furthermore, TPX2 co-immunoprecipitated with the Serine/Threonine Kinase AURORA1 (AUR1) and with γ-tubulin, both interactions that have been also observed in animal cells previously (Petrovská et al., 2012). TPX2 act as substrate and activator of AUR1 and AURORA A, in plants and animals respectively, and targets AURORA function within spindles. The down-regulation of AURORA1/2 in plants via RNAi silencing produces a range of developmental defects, including the impairment of primary root growth due to cell cycle arrest and ectopic re-initiation of cell division in mature tissues. The *Arabidopsis aur1aur2* double mutants exhibit characteristic defects in division plane orientation in formative divisions that promote embryo development, in divisions around the root stem cell niche, as well as in lateral root formation. However, spindle assembly *per se* does not seem disturbed, suggesting the existence of additional regulation of TPX2 dependent microtubule nucleation (Masoud et al., 2013a, Van Damme et al., 2011)

The regulation of downstream effectors such as TPX2, by the Ran cycle is one of the most conserved mechanisms among eukaryotes. The Ran GTPase controls, apart from the shuttling mechanisms between nucleus and cytoplasm, also the assembly of the mitotic spindle, nuclear envelope dynamics and the formation of the plant specific mitotic structures such as the PPB and the phragmoplast (Clarke and Zhang, 2008). The GTPase Ran acts as a molecular switch between two different functional states depending on its guanosine nucleotide-bound state. In higher plants, the activity of the small GTPase Ran is downregulated by two functionally redundant Ran GTPase ACTIVATING PROTEIN1 (RanGAP1) and RanGAP2 which promote the hydrolysis of GTP (GTP to GDP + Pi) via activation of the intrinsic GTPase domain of Ran (Bischoff and Görlich, 1997, Kim and Roux, 2003). On the contrary, the guanine nucleotide exchange factor (GEF) REGULATOR OF CHROMOSOME CONDENSATION1 (RCC1) promotes binding of Ran to GTP (Haizel et al., 1997). Simultaneous mutation in both RanGAP1 and 2, is gametophytic lethal, whereas downregulation of at least one of the transcripts combined with the absence of the other induces mild defects in growth and development (Rodrigo-Peiris et al., 2011, Boruc et al., 2015, Xu et al., 2008). Intriguingly, RanGAP1 localizes to the nuclear envelope and PPB in prophase and remains at the CDZ after PPB disassembly,

along with its presence at the kinetochores in mitosis and the cell plate during cytokinesis (Xu et al., 2008). How exactly Ran and RanGAP1 influence microtubule stabilization/nucleation during PPB and spindle assembly, and how it contributes to CDZ maintenance in plants, still remains an open question.

The opposing forces required to establish the bipolar symmetry of the spindle in plants are generated by different classes of microtubule dependent kinesin motor proteins that exert forces on spindle microtubules in opposite directions (Goshima and Kimura, 2010). At the spindle midzone, plus end directed kinesins are cross-linking anti-parallel microtubules and walk towards the microtubule plus ends. As a result, the opposite poles move apart. One the other hand, the minus end directed motor proteins substitute for the lack of dyneins in plants and mediate spindle pole focusing (Gadde and Heald, 2004). Contrary to animal cells, the plant spindle assembly factors and in particular the complex interplay of implicated molecular motors, is rather poorly understood. In human cells, members of up to five different plus end-directed kinesins are regulating microtubule dynamics and mediate bundling during spindle assembly. For instance, kinesin-7 (widely known as CENP-E) is responsible for the proper alignment of chromosomes (Bancroft et al., 2014), whereas kinesin-13 (MCAK) promotes microtubule depolymerization at the kinetochores (Kline-Smith et al., 2004). Nevertheless, the most important molecules facilitating the bipolar spindle arrangement belong to class-5, as well as to class-12. Interestingly, the homotetrameric kinesin-5 (Eg5) not only cross-links antiparallel overlapping microtubules at the spindle midzone but it also accumulates around the centrosomes and remains enriched at the spindle poles during metaphase, decorating K-fibers and interpolar microtubules as well (Ferenz et al., 2009). The ability to crosslink and to slide these microtubules apart, generates an outward force which drives centrosome separation during spindle assembly (Cole et al., 1994, Kashlna et al., 1996, Reber and Hyman, 2015). Therefore, it is not surprising that, loss of Eg5 leads to the formation of monopolar spindles and blockage of cell division. However, inhibition of Eg5 function by treatment with monastrol, or by RNAi silencing, can be restored upon simultaneous inhibition of cytoplasmic dyneins or members of the minus end-directed kinesin-14 class. Based on these observations a current model suggests that minus end-directed inward forces directly counteract kinesin-5 dependent outward forces (Hentrich and Surrey, 2010, Reber and Hyman, 2015). This so-called “force balance model” describes centrosome separation in animal cells as a result of cortical dynein function that is pulling the spindles poles apart, whilst pushing forces generated by Eg5 at the overlap region promote centrosome separation from prometaphase on (Sharp et al., 2000). Surprisingly, downregulation of either Eg5 or dynein produces an opposite effect on spindle length during metaphase. While Eg5 inhibition decreases the spindle length as an outcome of excessive inwards forces, inhibition of dynein, increases spindle length caused by immoderate outward Eg5 dependent forces suggesting the existence of additional force balancing, exerted by other proteins that contribute to the integrity of the bipolar spindle (Ferenz et al., 2009). Contrary to animals, *Arabidopsis* possesses four kinesins-5 class motor proteins, KINESIN RELATED PROTEIN125 (KRP) a-d (Reddy and Day, 2001). It has been shown that RADIALLY SWOLLEN7 (RSW, KRP125c), cannot complement the *eg5* phenotype in kidney epithelial (LLC-Pk1) cells and in addition it does not mislocalize upon monastrol application in wild-type *Arabidopsis* cells. Nonetheless, loss of *krp125c* severely compromises spindle structure, resulting in the generation of monopolar and aberrant spindles (Bannigan et al., 2007). These findings might indicate that the functional conservation of kinesin-5 motor proteins is extended into vascular plants as well, although the

molecular mechanism behind plant kinesin-5 contribution to spindle assembly needs to be determined. It has been assumed several years ago, that kinesin-12 motor Kif15 can complement for the loss of Eg5 in human cells (Tanenbaum et al., 2009). Upon Kif15 abundance, cells exhibit shorter spindles, a rather moderate phenotype compared to loss of Eg5 (Vanneste et al., 2009). However, simultaneous mutation of both *Eg5* and *Kif15* genes, leads to a total collapse of the spindle. Whereas in combination with the loss of dynein, spindle bipolarity is almost maintained, chromosome alignment fails in *eg5 kif15* (van Heesbeen et al., 2014). In addition, overexpression of Kif15 restored the Eg5 phenotype, suggesting that KİF15 and Eg5 act cooperatively (Vanneste et al., 2009, Tanenbaum et al., 2009). However, recent *in vivo* and *in vitro* findings indicate that Kif15 and Eg5 have opposing functions during spindle assembly. Eg5 acts predominantly on antiparallel microtubules, while Kif15 localizes to K-fibers and to parallel microtubule bundles between the kinetochore and the spindle poles in a TPX2 dependent manner (Sturgill and Ohi, 2013, Hancock, 2014, Tanenbaum et al., 2009). The first kinesin-12 protein was discovered in *Xenopus leavis* and is an orthologue of Kif15, XlKlp2 that gets directly targeted to spindle microtubules upon TPX2 recruitment through its intrinsic leucine-zipper domain (Wittmann et al., 1998, Wittmann et al., 2000). Although, TPX2 knockdown abolishes Kif15 spindle localization in human cells, evidence for direct interaction between Kif15 and TPX2 in the absence of microtubules was missing for a long time (Vanneste et al., 2009, Sturgill and Ohi, 2013, Tanenbaum et al., 2009). Notably, a recent study revealed that Kif15-dependent spindle formation *in vivo* as well as the inhibition of the Kif15 motor domain *in vitro*, requires interaction with the C-terminal domain of TPX2 (Mann et al., 2017). Nonetheless, the anticipated recruitment to K-fibers, regardless of a potential TPX2 dependence, is sufficient to explain the reduction in spindle length observed upon Kif15 knockdown, suggesting a role for Kif15 in regulating K-fiber length as well as their stability (Sturgill and Ohi, 2013). In case Kif15 preferentially binds to K-fibers the question arises, how Kif15 is able to restore the *eg5* phenotype, hence, contributing to spindle assembly and chromosome separation. Recent *in vitro* findings show that Kif15 preferentially binds to microtubule bundles independently of TPX2, utilizing a second, non-motor microtubule binding domain located in coiled-coil domain1 (coil1). Intriguingly, a model was proposed, suggesting that the motor domain of Kif15 is normally autoinhibited by the distal coiled-coil (coil-2) domain and becomes activated upon binding to coil1 and to microtubule bundles. The binding of Kif15 to two different microtubules with two different domains and the activation of the motor domain, enables the relative sliding of the microtubules within the bundle (Sturgill and Ohi, 2013). Intriguingly, the characterization of mitotic cells lacking K-fibers due to drug treatments revealed that full-length Kif15 re-localizes to non-K-fiber microtubule bundles, that assemble in treated cells (Sturgill and Ohi, 2013). The ability of binding either to K-fibers or to non-K-fibers suggests that Kif15 mode of function switches between pushing and pulling forces by simply binding to distinct microtubule populations, and hence, is capable of generating forces with opposite directionality (Sturgill and Ohi, 2013, Hancock, 2014) and of rescuing the *eg5* phenotype upon overexpression. On the contrary, several other reports show that Kif15 is able to form tetramers both *in vitro* and *in vivo* allowing the switching between microtubule tracks. In addition, Kif15 motor collectives display processive movement at steady velocity, on top of the capability of full length Kif15 to complement *eg5* mutants (Drechsler et al., 2014, Mann et al., 2017). Nonetheless, given the contradicting findings over the years, suggesting that Kif15 can bind to microtubule bundles either as homotetramers and as homodimers with an internal microtubule binding site, the mechanism

of Kif15 function during spindle assembly, is currently under debate.

The molecular mechanism underlying symmetric bipolar spindle organization in plants with respect to kinesin-12 function is unknown. *Arabidopsis thaliana* encompasses six members of kinesin-12 class, but only four have been characterized so far, none of which showed any functional or direct association to spindle assembly. Thus, further analyses/characterization are required in order to assert a potential conserved role for kinesin-12 proteins in plants during spindle assembly

The force balance generated by the interplay between plus end directed kinesins and the minus end directed dynein are essential for establishing a functional bipolar spindle in animal cells. However, plants do not contain a conserved functional orthologue of animal dynein. Instead, minus end directed kinesin-14 family members are expanded in land plants and probably substitute for the lack of dynein during cell division (Yamada and Goshima, 2017). Two closely related kinesin-14 family members, namely ARABIDOPSIS THALIANA KINESIN1 (ATK1) and ATK5 are essential for prospindle formation following nuclear envelope breakdown (Chen et al., 2002, Marcus et al., 2003). TDNA induced impairment of *ATK* function, results in the formation of abnormal prospindles and metaphase spindles with wider acentrosomal poles (Marcus et al., 2003), but without further impact on cell division. Intriguingly, ATK5 is tracking microtubule plus ends, due to an additional intrinsic microtubule binding domain at the N-terminal tail. Together with its central minus-end directed motor domain, ATK5 is able to slide and bundle the antiparallel microtubule overlap both *in vivo* and *in vitro*, to establish prospindle bipolarity (Ambrose et al., 2005). Therefore, it is likely, that kinesin-14 family members also counteract outward directed forces generated by plus end directed kinesins.

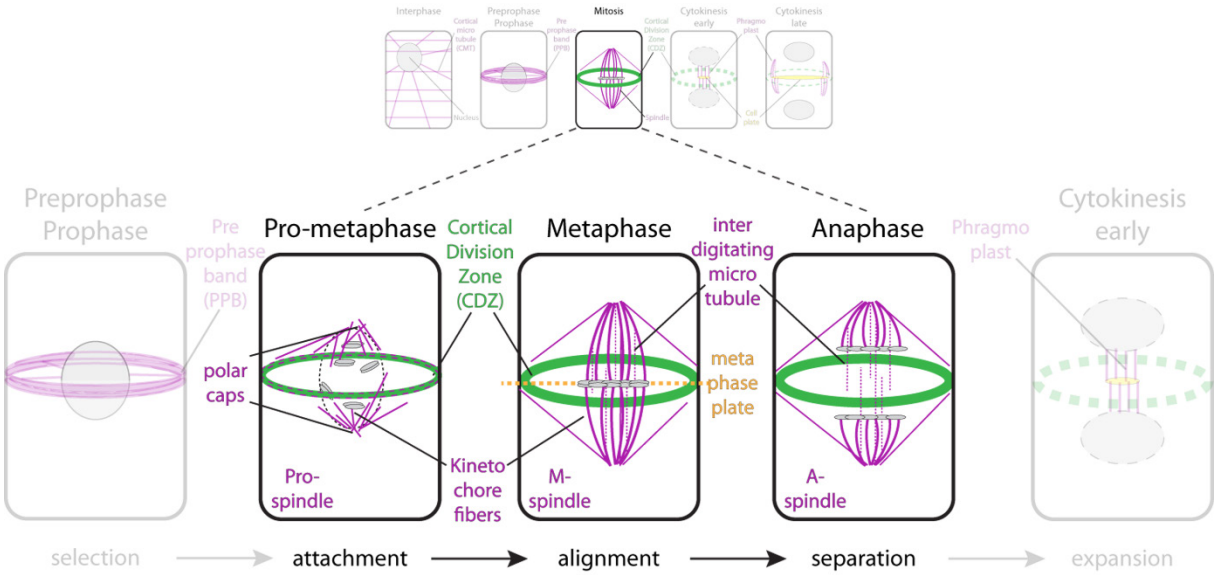

***Figure 2: Schematic illustration of plant spindle formation*:** The stages after NEB that lead to chromosome separation in a chronological order. Prospindle formation starts with the redistribution of microtubules into asters tangential to the nucleus, generating two polar caps on opposite sites before and during nuclear envelope breakdown that define spindle main axis. Microtubules are attaching to the kinetochores, forming kinetochore fibers (continuous magenta line). In metaphase, the barrel-shaped bipolar spindle leads to the alignment of chromosomes in the plane of cell division (metaphase plate). Interdigitating microtubules (dashed magenta lines) are nucleated. Microtubules connect the spindle with the CDZ. In anaphase, K-fiber microtubule-depolymerization facilitate chromosome pair movement towards opposite poles. Microtubules are depicted in magenta, the cortical division zone (CDZ) in green, and chromosomes in grey.

5.1.3 Establishment of the cytokinetic apparatus – the phragmoplast

The plant specific cytokinetic apparatus, the phragmoplast, is a bipolar array that consists of antiparallel microtubules, actin filaments and endomembranes (Staehelin and Hepler, 1996, Müller and Jürgens, 2016, Smertenko et al., 2017). While microtubule minus ends are pointing towards the daughter nuclei (distal zone), most of the microtubule plus ends in each phragmoplast half are facing towards the division plane, allowing for the directional transport of cell plate-forming vesicles. Furthermore, a subset of microtubules extends from both opposing phragmoplast half towards the phragmoplast middle plane, forming an antiparallel overlap within the plane of division (Park et al., 2012, Müller and Jürgens, 2016). It is assumed, based on the recent findings in *Physcomitrella patens*, that the phragmoplast midzone defines the region (width) of delivery of membrane material and of cell plate formation (de Keijzer et al., 2017). To accomplish cell plate synthesis and cell plate expansion by the addition of newly arriving vesicles requires timely co-ordination with the respective expansion of the phragmoplast towards the parental cell wall (Steiner et al., 2016b, Boruc and Van Damme, 2015). Simultaneously with the depolymerization of microtubules from the central zone (lagging zone) (Smertenko et al., 2011), polymerization of new microtubule at the margins (leading edge) of the phragmoplast occurs with dynamic acentrosomal microtubule nucleation, promoted by γ-tubulin ring complexes (γ-TuRCs) on stable microtubule bundles (Murata et al., 2013, Masoud et al., 2013b). Concurrently, translocation of γ-tubulin labelled microtubules at the distal region away from the midzone contribute to a constant length of phragmoplast microtubules during the homogenous centrifugal expansion (Murata et al., 2013). The phragmoplast is initially disk-shaped and is transformed into a ring-shaped structure as it expands radially, concurrently with the centrifugally evolving cell plate. Finally, the phragmoplast reaches the CDZ, the position of which was initially predicted by the PPB (Müller and Jürgens, 2016) (Figure 3).

Disruption of the microtubule-based expansion or the stabilization of the phragmoplast results in the generation of incomplete cell walls, multinucleated cells and wider phragmoplast midzones. For instance, a mutation in the kinesin-7 HINKEL (HIK)/NACK1 causes the persistence of phragmoplast microtubules and the formation of incomplete cell walls, pointing towards a regulatory function of HIK in the disassembly of the microtubules at the lagging zone (Strompen et al., 2002). Intriguingly, HIK/NACK1 triggers the activation of the mitogen activated protein kinase (MAPK) pathway upon direct binding to MAPK kinase kinase NUCLEUS AND PHRAGMOPLAST-LOCALIZED KINASE (NPK) and its prior release from the inhibitory effect of the active cyclin-dependent kinases (CDKs) during anaphase (Sasabe et al., 2011a). The target of the HIK/NAK1/NPK/MAPKK/MAPK signalling pathway is the conserved microtubule cross-linker family MAP65 (Otegui et al., 2005). Upon phosphorylation, MAP65 family members, cross-linking anti-parallel microtubules at the midzone are deactivated, allowing for the depolymerization of microtubules in the lagging zone (Sasabe and Machida, 2006, Sasabe et al., 2011a, Boruc et al., 2017). The function of certain MAP65 family members is critical for the integrity of the phragmoplast. For instance, compromised microtubule interdigitation by the loss of MAP65-3/PLEIADE (PLE) results in wider phragmoplast midzones and incomplete cell plate formation, reflected by cell wall stubs and oblique cell walls (Müller et al., 2004, Ho et al., 2011b, Kosetsu et al., 2013). MAP65-3 cross-links antiparallel microtubules *in vitro* and restricts Kinesin-12 family members (Kinsesin12-A/PAKRP1 and PAKRP1L) to the phragmoplast midzone *in vivo*. Thus, MAP65-3 activity along with kinesin motors contribute to phragmoplast assembly and function (Walczak and Shaw, 2010, Ho et al., 2011a).

Experimental evidence suggests that additional members of the MAP65 family with unique or overlapping functions might act redundantly with MAP65-3/PLE throughout cytokinesis (Van Damme et al., 2004, Li et al., 2017, Mao et al., 2005, Wicker-Planquart et al., 2004, Gaillard et al., 2008). Specifically, recent findings confirmed redundancy between MAP65-4 and MAP65-3/PLE at the phragmoplast midzone, contrary to MAP65-1, which is localized along the entire length of phragmoplast microtubules (Li et al., 2017, Sasabe et al., 2011b). Notably, it has been reported that in addition to the phragmoplast midzone MAP65-4 is localized also at the CDZ (Li et al., 2017, Gaillard et al., 2008) and associate with the early spindle and the kinetochores fibers (Van Damme et al., 2004, Fache et al., 2010). Moreover, phylogenetic analyses among the MAP65 family members revealed that MAP65-1 and MAP65-2 belong to a separate cluster within the family (Hussey et al., 2002). Both decorate almost all microtubule arrays including cortical microtubules, PPBs, spindles and phragmoplasts (Struk and Dhonukshe, 2014). Intriguingly, analyses of the dynamic behaviour of microtubules at the leading edge of the phragmoplast in tobacco bright yellow (BY)-2 cells revealed MAP65-1a dependent cross-linking of newly formed microtubule overlaps that probably leads to the stabilization of the leading edge during phragmoplast expansion (Murata et al., 2013). The latter combined with their capability of releasing microtubules upon phosphorylation, underscore a significant role for MAP65 protein family members as dynamic antiparallel microtubule cross-linkers that ensure proper phragmoplast integrity (lagging zone/ midzone) and expansion (leading edge) as well integrity.

During the anaphase-to-telophase transition, cell plate assembly initiates with the formation of the cell plate assembly matrix (CPAM) at the phragmoplast midzone (Smertenko et al., 2017), appearing as a ribosome free zone around the forming cell plate in electron micrographs (Seguí-Simarro et al., 2004). Over the years, application of various microscopy techniques, revealed that successful establishment of the CPAM requires a tense interplay of a huge set of different protein components. Mutations interfering with these components such as endomembrane structures (Golgi/ *trans*-Golgi network (TGN)), as well components of vesicle-associated molecular machineries (SNARE proteins/ Rab GTPases/ transport protein particle (TRAPP)II/ EXOCYST complex), are often lethal or at least dramatically affected at a cellular level (Steiner et al., 2016a, Hála et al., 2008, Ingouff et al., 2005, Rybak et al., 2014, Chow et al., 2008, Smertenko et al., 2017).

Cell plate biosynthesis, the establishment of a membrane-polysaccharide compartment, which partitions both daughter nuclei after separation, occurs within CPAM via fusion of TGN-derived secretory membrane vesicles, migrating along the phragmoplast towards the equatorial plane of cell division (Müller and Jürgens, 2016, Boruc and Van Damme, 2015). The fusion of vesicles within this plane is mediated by the formation of *trans*-SNARE (Qa-, Qb-, Qc and R-SNARE) and other tethering complexes, which are bridging membranes to be fused with one another (Boruc and Van Damme, 2015). These vesicles contain a whole set of different components, including enzymes (e.g. callose synthase) and different polysaccharides (e.g. pectins), which are forming a matrix that facilitates the incorporation of hemicelluloses and cellulose fibrils during cell plate maturation (Samuels et al., 1995) (Figure 3).

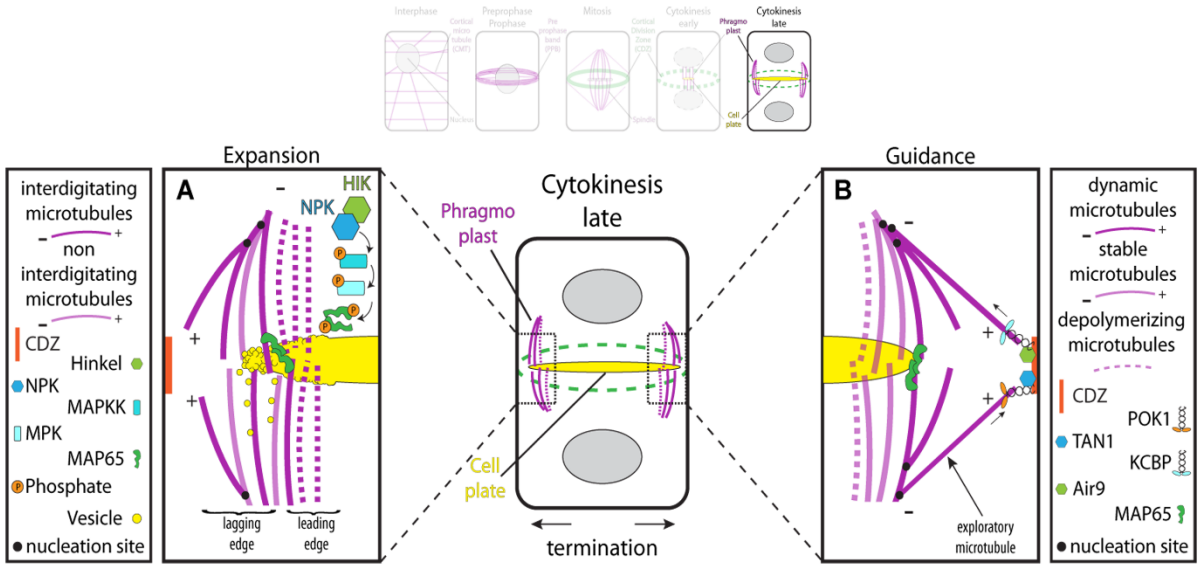

Figure 3: Schematic overview of phragmoplast expansion and guidance: **(A, Expansion)** Expansion of the phragmoplast proceeds with the nucleation and polymerization of microtubules at the phragmoplast leading zone, where Golgi derived vesicles (yellow) are fusing at the phragmoplast midzone, forming the centrifugally evolving cell plate. Antiparallel microtubules (interdigitating microtubules) are cross-linked in the phragmoplast midzone by the microtubule associated protein MAP65-3 (green), that form homo-dimers and ensure phragmoplast integrity. Upon phosphorylation by the HIK(green)/ NPK(blue)/ MAPKK(turquoise)/ MAPK(light blue) pathway, MAP65-3 releases the antiparallel microtubule overlap, resulting in the depolymerisation of microtubules at the lagging edge. Microtubule arrays are depicted in magenta, the CDZ in orange the cell plate in yellow. **(B, Guidance)** Exploratory microtubules are nucleating from the leading edge of the expanding phragmoplast and polymerize towards the CDZ. The plus end directed kinesin-12 class protein POK1 (orange) and its interactor TAN1 (blue) as well as the minus end directed kinesin-12 KCBP (turquoise) and MAP AIR9 (light green) resides at the CDZ throughout cytokinesis. Intriguingly, it might be possible, that both kinesins are able to bind with their motor domains at the plus ends of exploratory microtubules, originating from the phragmoplast. Generating force through motility, these kinesins would as consequence either push against (POK1) or pull (KCBP) the phragmoplast and therefore guide the phragmoplast towards the cell plate fusion site.

5.1.4 Maintenance of cell plate insertion site – the Cortical Division Zone

The positional information of the PPB provided in prophase is preserved through mitosis and cytokinesis by a unique and highly dynamic set of cellular components occupying the CDZ (Smertenko et al., 2017). The CDZ is an area of the plasma membrane and adjacent cell wall first detectable during PPB assembly in prophase as a broad ring like structure, which also includes the PPB. During cytokinesis this broad ring narrows, by, to date, an unknown mechanism, and is transformed into a distinct ring-shaped structure, marking more precisely the site of cell plate fusion (Rasmussen et al., 2013). The phragmoplast, guided by CDZ resident proteins, reaches the cell cortex at this pre-selected site, where the cell plate meets and fuses to the parental cell wall. Intriguingly, CDZ resident proteins involved in this process may also assist peripheral or exploratory microtubules which extend from the phragmoplast to contact the CDZ (Müller and Jürgens, 2016). The visualisation of the CDZ is rather challenging, nonetheless, sensitive microscopy technologies combined with fluorescent protein tagging shed light on its dynamic. Interaction screens and reverse genetics identified new players and connections between early and late events in spatial control of cytokinesis. For instance, it has been found that F-Actin remains at the cortex, marking a particular region after PPB disassembly at the margins of a zone of low actin abundance (Cleary et al., 1992, Cleary, 1995, Panteris, 2008). Whether this actin-depleted zone (ADZ) and the CDZ are precisely matching is still unknown, however, the enrichment of actin filaments described in BY2 cells at either side of the ADZ (twin peaks) is remarkable (Sano et al., 2005). Originally discovered in *Zea mays* (maize), TANGLED (TAN)1 is the first positive marker of the CDZ encoding for a highly basic MAP, which co-localizes in a ring-shaped pattern with the PPB and remains at the CDZ

until the termination of cytokinesis (Martinez et al., 2017, Walker et al., 2007, Rasmussen et al., 2011). Mutants of *TAN1* are characterized by defects in cell wall positioning in maize, however, PPBs and other mitotic structures are unaffected. Further analyses of mitotic microtubule arrays revealed that CDZ establishment or recognition by the centrifugally expanding phragmoplast is impaired, resulting in mis-aligned/tilting phragmoplasts and random cell plate insertions (Walker et al., 2007, Martinez et al., 2017). A recent finding suggests a more complex role for TAN1 during CDZ establishment alongside with a synergistic genetic interaction with the MAP AUXIN-INDUCED-IN-ROOTS9 (AIR9) (Mir et al., 2018). While single *tan1* or *air9* mutants have mild or no phenotype, the double *tan1 air9* mutants exhibit defects in root growth, division plane orientation in addition to a rotation in the cell files of the differentiation zone (Mir et al., 2018, Buschmann et al., 2006). Even though AIR9 is not a continuous marker, since it accumulates at the division site during prophase and reappears at the CDZ upon cell plate fusion (Buschmann et al., 2006), it might be possible that TAN1 and AIR9 function together in a common pathway (Mir et al., 2018). However, the existence of parallel or redundant pathways cannot be excluded. The predicted minus end directed kinesin-14 motor protein, KINESIN-like CALMODULIN-BINDING PROTEIN (KCBP), is an interactor of AIR9 and apart from its localization at the distal region of the phragmoplast, it resides from prophase on at the CDZ (Buschmann et al., 2015). Neither *kcbp* single mutant nor a *kcbp* and *air9* combination showed defects in division plane orientation, yet, KCBP might coordinate microtubule and actin mediated mechanisms in phragmoplast guidance, since KCBP binds to actin in addition to microtubules (Buschmann et al., 2015). Transient expression experiments in tobacco leaf cells showed that the association of KCBP to microtubules depends on AIR9 activity, whereas an internal MyTH4-FERM domain in KCBP, which is mostly shared among metazoan myosin X (Buschmann et al., 2015), is necessary for CDZ localization. These findings are of particular interest, since KCPB is the only predicted minus end directed kinesin known so far contributing to CDZ establishment and/or determination, mediating a potential crosstalk between microtubules and actin. Contrary to the AIR9-KCBP module however, CDZ maintenance of TAN1 from metaphase on depends on the C-terminal part of a pair of functional redundant plus end predicted motor proteins namely PHRAGMOPLAST ORIENTING KINESIN1 (POK1) and 2 (Walker et al., 2007, Lipka et al., 2014). Reminiscent of the *tan1* mutant in maize, the majority of phragmoplasts in symmetric cell divisions deviate from the PPB orientation in *pok1 pok2* double mutants (Müller et al., 2006), giving rise to a high frequency of random cell plate insertions and dwarfed plants. POK1 is dynamically recruited to the PPB during prophase in a microtubule-dependent manner, and maintained at the CDZ in the absence of cortical microtubules until the end of cytokinesis (Lipka et al., 2014) (Figure 4). Whether POK1 and POK2 act together in the same pathway to guide the expanding phragmoplast towards the CDZ is currently unclear. However, the persistent presence of POK1 at the CDZ, together with the requirement of POK1 and POK2 as scaffolds to retain resident proteins there, such as TAN1 or RanGAP1 from metaphase on, support a crucial role for these kinesins in CDZ establishment/ maintenance (Xu et al., 2008, Walker et al., 2007, Lipka et al., 2014).

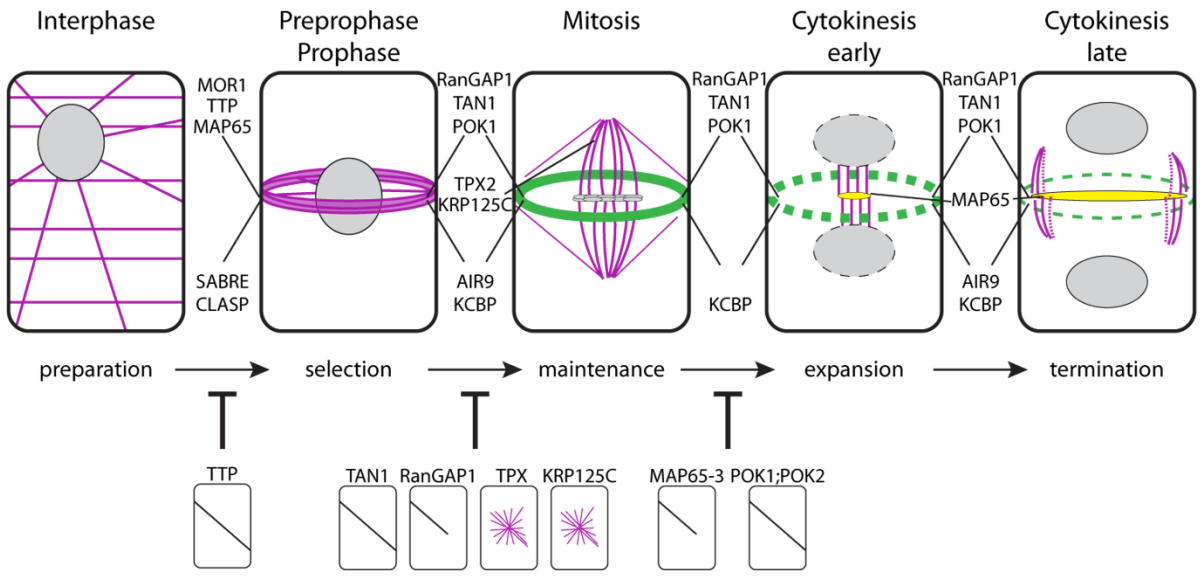

***Figure 4: Proteins involvement and function during cell division*:** Schematic representation of protein complexes and their involvement during cell division in the respective cell cycle stages. Alteration in specific protein function due to mutations leads to abnormal cell divisions, causing oblique cell walls (TTP, TAN1, RanGAP1, MAP65-3, POK1/2), cell wall stubs (RanGAP1/MAP65-3) or spindle disruption (TPX2, KRP125c). Microtubule arrays are depicted in magenta, the establishment and maintenance of the CDZ in green in addition to the cell plate in yellow.

5.2 Molecular motors in Arabidopsis thaliana – Kinesin-12 class proteins

The Arabidopsis genome encodes for an extraordinary high number of diverse kinesin-like proteins compared to metazoan (e.g. 45 human kinesins), encompassing at least 61 predicted kinesin-like proteins in *Arabidopsis thaliana* (Lee and Liu, 2004). These numerous and diverse molecular nano-motors are critical mediators of microtubule based cellular processes such as unidirectional transport of vesicles/organelles (eg. KCA1), microtubule organisation (e.g. FRA1), signal transduction (e.g. HINKEL) and cell division (e.g. POK1). (Ito et al., 1998, Lee and Liu, 2004, Menges et al., 2003, Miki et al., 2014, Suetsugu et al., 2010, Zhong et al., 2002, Sasabe et al., 2011a, Müller et al., 2006). The presence of an interior catalytic core domain of about 350 amino acids, containing both ATP- and a microtubule binding site is substantially conserved throughout the kingdoms, contributing to the known classification into different classes. In addition, and since they are capable of forming dimers, most kinesins possess two dis-ordered regions, with emerging regulatory function upstream of the catalytic core domain. Both, the catalytic core domain and the neck linker are forming the characteristic kinesin motor domain. Adjacent to the neck linker, a region called the stalk contains a structural motif named coiled coil domains (Vale and Milligan, 2000, Zhu and Dixit, 2012). Upon binding to and hydrolysing of adenosine triphosphate (ATP), the motor domain undergoes a conformational change, enabling stepping along microtubules. In spite of this, the ATP-dependent binding to microtubules is facilitated via an interior microtubule binding domain (Endow, 1999, Vale and Milligan, 2000). It's worthwhile noting that movement of kinesins is neither bidirectional nor sporadic. Kinesins possessing a motor domain at the amino-terminal (N-terminal) domain exhibit microtubule plus end-directed motility. On the contrary, kinesins, the motor domains of which are located at the carboxy-terminal (C-terminal) domain move towards the microtubule minus ends (Endow, 1999). The coiled coil domains within the stalk facilitate the homodimerization of protein molecules. This homodimerization in many cases results in the formation of additional binding

domains to cellular components such as vesicles, Golgi, and mitochondria (Hancock, 2008). The structural features and the functional interplay of kinesins are reflected in numerous specific cellular functions during various cellular and developmental processes (Endow, 1999). To accomplish their roles, the function of kinesins must be timely and spatially regulated. This requires a plethora of regulatory mechanisms (e.g. phosphorylation/ dephosphorylation) and additional interaction with several other proteins. Based on a phylogenetic analyses of motor domains, the kinesin superfamily has been further divided into 14 families. In *Arabidopsis* several families are either expanded with more than half kinesins belong to class 7 and 14 or are not represented at all (e.g. classes 2, 3, 9 and 11) (Zhu and Dixit, 2012, Vanstraelen et al., 2006). Intriguingly during cell division, 23 kinesins are upregulated in *Arabidopsis* (Vanstraelen et al., 2006) whereas in *Physcomitrella patens*, at least 43 kinesins are expressed during mitosis, most of them localizing to the spindle or the phragmoplast (Miki et al., 2014).The kinesin-12 family members are grouped into two clusters in *Arabidopsis*, with contain three members each (Figure 5B). These kinesins share N-terminal motor domain homology with their metazoan orthologues, thus indicating a plus end directed motility for the members of this family. One kinesin-12 cluster comprises the phragmoplast-associated kinesin-related protein1 (PAKRP1/Kinesin-12A), the PAKRP1-like protein (PAKRP1L, Kinesin-12B) along with a so far uncharacterized kinesin encoded by *At3g20150*. Both, Kinesin-12A and Kinesin-12B are located at the phragmoplast midzone in a MAP65-3/PLE dependent fashion and are necessary for proper cell plate formation in the male gametophyte (Ho et al., 2011a, Lee et al., 2007, Lee and Liu, 2000). The other cluster of kinesin-12 class protein consists of the functionally redundant protein pair of POK1 and POK2, which are required for the spatial regulation and maintenance of the CDZ (Müller et al., 2006), in addition to a yet uncharacterized kinesin, from now on referred to as PHRAGMOPLAST ORIENTING KINESIN-Like protein (POK-like; At3g44050). Co-alignment of PPB, phragmoplast and cell plate fusion site is impaired in the *pok1 pok2* double mutant, resulting in tilting of phragmoplasts and random cell plate insertions. Furthermore, in cytokinetic root cells of *pok1 pok2* mutants, the phragmoplast expansion rate is reduced compare to wild type cytokinetic cells, pointing towards an additional function of POKs in phragmoplast microtubule dynamics (Lipka et al., 2014).

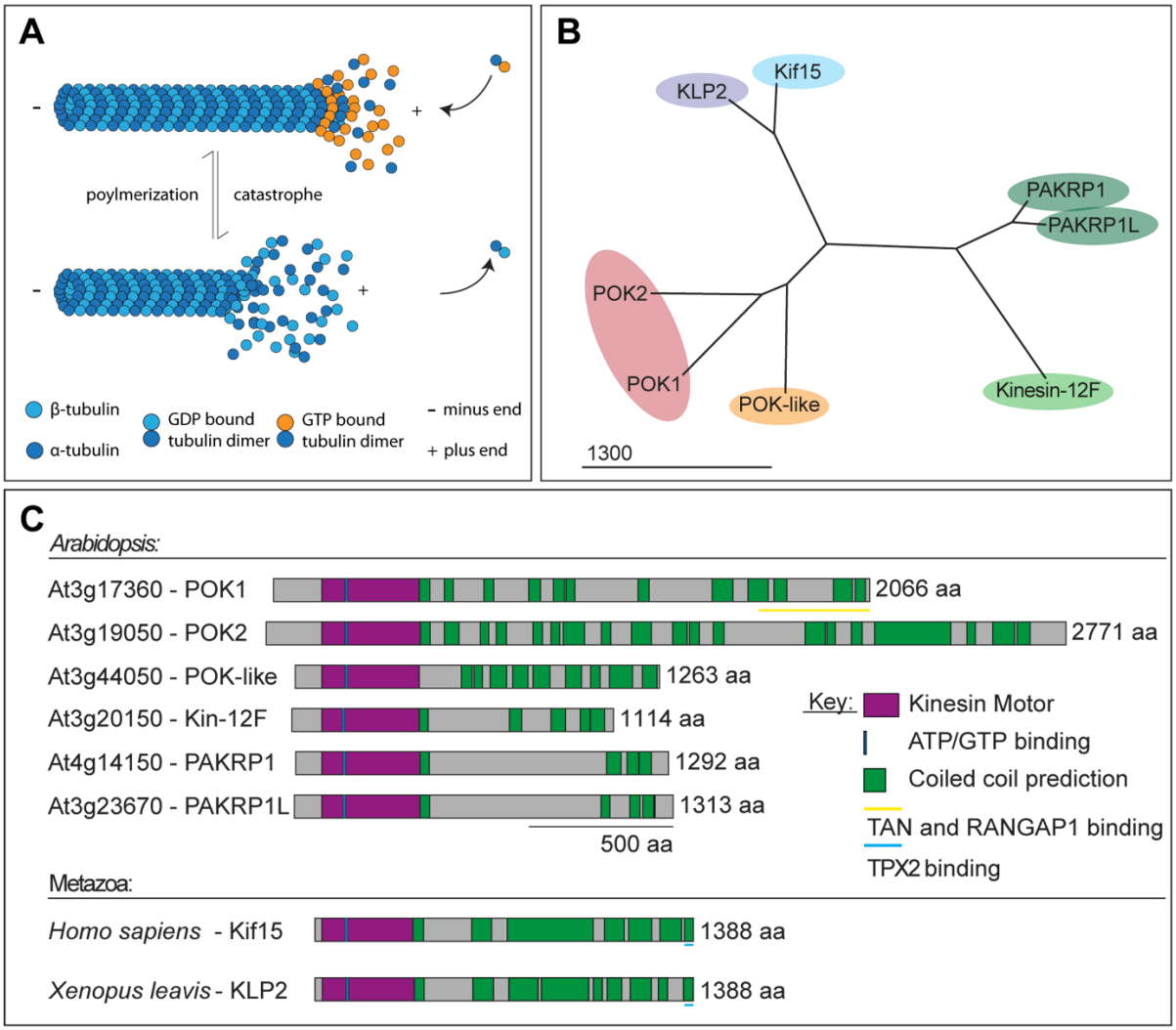

Figure 5: Microtubule structure/dynamics and, phylogenetic relationship and organization of kinesin-12 class motor proteins: (A) Schematic representation of microtubule dynamics and the switching of polymerisation (growth) and depolymerisation (catastrophe) at the microtubule plus end. GTP-bound α-(dark blue) and β-tubulin (orange) heterodimers are associating with another heterodimer via an α- and β-tubulin head-to-tail linkage, forming a tubule like structure, consisting of 13 protofilaments. The less dynamic end of a microtubule is defined as the minus end. Catastrophe occurs, since the GDP bound states of the α- and β-tubulin heterodimer is less stable compared to the GTP bound form, resulting in a fast shrinkage of the microtubule and the release of α- and β-tubulin hetero dimers (modified from *Dixit and Cyr,* 2004). **(B)** Phylogenetic tree of kinesin-12 class motor proteins and their next relatives from *Xenopus leavis* (KLP2) and *Homo sapiens* (Kif15), based on the amino acid sequence (aa). Note the clustering into two clades, namely POK and PAKRP. Phylogenetic tree was prepared with CLC main workbench ver. 7.7. **(C)** Comparative domain organization of kinesin-12 class proteins of *Arabidopsis* and Metazoan. Motor domains are depicted in purple (predicted by prosite (Sigrist et al., 2013)) with the internal ATP/GTP binding domain in blue. The coiled coil domains potentially aiding homo-dimerization are depicted in green (paircoil2.csail.mit.edu). Potential binding site for TAN and RanGAP1 interaction are depicted in yellow in case of POK1 and in blue for TPX2 in case of Kif15 and KLP2.

6. Objectives

Cell division, the duplication and physical separation of the cellular content is essential for life. Although cell division per se is more or less conserved throughout the kingdoms, different organisms developed evolution unique features during to effectively fulfil their individual requirements. The inward-to-outward separation mode involves specified cytoskeletal arrays and occurs exclusively in plant cells during cell division, as plants have to coping with the existence of a rigid cell wall. Many associating proteins as well as aspects of their spatial-temporal regulation mediating this process have been investigated and identified over the past decades,

Characterized by its ability to establish, maintain and recognize the CDZ, the resident kinesin-12-member POK1 acts together with its functional homologue POK2 in phragmoplast guidance, hence contributing in the proper positioning of the newly synthesized cell plate. Molecular characterization of POK1 identified its ability to act as scaffold to retain resident CDZ proteins to the latter cortical cell region, likely contributing in the spatial-temporal regulation of its presence during each individual cell division stage. To understand POK1 mode of function and its ability to act as scaffold in its entirety and gain further insight into the spatio-temporal regulation of its activity, we performed a Y2H screening with POK1 to identify novel interactors. We identified a pair of functional redundant putative ROP GTPase activating proteins (ROP-GAPs), the function and localization of which depends on POKs. By using molecular and genetic approaches, we discovered that these ROP-GAPs might both function in a continuous feedback loop as effectors of ROPs, to accurately determine division plane selection upstream of POK function. The requirement of POK activity for their localization at the CDZ from mitosis on might reflect implication of this module in additional cell division related processes such as vesicle trafficking and cytoskeletal reorganization. Collectively these findings provide further insight into the mechanism that regulates these two novel CDZ resident proteins, which possibly modulate ROP effector driven signalling pathways during cell division.

Another objective of this work was to decipher the molecular contribution of POK2 during cell division. We assumed that POK2 and POK1 act redundantly, contributing both to phragmoplast guidance, since simultaneous loss of function mutants exhibit strong developmental defects. However, the localization pattern of POK1 at the CDZ did not explain the additional decrease in the phragmoplast expansion velocity recorded in the double mutant. Such decrease in the expansion rate is indicative of an additional function of POKs in phragmoplast dynamics. Indeed, this work uncovered a dual localization pattern for POK2 mediated by distinct protein domains and its specific implication in phragmoplast expansion via interaction with the known phragmoplast midzone resided MAP65-3/PLE. These findings allowed the proposal of a hypothetical model, regarding POK2 functions in CDZ as well as in phragmoplast expansion during cell division

Considering that kinesin-12 members and their individual functions are conserved throughout the eukaryotic kingdom, the last objective of this work was to identify the yet missing kinesin-12 member involved in spindle assembly. We characterized for the first time Kinesin-12E, which we named POK-like. POK-like shares the evolutionary conserved function with mammalian kinesin-12 as it interferes with spindle assembly, whereas it displays also the plant specific localization typical of plant kinesin 12 class proteins during cytokinesis.

7. Results and Discussion

7.1 Division plane selection is controlled by two putative ROP-GAPS, which both depend on POK function

Over the years, there has been a plethora of work published towards understanding CDZ establishment and maintenance. However, essential key parts are still missing, making it difficult to understand this process in its entirety. The current model suggests that POK kinesins act as crucial scaffolds at the CDZ, retaining CDZ resident proteins such as TAN1 and RanGAP1. Nevertheless, little is known regarding the existence of additional proteins participating in CDZ establishment/ maintenance and their interplay with POKs (Lipka et al., 2014, Walker et al., 2007, Xu et al., 2008). In the research article entitled “Putative RopGAPs impact division plane selection and interact with kinesin-12 POK1”, we describe the identification of two closely related putative Rho-GTPase Activating Proteins (Rho-GAPs), as novel interactors of POK1 (Stöckle et al., 2016). It was found that the carboxy (C)-terminal located coiled coil domains of RhoGAP1 and 2 are sufficient for interaction with POK1. Protein domain prediction softwares (http://uniprot.org; http://paircoil2.csail.mit.edu) predicted the presence of an additional (N)-terminal pleckstrin homology (PH) domain upstream of the conserved GAP domain, putatively responsible for membrane association (Lemmon and Ferguson, 2000). Therefore, the proteins were named PHGAP1 and PHGAP2, respectively. The interaction with POK1C-terminal domain were confirmed using yeast mating-based split-ubiquitin-system (SUS) interaction assay (Karnik et al., 2015). Considering that two C-terminal protein truncations of POK1 were sufficient for CDZ localization (POK1C$_{1213\text{-}2066}$) or interaction with TAN1 (POK1C$_{1683\text{-}2066}$) (Lipka et al., 2014), these two C-terminal fragments were used as baits in the SUS-assay. As expected, yeast clones co-expressing POK1C$_{1213\text{-}2066}$ and POK1C$_{1683\text{-}2066}$ with either PHGAP1 or PHGAP2 were able to grow on selective media, indicative of POK1-PHGAP interaction. Furthermore, interactions were validated *in planta* by ratiometric bimolecular fluorescent complementation (rBiFC) experiments in *Arabidopsis* root protoplasts between nYFP-POK1C$_{1683\text{-}2066}$ and cYFP-PHGAP2, using appropriate controls (Hecker et al., 2015). Thus, we concluded that the C-terminal truncation of POK1 is sufficient for *in vitro* and *in vivo* interaction with PHGAP1 and PHGAP2.

PHGAPs might function during cell division and polarity establishment

It is well known that GAPs inactivate their small GTPase targets by stimulating the intrinsic GTPase activity, thus accelerating the hydrolysis of GTP to GDP. A highly conserved arginine (R) residue in the GAP domain seems to be critical for RhoGAP function in plants and animals (Hwang et al., 2008). On the other hand, the activation of small GTPases, is accomplished by distinct Guanine Nucleotide Exchange Factors (GEF) (Feiguelman et al., 2018, Bourne et al., 1990). As a result, these tightly regulated small GTPases act as molecular switches, contributing in the transduction of various stimuli via different molecular signalling cascades, hence, influencing a number of different cellular processes in the eukaryotic kingdom (Bourne et al., 1990). Apart from Rab, Ran, ARF, and Ras GTPases in eukaryotes, the Rho-small GTPases of Plants (ROPs) constitute a plant specific Rho/Rac-like GTPase subfamily (Zheng and Yang, 2000, Brembu et al., 2006), implicated in the organization and dynamics of the actin and microtubule cytoskeleton, the regulation of endo- and exocytosis as well as the control of

intracellular signalling cascades (Feiguelman et al., 2018). PHGAP1 and PHGAP2 both share conserved protein domain architecture with the, pollen specific, GAP ROP1 ENHANCER (REN1), a *bona fide* regulator of ROP1 activity during pollen tube growth in *Arabidopsis* (Hwang et al., 2008). Therefore, we tested whether PHGAPs could bind and interact with ROP GTPases *in vivo,* taking advantage of our established rBiFC system. Indeed, n/cYFP complementation upon interaction of PHGAP2 with either ROP1, ROP2, ROP3, ROP4 and ROP6 in *Arabidopsis* root protoplasts suggested a potential interaction. However, the interaction between PHGAP2 and ROPs in the rBiFC experiments is deemed rather unspecific considering the biological function of either of these ROP GTPases. ROP2/ROP4 and ROP6 are antagonistically regulating pavement cell development/expansion in the *Arabidopsis* leaf epidermis, ROP1 and ROP3 contribute in pollen tube growth, whereas ROP3 displays an additional function during embryo development (Feiguelman et al., 2018). To test whether the findings regarding POK1-PHGAP and ROP-PHGAP interaction provide substantial reasons for further characterization, we analysed the gene expression patterns of both PHGAPs in lines expressing *β*-Glucuronidase (GUS) under the control of each PHGAP promoter. PHGAP1 and PHGAP2 GUS reporter gene expression overlapped in root and leaf meristematic tissue, in young leaf and in the leaf-vascular tissue indicative of a common biological function. However, *pPHGAP1*:GUS reporter expression was predominantly detected in the epidermal and cortex cell files in roots and in root hairs as well. Comparison of our findings with available previous published data concerning POK1 reporter gene which is expressed in meristematic root and leaf tissue (Müller et al., 2006) or distinct ROP reporter gene expression (e.g. AtROP2, AtROP4, AtROP6 (expressed in young leaves); AtROP4, AtROP11 (function in root hair initiation); AtROP7: (expressed during vascular development) strongly supports a possible function in a common biological pathway. Collectively, these data imply that PHGAPs might function during cell division and cell polarity establishment prior to cell expansion.

PHGAP1 and PHGAP2 are recruited towards the CDZ

To examine the cellular localization of PHGAP1 and PHGAP2 during cell division in *Arabidopsis*, we took advantage of two ubiquitously expressed cDNA fusion constructs (*pUBN:GFP-PHGAP1*, *pUBN:GFP-PHGAP2*) and one full genomic construct (*pPHGAP2:GFP-PHGAP2*). The transgenic proteins were labelled with the green fluorescent protein (GFP). Considering POK1 localization in a cell cycle dependent pattern in meristematic tissue (Lipka et al., 2014), the putative PHGAP-POK1 interaction, as well as their similar gene expression pattern, we focused our investigation on *Arabidopsis* root meristem cells for further analyses. The cell cycle stages during cell division were determined after co-expression of either of the fusion proteins with the microtubule binding domain (MBD) fused to the red fluorescent protein (RFP-MBD). Intriguingly, both GFP-PHGAP1 and GFP-PHGAP2 display a cytoplasmic and membrane-associated signal in interphase. Upon entry into metaphase, a ring-shaped accumulation pattern at the plasma membrane, reminiscent of that formed by other CDZ resident proteins, appears and remains there until the termination of cytokinesis. In addition, we created a red version of PHGAP1 (RFP-PHGAP1) in order to perform co-localization experiments with YFP-POK1. As expected, the results confirmed the localization of PH-GAPs at the CDZ. RFP-PHGAP1 and YFP-POK1 co-localize at the CDZ from metaphase on until the end of cytokinesis, however, XFP-PHGAPs fusion proteins were never detected at the PPB in prophase when YFP-POK1 is already present.

Loss of *PHGAP* activity results in developmental defects

Since proteins such as TAN1 and RanGAP1 decorate the CDZ from metaphase onward in a POK1 dependent manner, our findings prompted us to investigate the localization pattern of both PH-GAPs fusion proteins in the *pok1 pok2* double mutant (*pok1-1 pok2-3*) (Lipka et al., 2014). Although these proteins were present at the cytoplasm and the plasma membrane neither GFP-PHGAP1 nor GFP-PHGAP2 rings were observed in the *pok1 pok2* double mutant. Thus, we concluded that CDZ localization of PHGAPs from metaphase on, but not membrane association, depends on the function of POKs. The *pok1 pok2* double mutant exhibit severe cell wall positioning defects due to misguidance of phragmoplasts in cytokinesis, thus pointing towards a crucial function for POK proteins in maintaining the positional information of the CDZ. To further characterize the role of PHGAP1 and PHGAP2 in the context of cell division, we used available T-DNA insertion lines. Semi-quantitative RT-PCR analyses of transcript levels of either *phgap1-1* or *phgap2-1* mutant confirmed the complete lack of *phgap1* transcripts and revealed a significant reduction of *phgap2* transcripts compared to wild type. Considering the likelihood of functional redundancy between PHGAP1 and PHGAP2, since neither *phgap1* nor *phgap2* single mutant exhibited any obvious vegetative or cellular phenotype, we investigated a *phgap1-1 phgap2-1* double mutant (from now on *phgap1 phgap2*) as well as a quadruple *pok1 pok2 phgap1 phgap2* mutant. Compared to the *pok1 pok2* double mutant, the quadruple mutant showed phenotypic enhancement of the developmental defects. Root growth and cell division patterns in the root meristem visualized with propidium iodide, were similar to *pok1 pok2* double mutants, however the quadruple mutant exhibited mostly non-fertilized ovules, in addition to very few and non-viable embryos. These findings suggest that PHGAP1 and PHGAP2 might have additional function in aerial tissues. On the contrary, the *phgap1 phgap2* mutants displayed a rather moderate root growth phenotype, which can be partially rescued by the *pPHGAP2:GFP-PHGAP2* construct. On the cellular level however, *phgap1 phgap2* exhibit mild cell wall positioning defects compared to the wild type. Intriguingly, substitution of the highly conserved catalytic arginine (R) residue within the GAP domain by leucin (L) in both PHGAP1 (R203L) and PHGAP2 (R198L) and overexpression in the *phgap1 phgap2* mutant background could not complement the phenotype of mild mispositioned cell walls. Thus, we concluded that the GAP activity and consequently the regulation of potential downstream effectors are necessary for proper cell wall alignment. Notably, the cell cycle dependent CDZ localization pattern of pUBN:GFP-PHGAP1^{R203L} and pUBN:GFP-PHGAP2^{R198L} was not affected, indicating that GAP activity is not required for the recruitment to the CDZ.

Division plane determination is mediated by PHGAP1 and PHGAP2

The mispositioning of the cell walls due to the absence of a functional GAP or GEF and the consequent mis-regulation of ROP and its effector proteins were even more obvious in the context of embryonal development, which requires a distinct sequence of cell divisions to create a regular cell pattern in Arabidopsis. For instance a dominant negative version of ROP3 (DN-*rop3*), in which the protein is in a GDP bound locked status, causes embryo patterning defects in *Arabidopsis*, leading to misshaped and irregular cell wall insertions (Huang et al., 2014). Similarly, globular and early heart stage embryos of *phgap1 phgap2* exhibit abnormally positioned cell walls and an irregular cellular pattern with a penetrance of 6.6% (n=366). This small penetrance of abnormal embryos can be reduced to 2.6% (n=638) by expressing the genomic construct of GAP2, suggesting an additional contribution of

PHGAP1 and PHGAP2 in cell division plane orientation during embryo development. In terms of the putative PHGAP2-ROP interactions, it can be assumed that PHGAP1 and PHGAP2 act as genuine ROP GTPase-activating proteins. The necessity of the catalytic arginine in the GAP domain for their function, as well as the observed mispositioned cell walls in the embryo corroborate our hypothesis. With respect to ROP mediated effector signalling and its implication in plane selection during cell division little is known so far, apart from the phenotype defects caused by the ectopically expressed DN-ROP3. However, it has been shown that during pavement cell morphogenesis the formation of the typical jigsaw puzzle shape of *Arabidopsis* leaf cells requires a balance between ROP2/ROP4- and ROP6-mediated signalling (Feiguelman et al., 2018). The active ROP2/ROP4 cooperate with their effector RIC4 and induce the formation of an actin filament network while concurrently inhibiting RIC1, an effector of ROP6. Thus, activation of KATANIN, which is a microtubule severing protein controlling microtubule bundle formation and a downstream component of the ROP6-RIC1 signalling pathway is impeded. On the contrary, activation of the ROP6-RIC1 signalling pathway leads to the inhibition of ROP2/ROP4 and their effectors (Fu et al., 2002, Fu et al., 2009, Fu et al., 2005, Lin et al., 2013). This implies that these actin and microtubule based antagonistically acting signalling pathways must be under strict spatio-temporal regulation by corresponding GAP(s) or GEF(s). To determine the involvement of PHGAPs in cell division and in particular, their potential role in the organization of microtubule based mitotic structures, we examined the organization of the microtubule cytoskeleton in mitosis by expressing our RFP-MBD reporter construct in the *phgap1 phgap2* double mutant. In a subset of cells, the orientation of PPBs and phragmoplasts in *phgap1 phgap2* deviates from the transverse orientation that is predominantly observed in wild type plants as well as in the rescue line. In addition, by expressing YFP-POK1 in *phgap1 phgap2*, it was ascertained that the YFP-POK1 localization is restricted to the PPBs even in cases were the PPB was oblique. Using POK1 localization position as a readout for the division plane and measuring the deviation angle of its orientation from an axis oriented transversely to the main root axis, confirmed the division plane positioning defects in *phgap1 phgap2* mutants, as the mean deviation angle was significantly increased compared to wild type or the rescue lines. Moreover, in order to validate the hypothesis that the oblique cell walls detected in the *phgap1 phgap2* double mutant are due to a failure of division site selection, we then compared the orientation of PPBs and phragmoplasts in wild type and *phgap1 phgap2* double mutant. Indeed, PPB and phragmoplast orientations significantly deviated in *phgap1 phgap2* compared to the controls. However, PPB and phragmoplast orientation in root cells of the same genotype were similar. Thus, we concluded that loss of PHGAP function increases deviation of PPB orientation and therefore affects POK1 positioning, which in turn results in an inaccurate demarcation of the CDZ and phragmoplast misguidance.

Discussion

Taken together, our findings suggest that PHGAPs act upstream of POK1 in division plane selection. Apart from the POK-dependent activity for CDZ recruitment/maintenance during mitosis, PHGAPs might also function in a continuous feedback loop as effectors of ROPs, and thus, might affect additional cell division related processes such as cytoskeletal organisation and vesicle trafficking at the CDZ (Stöckle et al., 2016). However, the exact mode of PHGAP contribution to the CDZ selection in prophase or the putative regulation of ROP signalling during mitosis and cytokinesis in plants is still an open question. In principle, GAPs negatively regulate the intrinsic GTPase activity of ROPs. In metazoans, up to twenty

Rho-GTPases have been identified/shown to play a critical role in actin nucleation and organization, critical for several cellular processes (Heasman and Ridley, 2008). With respect to cell division specific mechanisms, the small GTPase RhoA and yeast Cdc42 are both key regulators of the acto-myosin contractile ring assembly. In particular, they are inducing the formation of the cleavage furrow in an actomyosin dependent manner, and thereby aid the separation of the daughter cells (Heng and Koh, 2010). Intriguingly, an acto-myosin contractile ring-based mechanism is not functioning in higher plants and the role of actin cytoskeleton during cell division is not considered essential (Smertenko et al., 2017). Drug-induced alterations in actin cytoskeleton as well as mutations in genes encoding for actin related components often lead to cell wall positioning defects, yet, do not interfere with mitotic progression (Kojo et al., 2013). Recently, it was shown that myosin VIII interacts with F-actin and microtubules in cytokinetic cells of the moss *Physcomitrella*, thereby creating a connection between the cell cortex and the phragmoplast, prior to cell plate insertion (Wu and Bezanilla, 2014). In addition, myosin VIII quadruple knock out mutants show phragmoplast misguidance. Together, these findings indicate that actin is required for the last steps of cytokinesis to maintain phragmoplast integrity and assist its guidance. So far, there is no evidence regarding a PHGAP dependent involvement of actin mediated division site selection, however, phragmoplasts in the *phgap1 phgap2* double mutant are still expanding towards the pre-selected site indicated by the PPB, suggestive for an unobstructed function of actin filaments that mediate phragmoplast guidance towards the cell cortex. If PHGAPs are contributing to the latter, their role might be not critical, possibly through unresolved redundant protein functions. Indeed, PHGAPs share unresolved redundant functions with a family of six RhoGAPs members that contain a Cdc42/Rac interacting binding motif (CRIB) (Stöckle et al., 2016). In fact, a functional redundancy between REN1 and ROPGAP1 has already been shown during pollen tube growth (Hwang et al., 2008, Klahre and Kost, 2006). However, to date, it is not known whether POK dependent or independent ROPGAPs function redundantly with PHGAPs in plant mitosis and/or whether ROPGAPs together with PHGAPs might contribute to phragmoplast guidance.

The positional information of the PPB and hence the future plane of cell plate insertion, is assumed to be dictated by both the geometry of the cell and the proper placement of the nucleus at the cell centre in G2 (Murata and Wada, 1991). The nucleus migration might be controlled by distinct members of the myosin protein family. For instance, myosin XI-i/KAKU1 interconnects the outer nucleus membrane to actin filaments via binding to the WPP domain-interacting tail-anchored protein 2 (WIT2) and in order to promote dark-induced nuclear positioning to the centre of the periclinal wall in *Arabidopsis* leaf cells (Tamura et al., 2013). The function of PHGAP activity towards the accurate selection of the division plane seems to be independent of nucleus positioning. This is rather fascinating, since it might be first molecular evidence of small GTPase mediated signalling for proper division site selection in symmetric cell division. These findings stimulate discussions and allow speculations about the exact interplay between nuclear migration and the organization of the cytoskeleton. Notably, both are coordinated between interphase and prophase in G2. The nuclear movement to the cell centre is actin dependent (Tamura et al., 2013). On the other hand, cortical microtubule arrays, are initially oriented transversely to the elongation axis and uniformly distributed and start to re-organize to form the ring shaped microtubule based structure at the cell cortex, the PPB, which surrounds the nucleus in prophase(Wick and Duniec, 1983). In addition, endoplasmic microtubules are connecting the PPB with

the nucleus conferring further stabilization whereas short single F-actin microfilaments connected to the microtubules in the PPB, potentially facilitate the narrowing of the PPB during prophase (Mineyuki and Palewitz, 1990, Takeuchi et al., 2016). The formation of these cytoskeletal components as well as their interaction needs to be spatially regulated. Such a role in intracellular spatial organisation has been proposed for a small GTPase which influences microtubule nucleation/stabilization in metazoan during cell division (Clarke and Zhang, 2008). In this regard, one model proposes that spatial information is transmitted through a diffusible signalling switch between an active and inactive state of two antagonistically functioning proteins, where at least one of them is immobilized. The other protein is dispersed away from its origin of generation towards the site of activation. The distribution of these components leads to the formation of signalling gradients and feedback suppression between signals allowing a timely gradient in favour of either of the signals, in case a concentration threshold is required. On the other hand, a second model proposes that spatial information depends on the localization of the signal itself and is achieved if the signal is tethered to an existing structure or protein complex within the cell (Clarke and Zhang, 2008).

Considering the above described models, it is interesting that PHGAPS are localizing both at the plasma membrane and in the cytoplasm in interphase and prophase, but they are not enriched at the PPB, although POK1 is already present there. This could potentially indicate that posttranslational modification(s) of PHGAPs might be necessary to balance microtubule nucleation and stabilisation through their absence at the PPB. After PPB disassembly, F-actin becomes enriched at either side of the CDZ (twin peaks), establishing an actin depleted zone (ADZ) described at least for BY2 cells. It might be conceivable that deactivation of ROP through PHGAPs that bind to POK1 leads to a local decrease in actin filament nucleation at the CDZ, visible as an actin depleted zone. Along these lines, a GTPase activity at the cell cortex flanking the ADZ might mediate the accumulation of actin filaments on both sides of the ADZ (twin peaks). In addition, one could suggest, that PHGAPs might interfere with ROP activity during the final stages of cytokinesis, thus promoting the stabilization of microtubules, which extend towards the CDZ during late phragmoplast expansion.

However, this is just a hypothesis as the role of distinct ROPs and their effectors or the presence or the necessity of an actin depleted zone during cell division in the root meristem of *Arabidopsis* have not been verified yet. Contrary to BY-2 cells, dividing root cells of *Arabidopsis* are located within the meristem. As a result, visualization of an ADZ has been rather challenging due to signals from neighbouring cells obstructing the view onto the ADZ. Additionally, the use of actin reporters might induce secondary phenotypical effects. Despite the difficulties in visualization of the delicate actin filaments in root cells, it would be fascinating to validate the existence of an ADZ in *Arabidopsis* roots and compare the distribution of actin filaments in wild type and the *phgap1 phgap2* double mutant, in which the activity of PHGAPs is lost. Collectively our results favour for a dual role of PHGAPs in regulating the organization of the cytoskeleton. However, it is not entirely clear which ROPs are direct targets of PHGAP activity. Along these lines, our BIFC experiments confirmed a putative non-specific interaction between PHGAP2 and several ROPs. Besides, co-immunoprecipitation experiments (Fu et al., 2009), combined with mass spectrometry analyses in root-tips expressing different ROP-PHGAP reporter transgene combinations, would allow the identification of specific ROP targets for PHGAP activity during cell division and would set the basis for establishing an ROP activity reporter system.

On the other hand, the visualisation of a potential GTP gradient was performed based on a modified fluorescence resonance energy transfer (FRET) reporter between a cyan and a yellow fluorescent protein (CFP and YFP, respectively) in *Xenopus* egg extracts (Kalab et al., 2002). In principle, a specific GTPase binding domain is fused to CFP and YFP and should undergo FRET in the presence of a GTPase in its GDP bound state but not when bound in its GTP confirmation (Kalab et al., 2002). In our system, the identification of ROP effectors such as RIC1 (ROP6) or RIC4 (ROP2/ROP4) could lead to the generation of a FRET sensor system based on the intrinsic ROP binding CRIB domain (e.g. CRIB-RIC1; CRIB-RIC4) for each identified ROP as readout for active ROPs during cell division in root meristems. The latter, combined with a sensor containing only the GAP domain of our PHGAPs for negative ROP mediated signalling, might be helpful in visualizing GTPase activity gradients *in planta* related to the division plane selection and the later steps of cell division.

Collectively, these data suggest involvement of small GTPase signalling in cell division in plants and showed that PHGAPs participate in division plane selection in a POK1/2 dependent manner.

7.2 Dual localized kinesin-12 POK2 displays multiple functions during plant cell division and exhibit weak, plus-end directed motility.

The position of a functional CDZ, which in turn constitute a pre-selected region at the cell cortex for targeting of the rapidly expanding phragmoplast/cell plate is indicated by the position of the PPB and depends on both, POK1 and POK2 function (Lipka et al., 2014). Previous work showed that kinesin-12 POK1, via its C-terminus, is necessary and sufficient to retain CDZ resident proteins such as TAN1, RanGAP1 as well as the newly identified CDZ occupants PHGAP1 and 2 after prophase and thus, establishes a functional multimeric protein complex that maintains and identifies the future site of cell plate insertion (Walker et al., 2007, Xu et al., 2008, Stöckle et al., 2016). Contrary to the single *pok* mutants which are unremarkable, the *pok1 pok2* double mutant displays numerous mispositioned cell walls and several individual CDZ resident proteins are absent. Therefore, it has been assumed that POK2 and POK1 act redundantly as scaffold for CDZ resident proteins and contribute to phragmoplast guidance. However, the localization pattern of POK1 at the CDZ does not explain the decrease in the phragmoplast expansion velocity recorded in the *pok1 pok2* double mutant compared to wild type, indicative of an additional function of POKs in phragmoplast dynamics (Lipka et al., 2014). In the research article “Dual localized kinesin-12 POK2 plays multiple roles during cell division and interacts with MAP65-3”, we unravel the role of POK2 during cell division.

Timely phragmoplast expansion requires POK2

Since Kinesins-12A and -12B, relatives of POK1 and POK2, are essential for phragmoplast integrity during male gametogenesis and considering that POK1 is exclusively localized at the CDZ throughout cell division, we hypothesized that POK2 might contribute to phragmoplast expansion as well. Therefore, we investigated the expansion rate of the phragmoplast in dividing root cells of *pok2*-1 single mutants, as well as Col and *pok1 pok2*, expressing the microtubule marker GFP-MAP4. Kymograph analyses revealed a mean velocity of phragmoplast expansion for *pok2-1* single mutants comparable to the *pok1 pok2* double mutants (0.16 µm/min ± 0.04and 0.15 µm/min ± 0.02, respectively). Thus, we concluded that indeed POK2 is involved in phragmoplast dynamics independently of other known kinesin-12 family members.

POK2 exhibits dual localization pattern during cell division

To investigate the role of POK2 during cell division further, we generated transgenic plants expressing a Green Fluorescent Protein (GFP)-POK2 fusion protein under the control of the constitutive *Cauliflower* Mosaic Virus (CaMV) promoter *p35S* (p35S:GFP-POK2). Due to recombination of the DNA containing full genomic or full cDNA versions of POK2 we created a chimeric clone, consisting of cDNA and genomic DNA. Expression of this construct restored the strong phenotype of the *pok1 pok2* double mutants to wild type. To examine whether the localization pattern of GFP-POK2 is cell cycle specific, we co-expressed GFP-POK2 with our microtubule binding domain (MBD) fused to the red fluorescent protein (RFP-MBD). Intriguingly, live cell imaging analyses performed in *Arabidopsis* root meristem cells uncovered a dual localization pattern of GFP-POK2 restricted to cells undergoing division. As anticipated, GFP-POK2 marks the PPB in prophase and remains at the CDZ zone throughout cell division, reminiscent of POK1 localization (Lipka et al., 2014). Notably, we observed additional GFP-

POK2 accumulation at the midzone of early disk phragmoplasts in early telophase. GFP signal at the phragmoplast midzone is present throughout the expansion of the phragmoplast towards the cell cortex until the leading edge of the phragmoplast reaches the division site upon cell plate fusion. The presence of a GFP-POK2 population at the phragmoplast midzone supports the hypothesis that compared to POK1, POK2 serves non-redundant, additional functions during phragmoplast expansion. Using the microtubule destabilizing drug oryzalin and monitoring fluorescence recovery after photobleaching (FRAP), it was found that POK1 is dynamically recruited towards the PPB in a microtubule depended manner but remains at the CDZ independently of microtubules from metaphase on until the end of cytokinesis (Lipka et al., 2014). To test whether POK2 behaves like POK1, we treated transgenic seedlings expressing GFP-POK2 together with RFP-MBD with oryzalin. We imaged the cells before treatment and followed the response in the same cells over time. Shortly after application of oryzalin, GFP-POK2 signal vanished from PPBs and from the phragmoplast upon microtubule depolymerization whereas it persisted at the CDZ. Thus, we concluded that similarly to POK1, the localization pattern of POK2 at the CDZ is independent of microtubules, while its association with the phragmoplast midzone requires intact microtubule arrays. Therefore, we assumed that the dual localization pattern at the division site and the phragmoplast midzone of GFP-POK2 is mediated by distinct mechanisms.

Cortical division site localization requires the carboxy-terminal domain of POK2

Considering that two C-terminal protein truncations of POK1 were sufficient for CDZ localization (POK1C$_{1213-2066}$) as well as for interaction with TAN1 (POK1C$_{1683-2066}$), we decided to examine the localization of a truncated POK2 version containing the C-terminal domain (GFP-POK2C$_{2083-2771}$) that corresponds to the respective POK1 region responsible for targeting to the division site. When transiently expressed either in *Arabidopsis* root protoplasts or in *Tobacco* leaves the GFP-POK2C$_{2083-2771}$ displayed a punctuated or clustered pattern in the cytoplasm close to the plasma membrane three days after transfection. In addition, we observed recruitment of GFP-POK2C$_{2083-2771}$ towards filamentous cell structures reminiscent of microtubules when we stably expressed this construct in *Arabidopsis* interphase cells of meristematic tissues. Colocalization with our RFP-MBD marker confirmed that GFP-POK2C$_{2083-2771}$ is able to associate with microtubules in interphase cells. Moreover, in mitotic cells, GFP-POK2C$_{2083-2771}$ co-localizes with the PPB in prophase and at the division site until the completion of cytokinesis at the CDZ. Besides, it was found that GFP-POK2C$_{2083-2771}$ faintly decorates spindle and phragmoplast microtubules. GFP-POK2C$_{2083-2771}$ was not abolished from the CDZ upon treatments with oryzalin, similar to the full length GFP-POK2, but de-polymerization of microtubules abolished filamentous and PPB-localized GFP-POK2C$_{2083-2771}$. Since endogenous POK2 protein might interfere with the localization of the truncated POK2 version, we asked whether GFP-POK2C$_{2083-2771}$ exhibits a similar localization pattern in the *pok1 pok2* double mutant background, where endogenous POK2 is absent. Indeed, in the majority of mutant root cells POK2 C-terminus protein forms a continuous ring in mitotic cells in the *pok1 pok2* double mutant indicative of proper division site targeting. However, compared to wild type approximately 30% of GFP-POK2C$_{2083-2771}$ rings were discontinuous. This observation might point towards a reduction in the efficacy of CDZ targeting and/or retention of GFP-POK2C. In addition, the expanding phragmoplasts ignored the spatial information given by GFP-POK2C$_{2083-2771}$, incapable to rescue the mutant phenotype. Therefore, we concluded that the POK2 carboxy-terminal domain although it is sufficient to mark the division site at the cell cortex, it cannot

guide the phragmoplast by itself. This implies that the N-terminal motor domain contributes to proper POK2 function.

Phragmoplast midzone association is facilitated by the POK2 motor domain

To examine the latter hypothesis, we created a fusion protein containing the first 589 amino acid of POK2 fused to GFP (GFP-POK2MD$_{1-589}$) and investigated its localization. Transient expression in either *Arabidopsis* protoplasts or *Tobacco* leaf epidermal cells revealed association with microtubules. Intriguingly, in both *Arabidopsis* wild-type and *pok1 pok2* double mutant root meristem cells, only in rare occasions GFP-POK2MD$_{1-589}$ decorated cortical interphase microtubules or co-localized with PPB microtubules. Apart from the cytosolic signal in meta- and anaphase, GFP-POK2MD$_{1-589}$, locates at the midzone of the early phragmoplast as soon as the cells proceed to cytokinesis and persists at the midzone until complete depolymerization of phragmoplast microtubules. This specific accumulation at the phragmoplast midzone requires microtubules, similarly to the full-length POK2. Treatment with oryzalin showed disappearance of microtubules and simultaneous abolishment of GFP-POK2MD$_{1-589}$ association at the midzone. Nevertheless, the GFP-POK2MD$_{1-589}$ construct was not sufficient to rescue the mutant phenotype suggesting that both, the C-terminal domain and the motor domain are necessary for phragmoplast guidance.

The signal distribution of GFP-POK2MD$_{1-589}$ at the phragmoplast midzone appeared wider in comparison to full length POK2. Comparison of the full width at half maximum (FWHM) (de Keijzer et al., 2017) of GFP-POK2MD$_{1-589}$ and GFP-POK2 showed that the distribution of GFP-POK2MD$_{1-589}$ is considerably broader than GFP-POK2. These findings support the view that the POK2 localization at the phragmoplast midzone is fine-tuned by domains that are absent from GFP-POK2MD$_{1-589}$.

The prerequisite for POK2 phragmoplast midzone targeting is ATP-hydrolysis

The N-terminal motor domain of POK2 implies plus end directed movement on microtubules. Therefore, we asked whether the localization of POK2 motor at the phragmoplast midzone requires plus end directed motility, since at the midzone the microtubule plus ends of each phragmoplast half are overlapping. First, we performed time-laps imaging of GFP-POK2MD$_{1-589}$ and Kymograph analyses. The linear trajectories of GFP-POK2MD$_{1-589}$ along filamentous structures, which correspond to microtubules, revealed translocation with a mean velocity of 4.19 ± 1.03 µm/min. Intriguingly, GFP-POK2MD$_{1-589}$ co-expression with the *bona fide* microtubule plus end marker End-Binding (EB)1b fused to RFP validated co-localization, thus, confirming and supporting the plus end directed motility of the POK2 motor domain along microtubules *in planta*. Since hydrolysis of ATP is a prerequisite for kinesin motility, we created a hydrolysis-deficient POK2 and examined its behaviour. The rigor mutation, created by replacing the conserved threonine (T) in the ATP binding site within the motor domain with asparagine (N), is unable to hydrolyse the ATP and generate forces against microtubules, causing strong binding to microtubules and even promotes microtubule bundling (Anne et al., 1998, Nakata and Hirokawa, 1995). Intriguingly, examination of *Arabidopsis* meristems cells expressing the rigor mutant GFP-(POK2MD$_{1-589}$)^{T281N} together with RFP-MBD revealed that the rigor mutant indeed associates with all microtubules arrays. Collectively, our data suggests, that motility of the motor domain in a plus-end directed fashion is necessary to target POK2 towards the phragmoplast midzone.

POK2 at the phragmoplast midzone is retained by MAP65-3/PLE via two distinct binding sites

As previously discussed, the function of certain MAP65 family members are critical for the integrity of the phragmoplast. For instance, the impairment of MAP65-3/PLE causes widening of the phragmoplast midzone, incomplete cell walls and multinucleated cells. The similarity in the localization pattern between MAP65-3 and POK2 at the phragmoplast midzone prompted us to investigate whether these two proteins interact. First, we investigated the localization pattern of GFP-POK2 in the MAP65-3/PLE mutant *ple-2*. While accumulation of GFP-POK2 signal at the division site remained unaffected, and midzone association was not abolished, the intensity profile plot of GFP-POK2 signal from confocal images recorded with identical settings uncovered a reduction of GFP-POK2 signal at the phragmoplast midzone in the *ple-2* mutants compared to wild type plants. When expressed in the *ple-2* mutant, the motor domain GFP-POK2MD$_{1-589}$ lacked the confinement to the phragmoplast midzone but decorated the entire length of phragmoplast microtubules instead. On the other hand, the POK2 C-terminal construct GFP- POK2C$_{2083-2771}$ localized at the division zone and along phragmoplast microtubules, similarly to wild type, suggesting that the C-terminal fragment of POK2 is not affected by the loss of MAP65-3. In addition to the genetic analyses, we also asked whether loss of *POK1* or *POK2* interferes with the localization of MAP65-3 by expressing GFP-MAP65-3/PLE in meristematic root cells of the *pok1 pok2* double mutant. Intriguingly, we did not observe any mis-localization of GFP-MAP65-3/PLE compared to the reported distribution (Steiner et al., 2016b). These findings indicate that MAP65-3/PLE act upstream of POK2 and might be able to retain, directly or indirectly, GFP-POK2 at the phragmoplast midzone through its motor domain. Combined with previous observations, this result suggests that MAP65-3/PLE might serve as a local platform for kinesin-12 targeting. In particular, Kinesin 12-A/B midzone localization is completely abolished in the strong MAP65-3/PL3 allele *dyc283* whereas orphaned kinesin PAKRP2 becomes evenly distributed at the entire length of the phragmoplast (Lee and Liu, 2000, Lee et al., 2007, Lee and Liu, 2013). To further test the interaction between POK2 and MAP65-3/PLE, we used tobacco leaves as they do not express any MAP65-3 homolog (Smertenko et al., 2008). First, we investigated the interaction of GFP-POK2 domains and MAP65-3/PLE-RFP by transient co-expression in tobacco leaf epidermal cells. Co-expression of GFP-POK2MD$_{1-589}$ together with MAP65-3/PLE-RFP showed anticipated co-localization along microtubules. This is not surprising, since single expression controls of each of these fusion proteins revealed also microtubule association. We wondered whether the extraordinary large disordered region, upstream of the POK2 motor domain might be responsible for MAP65-3 interaction and therefore expressed a fusion protein containing only the first 189 amino acids of POK2 in *Tobacco* leaves. Intriguingly, GFP-POK2MD$_{1-189}$ remains cytosolic and does not localize to microtubule in these pavement cells. However, when co-expressed together with MAP65-3-RFP, GFP-POK2MD$_{1-189}$ co-localizes with MAP65-3-RFP at filamentous structures reminiscent of microtubules. Moreover, we expressed a motor domain construct of POK2 without the disordered region (GFP-POK2MD$_{183-589}$) alone and together with MAP65-3-RFP. In addition, we examined the potential interaction of MAP65-5, which also localizes to the phragmoplast midzone with the various POK2 domains. In each case, we did not detect co-localization of MAP65 family members with the POK2 motor domain that lacked the disordered region at the very N-terminus, suggesting that this region of POK2 is sufficient to promote the interaction with MAP65-3/PLE in *Tobacco* leaves. This allows the hypothesis that it might be also responsible to retain POK2 motor domain at the phragmoplast

midzone in *Arabidopsis*. These findings however, do not explain why GFP-POK2, despite the diminished signal intensity, is still able to reach the midzone in the *ple-2* mutant. Consequently, and with respect to the fact that GFP-POK2C$_{2083-2771}$ is also able to bind to microtubules in the phragmoplast, we investigated the interaction of POK2C$_{2083-2771}$ and MAP65-3/PLE in *Tobacco* pavement leaf epidermal cells.

Expression of GFP-POK2C$_{2083-2771}$ in *Tobacco* pavement cells displays punctate clusters, a pattern similar to that monitored in *Arabidopsis* interphase protoplasts, yet, it does not co-localize with microtubules when solely expressed in leaf epidermal cells. However, when GFP-POK2C$_{2083-2771}$ was co-expressed with MAP65-3/PLE-RFP, we observed a remarkable colocalization of GFP-POK2C$_{2083-2771}$ and MAP65-3-RFP signal. This suggests that MAP65-3-RFP promotes recruitment of POK2 C-terminal domain to microtubules. We validated these findings by using a mating-based split-ubiquitin yeast interaction assay (Karnik et al., 2015), using MAP65-3 as “bait” protein. As anticipated, co-expressing MAP65-3 with either POK2MD$_{1-589}$, POK2MD$_{1-189}$ or POK2C$_{2083-2771}$ were able to grow on selective media, hence, confirming a putative interaction of MAP65-3 with POK2 via two distinct binding sites. The expression of each fusion protein was confirmed by immuno-detection.

The truncated POK2 C-terminal region corresponds in size to the respective POK1 region that is responsible for division site targeting, yet, we never observed microtubule association of POK1 C-terminal domain other than the association with PPB microtubules in prophase. Since GFP-POK2C$_{2083-2771}$ was able to bind microtubules of all interphase or mitotic arrays *in planta* and is correctly localized in the *ple-2* mutant, we wondered about the specificity of the observed interaction between MAP65-3 and POK2 C-terminal domain. Therefore, we tested the localization pattern GFP-POK2C$_{2083-2771}$ when transiently co-expressed with other MAP65 family members which also have been reported to associate with the phragmoplast and other microtubule arrays. Intriguingly, GFP-POK2C$_{2083-2771}$ was co-localizing with MAP65-1-RFP as well as with MAP65-5-RFP along filamentous structures similar to those observed during the POK2C-MAP65-3 co-expression. This indicates that the POK2 C-terminal domain has a tendency to interact with MAP65 isoforms. Furthermore, we expressed a phospho-mimic version of MAP65-1 (MAP65-1(9D)-RFP), which is not capable of microtubule association (Boruc et al., 2017), together with GFP-POK2C$_{2083-2771}$. Although, MAP65-1(9D)-RFP distributes into the cytosol upon transient expression in leaf epidermal cells, GFP-POK2C$_{2083-2771}$ formed punctuated clusters close to the plasma membrane and did not accumulate in the cytosol, suggesting that the interaction of POK2C-terminal domain and a MAP65 isoform requires binding of the latter to microtubules. Along the same lines, the necessity for microtubules for the interaction of POK2C with MAPs was confirmed after treatments of leaves transfected with GFP-POK2C$_{2083-2771}$ and MAP65-5-RFP with the microtubule depolymerizing drug oryzalin. Upon treatment, GFP-POK2C$_{2083-2771}$ forms clusters close to the plasma membrane, while MAP65-5-RFP diffuses into the cytosol. Thus, our results show a novel spatio-temporal localization pattern of POK2 mediated by different protein domains and suggest a role in phragmoplast expansion via interaction of the intrinsically disordered N-terminal domain of POK2 with the conserved microtubule cross-linker MAP65-3/PLE. In addition, POK2C$_{2083-2771}$ interacts with microtubule bound-MAP65 isoforms and fine-tunes POK2 accumulation at the phragmoplast midzone.

Putative model for POK2 activities in cytokinesis

These findings can be summarized in a hypothetical model proposing that motile POK2 moves towards the plus ends of phragmoplast microtubules and reaches the midzone, where it interacts with its intrinsic disordered region with MAP65-3/PLE, thereby impounding POK2 at the midzone. Intriguingly, the C-terminal domain of POK2 contributes to the latter via interaction with MAP65-3/PLE or other MAP65 isoforms, since full length POK2 is still weakly recruited towards the phragmoplast midzone in the *ple-2* mutant. In analogy to HsKif15, POK2 might be able to form di- or tetramers and bind microtubules cross-linked by MAP65-3/PLE and other MAP65 isoforms, which potentially increases the binding affinity of POK2 C-terminal domain for microtubule interaction. Consequently, similarly to HsKif15, POK2 clusters might delay microtubule plus end catastrophe, hence conferring further stability to the expanding phragmoplast. However, this hypothetical model does not contain information regarding the spatio-temporal regulation of POK2 function in the phragmoplast.

The POK2 motor domain might be regulated by its disordered region

It has been shown for other kinesins that disordered regions upstream of motor domains may fulfil additional regulatory functions, that influence processive motility (Vale and Milligan, 2000, Zhu and Dixit, 2012). As mentioned previously, we expressed GFP-POK2MD$_{1-189}$ fusion protein in *Tobacco* leaf epidermal cells, which localizes to the cytosol and the nucleus and forms small aggregates in the cytosol. Besides, this domain re-localizes to microtubules when co-expressed with MAP65-3/PLE. Thus, we concluded that the region consisting of the first 189 amino acids is not able to bind microtubule by itself *in planta* (Appendix Supplementary Figure1E). To examine whether this domain promote microtubule binding of the rest of the motor domain, we transiently expressed GFP-POK2MD$_{183-589}$ in *Tobacco*. Intriguingly, single transformation of GFP-POK2MD$_{183-589}$ localizes to the cytosol *in planta* but not to microtubules although it contains the intrinsic microtubule binding site in the motor domain (Appendix Supplementary Figure1D). Although the possibility that GFP-POK2MD$_{183-589}$ is not able to form homodimers cannot be excluded, I propose that the N-terminal located disordered region POK2MD$_{1-189}$ upstream of the motor domain might fold onto the motor domain, thereby enhancing the binding of the motor domain to microtubules. This hypothetical intramolecular regulation of POK2 motor activity might explain the unique phragmoplast midzone association during cytokinesis. In this model, the intramolecular interaction between disordered region and motor domain, results in a temporal conformational change that favours microtubule association and processive motility at the end of anaphase. Then, POK2 would bind phragmoplast microtubules and walk along these towards the midzone, where it becomes retained by MAP65-3 to further promote the stabilization of the phragmoplast. To test this hypothesis, I co-expressed both GFP-POK2MD$_{183-589}$ and RFP-POK2MD$_{1-189}$ in tobacco leaf epidermal cells to examine whether both constructs relocate on microtubules (Appendix Supplementary Figure1A & C). This was not the case in this experiment. Several reasons might have had an influence, such as unequal expression levels of both constructs, or the degree of proximity between both proteins, which might be critical for the formation of a stable complex that is recruited towards cortical microtubules. An additional yeast two hybrid interaction assay should clarify, whether intramolecular interaction occurs, that potentially sustains microtubule association and processivity of POK2.

Phosphoregulation might control POK2 midzone localization and function

Although we can't rule out the possibility that intramolecular interaction of the disordered region and the motor domain might play a certain role in the spatio-temporal regulation of POK2, the mechanism behind a timely POK2 release from the phragmoplast overlap at the lagging edge is completely unknown. To get an idea of a potential regulation, I performed additional experiments which are not included in Herrmann et al. 2018. Upon phosphorylation, MAP65 family members residing at the midzone become deactivated by the HIK/NAK1/NPK/MAPKK/MAPK signalling cascade (Sasabe and Machida, 2006, Sasabe et al., 2011a, Boruc et al., 2017). Intriguingly, members of the MPK/ERK family MITOGEN ACTIVATED PROTEIN KINASE6 (MPK6), as well as MPK4 and the functionally redundant MPK11 are involved in several developmental processes regulating a variety of targets via phosphorylation such as the bHLH transcription factor SPEECHLESS critical for stomatal development (Lampard et al., 2008), the negative regulator of the jasmonate signal transduction pathway *ATMYC2/JASMONATE-INSENSITIVE1* (Takahashi et al., 2007), and isoforms of the microtubule cross linker MAP65 (Jens et al., 2010, Smékalová et al., 2014, Komis et al., 2011, Xu and Zhang, 2015). In meristematic root cells of Arabidopsis, MPK6 is restricted to the PPB and the phragmoplast, whereas it displays an additional plasma membrane and trans-Golgi network association (Jens et al., 2010, Komis et al., 2011). Phosphorylation assays revealed that MPK4 is able to phosphorylate MAP65-1, MAP65-2 and MAP65-3 *in vitro* (Sasabe et al., 2011b, Xu and Zhang, 2015), while MAP65-1 can also be phosphorylated by MPK6 *in vivo* (Hoehenwarter et al., 2013).

Since MAP65-3 releases the antiparallel microtubule overlap in the phragmoplast midzone upon its phosphorylation and interacts with the N-terminal disordered region of POK2 providing phragmoplast stabilization, we hypothesised that phosphorylation of the disordered region of POK2 may also contribute to the release of the protein complex and promote microtubule destabilization which is needed for phragmoplast expansion. To test our hypothesis, we specifically sought for predicted CMC/MAPK/ERK phosphorylation sites using appropriate software (http://gps.biocuckoo.org) and high threshold output setting. Intriguingly, POK2MD$_{1-189}$ possesses at least five predicted threonine phosphorylation sites (score >10, indicative of high phosphorylation probability) at positions T53, T70, T106, T126 as well as T128 (Appendix Supplementary Figure1B). To test whether MPKs have an influence on POK2 we created a red fluorescent version of MPK6 (MPK6-RFP) and its functionally redundant orthologue MPK3 (MPK3-RFP) as a control and co-transfected *Tobacco* epidermal leaves together with GFP-POK2MD$_{1-589}$ (Appendix Supplementary Figure1F-J). Single transfected leaves expressing GFP-POK2MD$_{1-589}$ exhibit the anticipated microtubule association as well as the ability to form microtubule bundles depending on its expression levels (Appendix Supplementary Figure1G & J). On the contrary, single expression in epidermal leave cells of either MPK6-RFP or MPK3-RFP displays by a primarily cytosolic signal along with a faint localization at the plasma membrane (Appendix Supplementary Figure1H & K). However, simultaneous expression of MPK6-RFP or MPK3-RFP with GFP-POK2MD$_{1-589}$ did not change the localization of each construct described previously. This indicates that both MPK6 and MPK3 are not interfering with GFP-POK2MD$_{1-589}$ localization in *Tobacco*, since GFP-POK2MD$_{1-589}$ binds to microtubules despite the presence or absence of these MPKs (Appendix Supplementary Figure1F-I). We also examined potential interactions using the mating based split ubiquitin yeast interaction assay by expressing MPK6 as bait protein and different motor domain

constructs as potential interactors. To our surprise, compared to the negative control, the co-expression of POK2MD$_{1-189}$ and MPK6, confirmed also by western immunoblotting, promoted yeast growth on selective media, suggesting a potential MPK6-POK2 interaction (Appendix Supplementary Figure1L-M). This raises questions regarding the exact mode by which MPK-related phosphorylation might regulate POK2 activity and contribute to its release from the phragmoplast midzone at the lagging edge. To retain POK2 at the phragmoplast midzone, the disordered region must bind MAP65-3 directly, This interaction might target POK2 to certain MPKs such as MPK6 or more likely the MPK4, which is largely involved in cytokinesis (Kosetsu et al., 2010), as soon MAP65-3 is phosphorylated. Consequently, the phosphorylation of POK2 would result in a highly negatively charged modification, potentially preventing further binding to the negatively charged microtubules. Whether disassociation from phragmoplast microtubules is followed by degradation or POK2 is dephosphorylated enabling a new cycle remains to be investigated.

POK2 is a plus end directed motor which switches motility modes

Our investigation about the dual localization pattern of POK2 *in planta* uncovered a new role in phragmoplast function. However, to date, information about mechanistic insight on POK2 function is missing. In collaboration with the Cellular nano-science group at the ZMPB, we examined biophysical properties of POK2 which lead to the generation of a mechanistic model to explain the prominent narrowing of the POKs at the cortical division site. The results were published recently in an article entitled “Phragmoplast orienting kinesin 2 is a weak motor switching between processive and diffusive mode” (Chugh et al., 2018). Briefly, fluorescently tagged POK2 motor domain fragments were expressed in insect cells. Purified proteins were used for *in vitro* single molecule imaging using total-internal-reflection-fluorescence (TIRF) microscopy. Furthermore, optical-tweezer-based force spectroscopy measured force generation of the POK2 motor fragment. The study confirmed that POK2MD$_{1-589}$-GFP is a plus end-directed motor protein that homo-dimerizes. The *in vitro* analyses of the N-terminal disordered region corroborated the assumption that it is needed for efficient microtubule binding of the motor. An exclusive-state-mean-squared-displacement (MSD) analyses (Helenius et al., 2006) combined with a speed correlation index (SCI) analyses (Chugh et al., 2018) allowed quantification of velocities of individual POK2 motors that switch between a processive and diffusive state while translocating along the microtubule lattice. The processive mode of a kinesin allows controlled walking in a directed manner along a microtubule, whereas the diffusive mode allows faster, thus less energy consuming motility over short distances than the directed one. In addition, using high-resolution optical tweezers Chung et al. measured the maximum force that a single POK2 molecule could exert on artificial cargo. POK2MD$_{1-589}$-GFP is trapped via its GFP-tag to a stationary microsphere, thereby upon motor activity on the microtubule lattice it displaces the trap from the centre of a light beam. According to Hooke’s law, the generating force is increasing proportionally to the displacement of the microsphere and the average maximum force calculated for POK2 single motor activity was 0.34 ± 0.02 pN. Although multiple POK2 motor molecules can increase the force up top 1 pN, it seems that the POK2 motor domain is among the weakest kinesin motors across taxa (Chugh et al., 2018).

POK2 might push against the phragmoplast

Taken all these findings into account and considering also that the polarity of peripheral microtubules at

the phragmoplast leading edge are plus end directed, the question that arises is whether POK2 motors at the CDS are able to either pull on or push against these microtubules. In other words, it is assumed that the entire POK2 molecules at the division site capture these peripheral microtubules emanating from the expanding phragmoplast and walk towards their plus-ends. Since the speed of the motors is faster than the phragmoplast expansion rate (Lipka et al., 2014), the kinesin will catch up with the microtubule plus ends, thereby counteracting and pushing against the expanding phragmoplast (Chugh et al., 2018). Consequently, according to Newton's third law, the net force on these peripheral microtubules generated by many POK2 motors causes an opposing force of equal magnitude exerted on the anchoring points of the motors, the C-terminal POK2 domains which are somehow anchored at the lipid bilayer of the division site. Considering the localized accumulation of POK2 motors at the division site and that POKs are capable of being mobile, it might be suggested that the joint forces emanating from single-motors are strong enough to move their anchoring points within the membrane/phospholipid bilayer. The synchronized movement of the individual motors would result in the focusing of the POK molecules, as observed for YFP-POK1 in meristematic cells of *Arabidopsis* at the end of cytokinesis (Lipka et al., 2014, Chugh et al., 2018)

The necessity of a CDZ resident kinesin motor: binding *versus* motility

Such a mechanically based mechanism for division site narrowing mediated by POK kinesins is remarkable and might shed new light on the metamorphosis of the division site from a broad to a narrow site from a different perspective. However, it is still speculative and there are no experimental *in vivo* data that supports this model. Moreover, in order to fully understand cortical division site narrowing and phragmoplast guidance in its entirety a lot of open question need to be addressed. For instance, the potential involvement of the second POK2 population residing at the phragmoplast midzone, contributing to phragmoplast stability during expansion. Since peripheral phragmoplast microtubules are extending towards the CDZ, it might be possible that phragmoplast-resident POK2 tracks these microtubules, forming either potential tetramers with the POK2 population at the CDZ or similarly to Kif15 preventing plus end destabilization on the peripheral microtubules to promote phragmoplast guidance and phragmoplast midzone stabilization. Nevertheless, several findings indicate that the presence/activity of POK1/2 motor is needed for correct protein function. The C-terminal domain of POK1/2, although in both cases is targeted to the division zone, is not sufficient to rescue the *pok1 pok2* double mutant phenotype. These findings indeed confirm that the presence of downstream elements absent from the C-terminal domain are necessary for accurate phragmoplast guidance. Whether binding of POKs to peripheral microtubules and/or their motor activity mediates the fine-tuned guidance of the phragmoplast, and thus facilitate cortical division site narrowing is currently unknown. Chugh et al. postulate that the motor activity is the main prerequisite to generate a potential pushing force for the latter. If this is the case a motor dead version, of *POK1* or *POK2* introduced into the *pok1 pok2* double mutant, should in theory not be able to induce narrowing of the division site and also should not complement the phenotype. In this direction, a full length POK2$_{T281N}$ rigor mutant might be useful. As a result of the mutation, division site narrowing should be impaired. However, in case narrowing of the cortical division site still occurs upon POK2$_{T281N}$ expression in *pok1 pok2* double mutant plant lines, POK2$_{T281N}$ would hypothetically still be able to push against the phragmoplast, but the driving force would only originate from the expansion of the phragmoplast and not from the mobility and force

generation of POK2 motor molecules, supporting the idea that the phragmoplast itself is responsible for CDZ narrowing. Whether microtubules or actin filaments, connecting the phragmoplast and the division zone, participate in this process and facilitate protein movement within the lipid bilayer, needs to be determined.

In this regard, the assumption proposed above might lead to another question: Is a POK motor activity specifically needed to guide the phragmoplast to its destination or can this be achieved by the motor domain of any kinesin, regardless of the orientation of its motility, when anchored at the division site. Simple rescue experiments of different motor domains fused to the C-terminal part of POK1, which facilitates cortical division site anchoring and introduced into the *pok1 pok2* double mutant expressed under a mitotic-specific promoter could clarify this.

In summary, the data presented in this section show that POK2 is a plus end directed kinesin that demarcates the cortical division site from prophase onward and accumulates at the phragmoplast midzone, where it interacts with the microtubule cross-liker MAP65-3 to ensure proper guidance of the phragmoplast and cell plate positioning during plant cell division. However, there are still a lot of open questions to be solved in the future to fully understand phragmoplast guidance and cortical division site narrowing in its entirety.

7.3 Manuscript:

A conserved kinesin-12 class protein, PHRAGMOPLAST ORIENTING KINESIN-LIKE is necessary for proper spindle assembly in *Arabidopsis thaliana*

Arvid Herrmann[1], Steffi Zimmermann[1], Sabine Müller[1]*

* Corresponding author: Sabine Müller
[1]Zentrum für Molekularbiologie der Pflanzen
Developmental Genetics
University of Tübingen
Auf der Morgenstelle 32
72076 Tübingen, Germany

Abstract

The assembly of a bipolar spindle, which mediates the chromosome alignment and separation, is a highly conserved process among the eukaryotic kingdom. The exact molecular mechanism of spindle assembly in land plants is still poorly understood, contrary to animal cells where a plethora of its aspects has been resolved. Here we show, that a member of the kinesin-12 class proteins PHRAGMOPLAST ORIENTING KINESIN-LIKE (POK-like) plays a role during spindle formation, similar to its animal orthologues KLP2 and Kif15. Examination of *pok-like* mutant with immunolabeling, as well as live cell imaging of a GFP-POK-like fusion protein revealed its specific involvement in prospindle assembly as it progressively enriches at the spindle overlap between the opposing kinetochore microtubule bundles/spindle midzone. Later POK-like displays a specific, and microtubule-dependent accumulation throughout the cell cycle whereas its timely recruitment is accomplished by distinct protein domains. In addition to its anticipated localization at opposing kinetochore microtubule bundles, co-localization analyses with the kinetochore marker RFP-HTR12 combined with the microtubule depolymerizer oryzalin revealed an accumulation of GFP-POK-like close to chromosomal structures. Furthermore, we could show, that replacing the conserved threonine of the ATP binding site within the motor domain of POK-like with asparagine abolishes specific midzone localization of POK-like from the bipolar microtubule arrays. In addition, we confirmed RanGAP1 as interaction partner of POK-like *in planta*. Our results suggest that, contrary to the other members of kinesin-12 family, POK-like operates as its orthologues in animals. Although several mechanistic details remain to be determined, this work supports the view that kinesin-12 might functions in land plants, contributing to the sliding mechanism for proper spindle segregation.

Results

Kinesin-12 proteins cluster in two sub-groups within the plant kingdom

It has been previously reported that the kinesin-12 orthologues, POK1 and POK2 are required for the establishment and maintenance of a functional CDZ in *Arabidopsis*, since co-alignment of PPB, phragmoplast expansion axis and cell plate fusion site is impaired in the *pok1 pok2* double mutant, causing oblique insertions of cell plates, hence, affecting meristem organization and growth (Figure 1B, D) (Müller et al., 2006). In addition to their anticipated localization at the CDZ (Lipka et al., 2014), POK2 exhibits an additional localization at the phragmoplast midzone. Restricted by the cross-linker MAP65-3, POK2 promotes the expansion of the phragmoplast during cytokinesis (Herrmann et al., 2018). Interestingly, none of the so far characterized kinesin-12 members in plants, including Kinesin-12A (PAKRP1), Kinesin-12B (PAKRPL) and POKs share the evolutionary conserved function of their respective mammalian ortholog, which are mainly involved in spindle assembly. To address this issue, we investigated the phylogenetic relationship among kinesin-12 family members in plants using the predicted protein sequences from a variety of plant species, as well as their animal counterparts (Supplement Figure S1). Intriguingly, the kinesin-12 members are clustering in two sub-groups, one comprising the Kinesin-12A, the Kinesin-12B along with a, so far, uncharacterized kinesin encoded by At3g20150 and their respective paralogues in one cluster. POK1, POK2 in addition to a second yet uncharacterized kinesin encoded by At3g44050 and their orthologs are forming the second cluster. Since Kinesin-12A and Kinesin-12B are located at the phragmoplast midzone in a MAP65-3/PLE dependent fashion and are necessary for proper cell plate formation in the male gametophyte (Ho et al., 2011a, Lee et al., 2007, Lee and Liu, 2000), and considering that both animal kinesin-12 proteins Kif15 and KLP2 are closer related to the POK cluster, we focused our attention on kinesin12E, which is from now on referred to as POK-like (accession number: At3g44050). POK-like consists of 1263 amino acids with a kinesin-12 characteristic N-terminal located motor domain and shares with its animal orthologue Kif15 26.3% identity and 41.9% similarity. POK1 and POK-like share 24.5% identity and 36.2% similarity while POK2 and POK-like share 17.9% identity and 27.1% similarity. Notably, the identity of POK1 and POK2 is 30.1% identity and their similarity is 43.2%. (pairwise sequence alignment (protein): https://www.ebi.ac.uk/Tools/psa/emboss_needle/).

POK triple knockdown influences plant growth and reproduction

In order to gain insight in the function of *POK-like*, we ordered respective T-DNA insertion lines and confirmed knockout of the gene by analysing transcript levels by RT-PCR (Supplemental Figure S2A). Neither *pok-like-1* (WiscDsLox4G07) nor *pok-like-2* (GabiKAT429E11) insertion lines exhibit transcript accumulation in 5-day old seedlings, contrary to the respective wild type controls (Supplemental Figure S2B). However, unlike *pok1 pok2* mutant allele combination, plants homozygous for these *pok-like* mutant alleles did not show a considerable growth phenotype (Supplemental Figure S2C). Analyses of gene expression pattern in GUS-reporter fusion lines showed *POK-like:GUS* expression predominantly in meristematic tissue, as well as in embryos and gametophytes (Supplemental Figure S2E) Next, we investigated whether functional redundancy among POKs might compensate for the loss of *POK-like*. To clarify this question, we created and analysed double mutant combinations between *pok-like* and either of *pok1* and *pok2* as well as a triple *pok* mutant (Figure 1A-D). To our surprise, neither the *pok1-*

2 pok-like-1 (Figure 1A [iV]) nor the *pok2-2 pok-like-1* (Figure 1A [V]) double mutant exhibited an obvious growth phenotype compared to the respective single mutants (Figure 1A [i-iii]) and wild type (Figure 1A [Vi]) controls. Similarly, none of the investigated double mutant combination (Figure 1D [iX-X]) exhibited any detectable aberrations in the organisation of the meristem (Figure 1D [Viii]). An examination at a later developmental stage of the *pok1-2 pok-like-1* double mutants, revealed that the length of silique was significantly reduced by 0.43 µm ± 0.03 µm in the double mutant (Figure 1C [b]) compared to the single mutant (Figure 1C [d. e]) or wild type (Figure 1C [a]) with 0.59 µm ± 0.05µm. Upon expression of a YFP-POK1 fusion protein under its native promoter in the *pok1-2 pok-like-1* double mutants this developmental defect was reverted (Figure 1C [c]), suggesting that POK1 and POK-like but not POK2 play a role, in silique elongation/organization. Since none of the investigated double mutant combination possessed any strong morphological aberration as it has been reported for the simultaneous loss of both *POK1* and *POK2*, we examined a *pok1-2 pok2-2 pok-like-1* triple mutant (from now referred to as *pok* triple mutant). Indeed, the *pok* triple mutant exhibited an enhanced phenotype compared to the *pok1 pok2* double mutant (Figure 1B), with smaller, curved leaves, delayed flowering and senescence and an overall enhancement of the dwarfism. In addition, reciprocal crosses of the *pok* triple mutant and wild type plants did not yield any fertile progenies, indicative of both male and female gametophyte lethality. These findings suggest that either POK-like act redundantly with POK1 and POK2 during specific developmental processes, or this is an additive phenotype seriously influencing plant growth and reproduction, as an outcome of the simultaneous loss of the three kinesin-12 members.

POK-like localization pattern is cell cycle specific and microtubule dependent

To investigate the function of POK-like, we analysed a functional GFP-POK-like fusion, driven by its own promoter, in 4- to 6- day old wild type seedlings. Confocal microscopy examination revealed GFP-POK-like expression only in a subset of meristematic cells, indicative of cell cycle specific regulation. To determine the cell cycle stages GFP-POK-like spatiotemporal pattern was analysed together with the microtubule reporter *pUBN:RFP-MBD* (Figure 2A). Although GFP-POK-like does not co-localizes with microtubules of the PPB in prophase (*n* = 26 cells, Figure 2A-B), it accumulates in the cytosol and at the nuclear envelope (see also Supplemental Figure S6). Following nuclear envelope breakdown, GFP-POK-like decorates prospindle microtubules. Specifically, it starts being enriched at the overlap between the opposing kinetochore microtubule bundles as soon as they are in close proximity. This became even better visible after investigation of GFP-POK-like co-expressed with the microtubule plus end marker RFP-EB1b (Supplemental Figure 3A). At metaphase, GFP-POK-like was particularly restricted to the central region of the spindle, colocalizing with all bundles of microtubules within the metaphase plate but being absent from the spindle poles (*n* = 48 cells, Figure 2A-B, Supplemental Figure 3B, Supplemental Figure S7). Co-localization of GFP-POK-like with the known spindle marker RFP-TPX2 confirms that GFP-POK-like exclusively restricted to the spindle overlap region and is absent from spindle poles (Supplemental Figure S5). During transition to cytokinesis, GFP-POK-like relocated towards the phragmoplast midzone until the end of cytokinesis (*n* = 34 cells, Figure1A-B, Supplemental Figure S6).

To examine whether this subcellular GFP-POK-like localization pattern depends on microtubules, seedlings co-expressing GFP-POK-like and RFP-MBD were treated with the microtubule

polymerization inhibitor oryzalin (Figure 2, C-G). Depolymerization of microtubules upon oryzalin treatment confirmed by the abolishment of the RFP-MBD signal, caused GFP-POK-like disappearance during metaphase and cytokinesis. Interestingly, the recruitment of GFP-POK-like towards the nuclear envelope in prophase remains unaffected following microtubule depolymerization. Quantification of cells displaying RFP-MBD and GFP-POK-like signal before (*n* = 16 metaphase; *n* = 21 cytokinesis) and after oryzalin revealed that only 6.25% of cells in metaphase and 9.52% of cytokinetic cells retained GFP localization after 10 min of treatment, respectively. However, GFP-POK-like localization at the nuclear envelope (*n* = 20 cells) persisted in 50% of the cells after 10 min treatment and was still present even after 30 min of treatment (data not shown). Consequently, we concluded that once POK-like is tethered at the nuclear envelope it remains there independently of microtubules, while its association at the spindle and phragmoplast midzone depends on the presence of intact microtubule arrays. These findings indicate that association of POK-like at the nuclear envelope is mediated by a different mechanism than its localization at the spindle and phragmoplast. Taken together, POK-like seems to play a specific role during cell division *in planta*, thus we next investigated the contribution of different protein domains of POK-like to the dynamic recruitment of the full-length protein monitored by analysing the localization patterns of different POK-like-domain deletion mutants.

Different domains are necessary for an accurate recruitment of POK-like during cell division

First, GFP-fusion proteins containing different domains of POK-like were generated and analysed in living cells using confocal microscopy (Supplemental Figure S2D). Time-laps imaging of full length GFP-POK-like revealed its localization at the overlapping microtubule bundles after nuclear envelope breakdown, an inimitable re-arrangement at the spindle midzone during metaphase and anaphase (Figure 3A) and a specific association with the phragmoplast midzone throughout cytokinesis (Figure 3A). However, this localization pattern is altered in the absence of the kinesin specific N-terminal motor domain of POK-like. The GFP-tagged POK-like C-terminal domain (GFP-POK-like$_{389-1265}$) decorates the nuclear envelope right before nuclear envelope breakdown. Upon prospindle formation, GFP-POK-like$_{389-1265}$ co-localizes with emerging microtubule-kinetochore bundles. Unlike the full-length protein, in metaphase, GFP-POK-like$_{389-1265}$ associates with the entire spindle. After segregation of chromosome pairs in anaphase, GFP-POK-like$_{389-1265}$ is drawn towards the poles, vanishes as soon as the phragmoplast forms and remains absent until the newly synthesized cell plate fuses with the parental cell wall (Figure 3C). To underline the differences in the localization patterns between GFP-POK-like and GFP-POK-like$C_{389-1265}$, multiple kymograph analyses have been performed (Figure 3B and D). Evidently, during metaphase GFP-POK-like does not completely co-localize with the RFP-MBD signal over time (Figure 3B), whereas GFP-POK-like$_{389-1265}$ shows largely the same accumulation pattern as RFP-MBD signal (Figure 3D).

Moreover, a truncated motor domain construct tagged with GFP (POK-like$_{1-631}$-GFP) driven by the 35S promoter has been analysed *in planta* together with the microtubule marker RFP-MBD. In both, leaf (Figure 3E) and root meristem cells (Figure 3F and G) undergoing phragmoplast expansion, showed a specific association of POK-like$_{1-631}$-GFP with the phragmoplast midzone. Furthermore, line plot analyses along the phragmoplast expansion axis in cytokinetic cells revealed that it is not exclusively co-localizing with the microtubule overlap in the phragmoplast midzone but might also accumulate at

the newly synthesized cell plate (Figure 3G and H).

Overall, these findings suggest, that the C-terminal domain is able to bind microtubules directly or indirectly and independent of the motor domain, whereas the motor domain specifically targets only the emerging phragmoplast midzone.

Loss of POK-like interferes with spindle organization

To further characterize the function of *POK-like*, we investigated in detail the mutant alleles on a cellular level by examining the organization of the mitotic microtubule arrays in the root meristem after immunolabeling. Intriguingly, PPBs or phragmoplasts in *pok-like* mutant alleles did not show any apparent defects, suggesting that *POK-like* does not interfere with either PPB or phragmoplast establishment (Supplemental Figure S4). However, a closer look at mitotic spindles in metaphase, revealed the presence of shortened spindles in mutant root cells (Figure 4A-B). Quantification of pole-to-pole spindle length revealed a significant reduction of average spindle length by about 27% (4.67 µM ± 0.54 µm, n=40, *P < 0.001) for the *pok-like-1* mutant allele compared to wild type (5.95 µM ± 0.82 µm, n=34) (Figure 4B). Expression of *pPOK-like*:GFP-POK-like in the *pok-like-1* mutant reduced the observed phenotype to 7% (5.56 µM ± 0.62 µm, n=50 *P < 0.001), suggesting that POK-like could contribute to spindle pole separation during mitosis. In addition, the above defects were also detected in the second allele of *pok-like* (*pok-like-2*), however, rescue experiments for this particular line are still ongoing (data not shown).

Next, we asked whether the formation of aberrant spindles in mutants interfered with the timely progression of mitosis. For this purpose, we introduced the microtubule reporter RFP-MBD in both mutant alleles obtaining time series from prophase until the beginning of cytokinesis (Figure 4C-D, Supplemental Figure S4). Quantification revealed a significant delay of *pok-like* mutants during the progression from prophase to pro-metaphase as well as in metaphase. The duration of these division stages was significantly extended in *pok-like* mutant alleles compared to wild type (Figure 4D). While in both wild type controls, the duration of pro-metaphase spindle (pro-M-spindle) assembly lasted 3.67 min ± 1.14 min (n=15, wild type 1) and 3.33 min ± 1.75 min (n=21, wild type 2) and metaphase lasted 5.20 min ± 2.51 min (n=15, wild type 1) and 4.24 min ± 1.88 min (n=25, wild type 2) on average; the pro-M-spindle stage lasted 5.39 min ± 2.4 min, *P < 0.01, (n=14,) for *pok-like-1* and 5.60 min ± 2.85 min (*P < 0.01, n=15) for *pok-like2* and also metaphase was significantly prolonged in both *pok-like* alleles (*pok-like-1*, 8.70 min ± 3.32 min, *P<0.01, n=15 and for *pok-like-2* 7.29 min ± 0.85 min, *P<0.01, n=17) respectively. Intriguingly, early prospindle assembly before nuclear envelope breakdown (Figure 4D, PPB, prospindle) as well as progression from anaphase through cytokinesis (Figure 4D, an-/telophase; early cytokinesis) are unaffected in the mutants compared to their respective controls. Comparison of the duration of the cell division from prophase until the beginning of cytokinesis (Figure 4E) revealed a delay of approximately about 5 to 6 min for both *pok-like* mutant alleles (*pok-like-1*: 24.01 min ± 11.36 min, *P < 0.01, n=16; *pok-like-2*: 22.97 min ± 11.65 min, *P < 0.01, n=17) compared to wild-type controls (wild type1: 18.90 min ± 8.49 min, n=16; wild type2: 17.13 min ± 8.90 min, n=26).

Taking these data together, we conclude that the function of POK-like is predominantly exerted during prospindle assembly and prometaphase by promoting the establishment of a functional spindle, thus contributing in the timely progression of cell division

POK-like is targeted to kinetochores

The striking localization of POK-like at kinetochore bundles and at the spindle as well as the observed phenotype in loss of function *pok-like* mutants also has been described for its animal orthologue hKif15 and XKLP2 (Xklp2) (Vanneste et al., 2009, Boleti et al., 1996). In addition, Kif15 is targeted to chromosomes via its interaction with the Ki-67 protein (Sueishi et al., 2000). During the investigation of GFP-POK-like distribution in meristematic cells, we noticed that POK-like also accumulates in puncta at the plus ends of microtubules of the opposing kinetochore bundles during prometaphase and upon the alignment of the chromosomes at the metaphase plate in metaphase (Figure 5A). Therefore, we wondered whether, in addition the association with prospindle and spindle microtubules, POK-like localizes at the chromosomes or any chromosome-associated protein structures. To test this, we examined meristematic cells expressing GFP-POK-like and the CENTROMERIC HISTONE H3 (CENH3/HTR12) fused to RFP. In *Arabidopsis*, CENH3/HTR12 (from now on referred as HTR12) accumulates at centromeres/kinetochores (Lermontova et al., 2011). During prophase, we observed RFP-HTR12 accumulation at the inner site of the nuclear envelope as punctate structure, whereas GFP-POK-like marked the outer membrane of the nuclear envelope. Intriguingly, when we applied oryzalin to cells undergoing nuclear envelope breakdown, filamentous GFP-POK-like re-distributed in a dot-like pattern adjacent to the RFP-HTR12 signal and these dots were more resistant to oryzalin (Figure 5B). Imaging at higher magnification of this localization pattern combined with line plot analyses (Figure 5C) revealed, that both signals were not co-localizing, but seemed to be tightly related. When metaphase cells were treated with oryzalin, a similar behaviour of GFP-POK-like was monitored. In particular, before oryzalin, RFP-HTR12 signal aligns pairwise at the metaphase plate and is surrounded by GFP-POK-like (Figure 5D). Although, after application of oryzalin most of the GFP-POK-like signal vanishes from the spindle, GFP-POK-like can still be observed in dots adjacent to RFP-HTR12 (Figure 5E), suggesting GFP-POK-like associates with kinetochores. Collectively, these findings suggest, that GFP-POK-like not only contribute to the stabilisation of the opposing kinetochore microtubule bundles in a microtubule depended manner but also might promote bridging of the latter to the kinetochores.

RanGAP1 co-localizes and interacts with the carboxy-terminal region of POK-like

The unexpected localization pattern of POK-like at the kinetochores, combined with its localization at the nuclear envelope is reminiscent of RanGAP1, an effector protein of the small GTPase Ran that is essential for cell division (Xu et al., 2008, Rodrigo-Peiris et al., 2011). Visualization of RanGAP1 fusion proteins in living cells or immunolocalization using specific antibodies revealed its association with the nuclear envelope, the PPB and the CDZ, the kinetochores as well as the developing cell plate. Since the maintenance of RanGAP1 at the CDZ depends on *POK* function and POK1 carboxy-terminal domain interacts directly with RanGAP1 (Xu et al., 2008), we asked whether POK-like interacts with RanGAP1. To test this hypothesis, we used ratiometric bimolecular fluorescent complementation (rBiFC) by transfecting *Arabidopsis* root protoplasts with nYFP- POK-like$_{389-1265}$ together with RanGAP1-cYFP or with appropriate controls (nYFP-TAN1) (Figure 6A). To estimate the strength of potential interaction, each combination was transformed separately and analysed by calculating the ratio of fluorescence intensity of an additional cytosolic RFP control and the reconstituted YFP upon interaction. As proof of

principle we first tested the observed interaction between POK1 carboxy-terminal domain and RanGAP1 by using the two different truncated versions of POK1C-terminal domain (Lipka et al., 2014). Intriguingly, the calculated relative fluorescence intensity ratio (YFP/RFP) of both nYFP-POK1C$_{1213-2066}$ (0.64 $\pm$ 0.43, P < 0.001) and nYFP-POK1C$_{1683-2066}$ (0.65 $\pm$ 0.55 P< 0.001) with RanGAP1-cYFP were six times higher compared to the negative control nYFP-TAN1 and RanGAP1-cYFP (0.1 $\pm$ 0.06), as expected of a direct interaction between POK1 and RanGAP1 *in planta* (Figure 6B). Next, we tested the interaction of n-YFP-POK-like$_{389-1265}$ and RanGAP1-cYFP. The relative fluorescence ratio was five times higher value (0.5 $\pm$ 0.24, P < 0.001) than the respective ratio calculated for the negative control (Figure 6B). Thus, we concluded that POK-like interacts *in vivo* with RanGAP1 and that the C-terminal truncation of POK-like is sufficient for this interaction.

To further investigate the biological interplay between RanGAP1 and POK-like, we first examined meristematic cells expressing GFP-POK-like and RanGAP1-RFP (Figure 6D). Indeed, co-localization studies combined with line plot analyses revealed that both signals co-localize at the nuclear envelope right before NEB in prophase. Afterwards, we investigated whether RanGAP1-RFP and GFP-POK-like co-localize also at kinetochores during spindle assembly, since GFP-POK-like also is probably targeted to the kinetochores as it was described previously. Indeed, GFP-POK-like and RanGAP1-RFP showed a perfect co-alignment indicative of co-localization at kinetochores during anaphase (Figure 6D, E). Subsequently, we examined cytokinetic cells and compared the distribution of both signals at the phragmoplast midzone Intriguingly, both signals co-localize at the midzone co-align in respective line intensity plots (Figure 6D, E). Since it has been reported that RanGAP1 is particularly localized at the cell plate (Xu et al., 2008), these results might reflect an enhanced recruitment of RanGAP1 at the phragmoplast midzone due to an overexpression of GFP-POK-like and/or might imply that POK-like is also recruited to the cell plate during cytokinesis.

Since POK1 and POK2 are crucial for the maintenance of RanGAP1 from metaphase on at the CDZ, which has been shown by RanGAP1 localization analyses in the *pok1 pok2* double mutant, we next asked whether dual loss of *POK1* and *POK-like* interferes with RanGAP1 maintenance (Figure 6C). For this, we expressed RanGAP1-GFP in the *pok1-2 pok-like-1* double mutant and imaged meristematic root cells of 4-day old seedlings. Intriguingly, RanGAP1-GFP localization was not altered in the *pok1-2 pok-like-1* double mutant, suggesting that the recruitment of RanGAP1 to the division site is mediated by POK2 in the absence of POK1 and POK-like.

Motor domain activity controls the microtubule overlaps from metaphase onward

We previously reported that phragmoplast midzone association of POK2 depends on its motor domain activity, since a specific mutation in the ATPase binding site cause the relocation of POK2 along phragmoplast microtubules and its absence from the midzone (Herrmann et al., 2018). To test whether GFP-POK-like distribution from metaphase to cytokinesis depends on the motor domain activity of POK-like, we generated an ATP hydrolysis deficient mutant GFP-POK-like(T181N) by replacing the conserved threonine (T) at position 181 of the ATP-binding site within the motor domain with asparagine (N). In stably transformed wild type plants, expressing the mutated POK-like version, the association with the midzone is abolished and the transgenic protein decorates the entire microtubule bipolar arrays including phragmoplasts (Figure 7B compare with 7A), as well as microtubule arrays of interphase and dividing cells (Supplemental Figure S8). Line plot analyses confirmed the distinct localization pattern

between GFP-POK-like and the ATP-hydrolysis deficient mutant GFP-POK-like(T181N) (Figure 7A-B). These findings suggest, that motor activity is necessary to target POK-like to the microtubule overlap in mitotic and cytokinetic bipolar arrays .

POK-like exhibits a differential sub-localization pattern, contributing mainly to prospindle assembly, contrary to the other family members of kinesin-12. Considering, its motility dependent association with the phragmoplast midzone, we were wondering about a potential specificity of the kinesin-12 during cytokinesis. Experimental evidence suggests that Kinesin-12A/B interfere with phragmoplast integrity and that POK2 is involved in phragmoplast expansion. Live cell imaging of *pok-like-1* mutant mitosis (Figure 7D) revealed abnormalities during the establishment of the overlap region of interdigitating microtubules during transition from anaphase to cytokinesis (Figure 7C). Specifically, as soon as the cell enters telophase, the interdigitating microtubules do not form a defined continuous midzone between the segregating spindle poles as observed in wild type, rather, the phragmoplast microtubules are unevenly distributed and predominantly bundled in the outer region of the emerging phragmoplast (Figure 7D). Consequently, in mutant cells, the early phragmoplast does not display the characteristic disc like structure as in wild type, yet, phragmoplast expansion and the overall progress of cytokinesis are not affected.

Collectively, these findings suggest that POK-like uses its motor activity to reach microtubule overlaps of mitotic and cytokinetic bipolar arrays, consequently defining the latter during the transition from anaphase to cytokinesis to establish the characteristic disc like phragmoplast.

Discussion

In this study, we provide further insight into the evolutionary conserved function of kinesin-12 class proteins in spindle assembly. We investigated the localization pattern and the functional implications of a so far uncharacterized kinesin-12 family member, namely POK-like. Its primary role seems to be related with the organization of the bipolar microtubule arrays during cell division formed right after nuclear envelope breakdown. Contrary to its closest relatives POK1 and POK2, which both reside at the CDZ throughout cell division, whereas POK2 also accumulates at the phragmoplast midzone, POK-like localizes at the nuclear envelope at the end of prophase and enriches at the overlap of opposing kinetochore microtubule bundles during the assembly of the metaphase spindle. Furthermore, experimental evidence shows that POK-like might act to promote the stabilization of kinetochore microtubule bundles at the kinetochores. In addition, POK-like associates with the phragmoplast midzone during cytokinesis and last but not least, we confirmed RanGAP1 as new interaction partner of POK-like.

POK-like maintains the conserved function of kinesin-12 class proteins

Previous work determined that two pairs of functionally redundant kinesin-12 class members are either essential for cell plate formation in the male gametophyte (Kinesin-12A/12B) or crucial for division site maintenance at the cell cortex (POK1/POK2) (Herrmann et al., 2018, Lipka et al., 2014, Lee and Liu, 2000, Lee et al., 2007). Of the six kinesin-12 members in Arabidopsis, so far, only POK-like is localized at the bipolar barrel shaped mitotic spindle, suggesting an evolutionary conserved function for POK-like in the establishment of the latter. Recruited towards the nuclear envelope at the end of prophase, POK-

like immediately appears at the opposing kinetochore bundles right after nuclear envelope breakdown, following a distinct localization pattern during formation of the metaphase spindle and finally residing at the kinetochore and overlapping/antiparallel microtubule bundles, decorating the entire spindle midzone. Therefore, as expected loss of *POK-like* induced prolonged duration of spindle assembly following nuclear envelope breakdown, and resulted in considerably shorter spindles, reminiscent of spindles observed in metazoan HsKif15 or KLP2 loss-of-function mutants (Tanenbaum et al., 2009, Boleti et al., 1996). Regarding the exact mode of POK-like function, at opposing kinetochore bundles and at the spindle midzone, only hypothesis can be made, since it is the first kinesin-12 representative identified so far that accumulates at mitotic spindles in plants. In metazoan, kinesin-12 are able to bundle microtubules and exhibit sliding activity *in vitro* (Mann et al., 2017), thus, counteracting inward directed forces produced within the spindle, originating from kinesin-14-dependent motor activity and dyneins (Hentrich and Surrey, 2010, Reber and Hyman, 2015). In addition, HsKif15, using a second non-motor microtubule binding site, preferentially binds to K-fibers *in vivo*, independently of the MAP TPX2. This binding enables the HsKif15-mediated relative sliding of microtubules within the bundles, consequently aiding in chromosome separation during anaphase (Sturgill and Ohi, 2013). On the contrary, other *in vitro* studies reported the presence of homotetrameric HsKif15 molecules, switching between microtubules tracks and displaying processive movement at steady velocities (Drechsler et al., 2014). Moreover, examination of mitotic cells lacking K-fibers revealed that HsKif15 re-localizes to non-K-fiber microtubule bundles upon overexpression, suggesting that mode of function of HsKif15 switches between exerting pushing and pulling forces (Sturgill and Ohi, 2013, Hancock, 2014).

Although *in vitro* data regarding the dynamic behaviour of POK-like molecules are still missing, genetic data combined with localization analyses strongly suggest that POK-like display microtubule bundling and sliding activity. Upon NEB, numerous microtubule bundles emanating from the prospindle elongate towards the kinetochores and attach to them. These parallel oriented K-fibers must be bundled and shortened to promote the lateral expansion of the metaphase plate, which in turn facilitates the alignment of the chromosomes within the plane of cell division. Although chromosome alignment is not significantly impaired in *pok-like* mutants, the extended prometaphase/metaphase combined with the specific localization pattern at opposing kinetochore microtubule bundles favours the hypothesis that POK-like contribute to the latter, and that the excessive delay in formation of the mitotic spindle in mutants is possibly due to a deficiency in microtubule bundling originating from an insufficient microtubule-microtubule sliding.

In addition to an involvement of POK-like in microtubule bundling and sliding, the observed spindle length phenotype in *pok-like* mutants compared to wild type might alternatively be explained by the force balance model which has been postulated for the minus end directed kinesin-14 family member ATK5 (Ambrose and Cyr, 2007). In *atk5-1* mutant cells, prophase/prometaphase spindles elongate prematurely and to a greater extent, resulting in the assembly of wider metaphase spindles (Ambrose and Cyr, 2007). Considering the ATK5 localization at the spindle midzone and its ability to co-align both anti-parallel and parallel microtubules bundles *in vitro*, it has been hypothesised that ATK5 counteract the outward forces exerted by other kinesins during the initial stages of spindle elongation in prometaphase. Moreover, it is thought, that ATK5 promotes lateral connections between microtubules and co-aligns them in linear bundles parallel to the spindle axis, explaining the wider spindle poles

observed upon loss of ATK5 function in mutants (Ambrose and Cyr, 2007). However, unlike ATK5, POK-like is a plus end directed kinesin the loss of function of which causes a significant reduction in spindle length. This phenotype might be an outcome of excessive inward forces, created by ATK5 or other minus end directed kinesins, normally counteracted by plus end directed outward forces potentially generated by POK-like. How exactly POK-like generate outward forces and hence contributes to K-fiber bundling and separation needs further clarification which should include a detailed genetic analysis of both antagonistic operating kinesins, ATK5 and POK-like.

The mode of function of POKs and in particular whether POK-like molecules form di- or tetramers and how they interact specifically with different microtubule populations within the metaphase spindle are also critical points. Our results show that the C-terminal domain of POK-like is able to bind spindle microtubules *in planta*, independently of the kinesin specific motor domain. However, unlike for HsKif15, it is not clear, whether the capability of binding spindle microtubules by the C-terminal domain of POK-like is direct through an intrinsic microtubule binding domain or facilitated by an additional interaction partner. Furthermore, there is evidence suggesting that POK-like can switch between K-fibers and interpolar microtubules, since it initially localizes at the opposing kinetochore bundles after NEB changes during the transition from metaphase to anaphase, were POK-like specifically decorates the antiparallel microtubule overlap within the plane of cell division. In case the C-terminal domain exhibit an internal microtubule binding domain, we might assume that POK-like might bind to- and switch between parallel as well as antiparallel microtubules bundles, as it has been suggested for HsKif15, via binding to microtubule bundles either as homotetramer or homodimer. Whether POK-like and HsKif15 share the same molecular characteristics requires further scrutiny.

The role of kinesin-12 during chromosome alignment

Notably, loss of *POK-like* does not significantly interfere with chromosome alignment in plants, as the loss of *HsKif15* induces in animal cells (Tanenbaum et al., 2009). However, our co-localization analyses with the known kinetochore resident HTR12 combined with oryzalin treatments clearly support the idea that GFP-POK-like accumulates at the spindle microtubule plus-ends in close proximity of the chromosomes or are even directly connected to kinetochores. Experimental evidence identified so far two interaction partners of HsKif15 in animals, KBP and Ki-67, which are required for the efficient alignment of all chromosomes to the metaphase plate. Intriguingly, both KBP and Ki-67 are necessary for HsKif15 localization to the spindle equatorial plane and the chromosomal area but do not interfere with the overall spindle localization of HsKIF15. In cells lacking *KBP* or *Ki-67* prometaphase stage is delayed and exhibit a small number of misaligned chromosomes (Vanneste et al., 2009, Sueishi et al., 2000, Brouwers et al., 2017), This is reminiscent of loss of *HsKif15* function mutants and points towards the functional importance of HsKif15 during chromosome alignment. Moreover, Sturgill et al. reported that HsKif15 co-localizes with HEC1, a component of the kinetochore-associated NDC80 complex in animal cells (Sturgill and Ohi, 2013). This complex is consists of several proteins, which are conserved from yeast to mammals, and forms a rod-like structure with globular region in each end bridging the inner kinetochore of chromosomes to the dynamic plus microtubule ends of the attached kinetochore bundles (Dhatchinamoorthy et al., 2018, Ciferri et al., 2005). Further work showed that an oligomeric array of Ndc80 complexes is able to move along these microtubule ends through biased diffusion (Powers et al., 2009) and to enable the loss or gain of tubulin subunits at the microtubule plus ends,

while the latter are still attached to the kinetochores (Powers et al., 2009). Similar observations have also been made maize (Du and Dawe, 2007, Li and Dawe, 2009). The exact mode of kinesin-12 contribution to chromosome alignment is still under investigation. However, in animals *in vitro* examination of high concentration of tetrameric HsKif15 molecules disables catastrophe at the microtubule plus ends (Drechsler and McAinsh, 2016). These findings imply that POK-like might contribute to microtubule plus end stabilization at kinetochore bundles to maintain steady kinetochore-K-fiber connection until the end of metaphase.

Kinesin-12 POK1 and POK-like interact with RanGAP1

Although the roles of POK1 and POK-like during cell division apparently differ, genetic evidence and our BiFC analysis suggest that both POK1 and POK-like interact with the GTPase activating protein RanGAP1 *in planta*. In addition, previous reports have shown that RanGAP1 maintenance at the CDZ from metaphase on depends on both POK1 and POK2 function, since RanGAP1 is absent from the CDZ in *pok1 pok2* double mutants (Xu et al., 2008). However, our investigation of a RanGAP1-GFP fusion protein in the *pok1 pok-like* double mutant did not show any alteration in the localization pattern of RanGAP1. Therefore, we may conclude, that the localization pattern of RanGAP1 at the nuclear envelope, at kinetochores and at the cell plate is not dependent on the function of POK-like. Since we did not investigate the localization pattern of our GFP-POK-like fusion protein in the inducible *rangap1 rangap2* double mutant (Xu et al., 2008, Rodrigo-Peiris et al., 2011, Boruc et al., 2015), we cannot exclude RanGAP1-dependency of POK-like accumulation. However, the striking localization pattern of POK-like at the nuclear envelope and its additional recruitment towards kinetochores would support the latter possibility.

Both RanGAP1 and RanGAP2 promote the hydrolysis of GTP via activation of the intrinsic GTPase domain of their target, the GTPase Ran (Bischoff and Görlich, 1997, Kim and Roux, 2003). Acting as a molecular switch, the small GTPase Ran functions in nuclear envelope dynamics, influencing microtubule stabilization/nucleation and contributes to the assembly of the mitotic spindle, the formation of the PPB and the phragmoplast in plant cells (Clarke and Zhang, 2008). How exactly Ran via RanGAP1 effect PPB assembly or CDZ maintenance is currently not known. However, over the years, reports for metazoan and plants discovered an evolutionary conserved function for Ran during spindle assembly (Masoud et al., 2013a). The active GTP-locked form of Ran triggers the release of the MAP TPX2 from importin β binding, forming an inhibitory complex (Vos et al., 2008). Upon release, TPX2 activates the serine/threonine kinase AUR1, which in returns phosphorylates TPX2 leading to its activation (Petrovská et al., 2012, Petrovská et al., 2013). Furthermore, in animal cells it has been reported that the AUR1 dependent phosphorylation enables TPX2 but also the recruitment of both, HsKif15 and KLP2 towards the early prometaphase spindle (Wittmann et al., 1998, Mann et al., 2017). Whether POK-like also interacts with plant TPX2 remains an open question. In our hands, neither the BiFC analysis in *Arabidopsis* root protoplasts nor the yeast mating-based split-ubiquitin-system interaction assay could reveal an interaction between TPX2 and the C-terminal domain of POK-like (data not shown). Since TPX2 contains two characterized nuclear localization sequences (NLS) (Evrard et al., 2009) and is cell cycle regulated, it would be challenging to investigate the latter. In addition to *TPX2*, plants display four additional, uncharacterized TPX-related genes and at least three of them exhibit a putative KLP2 binding motif (Evrard et al., 2009). Moreover, and contrary to animals, co-localization

analysis of an ubiquitously expressed RFP-TPX2 fusion protein and GFP-POK-like in Arabidopsis root meristems showed only partial co-localization during spindle assembly in plants (Supplemental Figure S5A-B) Considering that POK-like already localizes at the nuclear envelope right before NEB, possibly through the interaction with RanGAP1 or a yet unidentified protein, it would be also interesting to examine whether TPX2 mediated POK-like recruitment still exists in plants. Nevertheless, our findings support a direct interaction between the small GTPase activating protein RanGAP1 and POK-like. To our knowledge this is the first time where a direct link between the Ran Cycle and a member of the kinesin-12 class proteins during spindle assembly is described. How exactly the interplay of these proteins contributes to spindle assembly needs further scrutiny.

POK-like phragmoplast midzone targeting requires motility

The additional localization of POK-like at the phragmoplast midzone indicates a conserved function of plant kinesin-12 proteins. Specifically, four of the six members in *Arabidopsis* exhibit phragmoplast midzone association, whereas at least three of them maintain their localization to the phragmoplast midzone in a MAP65-3/PLE dependent manner (Herrmann et al., 2018, Ho et al., 2011b). However, none of the investigated *pok-like* alleles exhibited defects similar to those observed in *pok1 pok2* or *kinesin12a/12b* single mutants, uncovering an additional role for POK-like during phragmoplast assembly and function. Closer examination of our microtubule marker GFP-TUA6 revealed aberrations during the establishment of the overlap region of interdigitating microtubules during transition from anaphase to cytokinesis. Normally forming a define continuous midzone between the segregating spindle poles, in loss of *POK-like* the interdigitating microtubules are unevenly distributed and predominantly bundle at the leading edge of the emerging phragmoplast, rather than in its centre. It appears that the phragmoplast fails to efficiently form its initial disk organization. In addition, a catalytically-inactive, motility-impaired mutant POK-like(T181N) fails to be targeted to both, spindle and phragmoplast midzone and rather decorates microtubules in its entirety, independent of their cell cycle stage. Collectively, these findings imply that POK-like moves toward microtubule plus ends to reach the cell division plane, where it is likely contributing to microtubule plus end stabilization and bundling of phragmoplast microtubules. Whether the maintenance of POK-like at the phragmoplast midzone during cytokinesis is also MAP65-3/PLE dependent, is currently unknown. The *pok* triple mutant exhibited a more severe phenotype, possibly through an additive effect of their individual phenotypes. However, further genetic analysis between kinesin-12 members in plants might resolve possible redundant functions of kinesin-12 member during phragmoplast establishment.

The distinct localization pattern of POK-like essentially represents the intersection of the ancestral function of kinesin-12 proteins during spindle assembly and novel kinesin-12 proteins functions in plants, including its unique accumulation at the nuclear envelope. Regarding the exact mode of POK-like function, further investigation, combining both *in vivo* and *in vitro* analysis is required.

Material and Methods

Plant Material

Arabidopsis thaliana plants ecotype Colombia (Col-0, wild type) were used throughout the entire study. *POK-like* mutant lines are the Wisconsin line WiscDsLox4G07, *pok-like-1*, mapped to exon 13 by sequencing (Primers given in Supplement Table S1) and a Gabi-Kat T-DNA line (GABI-KAT_429E11, *pok-like-2*) mapped to the first. All the other mutant lines were obtained from the Arabidopsis stock centre NASC (University of Nottingham). *Agrobacterium tumefaciens*–mediated transformation of plasmids to generate different transgenic lines (Col-0) was performed according to Clough and Bent (1998). For visualization of the microtubule cytoskeleton the described microtubule reporter line pUBN:RFP-MBD (Lipka et al. 2014) was used, GFP-TUA6 line was obtained from NASC. RanGAP1-GFP in Col-0 background (Xu et al., 2007, Xu et al., 2008) was kindly provided by Iris Meier.

Growth Conditions

Seedlings of different lines were grown on plates containing 1/2 Murashige and Skoog basal media (Sigma Aldrich) and 1% agar. After two days of stratification at 4°C in dark, plates were transferred into growth chambers with long day conditions (cycling 16 h light / 8 h dark) at 22°C. For reproduction and crosses two to three-week-old seedlings were transferred onto soil.

Generation cDNA, amplification of PCR products and ligation

cDNA was generated as described (Müller et al., 2006), using Superscript Reverse Transcriptase II (Invitrogen, 18064-22). All enzymes used for restriction digests were purchased from Fermentas. PCR fragments used for cloning purposes were amplified with Phusion DNA Polymerase (New England Biolabs, M0530L). All amplified or digested PCR fragments were purified either by extraction from agarose gels or by PCR purification (Bioline, BIO-52060). Every construct generated was sequenced. All restriction sites described below and marked bold in section “Generation entry clones” are gene specific. Primer combinations are listed in Supplemental Table S1.

Generation entry clones

pENTR:POK-like (398-1265): Reversed transcribed cDNA from Arabidopsis flowers was used to amplify the respective coding sequence, which was cloned into *pGEM T-easy* vector (Promega, A1360). Initially, *POK-likeC_Subclone3* was cloned with **ClaI**/NotI into the *pGEM_POK-likeC_Subclone2* backbone and afterwards cloned into Gateway compatible *pENTR2B* vector (**EcoRI**/NotI).

pENTR:proPOK-like::GFP-POK-like (1-1265): The full length POK-like GFP fusion construct driven by its own promoter was cloned in several steps, using the *pENTR2B_POK-like C-terminus* as a backbone. The POK-like C-terminus, containing the subclone2 cDNA fragment was replaced by a genomic subclone2 fragment using the same primer combination and restrictions enzymes as described above, and Col-0 genomic DNA as template (*pENTR2B_genPOK-like C-terminus*). A genomic fragment (*At3g44050_1-3313* bp) was amplified, digested with Acc65I/**EcoRI** and cloned into *pENTR2B_genPOK-like C-terminus* containing now the full genomic DNA of POK-like (*pENTR2B_genPOK-like full length*). After using extension PCR to clone *proPOK-like:GFP-At3gg44050_992* a fusion fragment into *pGEM*, both were combined via Acc65I/**MlsI** using

pENTR2B_genPOK-like full length as a backbone. In a single Gateway LR reaction *proPOK-like::GFP-POK-like* full length construct was introduced into a binary *pMDC99* vector.

pENTR:EB1b: The coding sequence of EB1b, amplified from cDNA generated from seedlings, was cloned into the pGEM T-easy vector (Promega, A1360) and then it was cloned into *pENTR2B* via EcoRI/XhoI.

pENTR:HTR12: The coding sequence of HTR12 was amplified using seedling cDNA and cloned into *pENTR3C* (Invitrogen) via EcoRI/EcoRI digest and subsequent ligation.

pDONR221-P1P4: An amplicon of RanGAP1 coding sequence was cloned via a Gateway BP reaction (Invitrogen, 11789-020) into *pDONR221-P1P4*. Subsequently, Gateway LR reaction (Invitrogen, 11791-020) was performed with the *pBIFCt-2in1-NC* (257) as a destination vector.

pDONR221-P3P2: Coding sequence of POK1(1683-2066), POK1(1213-2066), POK-like(398-1265) and TAN1 were amplified and cloned via a Gateway BP reaction (Invitrogen, 11789-020) into *pDONR221-P3P2*. Subsequent Gateway LR reaction (Invitrogen, 11791-020) was performed using *pBIFCt-2in1-NC* (257) as destination vector.

pENTR:TPX2: Full length genomic sequence of TPX2 was amplified from genomic DNA extracted from leaves and cloned into *pGEM T-easy* vector (Promega, A1360). From there it was cloned into the *pENTR3C* by using EcoRI.

Generation XFP-expression vectors

GFP-POK-like (398-1265): *pENTR2B:POK-like (398-1265)* was recombined into *pUBN:GFP-Dest* via a Gateway LR reaction (Invitrogen, 11791-020).

GFP-POK-like (1-1265): In a single Gateway LR reaction (Invitrogen, 11791-020) pENTR:*proPOK-like::GFP-POK-like* full length construct was recombined into a binary *pMDC99* vector.

POK-like-GFP (1-631): A 3222 base pair genomic fragment containing the POK-like motor domain was amplified and cloned with additional Not/AscI digestion sites into the expression vector *pOCC12_T7::GFP-6xHIS*. *pOCC12_T7::POK-like-MD-GFP-6HIS* was initially digested with DraI, the binary vector *pFK241* with BsrGI and both were then blunt ended and digested with XbaI. Due to an additional XbaI restriction site in POK-like (1-631), a 700 bp fragment had to be reintegrated in a second cloning step (DraI/XbaI and XbaI/XbaI) finally ending up as *pFK241_35S::POK-like$_{1-631}$-GFP.*

RFP-EB1b: pENTR:EB1b was used in a Gateway LR reaction (Invitrogen, 11791-020) with *pUBN:RFP-*Destination vector, creating the N-terminal RFP-EB1b fusion protein.

RFP-HTR12: In a Gateway LR reaction (Invitrogen, 11791-020) the *pENTR:HTR12* construct was recombined into *pUBN:RFP-Dest*.

RFP-TPX2: In a Gateway LR reaction (Invitrogen, 11791-020) *pENTR:TPX2* was cloned into *pUBN:RFP-Dest*.

Extension PCR

For the genomic fusion construct of GFP-gPOK-LIKE (*pENTR2B:proPOK-LIKE::GFP-gPOK-LIKE*), a specific extension PCR was used to fuse three fragments containing complementary overlap sequences at their ends (modified after Atanassov et al. 2009). The three fragments were fused stepwise (Fragment I: *proPOK-like*; Fragment II: *GFP-linker*; Fragment III: *linker-At3g44050_992bp*), in a total of 30 µl

overlap extension mix containing 14 µl mixture of both PCR fragments (7 µl for each one; approximately 200-800 ng; ratio 1:1), 6 µl of 5x Phusion HF Buffer, 3 µl of 2 mM dNTP mix, 0.3 µl Phusion DNA Polymerase (2 U/µl) and 6.7 µl H2O). The reaction mix was incubated at 98°C for 10 min, 60°C for 1 min and 72°C for 10 min. This cycle was repeated for 5 times and then stopped at 72°C for 10 min. Half of the reaction mix was purified from an agarose gel after gel electrophoresis and the other half was used as a template for another PCR to enrich the overlap PCR product. After combining Fragment I and II, and in an additional round, Fragment III, the fused *proPOK-like:GFP-At3gg44050_992* PCR product was cloned into pGEM.

β-Glucuronidase (GUS)-Staining

For gene expression analyses, a promoter fragment of POK-like (referred as *proPOK-like*) of approximately 954 base pair upstream of the translation initiation site of *POK-like* was cloned in frame (HindIII/BamHI) with GUS in pWD137 vector. Experimental set up and analyses was performed as previously described by Muller et al. (2006), Blasquez et al. (1997) and Hauser & Bauer (2000). The substrate 5-bromo-4-chloro-3-indolyl glucuronide (X-Gluc) was received from Peqlab. Images were taken at a Zeiss Axiophot equipped with a digital camera.

Confocal imaging and image processing

The confocal Laser Scanning Microscope (CLSM) Leica SP8 was used in all cases unless otherwise stated. A water immersion objective lens (63x, numerical aperture (NA) = 1.20) was used for image acquisition. GFP protein was excited with a 488 nm laser line from an argon/krypton laser and the emission detected with a HyD detector set to a detection window between 490 and 530 nm. RFP protein was excited with a 561-nm He/Ne laser, and fluorescent signal was detected with a standard PMT detector with a detection window between 570 to 630 nm.

Two-dimensional projections of Z stacks and line plot analyses were performed using ImageJ 1.48 v (https://imagej.nih.gov/ij/docs). Colour merges were performed in Adobe Photoshop CS5 v12.0.4 and all figures generated with Adobe Illustrator CS5 v15.0.2. For visualization of fusion protein distribution, the ImageJ kymograph plug-in (http://www.embl.de/eamnet/html/body_kymograph.html) was used.

Oryzalin treatment

Four- to seven-day old seedlings co-expressing GFP-POK-like and RFP-MBD were imaged and subsequently treated with 10µM oryzalin solution (Sigma). Cells in different cell cycle stages were reanalysed during oryzalin treatment at 2 min intervals for 10-50 min.

Immuno-localization

Immunofluorescence staining was performed as previously described in (Stöckle et al., 2016) in four to five day old seedlings. Imaging was performed with the CLSM Leica TCS SP8. To determine spindle length and width in each plant line, stacks were imaged with 16 times line averaging and 4x zoom. Substacks including the entire spindle size were generated. Using the segmented line tool, the width of a spindle was determined by DAPI staining, whereas the length was measured as the distance from

pole to pole perpendicular to the width. Based on these measurements, all values were normalized to 1 on wild type.

Interaction studies using ratiometric bimolecular fluorescence complementation

The Gateways compatible 2 in 1 system (Grefen and Blatt, 2012) was used to test the putative interaction of RanGAP1 and selected POK kinesin domains with appropriate controls (TAN1). The potential interaction partner was fused to either nYFP or cYFP in the same plasmid under the control of 35S promoter. In addition, an internal RFP control (p35S:RFP) served as control. The BifC analyses were performed according to (Stöckle et al., 2016). Protoplasts were imaged at least 22h after transfection with identical settings for comparison of the interaction strength. The average fluorescence signal intensity was measured for both YFP and RFP in the selected ROI region by using the selected line tool in ImageJ 1.48 v, set to 3 pixels width of. Calculation of mean YFP/RFP ratios were performed in Excel and Boxplots were generated by using the open source software BloxplotR (http://shiny.chemgrid.org/boxplotr/).

Phylogenetic Analyses

Full length protein sequences of kinesin-12 class members of *Arabidopsis thaliana*, namely KINESIN12A-F, were obtained from TAIR (https://www.arabidopsis.org/) and used to perform BLAST analyses and Similarity Search using Phytozome (https://phytozome.jgi.doe.gov/pz/portal.html). We searched for protein sequence homologies in tomato (*Solanum lycopersicum)*, cotton (*Gossypium raimondii),* black cottonwood (*Populus trichocarpa*)*,* rice (*Oryza sativa*), purple false brome (*Brachypodium distachyon*), amborella (*Amborella trichopoda*), maize (or corn) (*Zea mays*), as well in the algae *Chlamydomonas reinhardtii* and *Klebsormidium nitens/flaccidum* (http://www.plantmorphogenesis. bio.titech.ac.jp). To obtain the sequence for kinesin-12 proteins from *Homo sapiens* and the African claw frog (*Xenopus leavis*) we used Uniprot (https://www.uniprot.org/). These proteins sequences were aligned using the MAFFT v6.864 algorithm (Katoh et al., 2005). The phylogenetic tree was created using http://www.trex.uqam.ca (Boc et al., 2012) and edited in Adobe Illustrator CS5 v15.0.2.

Acknowledgements

We acknowledge NASC and Bielefeld University CeBiTec / GABI-KatIII for distribution of seed used in this study. We thank Pantelis Livanos for critical reading of the manuscript. We appreciate the help of Jens Reich for collecting data concerning the *pok1pok-like* double mutant. We gratefully acknowledge support from the University of Tübingen and funding from the Deutsche Forschungsgemeinschaft to SM (SFB 1101).

Author contributions

AH performed, conceptualized experiments and analysed data together with SM. SZ contributed in establishing plant lines. AH wrote the initial manuscript. All authors contributed to editing of the final manuscript.

Competing interests

The authors declare no competing financial interests.

Figure legend

Figure 1. Phenotypic characteristics of different mutants

(A) Comparison of single and double mutants as indicated. Double mutants (*pok1-2 pok-like1* (iV)) or *pok2* (*pok2-2 pok-like1* (V) do not exhibit a visible vegetative growth phenotype compared to single mutants (pok1-2 (i), *pok2-2* (ii), *pok-like-1* (iii)) or wild type (Vi)), except for a significant reduction of the average silique length in case of *pok1-2 pok-like1* double mutant shown in **(C)**. Bar = 3 cm. **(B)** Simultaneous loss of *POK1*, *POK2* and *POK-like* causes a considerable enhancement of the growth phenotype compared to the *pok1-2 pok2-2* double mutant. Note that the triple mutant is sterile. Bar = 3 cm. **(C)** Comparison of the average silique length between the *pok1-2 pok-like-1* double mutant and the respective controls (n = 100). Note the statistically significant reduction in average silique length in *pok1-2 pok-like-1* double mutant (B): 0.43 µm ± 0.03 µm, compared to Col A: 0.59 µm ± 0.05 µm), The average silique length is not affected in single mutants (*pok1-2* (D): 0.59 µm ± 0.05 µm; *pok-like-1* (E): 0.59 µm ± 0.05 µm). Expression of proPOK1:YFP-gPOK1 in the *pok1-2 pok-like-1* double mutant restores the wild type phenotype (C: 0.54 µm ± 0.06 µm). **(D)** Propidium iodide stained root meristems of wild type (Vii: Col-0), *pok1-2 pok2-3* (Viii), *pok1-2 pok-like* (iX) and *pok2-2 pok-like* (X) double mutant combinations that do not display obvious aberrations in the organization of the root meristem after 3 dag (inverted grey scale images). Bar = 50 µm.

Figure 2. GFP-POK-like shows cell cycle specific subcellular localization and differential microtubule dependencies.

(A) Z-projections of confocal images of dividing root cells as indicated co-expressing GFP-POK-like with the microtubule reporter RFP-MBD. Upper row: GFP-POK-like is recruited to the nuclear envelope in prophase (arrow). Arrowheads mark the PPB. Central row: GFP signal accumulates in the spindle midzone (brackets). Lower row: During cytokinesis GFP-POK-like localizes exclusively at the phragmoplast midzone (arrows). Bar = 10 µm. **(B)** Percentage of cells (%) in which GFP-POK-like signal co-localizes with a specific mitotic array (PPB = preprophase band, SP = spindle, PhP = phragmoplast). **(C-G)** POK-like recruitment at the nuclear envelope is independent of microtubules. Z-projections of dividing root cells expressing both RFP-MBD and GFP-POK-like before **(C)** and after 10µM oryzalin treatment **(D)**. Cell shown in the right panel was recorded after 5 min of incubation and corresponds to the cell on the left panel. **(E)** Graph depicting the percentage of cells exhibiting GFP signal after 10 min of 10µM oryzalin treatment. Note the reduced amount of cells displaying POK-like signal during spindle (SP, n = 1) and phragmoplast development (PhP, n = 2) after treatment. The total number of cells investigated is indicated. **(F, G)** Fluorescence intensity profile plot along the dashed line in **(C)** and **(D),** depicting RFP-MBD (dashed, magenta) and GFP-POK-like (continuous, green) distribution before and after oryzalin. Obviously, although RFP-MBD peaks (PPB) disappear in the presence of oryzalin, the GFP-POK-like signal persists at the nuclear envelope (arrows).

Figure 3. Distinct localization pattern of different GFP-POK-like fusion proteins

Single-plane time frames of meristematic root cells expressing either full length POK-like or POK-like$_{389-1265}$ together with RFP-MBD to allow visualization of the different cell cycle stages (**A** and **C**). **(A)** GFP-POK-like decorates overlapping microtubules (arrowheads) during prospindle assembly and remains at the spindle midzone during meta- and anaphase. Finally, POK-like gets recruited to the phragmoplast midzone in cytokinesis (white arrow head). Contrary to that, GFP-POK-like$_{389-1265}$ is uniformly distributed along all prospindle and spindle microtubules but vanishes completely after anaphase **(C)**. Bars = 5 µm. (**B** and **D**) Kymograph analyses of along the yellow dashed line of GFP-POK-like **(A)** and POK-like$_{389-1265}$ **(C)**. Note that the distribution of GFP-POK-like is exclusively restricted to the centre of the kymograph (**B**) whereas GFP-POK-like$_{389-1265}$ signal overlaps/coincides with the respective RFP-MBD signal (magenta) over time (**D**). (**E** and **F**) Expression of POK-like$_{1-631}$–GFP and RFP-MBD in meristematic leaf cells (**E**) or roots (**F**). Note the recruitment of POK-like$_{1-631}$–GFP towards the phragmoplast midzone (white arrow) during all steps of cytokinesis (**E**, **F**). (**G** and **H**) Line plot analyses of POK-like$_{1-631}$–GFP signal (**H**) along the yellow dashed line perpendicular to the expansion axis of the phragmoplast (**G**). Fluorescence intensity profile plot (normalized to 1) depicting RFP-MBD (dashed, magenta) and POK-like$_{1-631}$–GFP (continuous, green) distribution. Signal intensity peak of POK-like$_{1-631}$–GFP in between RFP-MBD signal is indicative not only of phragmoplast midzone localization but also of association with the cell plate. Bar = 10 µm.

Figure 4. Loss of POK-like interferes with prospindle development

(A) Immunolocalization of tubulin and DAPI staining in wild type and *pok-like-1* mutant. Note the reduction in metaphase spindle size in *pok-like-1* mutant compared to wild type. **(B)** Boxplot diagram showing the differences in average spindle length between wild type (a, n = 34, normalized to 1), *pok-like-1* (b, n = 40) and *pPOK-like*:GFP-POK-like expressed in *pok-like-1* background (c, n = 50). **(C, D)** Average time duration (in min) of individual cell cycle stages of wild type and mutant cells expressing RFP-MBD. Representative single plane time laps performed in wild type dividing cells (**C**) as have been classified in (**D**). PPB+NEB transition as well timely mitotic progression from anaphase on are unaffected in *pok-like* mutants compared to wild type (*pok-like-1*: PPB + NEB prospindle, 3.0 min ± 1.6 min, n = 4, A-spindle 2.6 min ± 1.14 min, n = 15, telophase/cytokinesis 2.0 min ± 1.09 min, n = 11, early cytokinesis 2.40 min ± 1.81 min, n = 8, light pink; *pok-like2*: PPB + NEB prospindle 3.75 min ± 2.56 min, n = 8, A-spindle 2.47 min ± 0.85 min n = 17, telophase/cytokinesis 2 min ± 0.96 min, n = 11, early cytokinesis 1.86 min ± 0.78 min, n = 14, pink; wild type1: PPB+NEB prospindle 2.8 min ± 1.45 min n = 4, A-spindle 2.5 min ± 1.17 min, n = 13, telophase/cytokinesis 2.10 min ± 0.75 min, n = 13, early cytokinesis 2.7 min ± 1.49 min, n = 3 light green; wild type2: PPB + NEB prospindle 2.67 min ± 2.67 min, n = 12, A-spindle 2.50 min ± 0.84 min, n = 26, telophase/cytokinesis 2.35 min ± 1 min, n = 23, early cytokinesis 2.05 min ± 0.76 min, n = 22, dark green). On the contrary, pro-metaphase/prospindle and metaphase/M-spindle stages are considerably extended in both *pok-like* alleles (*pok-like-1*: prospindle 5.39 min ± 2.4 min, *P < 0.01, n=14, M-spindle 8.70 min ± 3.32 min, *P < 0.01, n = 15, light pink; *pok-like2*: prospindle 5.60 min ± 2.85 min, *P < 0.01, n = 15 , M-spindle 7.29 min ± 0.85 min, *P < 0.01, n = 17, pink) compared to their respective wild type controls (wild type1: prospindle 3.67 min ± 1.14 min n = 15, M-spindle 5.20 min ± 2.51 min, n = 15, light green; wild type2: prospindle 3.33 min ± 1.75 min, n = 21, M-spindle 4.24

min ± 1.88 min, n = 25, dark green). **(E)** The total duration of cell division from prophase until early cytokinesis is extended in *pok-like* mutant alleles (*pok-like-1*: 29.01 min ± 11.36 min, *P < 0.01, n = 16; *pok-like-2*: 27.97 min ± 11.65 min, *P < 0.01, n = 17) compared to their respective wild type control (wild type1: 23.90 min ± 8.49 min, n = 16; wild type2: 22.13 min ± 8.90 min, n = 26).

Figure 5. POK-like accumulates in the close proximity of the kinetochore marker HTR12

(A) Single image of a root cell in prometaphase expressing GFP-POK-like together with the microtubule marker RPF-MBD on. Note the distinct localization pattern of GFP-POK-like most likely at the tip of a kinetochore microtubule bundle during spindle formation (yellow dashed box). (**B, D**) Single frames showing meristematic root cells expressing both GFP-POK-like and RFP-HTR12, before and after the application of the microtubule depolymerization drug oryzalin. **(B)** Before oryzalin, GFP-POK-like accumulate at the nuclear envelope (white arrow), whereas RFP-HTR12 localizes in a punctate pattern within the nucleus (white arrowhead). Right after nuclear envelope breakdown and in the presence of oryzalin, GFP-POK-like re-localizes as puncta adjacent to RFP-HTR12. **(D)** During metaphase GFP-POK-like accumulates at the spindle midzone, whereas RFP-HTR12 localizes pairwise within the metaphase plate. After treatment with oryzalin, the distribution of GFP-POK-like is restricted next to the RFP-HTR12 signal. **(C, E)** Higher magnification showing GFP-POK-like and RFP-HTR12 localization within yellow dashed box in **(B)** and **(D)**. Line plot analyses along the white lines in **(C)** and **(E)** confirming a partial overlap of both signals. White continuous line depicts the shape of the cell in each case. Bar = 5 µm.

Figure 6. RanGAP1 interacts and co-localizes with POK-like in planta

(A, B) Ratiometric bimolecular fluorescence complementation (rBIFC) analyses of interaction between RanGAP1 and truncated protein domains of the kinesin12 members POK1 and POK-like as well TAN1 recorded in *Arabidopsis* root protoplasts. **(A)** Images show single optical sections of n/c YFP fluorescence and the cytosolic RFP fluorescence. TAN1 was used as a biological negative control as it does not interact with RanGAP1. **(B)** Box plots illustrating the YFP/RFP fluorescence ratio for each protein pairs tested. Both, the n/c YFP fluorescence and the co-expressed cytosolic RFP were recorded and the mean ratio of n/c YFP and RFP intensities were calculated for each protoplast. The higher the YFP/RFP ratio corresponding to n/cYFP complementation represents stronger interaction. Note that n/c YFP complementation because of protein interaction shown in **(A)** and calculated in **(B)** was detected only for both kinesin-12 members nYFP-POK1 and nYFP-POK-like with RanGAP1-cYFP and not for nYFP-TAN1. Statistically significant differences (*P < 0.0001, n ≥ 30 protoplasts) were determined by one-way ANOVA. Bar = 10µm. **(C)** The localization pattern of RanGAP1-GFP expressed in the *pok1-2 pok-like-1* meristematic cells is not altered. Note that RanGAP1-GFP localizes at the nuclear envelope and PPB in prophase (yellow arrow), at kinetochores (yellow asterisk) in metaphase and in a punctate pattern at the CDZ at the end of cytokinesis (yellow arrow head). Propidium iodide was used for cell wall staining. Bar = 5 µm. **(D)** Individual images of dividing root cells expressing both GFP-POK-like and RanGAP1-RFP. GFP-POK-like (white marks) and RanGAP1-RFP (yellow marks) are co-localizing at the nuclear envelope during prophase, at the microtubule overlap in anaphase and at the cell plate during cytokinesis. **(E)** Plot profiles illustrating GFP (green) and RFP (magenta) signal distribution along the dashed lines shown in **(D)**. Bar = 5 µm.

Figure 7. Motor activity of POK-like is necessary to define and maintain midzone integrity (A, B) Individual images of time series, showing GFP-POK-like **(A)** and GFP-POK-like(T181N) **(B)** signal co-expressed with the microtubule marker RFP-MBD from metaphase on until cytokinesis. Plot profiles illustrate GFP (green) and RFP (magenta) signal distribution of the average signal intensity within the dashed box in the respective figure panels above. Arrows in plot profiles point to intensity maxima (peaks) and the asterisks mark the midzone in each case. Note that from metaphase on, GFP-POK-like associates with the overlap of antiparallel microtubules in every cell stage. On the contrary, the dead motor domain version is absent from the midzone and decorates the entire microtubule arrays instead. **(C, D)** Time laps of meristematic root cells in wild type **(C)** and *pok-like-1* single mutant **(D)**, expressing the microtubule marker GFP-TUA6. **(C)** In wild type, microtubules are forming a distinct midzone (white arrow) during the transition from anaphase (50 sec) to cytokinesis (275 sec) within the plane of cell division, to form an early disc phragmoplast. **(D)** In *pok-like* mutant cells, during the transition from anaphase (75 sec) to cytokinesis (275 sec) the continuous midzone between the segregating spindle poles are not forming, as observed in wild type; furthermore, but phragmoplast microtubules are unevenly distributed and predominantly bundled at the leading edge of the emerging phragmoplast (yellow arrow). Consequently, in mutant cells, the early phragmoplast does not display the characteristic narrow disk organization. Bar = 5 µm.

Supplemental Figure S1. Rooted phylogenetic tree of selected kinesin-12 members

The phylogenetic tree was generated using T-REX (http://www.trex.uqam.ca). Sequences of full-length protein of selected kinesin-12 members were aligned using the MAFFT algorithm. Note that plant kinesin-12 members split up in two main clusters: Cluster I: Kinesin12C-POK1 (green), Kinesin12D-POK2 (light green) and Kinesin12E-POK-like (red). Cluster II: Kinesin12A-PAKRP1 (violet), Kinesin12B-PAKRPL (violet) and Kinesin12F-At3g20150 (blue). Sequences were obtained from Phytozyme and all accession numbers are listed in Supplement Table S2.

Supplemental Figure S2. Domain organization, transcript levels and mutant phenotypic analyses and GUS gene expression pattern of *POK-like*

Schematic representation of gene organization and T-DNA insertion site of POK-like (At3g44050) **(A)**. Exons of POK-like are depicted in black bars while black arrows demonstrate the positions of T-DNA insertions confirmed after sequencing. **(B)** Representative images after semi quantitative RT-PCR showing transcript levels in *pok-like* mutants as well as in wild type seedlings. Primer combination for transcript amplification of both *POK-like* alleles are depicted in **(A)** for *pok-like-2* [(**ii**)] and *pok-like-1* [(**i**)] (see also table Supplemental Table S1). A size of approximately 2086 bp (cDNA) and 3206 bp (genDNA) is expected for the first Primer combination (**i**) and 576 bp (cDNA) and 992 bp (genDNA) for the second combination (**ii**). Controls used were water (H_20, negative) and genomic DNA (genDNA, positive). Expression levels of *UBIQUITIN5 (UBQ)* gene (cDNA) were monitored as loading control (260 bp). **(C)** Overview of 12 dag seedlings of different genotypes as well images of 6-week-old plants. From left to right: Wild type (Col-0) and Wild type (Gabi-Kat), *pok-like-1* and *pok-like-2* single mutant, the rescue line of *pok-like-1* expressing *GFP-POK-like* under its endogenous promoter as well as the *pok1-1pok2-3* double mutant plants. Note that only *pok1-1pok2-3* double mutant plants display shorter roots compared to *pok-like* single mutants and their respective wild type. Bar = 5 cm. **(D)** POK-like domain organization

as indicated in the key. **(E-J)** GUS-reporter gene expression pattern of POK-like in stable transformed Col-0 plants (seven independent lines exhibiting comparable expression were analysed). Intense *GUS* staining was observed predominantly in meristematic tissues such as the leaf (**E,** bar = 1 mm) and root meristems (**G,** bar = 50 µm) after one to three hours of incubation with the substrate. In addition, expression was also detected in developing and mature stomata (**F,** bar = 50 µm) as well as in embryos (**H**, bar = 100 µM). Examination of *pPOK-like:GUS* expression in reproductive organs revealed its expression in both male (**I**, bar = 100µm) and female (**J**, bar = 50 µm) gametophyte two days after emasculation and overnight incubation with the substrate.

Supplemental Figure S3. POK-like is directed to the microtubule overlap

(A) Co-expression of GFP-POK-like and RFP-EB1b under the ubiquitin promoter in stable transformed plants. White arrowheads point towards the microtubule overlaps localization of GFP-POK-like, in contrast to RFP-EB1b signal which decorates most of the prospindle (t1 = 0 sec). Over time both signals are narrowing towards the metaphase plate during spindle formation (t2-t4 = 60-270 sec). Bar = 5 µm **(B)** Single images of a meristematic root cell expressing GFP-POK-like together with the microtubule marker RPF-MBD from metaphase on (t1 = 0 sec) until late cytokinesis (t15 = 869 sec). Note the distinct localization pattern of GFP-POK-like at interdigitating microtubule bundles during metaphase and anaphase together with a re-distribution in cytokinesis towards the phragmoplast midzone. **(C)** Kymograph along the yellow dashed line of GFP-POK-like and RFP-MBD in **(B)**. Note that the distribution of GFP-POK-like is mostly restricted to the centre of the kymograph compared to RFP-MBD. Bar = 5 µm.

Supplemental Figure S4. Microtubule organization in *pok-like* mutants

(A) Immuno-localization of tubulin and DAPI staining in *pok-like-1* meristematic cells. Note that there is no defects in both PPB formation in prophase (upper panel) and during phragmoplast expansion throughout cytokinesis (lower panel). Bar = 5 µm. **(B)** Boxplot diagram showing the percentage of meristematic root cells in different cell cycle stages of *pok-like1* mutants (n = 399; 6 roots) and *pok-like-1* mutants (n = 300; 6 roots) expressing the full length genomic GFP-fusion protein. The dividing cells have been classified according to their cell cycle stage determined by the organisation of microtubule arrays as shown in Figure 4. The increase in the percentage of cells being in pro-metaphase/metaphase indicates a significant delay at the respective stage. Note that in the rescue line the effect is alleviated.

Supplemental Figure S5. Co-expression of POK-like C-terminal domain and TPX2

(A) Expression of the C-terminal domain of POK-like (GFP- POK-like$_{389-1265}$, green) and RFP-TPX2 (magenta) in Arabidopsis root protoplasts. Note that POK-like$_{389-1265}$ localizes exclusively in the cytosol, whereas RFP-TPX2 accumulates in the nucleus. Bar = 10 µm. **(B)** Co-localization analyses of GFP-POK-like (green) full length protein together with RFP-TPX2 (magenta). While GFP-POK-like localizes at the nuclear envelope (arrow, upper row) and at the cell plate in cytokinesis, RFP-TPX2 accumulates in the nucleus (yellow asterisk, upper row) in prophase and is completed vanished in cytokinesis. On the contrary, both GFP-POK-like and RFP-TPX2 are restricted at the spindle in metaphase (lower panel). However, RFP-TPX2 is confined at the spindle poles (yellow arrow head), whereas GFP-POK-like decorates the spindle midzone (white arrow head). Average intensity plot along the dashed box confirmed the distinct localization pattern. Bar = 10 µm.

Supplemental Figure S6. Recruitment of POK-like towards the nuclear envelope

Individual time points (as indicated) of a meristematic root cell showing the dynamic recruitment of GFP-POK-like at the nuclear envelope during prophase. GFP-POK-like signal is indicated with white arrows. Images acquired using scanning confocal microscopy at 2.3 sec interval. Bar = 10 µm.

Supplemental Figure S7. POK-like localization throughout the cell cycle

Individual time points (as indicated) of two cytokinetic root cells expressing GFP-POK-like (green) and the microtubule marker RFP-MBD (magenta). obtained every 30 sec Images acquired using a scanning confocal microscope at 5 sec intervals.

Supplemental Figure S8. POK-like(T181N) localizes to all microtubule arrays

Individual time points (as indicated) of a cytokinetic wild type cell from prophase on, expressing the ATP-hydrolysis deficient mutant GFP-POK-like(T181N) (green) and the microtubule marker RFP-MBD (magenta). CLS microscopy was used to acquire images.

Supplement Table S1

Primer	Sequence
Cloning	
At3g44050_SacII-Kpn_ATG_F	atccgcggtaccatgccgtttatctccgagact
At3g44050_STOP_Not_R	gcggccgctcagtgagaaacttcaagcaa
At3g44050_2211R	gttgatgttggtagcttctttg
At3g44050_2660F	tgctcattggagaccctaagta
At3g44050_2681R	tacttagggtctccaatgagca
At3g44050_4741R	gttctgagcgtccgcattattacttg
At3g44050_970F	ttggagatatcgagggaggaaca
At3g44050_992R	tgttcctccctcgatatctccaa
NotI_POK3_ATG_F_correct	aataataacatgcggccgcaatgccgtttatctccgagactgc
KAT3_ClaI F	agagaaatcgatgctgctatg
KAT3_ClaI R	catagcagcatcgatttctct
NotI_POK3_ATG_F_correct	aataataacatgcggccgcaatgccgtttatctccgagactgc
Asc_POK3_1893 R	aataataacatggcgcgccatcccgttccccttcctcacct
Asc_POK3_1893 stop R	aataataacatggcgcgcctta*ccgttccccttcctcacct*
ProPOK3_1kb_KPNI	aaggtaccatacatcaaaggcgatagaaca
proPOK3_GFP_R	cagctcctcgcccttgctcaccatgcttgatttggttgggtgatgagag
proPOK3_GFP_F	ctctcatcacccaaccaaatcaagcatggtgagcaagggcgaggagctg
linkerPOK3_F	tatactttctagagaataggaacttcatgccgtttatctccgagact
HTR12_ATG	atgaattctcaccatggtctgccttttcctcc
HTR12_STOP	tactcgagtaccgatatcttgtaccagagctct
Eb 1B ecoRI F	gaattcaaaaatggcgacgaacatt

Eb 1B xhoI R	ctcgagttaagtttgggtctctgcagca
rBifC cloning	
attB3 POK3C_EcoRI_F	ggggacaactttgtataataaagttgtaatggggaattcaaagacaattataat
attB2 POK3_R	ggggaccactttgtacaagaaagctgggtttcagtgagaaacttcaagcaa
attB3 POK1C-short _F	ggggacaactttgtataataaagttgtaatggatgaagaagtaaaaaggcatcgt
attB2 POK1C-short_R	ggggaccactttgtacaagaaagctgggttttaccgat atcttgtaccagagct
attB3 TAN1_F	ggggacaactttgtataataaagttgtaatggttgcaa gaaccccacagaagca
attB2 TAN1_R	ggggaccactttgtacaagaaagctgggttctacactt tcctgctcttcattgga
attB1 RanGAP1_F	*ggggacaagtttgtacaaaaaagcaggctta*atggatcattcagcgaaaacca
attB4 RanGAP1_r	*ggggacaactttgtatagaaaagttgggtg*ttcctccccttgcttgattt
TPX2 cloning and BifC	
EcoRI TPX2 START	gaattcatggaagcaacggcggaggaat
EcoRI TPX2 STOP	gaattcctatctcatctgaccagcagaggc
TPX2 MfeI F	accagtagttccaattgtttct
TPX2 MfeI R	agaaacaattggaactactggtt
TPX2 EcoRV F	tgagaggatatcacgaccagaa
TPX2 EcoRV R	ttctggtcgtgatatcctctcat
attB1 TPX2_F	ggggacaagtttgtacaaaaaagcaggcttaatggaagcaacggcggaggaatca
attB4 TPX2_r	ggggacaactttgtatagaaaagttgggtgtcagtttaataaacttgaatcagga
genotyping	
LBaI	tggttcacgtagtgggccatcg
KAT3_01 F	caaagaagctaccaacatcaac
KAT3_01 R	tcaaagcctgtaaagcaacgtc
LlbsLox	cacatggtcctgctggagttc
At3g44050_992R	tgttcctccctcgatatctccaa
At3g44050_SacII-Kpn_ATG_F	atccgcggtaccatgccgtttatctccgagact

Supplement Table S2

Kinesin-12 class	**Species**	**Accession number**
Kinesin12A	*Arabidopsis thaliana*	At4g14150
	Gossypium raimondii	Gorai.009G351600.1
	Populus trichocarpa	Potri.002G235500.1
	Solanum lycopersicum	Solyc09g097860.2.1
	Oryza sativa	LOC_Os04g28260.1

	Brachypodium distachyon	Bradi5g06640.1
	Amborella trichopoda	evm_27.model.AmTr_v1.0_scaffold00013.210
Kinesin12B	*Arabidopsis thaliana*	At3g23670
	Gossypium raimondii	Gorai.011G150300.1
	Populus trichocarpa	Potri.014G149000.1
	Solanum lycopersicum	Solyc12g098630.1.1
	Oryza sativa	LOC_Os02g28850.1
	Zea mays	GRMZM2G471186_T01
	Brachypodium distachyon	Bradi3g43587.3
	Klebsormidium nitens/flaccidum	kfl00364_0100_v1.1
Kinesin12C	*Arabidopsis thaliana*	At3g17360
	Gossypium raimondii	Gorai.006G081200.1
	Populus trichocarpa	Potri.010G153000.1
	Solanum lycopersicum	Solyc01g057320.1.1
	Oryza sativa	LOC_Os12g39980.1
	Zea mays	GRMZM2G300709_T01
	Brachypodium distachyon	Bradi4g03050.1
	Amborella trichopoda	evm_27.model.AmTr_v1.0_scaffold00045.35
Kinesin12D	*Arabidopsis thaliana*	At3g19050
	Gossypium raimondii	Gorai.005G239700.1
	Populus trichocarpa	Potri.004G145800.2
	Solanum lycopersicum	Solyc01g108670.2.1
	Zea mays	GRMZM5G839416_T01
	Brachypodium distachyon	Bradi1g20060.1
	Amborella trichopoda	evm_27.model.AmTr_v1.0_scaffold00169.37
	Klebsormidium nitens/flaccidum12D	kfl00364_0070_v1.1 POK2
Kinesin12E	*Arabidopsis thaliana*	At3g44050
	Gossypium raimondii	Gorai.009G081900.1
	Populus trichocarpa	Potri.004G193700.1
	Populus trichocarpa	Potri.009G156000.1
	Solanum lycopersicum	Solyc11g071730.1.1
	Oryza sativa	LOC_Os03g53920.1
	Zea mays	GRMZM2G177867_T02
	Zea mays	AC220970.4_FGT001
	Brachypodium distachyon	Bradi1g08500.1
	Amborella trichopoda	evm_27.model.AmTr_v1.0_scaffold00004.146
	Klebsormidium nitens/flaccidu12-E	kfl00041_0070_v1.1 POK-like
Kinesin12F	*Arabidopsis thaliana*	At3g20150
	Gossypium raimondii	Gorai.013G156400.3
	Populus trichocarpa	Potri.001G360200.1

	Solanum lycopersicum	Solyc07g065210.2.1
	Oryza sativa	LOC_Os03g39020.1
	Zea mays	GRMZM2G034828_T02
	Brachypodium distachyon	Bradi1g15330.1
	Amborella trichopoda	evm_27.model.AmTr_v1.0_scaffold00055.66
Kinesin12	Chlamydomonas reinhardtii	Cre03.g164050.t2.1
	Homo sapiens (hKif15)	NP_064627
	Xenopus leavis (X-KLP2)	NP_001081543
Kinesin4	*Klebsormidium nitens/flaccidum*	kfl00785_0060_v1.1 Protein

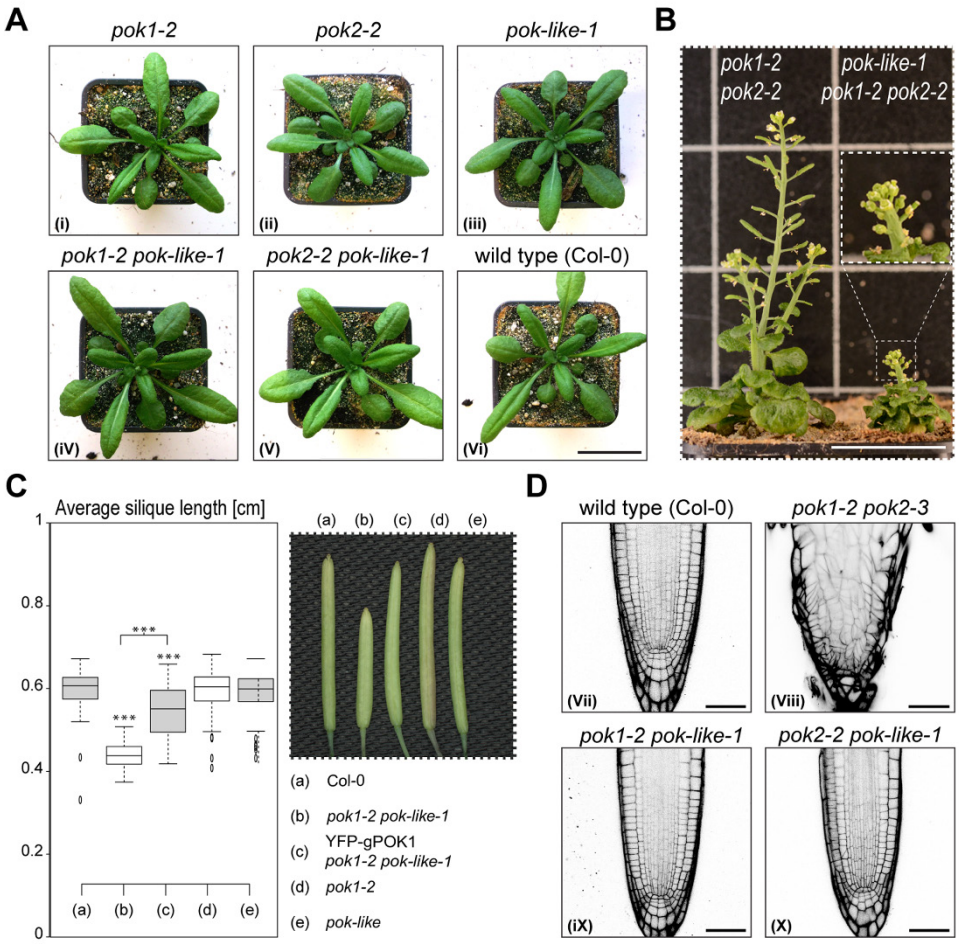
A
pok1-2
pok2-2
pok-like-1
(i)
(ii)
(iii)
pok1-2 pok-like-1
pok2-2 pok-like-1
wild type (Col-0)
(iV)
(V)
(Vi)
B
pok1-2
pok2-2
pok-like-1
pok1-2 pok2-2
C
Average silique length [cm]
1
0.8
0.6
0.4
0.2
0
***
***
***
(a) (b) (c) (d) (e)
(a) Col-0
(b) pok1-2 pok-like-1
(c) YFP-gPOK1
pok1-2 pok-like-1
(d) pok1-2
(e) pok-like
D
wild type (Col-0)
pok1-2 pok2-3
(Vii)
(Viii)
pok1-2 pok-like-1
pok2-2 pok-like-1
(iX)
(X)

Figure 1

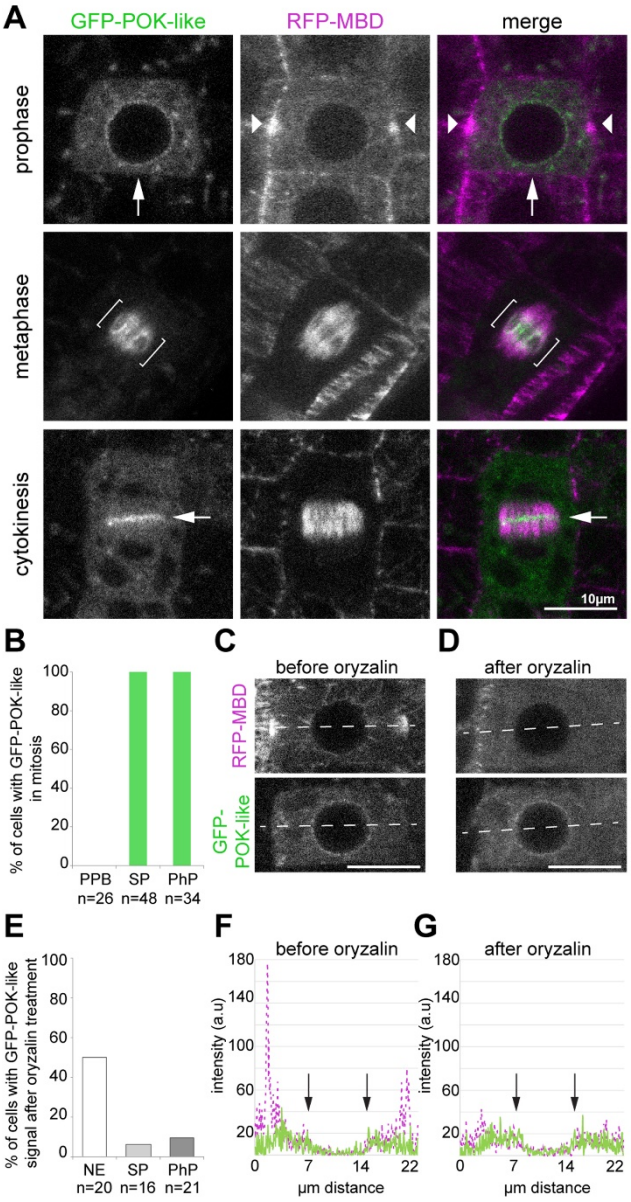
A
GFP-POK-like
RFP-MBD
merge
prophase
metaphase
cytokinesis
10µm
B
% of cells with GFP-POK-like in mitosis
100
80
60
40
20
0
PPB n=26
SP n=48
PhP n=34
C
before oryzalin
RFP-MBD
GFP-POK-like
D
after oryzalin
E
% of cells with GFP-POK-like signal after oryzalin treatment
100
80
60
40
20
0
NE n=20
SP n=16
PhP n=21
F
before oryzalin
intensity (a.u)
180
140
100
60
20
0
7
14
22
µm distance
G
after oryzalin
intensity (a.u)
180
140
100
60
20
0
7
14
22
µm distance

Figure 2

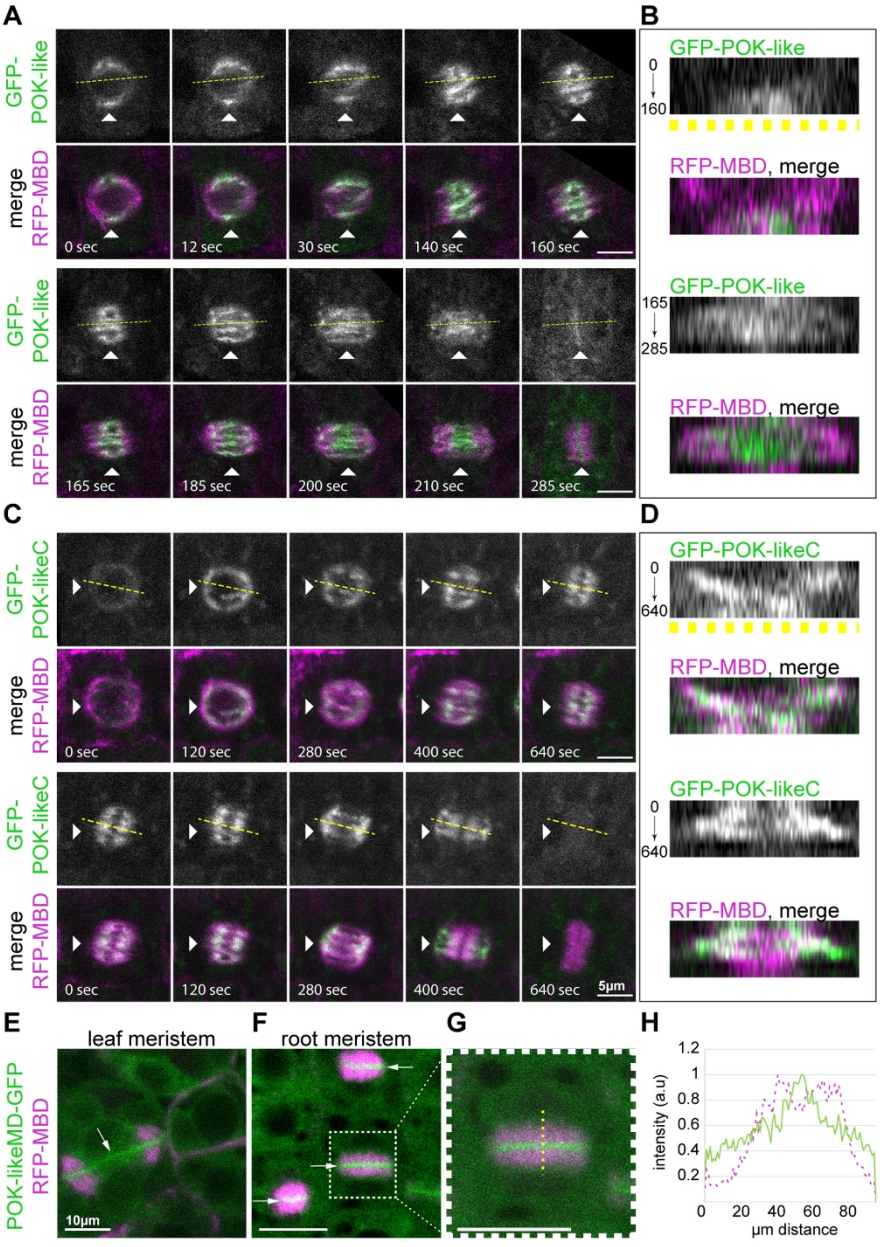
A
B
GFP-POK-like
merge RFP-MBD
0 sec
12 sec
30 sec
140 sec
160 sec
165 sec
185 sec
200 sec
210 sec
285 sec
GFP-POK-like
RFP-MBD, merge
0
160
165
285
C
D
GFP-POK-likeC
merge RFP-MBD
0 sec
120 sec
280 sec
400 sec
640 sec
5µm
GFP-POK-likeC
RFP-MBD, merge
0
640
E
F
G
H
leaf meristem
root meristem
POK-likeMD-GFP
RFP-MBD
10µm
intensity (a.u)
1.2
1
0.8
0.6
0.4
0.2
0
20
40
60
80
µm distance

Figure 3

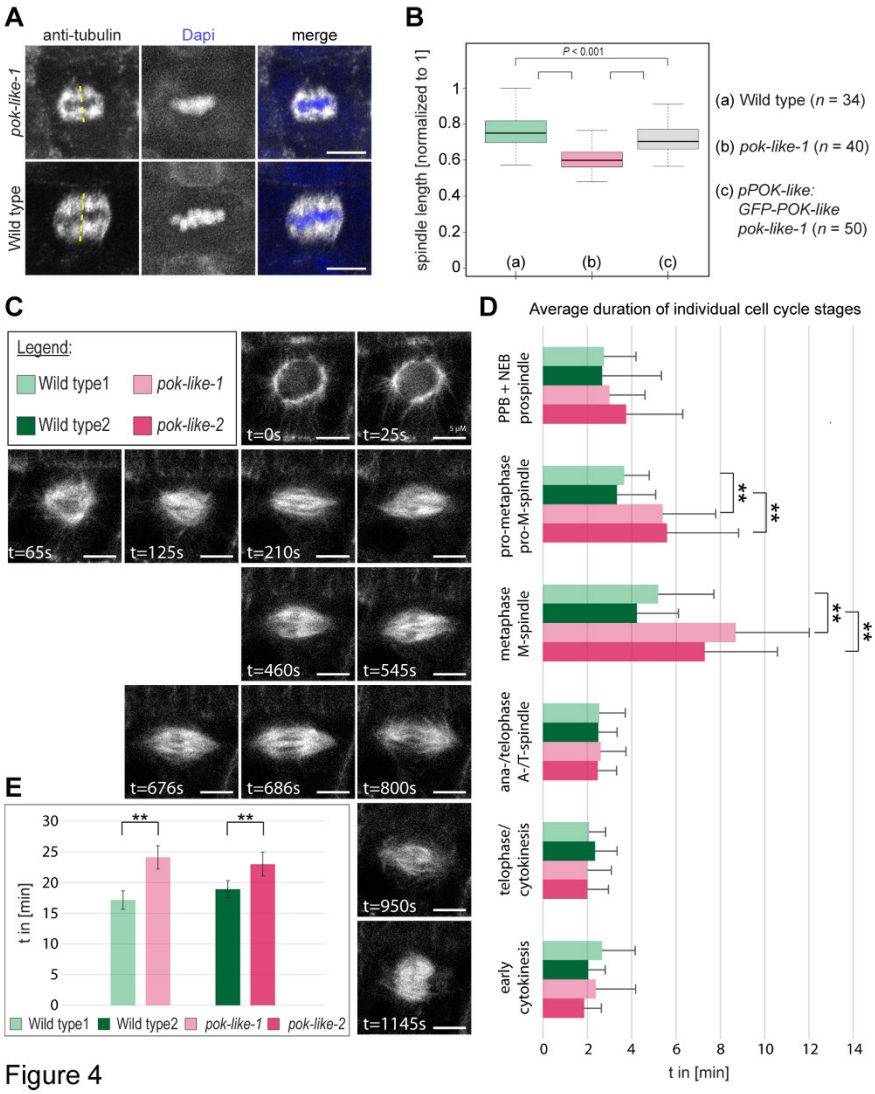
A
anti-tubulin
Dapi
merge
pok-like-1
Wild type
B
P < 0.001
spindle length [normalized to 1]
1
0.8
0.6
0.4
0.2
0
(a)
(b)
(c)
(a) Wild type (n = 34)
(b) pok-like-1 (n = 40)
(c) pPOK-like: GFP-POK-like pok-like-1 (n = 50)
C
Legend:
Wild type1
pok-like-1
Wild type2
pok-like-2
t=0s
t=25s
t=65s
t=125s
t=210s
t=460s
t=545s
t=676s
t=686s
t=800s
t=950s
t=1145s
D
Average duration of individual cell cycle stages
PPB + NEB prospindle
pro-metaphase pro-M-spindle
metaphase M-spindle
ana-/telophase A-/T-spindle
telophase/ cytokinesis
early cytokinesis
**
0
2
4
6
8
10
12
14
t in [min]
E
t in [min]
30
25
20
15
10
5
0
**
**
Wild type1
Wild type2
pok-like-1
pok-like-2

Figure 4

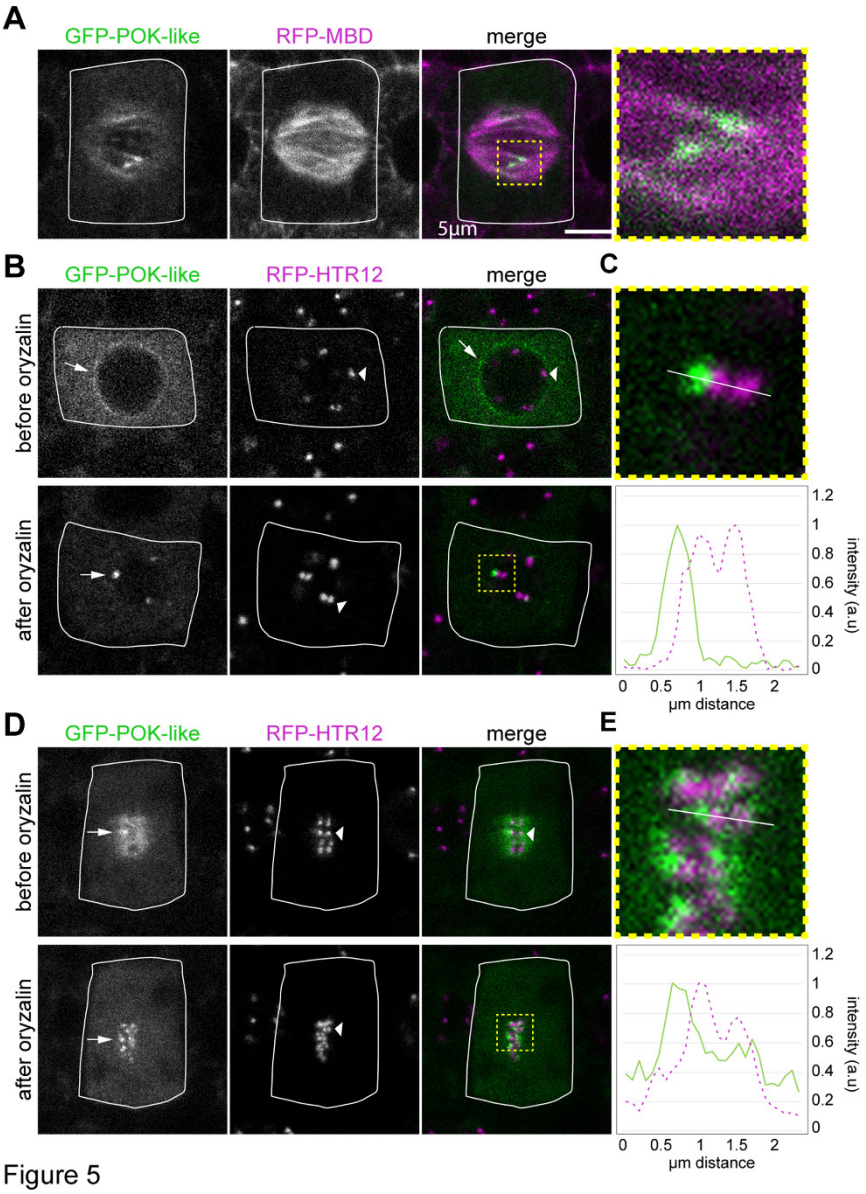
A
GFP-POK-like
RFP-MBD
merge
5µm
B
GFP-POK-like
RFP-HTR12
merge
C
before oryzalin
after oryzalin
1.2
1
0.8
0.6
0.4
0.2
0
intensity (a.u)
0 0.5 1 1.5 2
µm distance
D
GFP-POK-like
RFP-HTR12
merge
E
before oryzalin
after oryzalin
1.2
1
0.8
0.6
0.4
0.2
0
intensity (a.u)
0 0.5 1 1.5 2
µm distance

Figure 5

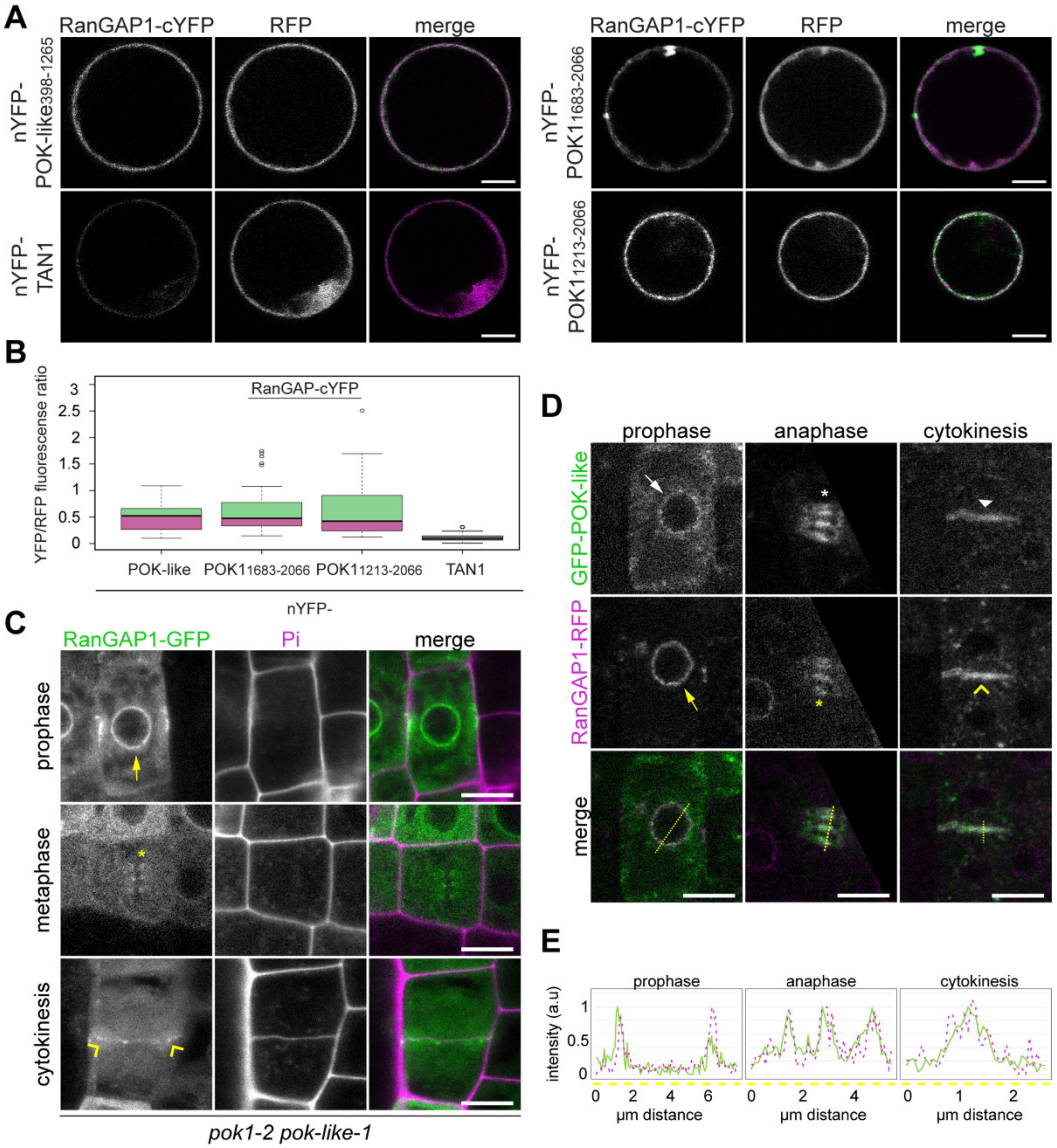
A
RanGAP1-cYFP
RFP
merge
nYFP-POK-like398-1265
nYFP-TAN1
nYFP-POK11683-2066
nYFP-POK11213-2066
B
RanGAP-cYFP
YFP/RFP fluorescense ratio
POK-like
POK11683-2066
POK11213-2066
TAN1
nYFP-
C
RanGAP1-GFP
Pi
merge
prophase
metaphase
cytokinesis
pok1-2 pok-like-1
D
prophase
anaphase
cytokinesis
GFP-POK-like
RanGAP1-RFP
merge
E
intensity (a.u)
µm distance

Figure 6

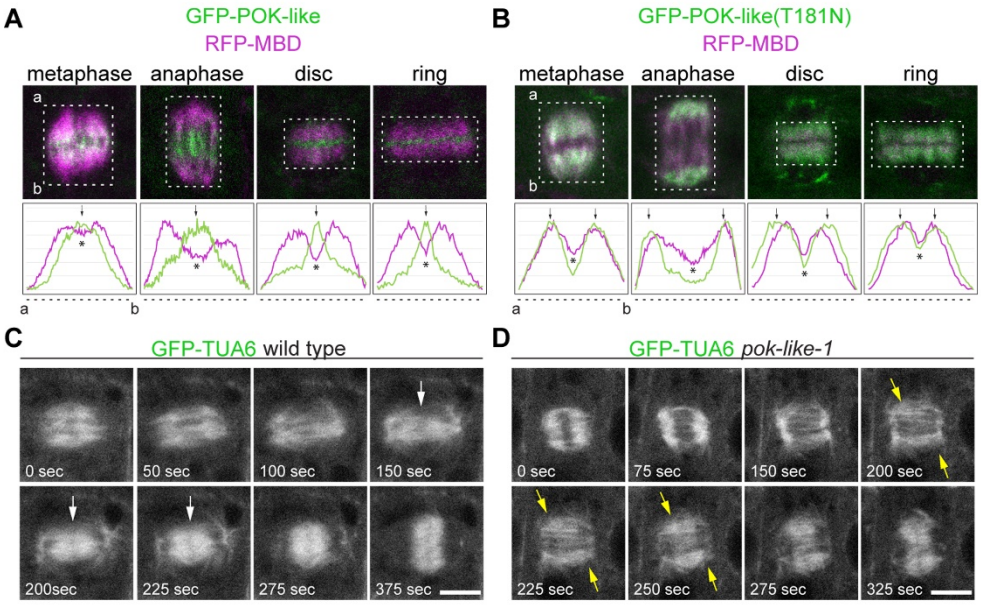
A
GFP-POK-like
RFP-MBD
metaphase
anaphase
disc
ring
a
b
B
GFP-POK-like(T181N)
RFP-MBD
metaphase
anaphase
disc
ring
C
GFP-TUA6 wild type
0 sec
50 sec
100 sec
150 sec
200sec
225 sec
275 sec
375 sec
D
GFP-TUA6 pok-like-1
0 sec
75 sec
150 sec
200 sec
225 sec
250 sec
275 sec
325 sec

Figure 7

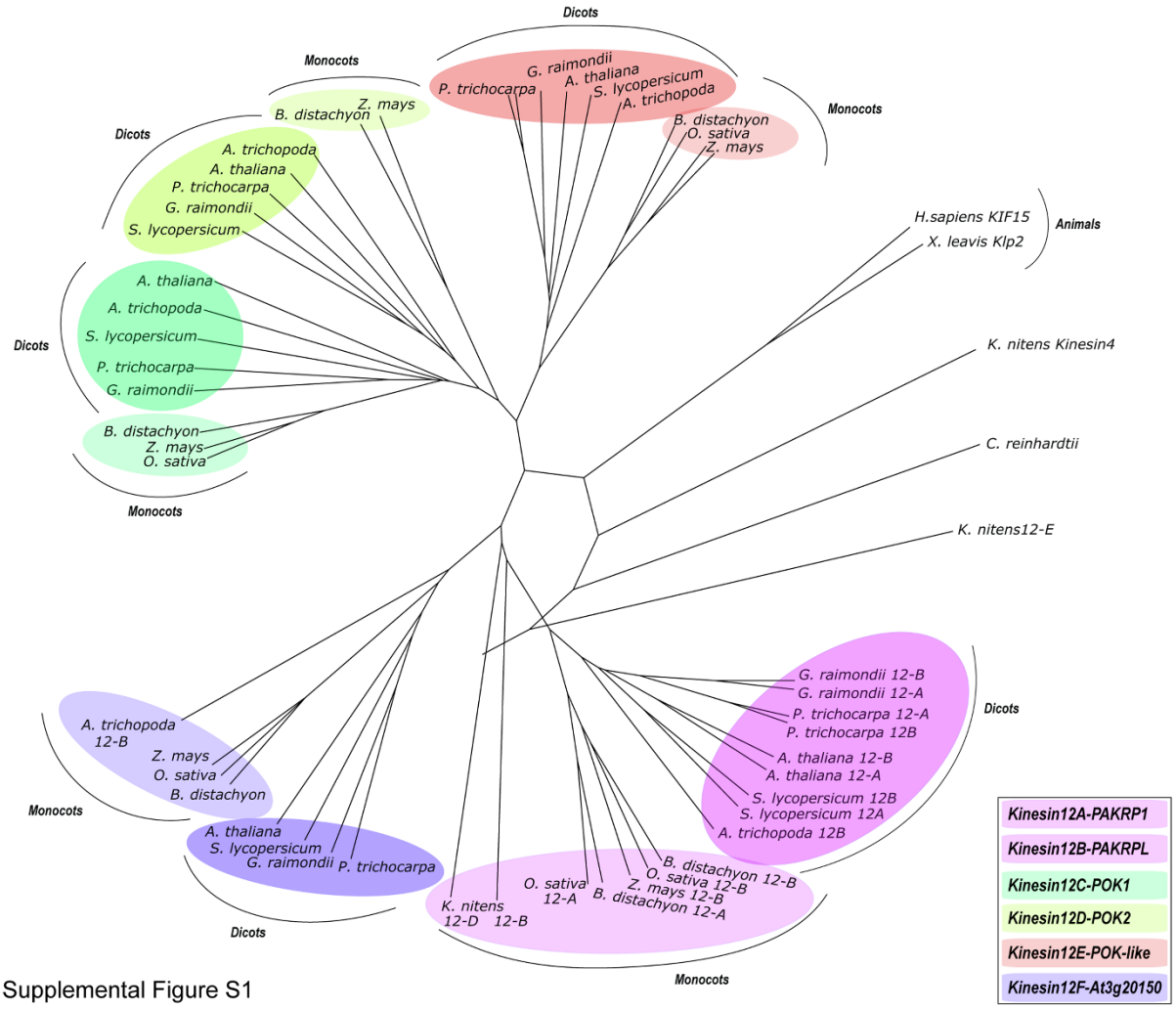

Supplemental Figure S1

Supplemental Figure S2

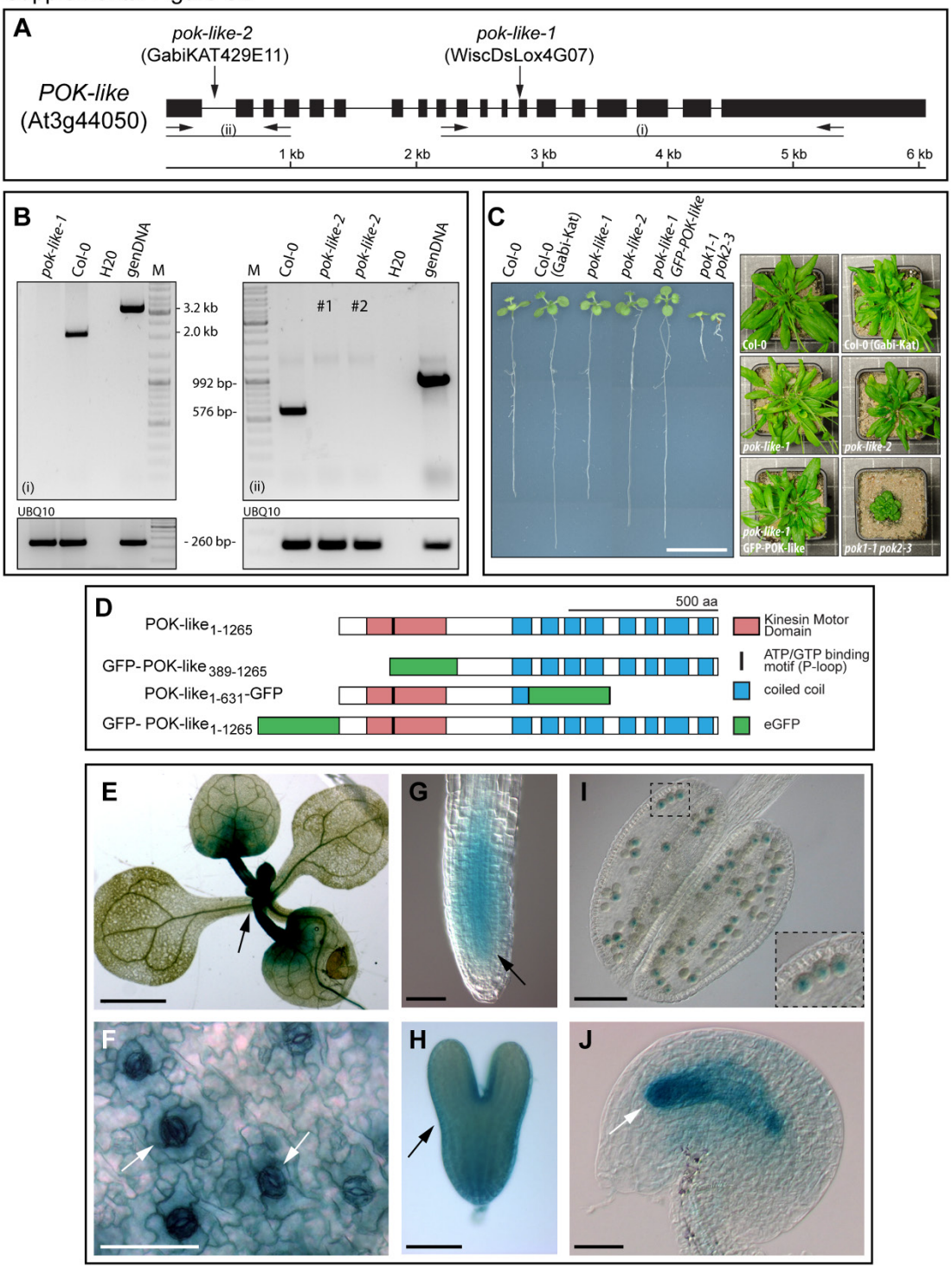

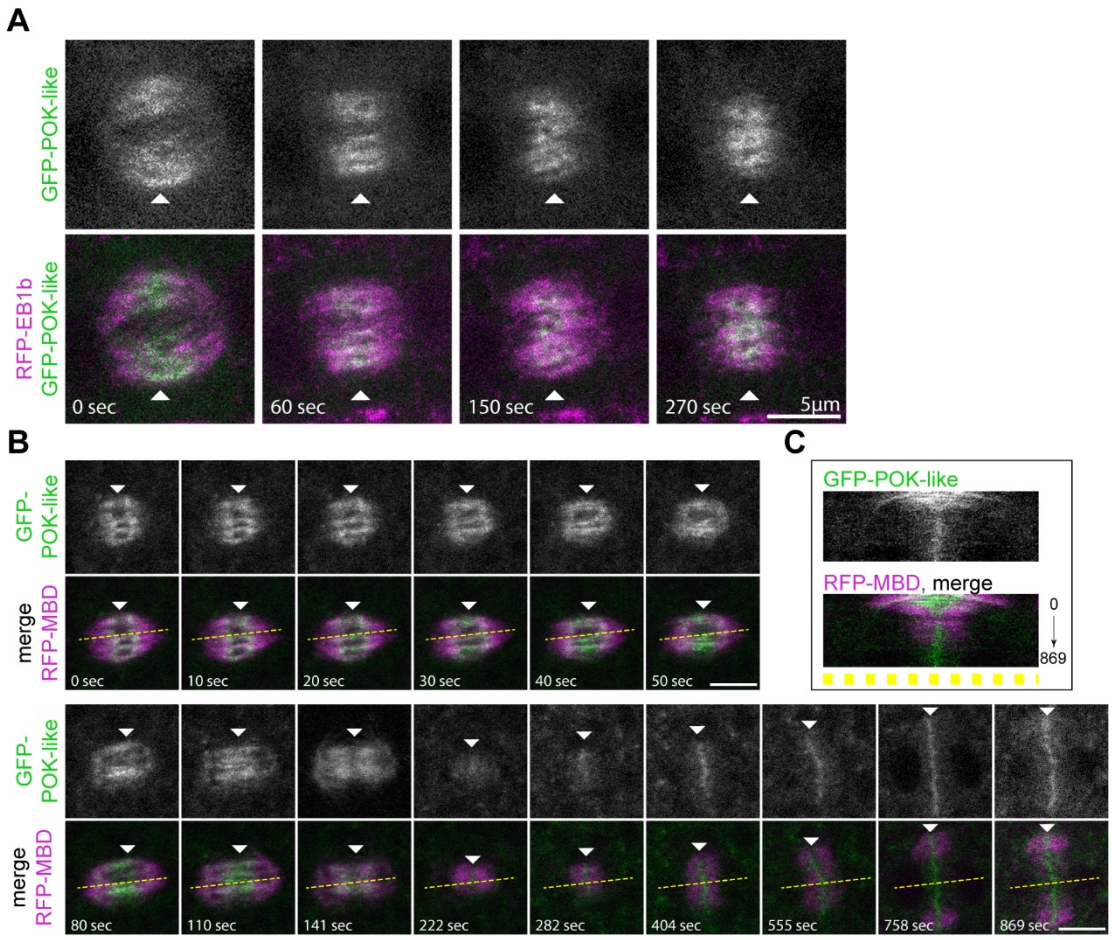

Supplemental Figure S3

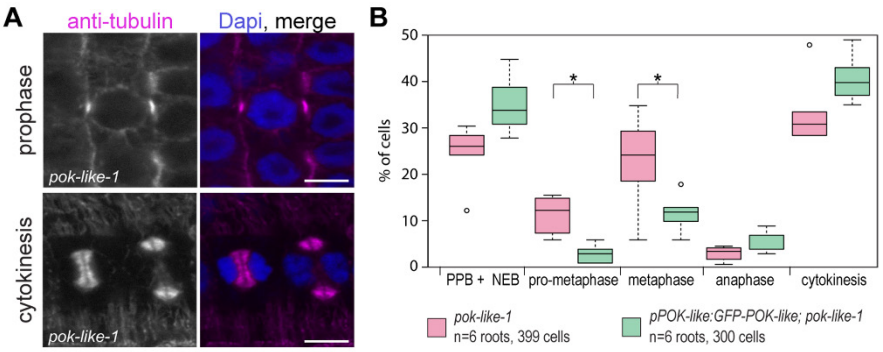

Supplemental Figure S4

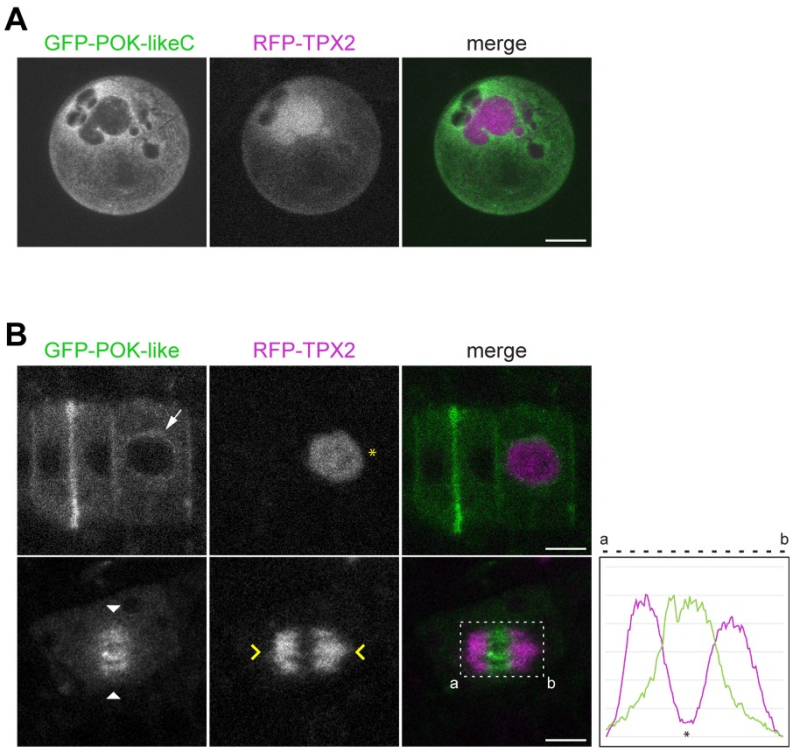

Supplemental Figure. S5

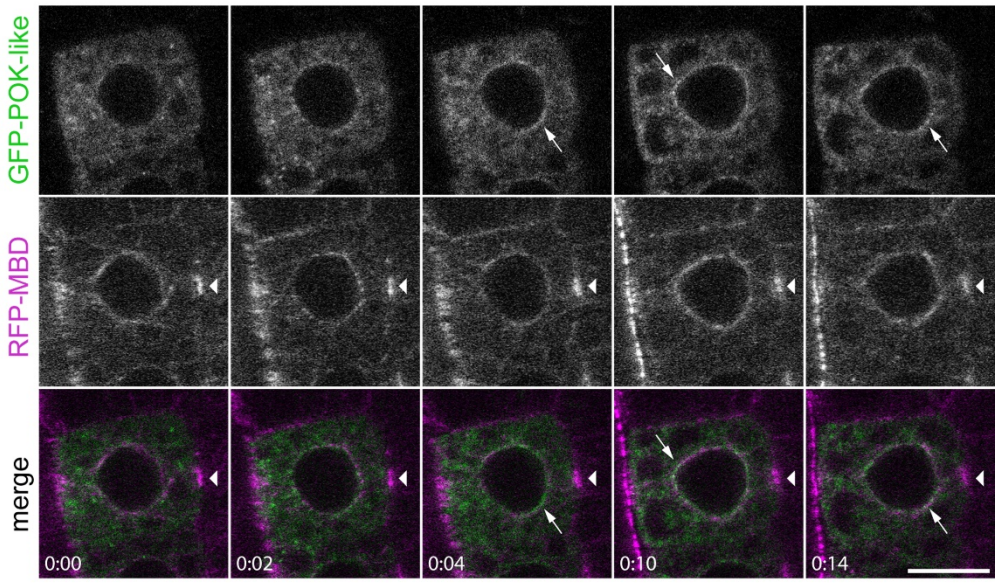

Supplemental Figure S6

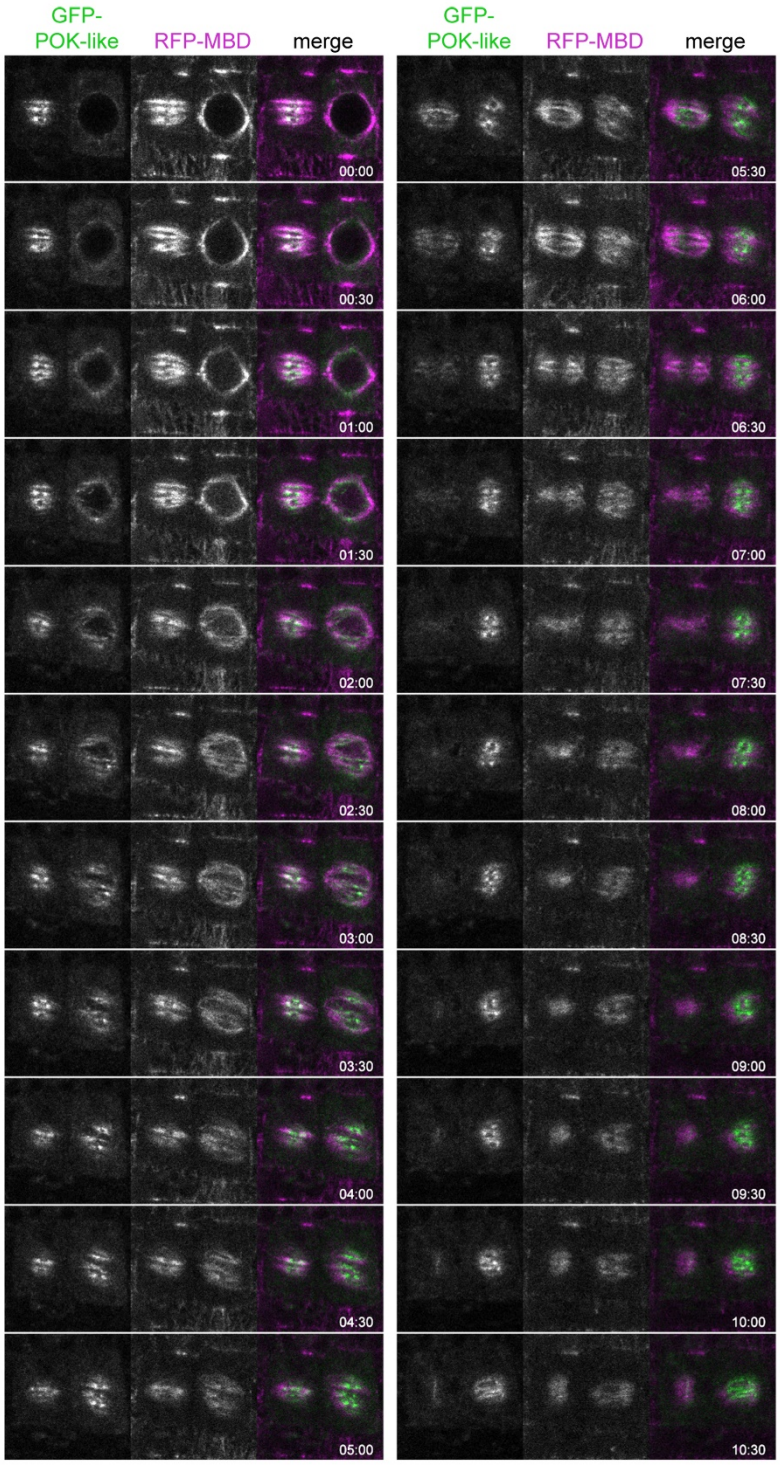

Supplemental Figure S7

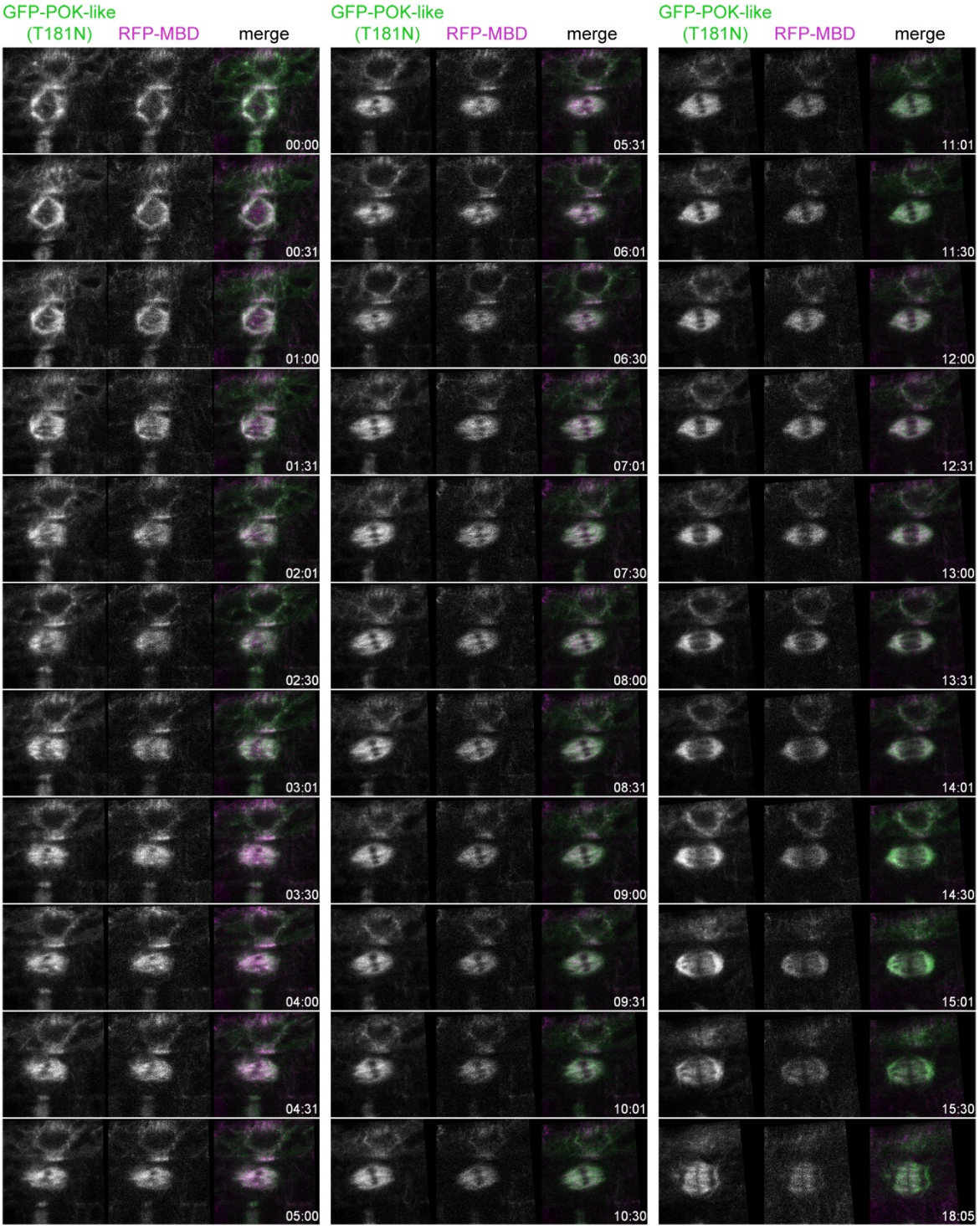

Supplemental Figure S8

8. References

Ambrose, C., Allard, J. F., Cytrynbaum, E. N. and Wasteneys, G. O. (2011) 'A CLASP-modulated cell edge barrier mechanism drives cell-wide cortical microtubule organization in Arabidopsis', *Nat Commun,* 2, pp. 430.

Ambrose, J. C. and Cyr, R. (2007) 'The Kinesin ATK5 Functions in Early Spindle Assembly in Arabidopsis', *The Plant Cell,* 19(1), pp. 226-236.

Ambrose, J. C. and Cyr, R. (2008) 'Mitotic spindle organization by the preprophase band', *Mol Plant,* 1(6), pp. 950-60.

Ambrose, J. C., Li, W., Marcus, A., Ma, H. and Cyr, R. (2005) 'A Minus-End–directed Kinesin with Plus-End Tracking Protein Activity Is Involved in Spindle Morphogenesis', *Molecular Biology of the Cell,* 16(4), pp. 1584-1592.

Ambrose, J. C., Shoji, T., Kotzer, A. M., Pighin, J. A. and Wasteneys, G. O. (2007) 'The Arabidopsis CLASP Gene Encodes a Microtubule-Associated Protein Involved in Cell Expansion and Division', *The Plant Cell,* 19(9), pp. 2763-2775.

Ambrose, J. C. and Wasteneys, G. O. (2008) 'CLASP modulates microtubule-cortex interaction during self-organization of acentrosomal microtubules', *Mol Biol Cell,* 19(11), pp. 4730-7.

Anne, B., Patrick, C. and A., N. E. (1998) 'Rigor-type mutation in the kinesin-related protein HsEg5 changes its subcellular localization and induces microtubule bundling', *Cell Motility,* 40(2), pp. 174-182.

Azimzadeh, J., Nacry, P., Christodoulidou, A., Drevensek, S., Camilleri, C., Amiour, N., Parcy, F., Pastuglia, M. and Bouchez, D. (2008) 'Arabidopsis TONNEAU1 proteins are essential for preprophase band formation and interact with centrin', *Plant Cell,* 20(8), pp. 2146-59.

Bancroft, J., Auckland, P., Samora, C. P. and McAinsh, A. D. (2014) 'Chromosome congression is promoted by CENP-Q- and CENP-E-dependent pathways', *Journal of Cell Science*.

Bannigan, A., Scheible, W.-R., Lukowitz, W., Fagerstrom, C., Wadsworth, P., Somerville, C. and Baskin, T. I. (2007) 'A conserved role for kinesin-5 in plant mitosis', *Journal of Cell Science,* 120(16), pp. 2819-2827.

Bischoff, F. R. and Görlich, D. (1997) 'RanBP1 is crucial for the release of RanGTP from importin β-related nuclear transport factors', *FEBS Letters,* 419(2-3), pp. 249-254.

Boc, A., Diallo, A. B. and Makarenkov, V. (2012) 'T-REX: a web server for inferring, validating and visualizing phylogenetic trees and networks', *Nucleic Acids Research,* 40(W1), pp. W573-W579.

Boleti, H., Karsenti, E. and Vernos, I. (1996) 'Xklp2, a Novel Xenopus Centrosomal Kinesin-like Protein Required for Centrosome Separation during Mitosis', *Cell,* 84(1), pp. 49-59.

Boruc, J., Griffis, A. H. N., Rodrigo-Peiris, T., Zhou, X., Tilford, B., Van Damme, D. and Meier, I. (2015) 'GAP Activity, but Not Subcellular Targeting, Is Required for Arabidopsis RanGAP Cellular and Developmental Functions', *The Plant Cell,* 27(7), pp. 1985-1998.

Boruc, J. and Van Damme, D. (2015) 'Endomembrane trafficking overarching cell plate formation', *Current Opinion in Plant Biology,* 28, pp. 92-98.

Boruc, J., Weimer, A. K., Stoppin-Mellet, V., Mylle, E., Kosetsu, K., Cedeno, C., Jaquinod, M., Njo, M., De Milde, L., Tompa, P., Gonzalez, N., Inze, D., Beeckman, T., Vantard, M. and Van Damme, D. (2017) 'Phosphorylation of MAP65-1 by Arabidopsis Aurora Kinases Is Required for Efficient Cell Cycle Progression', *Plant Physiol,* 173(1), pp. 582-599.

Bourne, H. R., Sanders, D. A. and McCormick, F. (1990) 'The GTPase superfamily: a conserved switch for diverse cell functions', *Nature,* 348, pp. 125.

Brembu, T., Winge, P., Bones, A. M. and Yang, Z. (2006) 'A RHOse by any other name: a comparative analysis of animal and plant Rho GTPases', *Cell Research,* 16, pp. 435.

Brouhard, G. J., Stear, J. H., Noetzel, T. L., Al-Bassam, J., Kinoshita, K., Harrison, S. C., Howard, J. and Hyman, A. A. (2008) 'XMAP215 Is a Processive Microtubule Polymerase', *Cell,* 132(1), pp. 79-88.

Brouwers, N., Mallol Martinez, N. and Vernos, I. (2017) 'Role of Kif15 and its novel mitotic partner KBP in K-fiber dynamics and chromosome alignment', *PLOS ONE,* 12(4), pp. e0174819.

Buschmann, H., Chan, J., Sanchez-Pulido, L., Andrade-Navarro, M. A., Doonan, J. H. and Lloyd, C. W. (2006) 'Microtubule-associated AIR9 recognizes the cortical division site at preprophase and cell-plate insertion', *Curr Biol,* 16(19), pp. 1938-43.

Buschmann, H., Dols, J., Kopischke, S., Peña, E. J., Andrade-Navarro, M. A., Heinlein, M., Szymanski, D. B., Zachgo, S., Doonan, J. H. and Lloyd, C. W. (2015) 'Arabidopsis KCBP interacts with AIR9 but stays in the cortical division zone throughout mitosis via its MyTH4-FERM domain', *Journal of Cell Science,* 128(11), pp. 2033-2046.

Camilleri, C., Azimzadeh, J., Pastuglia, M., Bellini, C., Grandjean, O. and Bouchez, D. (2002) 'The Arabidopsis TONNEAU Gene Encodes a Putative Novel Protein Phosphatase 2A Regulatory Subunit Essential for the Control of the Cortical Cytoskeleton', *The Plant Cell,* 14(4), pp. 833-845.

Chen, C., Marcus, A., Li, W., Hu, Y., Calzada, J.-P. V., Grossniklaus, U., Cyr, R. J. and Ma, H. (2002) 'The Arabidopsis ATK1 gene is required for spindle morphogenesis in male meiosis', *Development,* 129(10), pp. 2401-2409.

Chow, C.-M., Neto, H., Foucart, C. and Moore, I. (2008) 'Rab-A2 and Rab-A3 GTPases Define a trans-Golgi Endosomal Membrane Domain in ArabidopsisThat Contributes Substantially to the Cell Plate', *The Plant Cell,* 20(1), pp. 101-123.

Chugh, M., Reißner, M., Bugiel, M., Lipka, E., Herrmann, A., Roy, B., Müller, S. and Schäffer, E. (2018) 'Phragmoplast Orienting Kinesin 2 Is a Weak Motor Switching between Processive and Diffusive Modes', *Biophysical Journal,* 115(2), pp. 375-385.

Ciferri, C., De Luca, J., Monzani, S., Ferrari, K. J., Ristic, D., Wyman, C., Stark, H., Kilmartin, J., Salmon, E. D. and Musacchio, A. (2005) 'Architecture of the Human Ndc80-Hec1 Complex, a Critical Constituent of the Outer Kinetochore', *Journal of Biological Chemistry,* 280(32), pp. 29088-29095.

Clarke, P. R. and Zhang, C. (2008) 'Spatial and temporal coordination of mitosis by Ran GTPase', *Nature Reviews Molecular Cell Biology,* 9, pp. 464.

Cleary, A. L. (1995) 'F-actin redistributions at the division site in livingTradescantia stomatal complexes as revealed by microinjection of rhodamine-phalloidin', *Protoplasma,* 185(3), pp. 152-165.

Cleary, A. L., Gunning, B. E. S., Wasteneys, G. O. and Hepler, P. K. (1992) 'Microtubule and F-actin dynamics at the division site in living Tradescantia stamen hair cells', *Journal of Cell Science,* 103(4), pp. 977-988.

Cleveland, D. W., Mao, Y. and Sullivan, K. F. (2003) 'Centromeres and Kinetochores: From Epigenetics to Mitotic Checkpoint Signaling', *Cell,* 112(4), pp. 407-421.

Cole, D. G., Saxton, W. M., Sheehan, K. B. and Scholey, J. M. (1994) 'A "slow" homotetrameric kinesin-related motor protein purified from Drosophila embryos', *Journal of Biological Chemistry,* 269(37), pp. 22913-22916.

Conduit, P. T., Richens, J. H., Wainman, A., Holder, J., Vicente, C. C., Pratt, M. B., Dix, C. I., Novak, Z. A., Dobbie, I. M., Schermelleh, L. and Raff, J. W. (2014) 'A molecular mechanism of mitotic centrosome assembly in Drosophila', *eLife,* 3, pp. e03399.

de Keijzer, J., Kieft, H., Ketelaar, T., Goshima, G. and Janson, M. E. (2017) 'Shortening of Microtubule Overlap Regions Defines Membrane Delivery Sites during Plant Cytokinesis', *Current Biology,* 27(4), pp. 514-520.

Dhatchinamoorthy, K., Mattingly, M. and Gerton, J. L. (2018) 'Regulation of kinetochore configuration during mitosis', *Current Genetics*.

Drechsler, H. and McAinsh, A. D. (2016) 'Kinesin-12 motors cooperate to suppress microtubule catastrophes and drive the formation of parallel microtubule bundles', *Proceedings of the National Academy of Sciences*.

Drechsler, H., McHugh, T., Singleton, M. R., Carter, N. J. and McAinsh, A. D. (2014) 'The Kinesin-12 Kif15 is a processive track-switching tetramer', *eLife,* 3, pp. e01724.

Drevensek, S., Goussot, M., Duroc, Y., Christodoulidou, A., Steyaert, S., Schaefer, E., Duvernois, E., Grandjean, O., Vantard, M., Bouchez, D. and Pastuglia, M. (2012) 'The Arabidopsis TRM1–TON1 Interaction Reveals a Recruitment Network Common to Plant Cortical Microtubule Arrays and Eukaryotic Centrosomes', *The Plant Cell,* 24(1), pp. 178-191.

Du, Y. and Dawe, R. K. (2007) 'Maize NDC80 is a constitutive feature of the central kinetochore', *Chromosome Research,* 15(6), pp. 767-775.

Endow, S. A. (1999) 'Determinants of molecular motor directionality', *Nature Cell Biology,* 1, pp. E163.

Euteneuer, U., Jackson, W. T. and McIntosh, J. R. (1982) 'Polarity of spindle microtubules in Haemanthus endosperm', *The Journal of Cell Biology,* 94(3), pp. 644-653.

Evrard, J.-L., Pieuchot, L., Vos, J. W., Vernos, I. and Schmit, A.-C. (2009) 'Plant TPX2 and related proteins', *Plant Signaling & Behavior,* 4(1), pp. 69-72.

Fache, V., Gaillard, J., Van Damme, D., Geelen, D., Neumann, E., Stoppin-Mellet, V. and Vantard, M. (2010) 'Arabidopsis kinetochore fiber-associated MAP65-4 cross-links microtubules and promotes microtubule bundle elongation', *Plant Cell,* 22(11), pp. 3804-15.

Feiguelman, G., Fu, Y. and Yalovsky, S. (2018) 'ROP GTPases Structure-Function and Signaling Pathways', *Plant Physiology,* 176(1), pp. 57-79.

Ferenz, N. P., Paul, R., Fagerstrom, C., Mogilner, A. and Wadsworth, P. (2009) 'Dynein Antagonizes Eg5 by Crosslinking and Sliding Antiparallel Microtubules', *Current Biology,* 19(21), pp. 1833-1838.

Fu, Y., Gu, Y., Zheng, Z., Wasteneys, G. and Yang, Z. (2005) 'Arabidopsis Interdigitating Cell Growth Requires Two Antagonistic Pathways with Opposing Action on Cell Morphogenesis', *Cell,* 120(5), pp. 687-700.

Fu, Y., Li, H. and Yang, Z. (2002) 'The ROP2 GTPase Controls the Formation of Cortical Fine F-Actin and the Early Phase of Directional Cell Expansion during Arabidopsis Organogenesis', *The Plant Cell,* 14(4), pp. 777-794.

Fu, Y., Xu, T., Zhu, L., Wen, M. and Yang, Z. (2009) 'A ROP GTPase Signaling Pathway Controls Cortical Microtubule Ordering and Cell Expansion in Arabidopsis', *Current Biology,* 19(21), pp. 1827-1832.

Gadde, S. and Heald, R. (2004) 'Mechanisms and Molecules of the Mitotic Spindle', *Current Biology,* 14(18), pp. R797-R805.

Gaillard, J., Neumann, E., Damme, D. V., Stoppin-Mellet, V., Ebel, C., Barbier, E., Geelen, D., Vantard, M. and Drubin, D. G. (2008) 'Two Microtubule-associated Proteins of Arabidopsis MAP65s Promote Antiparallel Microtubule Bundling', *Molecular Biology of the Cell,* 19(10), pp. 4534-4544.

Goshima, G. and Kimura, A. (2010) 'New look inside the spindle: microtubule-dependent microtubule generation within the spindle', *Current Opinion in Cell Biology,* 22(1), pp. 44-49.

Grefen, C. and Blatt, M. R. (2012) 'A 2in1 cloning system enables ratiometric bimolecular fluorescence complementation (rBiFC)', *BioTechniques,* 53(5), pp. 311-314.

Haizel, T., Merkle, T., Pay, A., Fejes, E. and Nagy, F. (1997) 'Characterization of proteins that interact with the GTP-bound form of the regulatory GTPase Ran in Arabidopsis', *The Plant Journal,* 11(1), pp. 93-103.

Hála, M., Cole, R., Synek, L., Drdová, E., Pečenková, T., Nordheim, A., Lamkemeyer, T., Madlung, J., Hochholdinger, F., Fowler, J. E. and Žárský, V. (2008) 'An Exocyst Complex Functions in Plant Cell Growth in Arabidopsis and Tobacco', *The Plant Cell,* 20(5), pp. 1330-1345.

Hancock, W. O. (2008) 'Intracellular Transport: Kinesins Working Together', *Current Biology,* 18(16), pp. R715-R717.

Hancock, William O. (2014) 'Mitotic Kinesins: A Reason to Delve into Kinesin-12', *Current Biology,* 24(19), pp. R968-R970.

Heald, R., Tournebize, R., Blank, T., Sandaltzopoulos, R., Becker, P., Hyman, A. and Karsenti, E. (1996) 'Self-organization of microtubules into bipolar spindles around artificial chromosomes in Xenopus egg extracts', *Nature,* 382, pp. 420.

Heasman, S. J. and Ridley, A. J. (2008) 'Mammalian Rho GTPases: new insights into their functions from in vivo studies', *Nature Reviews Molecular Cell Biology,* 9, pp. 690.

Hecker, A., Wallmeroth, N., Peter, S., Blatt, M. R., Harter, K. and Grefen, C. (2015) 'Binary 2in1 Vectors Improve in Planta (Co)localization and Dynamic Protein Interaction Studies', *Plant Physiology,* 168(3), pp. 776-787.

Helenius, J., Brouhard, G., Kalaidzidis, Y., Diez, S. and Howard, J. (2006) 'The depolymerizing kinesin MCAK uses lattice diffusion to rapidly target microtubule ends', *Nature,* 441, pp. 115.

Heng, Y.-W. and Koh, C.-G. (2010) 'Actin cytoskeleton dynamics and the cell division cycle', *The International Journal of Biochemistry & Cell Biology,* 42(10), pp. 1622-1633.

Hentrich, C. and Surrey, T. (2010) 'Microtubule organization by the antagonistic mitotic motors kinesin-5 and kinesin-14', *The Journal of Cell Biology,* 189(3), pp. 465-480.

Herrmann, A., Livanos, P., Lipka, E., Gadeyne, A., Hauser, M. T., Van Damme, D. and Müller, S. (2018) 'Dual localized kinesin-12 POK2 plays multiple roles during cell division and interacts with MAP65-3', *EMBO reports*.

Ho, C.-M. K., Hotta, T., Guo, F., Roberson, R. W., Lee, Y.-R. J. and Liu, B. (2011a) 'Interaction of Antiparallel Microtubules in the Phragmoplast Is Mediated by the Microtubule-Associated Protein MAP65-3 in Arabidopsis', *The Plant Cell,* 23(8), pp. 2909-2923.

Ho, C. M., Hotta, T., Guo, F., Roberson, R. W., Lee, Y. R. and Liu, B. (2011b) 'Interaction of antiparallel microtubules in the phragmoplast is mediated by the microtubule-associated protein MAP65-3 in Arabidopsis', *Plant Cell,* 23(8), pp. 2909-23.

Hoehenwarter, W., Thomas, M., Nukarinen, E., Egelhofer, V., Röhrig, H., Weckwerth, W., Conrath, U. and Beckers, G. J. M. (2013) 'Identification of Novel in vivo MAP Kinase Substrates in Arabidopsis thaliana Through Use of Tandem Metal Oxide Affinity Chromatography', *Molecular & Cellular Proteomics,* 12(2), pp. 369-380.

Huang, J.-b., Liu, H., Chen, M., Li, X., Wang, M., Yang, Y., Wang, C., Huang, J., Liu, G., Liu, Y., Xu, J., Cheung, A. Y. and Tao, L.-z. (2014) 'ROP3 GTPase Contributes to Polar Auxin Transport and Auxin Responses and Is Important for Embryogenesis and Seedling Growth in Arabidopsis', *The Plant Cell,* 26(9), pp. 3501-3518.

Hussey, P. J., Hawkins, T. J., Igarashi, H., Kaloriti, D. and Smertenko, A. (2002) 'The plant cytoskeleton: recent advances in the study of the plant microtubule-associated proteins MAP-65, MAP-190 and the Xenopus MAP215-like protein, MOR1', *Plant Mol Biol,* 50(6), pp. 915-24.

Hwang, J.-U., Vernoud, V., Szumlanski, A., Nielsen, E. and Yang, Z. (2008) 'A Tip-Localized RhoGAP Controls Cell Polarity by Globally Inhibiting Rho GTPase at the Cell Apex', *Current Biology,* 18(24), pp. 1907-1916.

Hyman, A. A. and Karsenti, E. (1996) 'Morphogenetic Properties of Microtubules and Mitotic Spindle Assembly', *Cell,* 84(3), pp. 401-410.

Ingouff, M., Gerald, J. N. F., Guérin, C., Robert, H., Sørensen, M. B., Damme, D. V., Geelen, D., Blanchoin, L. and Berger, F. (2005) 'Plant formin AtFH5 is an evolutionarily conserved actin nucleator involved in cytokinesis', *Nature Cell Biology,* 7, pp. 374.

Ito, M., Iwase, M., Kodama, H., Lavisse, P., Komamine, A., Nishihama, R., Machida, Y. and Watanabe, A. (1998) 'A Novel cis-Acting Element in Promoters of Plant B-Type Cyclin Genes Activates M Phase–Specific Transcription', *The Plant Cell,* 10(3), pp. 331-341.

Jens, M., Martina, B., Ursula, M., George, K., Gerd, H., Diedrik, M. and Jozef, Š. (2010) 'Arabidopsis MPK6 is involved in cell division plane control during early root development, and localizes to the pre-prophase band, phragmoplast, trans-Golgi network and plasma membrane', *The Plant Journal,* 61(2), pp. 234-248.

Kalab, P., Weis, K. and Heald, R. (2002) 'Visualization of a Ran-GTP Gradient in Interphase and Mitotic Xenopus Egg Extracts', *Science,* 295(5564), pp. 2452-2456.

Karnik, R., Zhang, B., Waghmare, S., Aderhold, C., Grefen, C. and Blatt, M. R. (2015) 'Binding of SEC11 Indicates Its Role in SNARE Recycling after Vesicle Fusion and Identifies Two Pathways for Vesicular Traffic to the Plasma Membrane', *The Plant Cell,* 27(3), pp. 675-694.

Kashlna, A. S., Baskin, R. J., Cole, D. G., Wedaman, K. P., Saxton, W. M. and Scholey, J. M. (1996) 'A bipolar kinesin', *Nature,* 379, pp. 270.

Katoh, K., Kuma, K.-i., Toh, H. and Miyata, T. (2005) 'MAFFT version 5: improvement in accuracy of multiple sequence alignment', *Nucleic Acids Research,* 33(2), pp. 511-518.

Kawamura, E., Himmelspach, R., Rashbrooke, M. C., Whittington, A. T., Gale, K. R., Collings, D. A. and Wasteneys, G. O. (2006) 'MICROTUBULE ORGANIZATION 1 Regulates Structure and Function of Microtubule Arrays during Mitosis and Cytokinesis in the Arabidopsis Root', *Plant Physiology,* 140(1), pp. 102-114.

Kawamura, E. and Wasteneys, G. O. (2008) 'MOR1, the Arabidopsis thaliana homologue of Xenopus MAP215, promotes rapid growth and shrinkage, and suppresses the pausing of microtubules in vivo', *Journal of Cell Science,* 121(24), pp. 4114-4123.

Khodjakov, A., Copenagle, L., Gordon, M. B., Compton, D. A. and Kapoor, T. M. (2003) 'Minus-end capture of preformed kinetochore fibers contributes to spindle morphogenesis', *The Journal of Cell Biology,* 160(5), pp. 671-683.

Kim, S.-H. and Roux, S. J. (2003) 'An Arabidopsis Ran-binding protein, AtRanBP1c, is a co-activator of Ran GTPase-activating protein and requires the C-terminus for its cytoplasmic localization', *Planta,* 216(6), pp. 1047-1052.

Kirik, A., Ehrhardt, D. W. and Kirik, V. (2012) 'TONNEAU2/FASS Regulates the Geometry of Microtubule Nucleation and Cortical Array Organization in Interphase Arabidopsis Cells', *The Plant Cell,* 24(3), pp. 1158-1170.

Kirik, V., Herrmann, U., Parupalli, C., Sedbrook, J. C., Ehrhardt, D. W. and Hülskamp, M. (2007) 'CLASP localizes in two discrete patterns on cortical microtubules and is required for cell morphogenesis and cell division in Arabidopsis', *Journal of Cell Science,* 120(24), pp. 4416-4425.

Kirschner, M. and Mitchison, T. (1986) 'Beyond self-assembly: From microtubules to morphogenesis', *Cell,* 45(3), pp. 329-342.

Klahre, U. and Kost, B. (2006) 'Tobacco RhoGTPase ACTIVATING PROTEIN1 Spatially Restricts Signaling of RAC/Rop to the Apex of Pollen Tubes', *The Plant Cell,* 18(11), pp. 3033-3046.

Kline-Smith, S. L., Khodjakov, A., Hergert, P. and Walczak, C. E. (2004) 'Depletion of Centromeric MCAK Leads to Chromosome Congression and Segregation Defects Due to Improper Kinetochore Attachments', *Molecular Biology of the Cell,* 15(3), pp. 1146-1159.

Kojo, K. H., Higaki, T., Kutsuna, N., Yoshida, Y., Yasuhara, H. and Hasezawa, S. (2013) 'Roles of Cortical Actin Microfilament Patterning in Division Plane Orientation in Plants', *Plant and Cell Physiology,* 54(9), pp. 1491-1503.

Komaki, S., Abe, T., Coutuer, S., Inzé, D., Russinova, E. and Hashimoto, T. (2010) 'Nuclear-localized subtype of end-binding 1 protein regulates spindle organization in Arabidopsis', *Journal of Cell Science*.

Komis, G., Illés, P., Beck, M. and Šamaj, J. (2011) 'Microtubules and mitogen-activated protein kinase signalling', *Current Opinion in Plant Biology,* 14(6), pp. 650-657.

Kosetsu, K., de Keijzer, J., Janson, M. E. and Goshima, G. (2013) 'MICROTUBULE-ASSOCIATED PROTEIN65 Is Essential for Maintenance of Phragmoplast Bipolarity and Formation of the Cell Plate in Physcomitrella patens', *The Plant Cell,* 25(11), pp. 4479-4492.

Kosetsu, K., Matsunaga, S., Nakagami, H., Colcombet, J., Sasabe, M., Soyano, T., Takahashi, Y., Hirt, H. and Machida, Y. (2010) 'The MAP Kinase MPK4 Is Required for Cytokinesis in Arabidopsis thaliana', *The Plant Cell Online*.

Lampard, G. R., MacAlister, C. A. and Bergmann, D. C. (2008) 'Arabidopsis Stomatal Initiation Is Controlled by MAPK-Mediated Regulation of the bHLH SPEECHLESS', *Science,* 322(5904), pp. 1113-1116.

Lee, Y.-R. J., Li, Y. and Liu, B. (2007) 'Two Arabidopsis Phragmoplast-Associated Kinesins Play a Critical Role in Cytokinesis during Male Gametogenesis', *The Plant Cell,* 19(8), pp. 2595-2605.

Lee, Y.-R. J. and Liu, B. (2004) 'Cytoskeletal Motors in Arabidopsis. Sixty-One Kinesins and Seventeen Myosins', *Plant Physiology,* 136(4), pp. 3877-3883.

Lee, Y.-R. J. and Liu, B. (2013) 'The rise and fall of the phragmoplast microtubule array', *Current Opinion in Plant Biology,* 16(6), pp. 757-763.

Lee, Y. R. J. and Liu, B. (2000) 'Identification of a phragmoplast-associated kinesin-related protein in higher plants', *Current Biology,* 10(13), pp. 797-800.

Lemmon, M. A. and Ferguson, K. M. (2000) 'Signal-dependent membrane targeting by pleckstrin homology (PH) domains', *Biochemical Journal,* 350(Pt 1), pp. 1-18.

Lermontova, I., Rutten, T. and Schubert, I. (2011) 'Deposition, turnover, and release of CENH3 at Arabidopsis centromeres', *Chromosoma,* 120(6), pp. 633-640.

Li, H., Sun, B., Sasabe, M., Deng, X., Machida, Y., Lin, H., Julie Lee, Y. R. and Liu, B. (2017) 'Arabidopsis MAP65-4 plays a role in phragmoplast microtubule organization and marks the cortical cell division site', *New Phytol,* 215(1), pp. 187-201.

Li, X. and Dawe, R. K. (2009) 'Fused sister kinetochores initiate the reductional division in meiosis I', *Nature Cell Biology,* 11, pp. 1103.

Lin, D., Cao, L., Zhou, Z., Zhu, L., Ehrhardt, D., Yang, Z. and Fu, Y. (2013) 'Rho GTPase Signaling Activates Microtubule Severing to Promote Microtubule Ordering in Arabidopsis', *Current Biology,* 23(4), pp. 290-297.

Lipka, E., Gadeyne, A., Stöckle, D., Zimmermann, S., De Jaeger, G., Ehrhardt, D. W., Kirik, V., Van Damme, D. and Muller, S. (2014) 'The Phragmoplast-Orienting Kinesin-12 Class Proteins Translate the Positional Information of the Preprophase Band to Establish the Cortical Division Zone in Arabidopsis thaliana', *Plant Cell,* 26(6), pp. 2617-2632.

Lipka, E., Herrmann, A. and Mueller, S. (2015) 'Mechanisms of plant cell division', *Wiley Interdiscip Rev Dev Biol,* 4(4), pp. 391-405.

Lipka, E. and Muller, S. (2012) 'Potential roles for Kinesins at the cortical division site', *Front Plant Sci,* 3, pp. 158.

Mann, B. J., Balchand, S. K., Wadsworth, P. and Zheng, Y. (2017) 'Regulation of Kif15 localization and motility by the C-terminus of TPX2 and microtubule dynamics', *Molecular Biology of the Cell,* 28(1), pp. 65-75.

Mao, G., Buschmann, H., Doonan, J. H. and Lloyd, C. W. (2006) 'The role of MAP65-1 in microtubule bundling during Zinnia tracheary element formation', *J Cell Sci,* 119(Pt 4), pp. 753-8.

Mao, T., Jin, L., Li, H., Liu, B. and Yuan, M. (2005) 'Two microtubule-associated proteins of the Arabidopsis MAP65 family function differently on microtubules', *Plant Physiol,* 138(2), pp. 654-62.

Marcus, A. I., Li, W., Ma, H., Cyr, R. J. and Preuss, D. (2003) 'A Kinesin Mutant with an Atypical Bipolar Spindle Undergoes Normal Mitosis', *Molecular Biology of the Cell,* 14(4), pp. 1717-1726.

Martinez, P., Luo, A., Sylvester, A. and Rasmussen, C. G. (2017) 'Proper division plane orientation and mitotic progression together allow normal growth of maize', *Proceedings of the National Academy of Sciences*.

Masoud, K., Herzog, E., Chabouté, M.-E. and Schmit, A.-C. (2013a) 'Microtubule nucleation and establishment of the mitotic spindle in vascular plant cells', *The Plant Journal,* 75(2), pp. 245-257.

Masoud, K., Herzog, E., Chabouté, M. E. and Schmit, A. C. (2013b) 'Microtubule nucleation and establishment of the mitotic spindle in vascular plant cells', *The Plant Journal,* 75(2), pp. 245-257.

Meng, Q., Du, J., Li, J., Lu, X., Zeng, X., Yuan, M. and Mao, T. (2010) 'Tobacco microtubule-associated protein, MAP65-1c, bundles and stabilizes microtubules', *Plant Mol Biol,* 74(6), pp. 537-47.

Menges, M., Hennig, L., Gruissem, W. and Murray, J. A. H. (2003) 'Genome-wide gene expression in an Arabidopsis cell suspension', *Plant Molecular Biology,* 53(4), pp. 423-442.

Miki, T., Naito, H., Nishina, M. and Goshima, G. (2014) 'Endogenous localizome identifies 43 mitotic kinesins in a plant cell', *Proceedings of the National Academy of Sciences of the United States of America,* 111(11), pp. E1053-E1061.

Mineyuki, Y. and Palewitz, B. A. (1990) 'Relationship between preprophase band organization, F-actin and the division site in Allium', *Fluorescence and morphometric studies on cytochalasin-treated cells,* 97(2), pp. 283-295.

Mir, R., Morris, V. H., Buschmann, H. and Rasmussen, C. G. (2018) 'Division Plane Orientation Defects Revealed by a Synthetic Double Mutant Phenotype', *Plant Physiology,* 176(1), pp. 418-431.

Müller, S., Han, S. and Smith, L. G. (2006) 'Two Kinesins Are Involved in the Spatial Control of Cytokinesis in Arabidopsis thaliana', *Current Biology,* 16(9), pp. 888-894.

Müller, S. and Jürgens, G. (2016) 'Plant cytokinesis—No ring, no constriction but centrifugal construction of the partitioning membrane', *Seminars in Cell & Developmental Biology,* 53, pp. 10-18.

Müller, S., Smertenko, A., Wagner, V., Heinrich, M., Hussey, P. J. and Hauser, M.-T. (2004) 'The Plant Microtubule-Associated Protein AtMAP65-3/PLE Is Essential for Cytokinetic Phragmoplast Function', *Current Biology,* 14(5), pp. 412-417.

Murata, T., Sano, T., Sasabe, M., Nonaka, S., Higashiyama, T., Hasezawa, S., Machida, Y. and Hasebe, M. (2013) 'Mechanism of microtubule array expansion in the cytokinetic phragmoplast', *Nature Communications,* 4, pp. 1967.

Murata, T. and Wada, M. (1991) 'Effects of centrifugation on preprophase-band formation in Adiantum protonemata', *Planta,* 183(3), pp. 391-8.

Nakata, T. and Hirokawa, N. (1995) 'Point mutation of adenosine triphosphate-binding motif generated rigor kinesin that selectively blocks anterograde lysosome membrane transport', *The Journal of Cell Biology,* 131(4), pp. 1039-1053.

Otegui, M. S., Verbrugghe, K. J. and Skop, A. R. (2005) 'Midbodies and phragmoplasts: analogous structures involved in cytokinesis', *Trends in Cell Biology,* 15(8), pp. 404-413.

Panteris, E. (2008) 'Cortical actin filaments at the division site of mitotic plant cells: a reconsideration of the 'actin-depleted zone'', *New Phytologist,* 179(2), pp. 334-341.

Park, M., Touihri, S., Müller, I., Mayer, U. and Jürgens, G. (2012) 'Sec1/Munc18 Protein Stabilizes Fusion-Competent Syntaxin for Membrane Fusion in Arabidopsis Cytokinesis', *Developmental Cell,* 22(5), pp. 989-1000.

Petrovská, B., Cenklová, V., Pochylová, Ž., Kourová, H., Doskočilová, A., Plíhal, O., Binarová, L. and Binarová, P. (2012) 'Plant Aurora kinases play a role in maintenance of primary meristems and control of endoreduplication', *New Phytologist,* 193(3), pp. 590-604.

Petrovská, B., Jeřábková, H., Kohoutová, L., Cenklová, V., Pochylová, Ž., Gelová, Z., Kočárová, G., Váchová, L., Kurejová, M., Tomaštíková, E. and Binarová, P. (2013) 'Overexpressed TPX2 causes ectopic formation of microtubular arrays in the nuclei of acentrosomal plant cells', *Journal of Experimental Botany,* 64(14), pp. 4575-4587.

Pietra, S., Gustavsson, A., Kiefer, C., Kalmbach, L., Horstedt, P., Ikeda, Y., Stepanova, A. N., Alonso, J. M. and Grebe, M. (2013) 'Arabidopsis SABRE and CLASP interact to stabilize cell division plane orientation and planar polarity', *Nat Commun,* 4, pp. 2779.

Powers, A. F., Franck, A. D., Gestaut, D. R., Cooper, J., Gracyzk, B., Wei, R. R., Wordeman, L., Davis, T. N. and Asbury, C. L. (2009) 'The Ndc80 Kinetochore Complex Forms Load-Bearing Attachments to Dynamic Microtubule Tips via Biased Diffusion', *Cell,* 136(5), pp. 865-875.

Rasmussen, C. G., Sun, B. and Smith, L. G. (2011) 'Tangled localization at the cortical division site of plant cells occurs by several mechanisms', *J Cell Sci,* 124(Pt 2), pp. 270-9.

Rasmussen, C. G., Wright, A. J. and Muller, S. (2013) 'The role of the cytoskeleton and associated proteins in determination of the plant cell division plane', *Plant J,* 75(2), pp. 258-69.

Reber, S. and Hyman, A. A. (2015) 'Emergent Properties of the Metaphase Spindle', *Cold Spring Harbor Perspectives in Biology,* 7(7).

Reddy, A. S. and Day, I. S. (2001) 'Kinesins in the Arabidopsis genome: A comparative analysis among eukaryotes', *BMC Genomics,* 2(1), pp. 2.

Rodrigo-Peiris, T., Xu, X. M., Zhao, Q., Wang, H.-J. and Meier, I. (2011) 'RanGAP is required for post-meiotic mitosis in female gametophyte development in Arabidopsis thaliana', *Journal of Experimental Botany,* 62(8), pp. 2705-2714.

Rybak, K., Steiner, A., Synek, L., Klaeger, S., Kulich, I., Facher, E., Wanner, G., Kuster, B., Zarsky, V., Persson, S. and Assaad, Farhah F. (2014) 'Plant Cytokinesis Is Orchestrated by the Sequential Action of the TRAPPII and Exocyst Tethering Complexes', *Developmental Cell,* 29(5), pp. 607-620.

Samuels, A. L., Giddings, T. H. and Staehelin, L. A. (1995) 'Cytokinesis in tobacco BY-2 and root tip cells: a new model of cell plate formation in higher plants', *The Journal of Cell Biology,* 130(6), pp. 1345-1357.

Sano, T., Higaki, T., Oda, Y., Hayashi, T. and Hasezawa, S. (2005) 'Appearance of actin microfilament 'twin peaks' in mitosis and their function in cell plate formation, as visualized in tobacco BY-2 cells expressing GFP–fimbrin', *The Plant Journal,* 44(4), pp. 595-605.

Santaguida, S. and Musacchio, A. (2009) 'The life and miracles of kinetochores', *The EMBO Journal,* 28(17), pp. 2511-2531.

Sasabe, M., Boudolf, V., De Veylder, L., Inzé, D., Genschik, P. and Machida, Y. (2011a) 'Phosphorylation of a mitotic kinesin-like protein and a MAPKKK by cyclin-dependent kinases (CDKs) is involved in the transition to cytokinesis in plants', *Proceedings of the National Academy of Sciences,* 108(43), pp. 17844-17849.

Sasabe, M., Kosetsu, K., Hidaka, M., Murase, A. and Machida, Y. (2011b) 'Arabidopsis thaliana MAP65-1 and MAP65-2 function redundantly with MAP65-3/PLEIADE in cytokinesis downstream of MPK4', *Plant Signal Behav,* 6(5), pp. 743-7.

Sasabe, M. and Machida, Y. (2006) 'MAP65: a bridge linking a MAP kinase to microtubule turnover', *Curr Opin Plant Biol,* 9(6), pp. 563-70.

Schaefer, E., Belcram, K., Uyttewaal, M., Duroc, Y., Goussot, M., Legland, D., Laruelle, E., de Tauzia-Moreau, M. L., Pastuglia, M. and Bouchez, D. (2017) 'The preprophase band of microtubules controls the robustness of division orientation in plants', *Science,* 356(6334), pp. 186-189.

Seguí-Simarro, J. M., Austin, J. R., White, E. A. and Staehelin, L. A. (2004) 'Electron Tomographic Analysis of Somatic Cell Plate Formation in Meristematic Cells of Arabidopsis Preserved by High-Pressure Freezing', *The Plant Cell,* 16(4), pp. 836-856.

Sharp, D. J., Rogers, G. C. and Scholey, J. M. (2000) 'Microtubule motors in mitosis', *Nature,* 407, pp. 41.

Sigrist, C. J. A., de Castro, E., Cerutti, L., Cuche, B. A., Hulo, N., Bridge, A., Bougueleret, L. and Xenarios, I. (2013) 'New and continuing developments at PROSITE', *Nucleic Acids Research,* 41(D1), pp. D344-D347.

Smékalová, V., Luptovčiak, I., Komis, G., Šamajová, O., Ovečka, M., Doskočilová, A., Takáč, T., Vadovič, P., Novák, O., Pechan, T., Ziemann, A., Košútová, P. and Šamaj, J. (2014) 'Involvement of YODA and mitogen activated protein kinase 6 in Arabidopsis post-embryogenic root development through auxin up-regulation and cell division plane orientation', *New Phytologist,* 203(4), pp. 1175-1193.

Smertenko, A. (2014) 'Determination of phosphorylation sites in microtubule associated protein MAP65-1', *Methods Mol Biol,* 1171, pp. 161-70.

Smertenko, A., Assaad, F., Baluska, F., Bezanilla, M., Buschmann, H., Drakakaki, G., Hauser, M. T., Janson, M., Mineyuki, Y., Moore, I., Muller, S., Murata, T., Otegui, M. S., Panteris, E., Rasmussen, C., Schmit, A. C., Samaj, J., Samuels, L., Staehelin, L. A., Van Damme, D., Wasteneys, G. and Zarsky, V. (2017) 'Plant Cytokinesis: Terminology for Structures and Processes', *Trends Cell Biol,* 27(12), pp. 885-894.

Smertenko, A. P., Kaloriti, D., Chang, H. Y., Fiserova, J., Opatrny, Z. and Hussey, P. J. (2008) 'The C-terminal variable region specifies the dynamic properties of Arabidopsis microtubule-associated protein MAP65 isotypes', *Plant Cell,* 20(12), pp. 3346-58.

Smertenko, Andrei P., Piette, B. and Hussey, Patrick J. (2011) 'The Origin of Phragmoplast Asymmetry', *Current Biology,* 21(22), pp. 1924-1930.

Smirnova, E. A. and Baje, r. A. S. (1998) 'Early stages of spindle formation and independence of chromosome and microtubule cycles in Haemanthus endosperm', *Cell Motility,* 40(1), pp. 22-37.

Smirnova, E. A. and Bajer, A. S. (1992) 'Spindle poles in higher plant mitosis', *Cell Motility,* 23(1), pp. 1-7.

Spinner, L., Gadeyne, A., Belcram, K., Goussot, M., Moison, M., Duroc, Y., Eeckhout, D., De Winne, N., Schaefer, E., Van De Slijke, E., Persiau, G., Witters, E., Gevaert, K., De Jaeger, G., Bouchez, D., Van Damme, D. and Pastuglia, M. (2013) 'A protein phosphatase 2A complex spatially controls plant cell division', *Nature Communications,* 4, pp. 1863.

Staehelin, L. A. and Hepler, P. K. (1996) 'Cytokinesis in Higher Plants', *Cell,* 84(6), pp. 821-824.

Steiner, A., Müller, L., Rybak, K., Vodermaier, V., Facher, E., Thellmann, M., Ravikumar, R., Wanner, G., Hauser, M.-T. and Assaad, Farhah F. (2016a) 'The Membrane-Associated Sec1/Munc18 KEULE is Required for Phragmoplast Microtubule Reorganization During Cytokinesis in Arabidopsis', *Molecular Plant,* 9(4), pp. 528-540.

Steiner, A., Rybak, K., Altmann, M., McFarlane, H. E., Klaeger, S., Nguyen, N., Facher, E., Ivakov, A., Wanner, G., Kuster, B., Persson, S., Braun, P., Hauser, M. T. and Assaad, F. F. (2016b) 'Cell cycle-regulated PLEIADE/AtMAP65-3 links membrane and microtubule dynamics during plant cytokinesis', *The Plant Journal,* 88(4), pp. 531-541.

Stöckle, D., Herrmann, A., Lipka, E., Lauster, T., Gavidia, R., Zimmermann, S. and Muller, S. (2016) 'Putative RopGAPs impact division plane selection and interact with kinesin-12 POK1', *Nat Plants,* 2, pp. 16120.

Stoppin-Mellet, V., Fache, V., Portran, D., Martiel, J. L. and Vantard, M. (2013) 'MAP65 coordinate microtubule growth during bundle formation', *PLoS One,* 8(2), pp. e56808.

Strompen, G., El Kasmi, F., Richter, S., Lukowitz, W., Assaad, F. F., Jürgens, G. and Mayer, U. (2002) 'The Arabidopsis HINKEL Gene Encodes a Kinesin-Related Protein Involved in Cytokinesis and Is Expressed in a Cell Cycle-Dependent Manner', *Current Biology,* 12(2), pp. 153-158.

Struk, S. and Dhonukshe, P. (2014) 'MAPs: cellular navigators for microtubule array orientations in Arabidopsis', *Plant Cell Reports,* 33(1), pp. 1-21.

Sturgill, Emma G. and Ohi, R. (2013) 'Kinesin-12 Differentially Affects Spindle Assembly Depending on Its Microtubule Substrate', *Current Biology,* 23(14), pp. 1280-1290.

Sueishi, M., Takagi, M. and Yoneda, Y. (2000) 'The Forkhead-associated Domain of Ki-67 Antigen Interacts with the Novel Kinesin-like Protein Hklp2', *Journal of Biological Chemistry,* 275(37), pp. 28888-28892.

Suetsugu, N., Yamada, N., Kagawa, T., Yonekura, H., Uyeda, T. Q. P., Kadota, A. and Wada, M. (2010) 'Two kinesin-like proteins mediate actin-based chloroplast movement in Arabidopsis thaliana', *Proceedings of the National Academy of Sciences,* 107(19), pp. 8860-8865.

Takahashi, F., Yoshida, R., Ichimura, K., Mizoguchi, T., Seo, S., Yonezawa, M., Maruyama, K., Yamaguchi-Shinozaki, K. and Shinozaki, K. (2007) 'The Mitogen-Activated Protein Kinase Cascade MKK3–MPK6 Is an Important Part of the Jasmonate Signal Transduction Pathway in Arabidopsis', *The Plant Cell,* 19(3), pp. 805-818.

Takeuchi, M., Karahara, I., Kajimura, N., Takaoka, A., Murata, K., Misaki, K., Yonemura, S., Staehelin, L. A. and Mineyuki, Y. (2016) 'Single microfilaments mediate the early steps of microtubule bundling during preprophase band formation in onion cotyledon epidermal cells', *Mol Biol Cell,* 27(11), pp. 1809-20.

Tamura, K., Iwabuchi, K., Fukao, Y., Kondo, M., Okamoto, K., Ueda, H., Nishimura, M. and Hara-Nishimura, I. (2013) 'Myosin XI-i Links the Nuclear Membrane to the Cytoskeleton to Control Nuclear Movement and Shape in Arabidopsis', *Current Biology,* 23(18), pp. 1776-1781.

Tanenbaum, M. E., Macůrek, L., Janssen, A., Geers, E. F., Alvarez-Fernández, M. and Medema, R. H. (2009) 'Kif15 Cooperates with Eg5 to Promote Bipolar Spindle Assembly', *Current Biology,* 19(20), pp. 1703-1711.

Torres-Ruiz, R. A. and Jurgens, G. (1994) 'Mutations in the FASS gene uncouple pattern formation and morphogenesis in Arabidopsis development', *Development,* 120(10), pp. 2967-78.

Traas, J., Bellini, C., Nacry, P., Kronenberger, J., Bouchez, D. and Caboche, M. (1995) 'Normal differentiation patterns in plants lacking microtubular preprophase bands', *Nature,* 375, pp. 676.

Vale, R. D. and Milligan, R. A. (2000) 'The Way Things Move: Looking Under the Hood of Molecular Motor Proteins', *Science,* 288(5463), pp. 88-95.

Van Damme, D., De Rybel, B., Gudesblat, G., Demidov, D., Grunewald, W., De Smet, I., Houben, A., Beeckman, T. and Russinova, E. (2011) 'Arabidopsis α Aurora Kinases Function in Formative Cell Division Plane Orientation', *The Plant Cell Online*.

Van Damme, D., Van Poucke, K., Boutant, E., Ritzenthaler, C., Inze, D. and Geelen, D. (2004) 'In vivo dynamics and differential microtubule-binding activities of MAP65 proteins', *Plant Physiol,* 136(4), pp. 3956-67.

van Heesbeen, Roy G. H. P., Tanenbaum, Marvin E. and Medema, René H. (2014) 'Balanced Activity of Three Mitotic Motors Is Required for Bipolar Spindle Assembly and Chromosome Segregation', *Cell Reports,* 8(4), pp. 948-956.

Vanneste, D., Takagi, M., Imamoto, N. and Vernos, I. (2009) 'The Role of Hklp2 in the Stabilization and Maintenance of Spindle Bipolarity', *Current Biology,* 19(20), pp. 1712-1717.

Vanstraelen, M., Inzé, D. and Geelen, D. (2006) 'Mitosis-specific kinesins in Arabidopsis', *Trends in Plant Science,* 11(4), pp. 167-175.

Vinh, D. B. N., Kern, J. W., Hancock, W. O., Howard, J., Davis, T. N. and Stearns, T. (2002) 'Reconstitution and Characterization of Budding Yeast γ-Tubulin Complex', *Molecular Biology of the Cell,* 13(4), pp. 1144-1157.

Vos, J. W., Dogterom, M. and Emons, A. M. (2004) 'Microtubules become more dynamic but not shorter during preprophase band formation: a possible "search-and-capture" mechanism for microtubule translocation', *Cell Motil Cytoskeleton,* 57(4), pp. 246-58.

Vos, J. W., Pieuchot, L., Evrard, J.-L., Janski, N., Bergdoll, M., de Ronde, D., Perez, L. H., Sardon, T., Vernos, I. and Schmit, A.-C. (2008) 'The Plant TPX2 Protein Regulates Prospindle Assembly before Nuclear Envelope Breakdown', *The Plant Cell,* 20(10), pp. 2783-2797.

Walczak, C. E. and Heald, R. (2008) 'Chapter Three - Mechanisms of Mitotic Spindle Assembly and Function', in Jeon, K.W. (ed.) *International Review of Cytology*: Academic Press, pp. 111-158.

Walczak, C. E. and Shaw, S. L. (2010) 'A MAP for Bundling Microtubules', *Cell,* 142(3), pp. 364-367.

Walker, K. L., Müller, S., Moss, D., Ehrhardt, D. W. and Smith, L. G. (2007) 'Arabidopsis TANGLED Identifies the Division Plane throughout Mitosis and Cytokinesis', *Current Biology,* 17(21), pp. 1827-1836.

Wick, S. M. and Duniec, J. (1983) 'Immunofluorescence microscopy of tubulin and microtubule arrays in plant cells. I. Preprophase band development and concomitant appearance of nuclear envelope-associated tubulin', *J Cell Biol,* 97(1), pp. 235-43.

Wicker-Planquart, C., Stoppin-Mellet, V., Blanchoin, L. and Vantard, M. (2004) 'Interactions of tobacco microtubule-associated protein MAP65-1b with microtubules', *Plant J,* 39(1), pp. 126-34.

Wittmann, T., Boleti, H., Antony, C., Karsenti, E. and Vernos, I. (1998) 'Localization of the Kinesin-like Protein Xklp2 to Spindle Poles Requires a Leucine Zipper, a Microtubule-associated Protein, and Dynein', *The Journal of Cell Biology,* 143(3), pp. 673-685.

Wittmann, T., Wilm, M., Karsenti, E. and Vernos, I. (2000) 'Tpx2, a Novel XenopusMap Involved in Spindle Pole Organization', *The Journal of Cell Biology,* 149(7), pp. 1405-1418.

Wu, S.-Z. and Bezanilla, M. (2014) 'Myosin VIII associates with microtubule ends and together with actin plays a role in guiding plant cell division', *eLife,* 3, pp. e03498.

Xu, J. and Zhang, S. (2015) 'Mitogen-activated protein kinase cascades in signaling plant growth and development', *Trends in Plant Science,* 20(1), pp. 56-64.

Xu, X. M., Meulia, T. and Meier, I. (2007) 'Anchorage of Plant RanGAP to the Nuclear Envelope Involves Novel Nuclear-Pore-Associated Proteins', *Current Biology,* 17(13), pp. 1157-1163.

Xu, X. M., Zhao, Q., Rodrigo-Peiris, T., Brkljacic, J., He, C. S., Müller, S. and Meier, I. (2008) 'RanGAP1 is a continuous marker of the Arabidopsis cell division plane', *Proceedings of the National Academy of Sciences,* 105(47), pp. 18637-18642.

Yamada, M. and Goshima, G. (2017) 'Mitotic Spindle Assembly in Land Plants: Molecules and Mechanisms', *Biology,* 6(1), pp. 6.

Yoneda, A., Akatsuka, M., Hoshino, H., Kumagai, F. and Hasezawa, S. (2005) 'Decision of Spindle Poles and Division Plane by Double Preprophase Bands in a BY-2 Cell Line Expressing GFP–Tubulin', *Plant and Cell Physiology,* 46(3), pp. 531-538.

Zhang, H. and Dawe, R. K. (2011) 'Mechanisms of plant spindle formation', *Chromosome Research,* 19(3), pp. 335-344.

Zhang, Y., Iakovidis, M. and Costa, S. (2016) 'Control of patterns of symmetric cell division in the epidermal and cortical tissues of the Arabidopsis root', *Development,* 143(6), pp. 978-982.

Zheng, Z.-L. and Yang, Z. (2000) 'The Rop GTPase: an emerging signaling switch in plants', *Plant Molecular Biology,* 44(1), pp. 1-9.

Zhong, R., Burk, D. H., Morrison, W. H. and Ye, Z.-H. (2002) 'A Kinesin-Like Protein Is Essential for Oriented Deposition of Cellulose Microfibrils and Cell Wall Strength', *The Plant Cell,* 14(12), pp. 3101-3117.

Zhu, C. and Dixit, R. (2012) 'Functions of the Arabidopsis kinesin superfamily of microtubule-based motor proteins', *Protoplasma,* 249(4), pp. 887-899.

9. Appendix

9.1 Appendix Supplementary Figure1

9.2 Putative RopGAPs impact division plane selection and interact with kinesin 12 POK1.

9.3 Dual localized kinesin-12 POK2 plays multiple roles during cell division and interacts with MAP65-3.

9.4 Phragmoplast Orienting Kinesin 2 is a weak motor switching between pro cessive and diffusive modes.

9.5 Mechanisms of plant cell division.

9.1 Appendix Supplementary Figure1

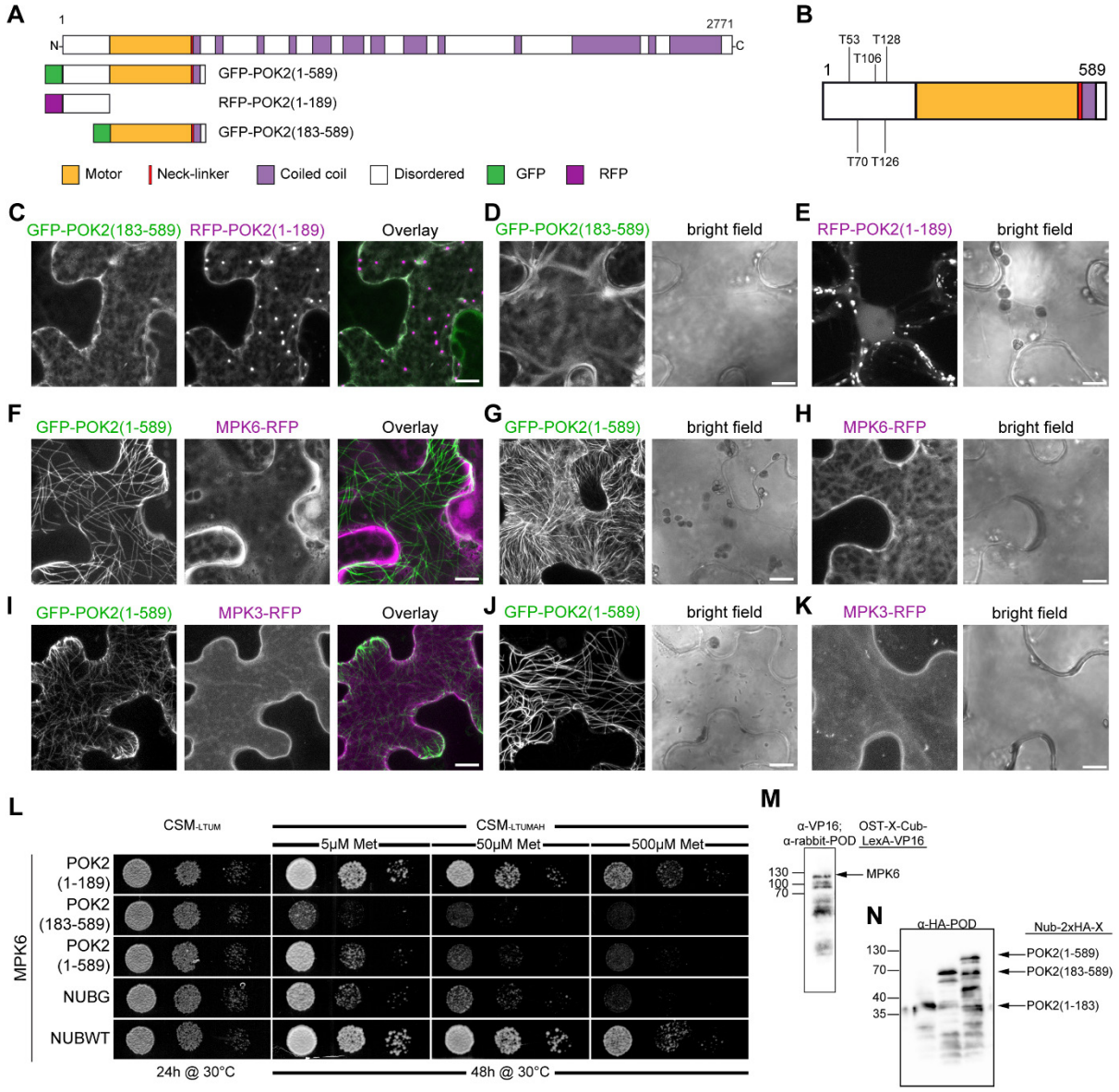

Apendix Supplementary Figure1: Additional experiments for a potential phosphoregulation of POK2: (A) Protein domain organization of POK2 and truncated POK2 fusion domains. **(B)** Predicted phosphorylation sites of conserved ERK kinases within the disordered region of POK2 (http://gps.biocuckoo.org/). **(C-E)** Expression of RFP-POK2MD$_{1-189}$ and GFP-POK2MD$_{183-589}$ in *Tobacco* leaf epidermis cells. Note that both RFP-POK2MD$_{1-189}$ **(E)** and GFP-POK2MD$_{183-589}$ **(D)** localizes into the cytosol in addition to a punctated pattern and nucleus localization for RFP-POK2MD$_{1-189}$ in **(E)**. Co-transfection of both constructs does not alter the localization pattern **(C)**. **(F-K)** Co-expression of either MPK6 **(F)** or MPK3 **(I)** with POK2MD1-589 in *Tobacco* leaf epidermis cells, with their respective controls for POK2MD1-589 **(G,J)**, MPK6 **(H)** and MPK3 **(K)**. In each cases POK2MD$_{1-589}$ **(G,J)**, localizes as filamentous structures, considered to be microtubules. On the contrary both MPK6 **(H)** and MPK3 **(K)** are localizing into the cytosol in addition to a potential plasma membrane localization. Note that co-transfection **(F,I)** does not alter the localization pattern. **(L)** Interaction of OST-MAPK6-Cub and NubG–POK2x fusion as indicated, with controls (NubG, negative; NubWT (wild type), positive). Yeast diploids were spotted (from left to right, dropped at 1.0, 0.1, and 0.01 A600 in each case) on CSM-Leu-, Met-, Trp-, Ura- (CSM-LTUM) medium to verify mating, and on CSM-Ade-, His-, Leu-, Met-, Trp-, Ura- (CSM-LTUMAH) with the addition of different methionine concentrations to assay for interaction. Note the restored yeast growth for NubG-POK2$_{1-189}$. **(M,N)** Immunoblot-detection of fusion proteins expressed in yeast. (M) Immunoblot-detection of MPK6-Cub-VP16 (101 kDa) in yeast protein extracts, using an anti-VPS16 as a primary antibody and anti-rabbit-POD as a secondary antibody. (N) Nub-2xHA-POK2 (1–189) (31 kDa), Nub-2xHA-POK2 (183–589) (57 kDa) and Nub-2xHA-POK2 (1–589) (75 kDa) corresponding to (L), using an anti-HA antibody conjugated with peroxidase (POD).

9.2 Stöckle et al. 2016

Putative RopGAPs impact division plane selection and interact with kinesin-12 POK1.

Dorothe Stöckle, **Arvid Herrmann**, Elisabeth Lipka, Theresa Lauser, Richard Gavidia, Steffi Zimmermann and Sabine Müller

Nature Plants 2, 16120 (2016), DOI: 10.0.38/nplants.2016.120

Putative RopGAPs impact division plane selection and interact with kinesin-12 POK1

Dorothee Stöckle[1], Arvid Herrmann, Elisabeth Lipka, Theresa Lauster, Richard Gavidia, Steffi Zimmermann, Sabine Müller[*]

Developmental Genetics, Centre for Plant Molecular Biology (ZMBP), University of Tübingen

Auf der Morgenstelle 32, 72076 Tübingen, Germany

[1] current address: The Sainsbury Laboratory, University of Cambridge, Bateman Street, Cambridge CB2 1LR, United Kingdom

email: sabine.mueller@zmbp.uni-tuebingen.de

[*] Corresponding author: Sabine Müller

In plants, cell shape is defined by the surrounding cell walls. Thus, spatial control over cell division planes and cell expansion polarity are essential to maintain cell morphology. As in non-plant organisms cell polarity and expansion in plants are controlled by Rho GTPase signalling, regulating cytoskeletal reorganization and vesicle trafficking [1]. However, unlike non-plant eukaryotes, Rho signalling was not implicated in mitotic events in plants. Here, we report on a pair of putative Rho GTPase activating proteins (RhoGAPs) that interact with the mitosis-specific kinesin-12 POK1, a core component of the cortical division zone/site (CDZ/CDS) that is required for division plane maintenance in *Arabidopsis* [2-4]. While designated PHGAPs are cytoplasmic and plasma membrane associated in interphase, during mitosis they additionally localize to the CDZ/CDS in a POK-dependent manner. In contrast to *pok1 pok2* mutants, *phgap1 phgap2* double mutants show moderate cell wall positioning defects as a consequence of inaccurate positioning of the cortical division zone marker POK1. We conclude that loss of PHGAP function interferes with division plane selection in proliferative cell divisions.

In recent years, several CDZ/CDS-resident proteins were identified, memorizing the positional information given by the preprophase band (PPB). The kinesin-12 class motor protein, POK1 is one critical component of the CDZ/CDS, required for the efficient recruitment and maintenance of CDZ identity-markers TANGLED (TAN) and RanGAP1 [2-4]. In the *Arabidopsis* root meristem, simultaneous loss of POK1 and POK2 leads to phragmoplast guidance defects and severe cell plate mis-positioning resulting in deformed cells [4].
In search for novel POK1 interactors, we identified a pair of putative Rho-GAPs in a yeast two-hybrid screen. Commonly, GAPs stimulate the intrinsic GTPase activity of their respective small GTPase targets, rendering the GTPase inactive [5]. Rho-based regulatory mechanism control numerous cellular processes via polarity establishment, cytoskeletal reorganization and vesicle-trafficking in distinct subcellular domains of plant cells. Well documented examples are multipolar pavement cell formation, polar pollen tubes growth, secondary cell wall formation [1,6-8] in *Arabidopsis* and division asymmetry of maize stomatal complexes [9]. In non-plant eukaryotes, Rho-activity directs polarity establishment, motility and cell division [10,11]. However, there is no prior evidence of a role for ROP signalling in division plane orientation for symmetric divisions in the root meristem. The novel POK1 interactors share conserved protein domain architecture (Figure 1a) with the *bona fide*, pollen-specific GAP, ROP1 enhancer (REN1) [12]. The N-terminal pleckstrin-homology (PH) domain is flanked by the GAP domain that contains a conserved arginine (R, Figure 1a) essential for GAP-function of REN1 and of mammalian RhoGAPs [12]. The C-terminal, coiled coil containing domain, interacted with POK1 (CC, Figure1a, 1c, 1d) in the initial yeast two-hybrid screen. We performed mating-based split-ubiquitin interaction assays in yeast [13] to confirm the interaction between PHGAPs and two POK1 C-terminal protein truncations. The longer POK1$_{1213\text{-}2066}$ C-terminal is sufficient for CDZ/CDS localization, whereas the shorter POK1$_{1683\text{-}2066}$ is sufficient for interaction with TAN [4,14]. PHGAP1 and PHGAP2 interacted with both POK1-C terminal variants (Figure 1b, 1c). Furthermore, ratiometric bimolecular fluorescent complementation (rBiFC) experiments [15] between nYFP-POK1$_{1683\text{-}2066}$ and cYFP-PHGAP2 corroborated *in planta* protein interaction in *Arabidopsis* root protoplasts (Figure S1a-S1d). Thus, we conclude that PHGAP1 and PHGAP2, both interact with the C-terminus of POK1.

rBiFC experiments also support an expected interaction between PHGAP2 and ROPs. As proof of principle we tested interaction with ROP2 and ROP6 (Figure 1d, 1e, 1g), a pair of ROP proteins, antagonistically regulating cytoskeletal dynamic and organization during pavement cell development, as well as ROP1, ROP3 and ROP4 (Figure S1j, 1k, 1l). While PHGAP2 interacted with all tested ROPs, neither PHGAP2 nor ROPs showed explicit n/cYFP complementation when tested with TAN (Figure 1f, 1g, 1h, 1i and Figure S1) [4]. These results suggest interaction between PHGAPs and ROPs, as has been reported for the PHGAP homolog REN1, which regulates ROP1 activity in pollen tube expansion [12]. The BiFC experiments showed unspecific interaction of PHGAPs and ROPs. Thus, the physiologically relevant ROP-targets of PHGAPs still need to be determined.

We further characterized POK1 and PHGAP interactions by examining the subcellular localization of PHGAPs. Expression of PHGAPs using cDNA constructs *pUBN:GFP-PHGAP1* and *pUBN:GFP-PHGAP2*, and the full genomic construct *pPHGAP2:GFP-PHGAP2* resulted in comparable localization patterns in transgenic wild type plants (Figure 2 and S2). Interphase cells displayed cytoplasmic and plasma membrane associated fluorescent signal (Figure 2a-2f and S2a-S2j). However, a subset of cells showed continuous GFP-PHGAP1 and GFP-PHGAP2 rings at the plasma membrane (Figure 2a-d and S2a, S2b), reminiscent of the prominent YFP-POK1 rings at the CDZ/CDS [4]. As previously reported, YFP-POK1 is recruited to the PPB in prophase and occupies the CDZ/CDS throughout mitosis by a yet unknown mechanism [4].

Therefore, we determined the cell cycle stage of PHGAP ring-localization at the plasma membrane and its dependency on POK function. While cells displaying spindles, exhibit moderate GFP-PHGAP1 ring accumulation that exceeds the cytoplasmic and membrane associated GFP-PHGAP1 pool, distinctive GFP-PHGAP1 rings were observed during cytokinesis (Figure 2f, 2i, S2c). Co-expression of YFP-POK1 and RFP-PHGAP1 confirmed the expected co-localization in a subset of cells with YFP-POK1 rings (Figure 2j, n= 9 roots, displaying (n = 21) YFP-POK1 rings and (n = 12) RFP-PHGAP1 rings). We know from our previous POK1 analysis [4], that YFP-POK1 starts accumulating at the CDZ in prophase, while PHGAPs are uniformly distributed in the cytoplasm and at the plasma membrane in prophase and visibly accumulate at the CDZ in meta- and anaphase (Figure 2f and S2c), when YFP-POK1 is already present. Similarly, GFP-PHGAP2 faintly accumulates at the CDZ during meta-/anaphase (Figure 2e, S2d-S2g) and remains present during cytokinesis (Figure 2e and 2h, S2h-S2j). Therefore, we conclude that both PHGAP1 and PHGAP2 localize uniformly in the cytoplasm and the plasma membrane in prophase cells and enrichment at the CDZ becomes noticeable in meta-/anaphase and remains throughout cytokinesis (Figure 2 and S2).

Next, we asked whether PHGAP localization at the CDZ/CDS depended on POK-function. In the *pok1-1 pok2-3* mutant GFP-PHGAP1 rings were absent from the CDZ/CDS in cells with PPBs (n = 4), spindles (n = 6) and phragmoplasts (n = 19), despite detectable cytoplasmic and plasma membrane associated GFP-PHGAP signal (Figure 2g). Likewise, GFP-PHGAP2 rings were never observed in *pok1-1 pok2-3* mutants (n = 20 cytokinetic cells with cell plates in eight mutant roots, Figure S2k). These observations suggest that POK function is critically required for the distinct accumulation of PHGAPs at the CDZ/CDS, as has been reported before, for the CDZ/CDS resident proteins TAN and RanGAP1 [3,4]. However, TAN and RanGAP1 recruitment

to the PPB occurs independent of POKs during prophase and only their maintenance at the CDZ upon metaphase is POK-dependent. In contrast, PHGAPs are uniformly distributed in prophase and POK-dependent PHGAP accumulation at the CDZ becomes detectable only during metaphase. Remarkably, PHGAPs cytoplasmic and plasma membrane localization are not noticeably affected by the loss of POK function.

The protein interaction and dependency of PHGAPs on the mitosis specific POK1 motivated our analysis of PHGAPs roles in cell division using available T-DNA insertion lines (Figure S3a). *PHGAP1* transcript was abolished in the *phgap1* allele (Figure S3b) and *PHGAP2* transcript was massively diminished in the *phgap2* allele (Figure S3c). However, the *phgap1* and *phgap2* single mutants did not show appreciable mutant phenotypes. Thus, the double mutant *phgap1 phgap2* was used for further experimentation (Figure S3d, S3e, S3f).

The *Arabidopsis* root meristem exhibits regular cell divisions, reflected in a well-ordered cell wall pattern. *phgap1 phgap2* seedling roots showed moderate reduction in root growth compared to wild type (Figure 3a). The complementation line, expressing *pPHGAP2:GFP-PHGAP2* showed a partial rescue of root growth, as it did not differ from wild type nor *phgap1 phgap2* mutant (Figure 3a). The *phgap1 phgap2* phenotype was less severe than the *pok1 pok2* double mutant (Figure S4a). On the cellular level, *phgap1 phgap2* root meristems displayed moderate cell wall positioning defects compared to wild type (Figure 3b, 3c), which were markedly diminished by *pPHGAP2:GFP-PH*GAP2 expression (Figure 3d).

The *pok1-1 pok2-3 phgap1 phgap2* quadruple mutant (Figure S3g, S3h, S3k, S3i) did show phenotype enhancement in aerial tissues, suggesting *PHGAP1* and *PHGAP2* might serve additional functions. While *pok1-1 pok2-3* double mutants, and *pok1-1 pok2-3 phgap1/+ phgap2* or *pok1-1 pok2-3 phgap1 phgap2/+* sesqui-mutants still produce viable progeny, the quadruple mutant *pok1-1 pok2-3 phgap1-1 phgap2-1* descendants contained mostly non-fertilized ovules and produced very few non- viable embryos (Figure S3g-m). However, root growth and cell division pattern in the root meristem were similar to that of *pok1-1 pok2-3* double mutant (Figure S4a, S4c).

Also, *Arabidopsis* early embryo development follows a recurring sequence of cell divisions creating a typecast cell pattern [16]. Globular and early heart stage embryos of *phgap1 phgap2* double mutants displayed irregular cell patterns and abnormally positioned cell walls (Figure 3e-3j). Although the penetrance of the defect was 6.6 % of the investigated embryos (n = 366), expression of *pGAP2:GFP-gPHGAP2* (n = 638, Figure 3g) reduced the number of abnormal embryos to 2.6 %, while only 0.9% of wild type embryos (n = 685) were abnormal (Figure 3d, 3h). Thus, we suggest that redundant function of PHGAP1 and PHGAP2 play a role in cell division plane positioning in the root meristem and in the early stages of embryo development.

To determine PHGAPs requirement during cell division, we investigated the organization of mitotic microtubule arrays in the *phgap1 phgap2* double mutant root meristem and found instances, where PPBs and phragmoplasts deviated from the expected transverse orientation, predominant in wild type (Figure 4a-4d). Since POK1 is recruited to the PPB in prophase and preserves the PPBs positional information at the CDZ/CDS [4], we examined whether POK1 orientation co-aligned with PPBs and phragmoplasts in the *phgap1 phgap2* mutant (Figure 4e). We never observed miss-alignments of microtubule array orientation and POK1 orientation (n > 100 POK1 rings), indicating that POK1 orientation also reiterate the PPB position in the *phgap1*

phgap2 double mutant, even in cases of oblique PPBs. Thus, we determined the position of POK1 rings relative to the expected transverse orientation, usually observed in wild type, as a read-out for division plane positioning defects. We defined different angle classes of deviation (>5° - ≤ 10°, >10° - ≤ 15°, > 15° and ellipse, which we observe when the division plane tilted perpendicular to the focal plane, Figure 4f) from the ideal transverse (0° to ≤5°) orientation. The mean deviation of POK1 from the transverse increased significantly in the *phgap1 phgap2* mutant (Figure 4g). While the majority of POK1 rings deviated only up to 5° from the expected transverse orientation in wild type (74 %), the frequency of POK1 rings in this class dropped in the *phgap1 phgap2* mutants (46 %) (Figure 4h). Instead, the frequency of POK1 rings, deviating between >5° - ≤ 10°, >10° - ≤ 15° and > 15° from the transverse, increased in the *phgap1 phgap2* mutant (Figure 4h). Thus, we conclude that loss of PHGAP function interferes with division plane selection and appropriate PPB positioning. To validate this notion, we compared PPB and phragmoplast orientations between wild type, the *phgap1 phgap2* mutant and the rescue line expressing *pPHGAP2:GFP-gPHGAP2* in *phgap1 phgap2*. Both, the mean PPB deviation angle and the mean phragmoplast deviation angle differed significantly in the *phgap1 phgap2* mutant compared to wild type and compared to the rescue line (Figure 4i, 4j), while PPB orientation and phragmoplast orientations of the same genotype (i.e. wild type PPB vs. wild type phragmoplast, etc.) did not differ. Like POK1, PPBs and phragmoplasts, displayed a shift towards larger angle classes in the *phgap1 phgap2* double mutant compared to wild type, a tendency that was reversed in the rescue line (Figure 4k, 4l). These observations suggest that loss of PHGAP function leads to an inaccurate demarcation of the CDZ due to mis-oriented PPBs, which consequently affects POK1 positioning.

To determine, whether PHGAPs localization at the CDZ depend on their GAP function, we generated non-functional GFP-PHGAP mutants and introduced them into the *phgap1 phgap2* double mutant. In REN1, the conserved arginine of the GAP domain was required for REN1 activity towards ROP1. Mutation of the conserved catalytic arginine in GFP-PHGAPs (*pUBN:GFP-PHGAP1*^{R203L} and *pUBN:GFP-PHGAP2*^{R198L}, Figure 1a) did not alter their cell cycle dependent localization at the CDZ/CDS, indicating that GAP activity was not required for CDZ/CDS localization (Figure S4g, S4h). Furthermore, defects in root growth, cell wall positions and mitotic microtubule array orientation were similar to *phgap1 phgap2* suggesting that a functional GAP domain was required for accurate cell wall positioning (Figure S4d, S4e, S4f, S4i).

Our results suggest that PHGAPs and POK1 most likely act in a feedback loop, where PHGAPs act upstream of division plane selection and subsequent POK1 localization at the CDZ, but still require POK activity for their localized enrichment at the CDZ/CDS during mitosis. Loss of PHGAP activity leads to cell division phenotypes, that are modest compared to *pok1-1 pok2-3* double mutants (Figure 3c and S4b). However, knock-down of *Arabidopsis TAN* also causes mild cell wall miss-positioning in the root meristem [2], comparable to *phgap1 phgap2*. Similarly to *tan*, *PHGAP2* transcripts are not fully abolished in the *phgap2* allele and residual PHGAP2 activity might be present in most tissues. Furthermore, gene expression patterns of *PHGAP1* and *PHGAP2* are overlapping, but not identical in root meristematic tissue (Figure S3n, S3o) and unresolved redundant functions with CRIB domain containing RhoGAP proteins are likely [17,18]. In fact, functional redundancy of REN1 and ROPGAP1 has been reported in the case of in *Arabidopsis* pollen tube growth [19].

The potential interaction of PHGAPs and ROPs (Figure 1), together with the requirement of the catalytic arginine for PHGAP function (Figure S4) suggest, that PHGAPs act as genuine ROP GTPase activating proteins. Thus, we propose that loss of *PHGAP1* and *PHGAP2* likely leads to localized, subcellular imbalance of ROP activities. Indeed, down-regulation or loss of ROP3 affects early embryo development [20], resembling the *phgap1 phgap2* embryo phenotype.

However, the localization of PHGAPs at the CDZ/CDS is not affected by the arginine mutation (Figure S4g, S4h), indicating that the localization of PHGAPs at the CDZ/CDS *per se* is independent of its GAP function. Likely, the POK dependent localization of PHGAPs at the CDZ/CDS is mediated by PHGAPs C-terminal domains and independent of GAP function. The interaction with the CDZ/CDS master-organizer POK1 and PHGAPs localization at the CDZ/CDS might indicate a localized down-regulation of ROP activities at the CDZ which could affect cytoskeletal organization and vesicle trafficking.

Our findings, that a pair of Rop-GAPs are necessary for accurate division plane selection and subsequent division plane establishment via POK1, might reflect the requirement for precautious spatio-temporal control over ROP activity and its downstream effects on cytoskeletal organization during cell division.

Methods

More information is provided in Supplemental Information.

Confocal Microscopy

Fluorescence was recorded using the Leica TCS SP8 equipped with resonant scanner with a 63x, NA = 1.20, water immersion objective lens or a 20x, NA = 0.75, water immersion objective lens. GFP fluorescence was excited with a 488-nm laser line from an argon/krypton laser and detected with a hybrid detector (HyD) set to 500 to 550 nm detection window. YFP excitation by the 514-nm laser line from an argon/krypton laser was detected between 520 and 550 nm with a HyD detector. RFP and Propidium Iodide, respectively, were excited with a 561-nm He/Ne laser, and fluorescence was detected with a HyD detector or standard PMT detector set at 570 to 650 nm.

Two-dimensional projections and three-dimensional reconstructions of Z stacks were generated with either Fiji (http://rsb.info.nih.gov/ij/) or Leica LF Image processing. Color merges were carried out with Adobe Photoshop CS5 v12.0.4 (Adobe Systems). Only linear adjustments to pixel values were applied. Figures were assembled in Adobe IllustratorCS5 v15.0.2.

Interaction studies using ratiometric Bimolecular Fluorescence Complementation (rBiFC)

Imaging of the protoplasts was carried out at least 22 h after transfection. For comparison of interaction strength rBiFC, identical confocal settings were used for respective experiments. YFP and RFP confocal images of individual transfected protoplasts were recorded. RFP is expressed from the same plasmid as the n-YFP and c-YFP fusion pairs. Image acquisition and quantification was performed as previously described [4]. YFP signal was selected with the segmented line tool in ImageJ 1.44, set to a width of 3 pixel. Average Fluorescence signal intensity was measured for YFP and RFP in the selected region. Calculation of mean YFP/RFP ratios were performed in Excel. Each protoplast represents an independent transformation event. Box plot was assembled in MATLAB.We also attempted to analyze PHGAP1 interactions with POK1-Cterminus and ROPs using BiFC, however, in no instance we observed fluorophore complementation.

Analysis of embryo development

Embryos were fixed in methanol:acetic acid (3:1) and cleared in chloral-hydrate, according to [14], and visualized using DIC optics with a Zeiss Axiophot microscope.

Quantification of microtubule array orientation and YFP-POK1 orientation.

For preprophase band and phragmoplast orientation we performed immuno-localization and measured intact root meristems. In case of YFP-POK1 we used life samples. We collected image stacks of root meristems at 2µm z-intervals. The longitudinal (main) axis of the root was determined and selected as a region of interest (ROI) using Imagej 1.50g (Fiji). The angle (α) between preprophase band, phragmoplast or YFP-POK1 and the main axis was determined in Fiji. The deviation from the expected transverse orientation (perpendicular, at 90 ° relative to the longitudinal main axis) was calculated. If α > 90°, we calculated the deviation angle = α-

90°, in case α < 90° we calculated the deviation angle = 90°-α. Thus, all deviation angle values were positive. We used BoxPlotR (http://boxplot.tyerslab.com/) to create boxplots depicting the mean deviation angle (plus) and the 95% confidence interval of the mean (grey bar flanking the mean). Altman Whiskers extend to 5th and 95th percentile. Significance was determined using one-way ANOVA with post-hoc Turkey HSD. Number of analysed roots was ≥ 6 ≥ 12. Using Excel, deviation angles were sorted into bins as indicated and the frequencies of angles in each bin were depicted in a bar chart. Significance of distribution was determined using Mann-Whitney U test.

Author contribution

We describe contributions to the paper using the CRediT taxonomy. Writing – Original Draft: S.M., D. S., A.H.; Writing – Review & Editing: S.M.; Conceptualization: D.S., S.M.; Investigation: D.S., A.H., E.L., T.L.,; Methodology: S.M.; Formal Analysis: D.S., A.H., E.L. and S.M.; Funding Acquisition: S.M.

Acknowledgements

We thank Dr. Manoj Singh for helpful discussion and Dr. Christopher Grefen for discussion and reagents. We thank anonymous reviewers for their constructive comments. Funding was provided by the Deutsche Forschungsgemeinschaft (DFG, grants MU3133/3-1 and SFB1101).

Figure legends

Figure 1: Organization of PHGAP protein domains and protein interaction assays. (a) PHGAP1 and PHGAP2 contain Pleckstrin homology (PH),GTPase activating protein (GAP) domains and coiled coil domains (CC, predicted by Paircoil, http://paircoil2.csail.mit.edu). The dashed lines indicate the shortest identified PHGAP clones found to interact with POK1$_{1213\text{-}2066}$ C-terminus in the initial yeast-two-hybrid experiment. PHGAP1 and PHGAP2 share 59% overall amino acid identity and 68% identical charge. (b and c) Yeast mating-based Split-Ubiquitin Cyto-SUS assay was performed with PHGAP1 and PHGAP2 with either (**b**) OST-POK1$_{1683\text{-}2066}$-Cub or (c) OST-POK1$_{1213\text{-}2066}$-Cub as baits. Yeast diploids were created with NubG-PHGAPx fusion construct together with controls (TAN, biological positive; NubG, negative; Nubl [wild type], positive) and spotted (left to right) on CSM- Leu-, Met-, Trp-, Ura- (CSM-LMWU) medium to verify mating, and on CSM-Ade-, His-, Leu-, Met-, Trp-, Ura- (AHLMWU) with the addition of different methionine concentrations to assay for interaction. Diploid yeast was dropped at 1.0, 0.1 and 0.001 OD_{600} in each case. Differences in interaction efficiency might be due to the heterologous system used for the assay and might not be biologically relevant. (d to i) Ratiometric bimolecular fluorescence complementation (rBiFC) analysis of interaction between PHGAP2 and (d) ROP2 and (e) ROP6 assayed in *Arabidopsis thaliana* protoplasts. Images show single optical sections of n/cYFP fluorescence and corresponding bright field. (f-h) TANGLED (TAN) was tested for interaction with (f) PHGAP2, (h) ROP2 and (i) ROP6 as a biological negative control. (g) Box plot of YFP/RFP fluorescence ratios for protein pairs as indicated. For each protein pair were imaged and n/cYFP fluorescence and co-expressed cytosolic

RFP serving as an internal control (see Figure S1e-S1i) were recorded. Mean n/cYFP and RFP fluorescence intensities were determined and ratioed for each protoplast. No or less efficient interaction results in low YFP/RFP ration, while efficient n/cYFP complementation due to protein interaction, results in elevated YFP/RFP ratios. Significant differences (*P<0.01) were determined by One Way Anova (n ≥ 24 protoplasts). Scale bars indicate 10 µm.

Figure 2: PHGAP accumulation at the cortical division zone is cell cycle- and POK-dependent. (a, b) Root meristem cells expressing *pUBN:GFP-PHGAP2.* (a) Arrowhead points to the distinct GFP-PHGAP2 localization, which represents the face view of a ring-shaped pattern, apparent in the 3-D reconstruction shown in (b, arrowhead). (c, d) Root meristem cells expressing *pPHGAP2:GFP-gPHGAP2.* (c) Arrowhead points to the distinct GFP-PHGAP2 localization, which represents the face view of a ring-shaped pattern, apparent in the 3-D reconstruction shown in (d, arrowhead). (e) Root meristem expressing *pUBN:GFP-PHGAP2* and the microtubule reporter construct *35S:mCherry-TUA5*. In cross sections, PHGAP2 is visible as lateral accumulations in cells with spindles (arrows) and phragmoplasts (arrow heads). (f) Root meristem expressing *pUBN:GFP-PHGAP1* and *35S:mCherry-TUA5*. Cells displaying PPB (arrows), spindle (asterisk) and phragmoplast (arrow heads). Cytokinetic cell (arrow heads) exhibits prominent GFP-PHGAP1 ring (arrow heads). (g) Root meristem of *pok1-1 pok2-3*. Note the absence of GFP-PHGAP1 from the cortical division site (arrow heads). Yellow arrows indicate the orientation of the root axis. (h, i) Correlation of PHGAP accumulation in a ring with cell cycle stage. (h) While prophase cells with preprophase bands (PPBs, n=13) do not show discernable rings, 73 % of cells with spindles (n=11) and 86 % of cells with phragmoplasts (n=29) show PHGAP2 rings. (i) Prophase cells with preprophase bands (PPBs, n=20) do not show discernable PHGAP1 rings, while 33 % of cells with spindles (n=9) and 97 % of cells with phragmoplasts (n=39) show PHGAP1 rings. In contrast, mitotic cells in the *pok1-1 pok2-3* double mutant never exhibit PHGAP1 rings. (j) Cells express *pPOK1:YFP-POK1* [4] and *p35S:RFP-PHGAP1*. Co-localization of YFP-POK1 and RFP-PHGAP1 (yellow arrow head) in root meristem. Note that some cells exhibit YFP-POK1 only (white arrow heads). Arrow heads indicate the cortical division site. Yellow arrows represent the long axis of the root. All images are z-projections of image stacks. Scale bars indicate 10 µm. See also Figure S2.

Figure 3: Phenotype analysis of *phgap1 phgap2* mutants compared to wild type. (a) Box plot comparing primary root length of wild type (A, Col-0, mean 2.5 cm ± 0.8 STD), (B) *phgap1 phgap2* double mutant (mean 2.1 cm ± 0.8 STD and (C) complementation line, expressing *pPHGAP2:GFP-PHGAP2* in the *phgap1 phgap2* double mutant (mean 2.3 cm ± 0.5 STD). Col-0 and *phgap1 phgap2* are significantly different (P< 0.01) (n = number of roots analyzed for each genotype. (b to d) Single confocal images of Propidium iodide stained primary root meristems visualizing cell wall patterns. (b) Wild type (Col-0), (c) *phgap1 phgap2* (d) complementation line *pPHGAP2:GFP-PHGAP2 phgap1 phgap2.* (e, f, h-j) DIC images of cleared embryos. **e,h** Wild type embryos display the typical regular, cellular pattern. (f, I, j) *phgap1 phgap2* embryos show abnormal cell pattern (brackets) and irregular positioned cell walls (arrows). (g) 3D reconstruction of globular stage embryo of complementation line expressing *pPHGAP2:GFP-PHGAP2 in phgap1 phgap2.* Arrows point

to continuous ring-shaped GFP-PHGAP2 pattern. Dashed line indicates outline of embryo. Scale bars indicate 20 µm in all images.

Figure 4: Mitotic microtubule array orientation and POK1-ring position. Microtubules are visualized using RFP-MBD. (a) and (b) prophase. (a) Transverse preprophase band (PPB, arrows) in wild type. (b) Oblique PPB (arrows) in *phgap1 phgap2*. (c) Transverse phragmoplast in wild type (arrows) and (d) obliquely expanding phragmoplast (arrows) and cell plate (arrow, bright field) in *phgap1 phgap2* cytokinesis. Dashed lines mark cell outlines. (e) Transverse (arrow) and obliquely (arrow head) oriented POK1 signal in *phgap1 phgap2*cytokinesis. Yellow arrows indicate longitudinal root axis. Images are z-projections or single images. Scale bars indicate 10 µm.

(f) Schematic of observed POK1-ring orientation. Deviation from the transverse (0° - 5°) were sorted into angle classes (>5° - ≤ 10°, >10° - ≤ 15°, >15°, ellipse). (g) Boxplot of YFP-POK1 orientation. Mean deviation angle (indicted by +, grey bar indicates the 95% confidence interval for the mean) of POK1 in wild type and in *phgap1 phgap2* differ significantly (** $p<0.01$ one-way ANOVA, post-hoc Turkey HSD). (h) Frequencies of different POK1-ring orientations in wild type (white bars) and *phgap1 phgap2* (pink bars). Distributions are significantly different from each other (Mann-Whitney U test, $p<0.01$). (i and j) Boxplots. Mean deviation angle is indicted by (+, grey bar indicates 95% confidence interval. (h) Deviation angle of PPBs, (i) deviation angle of phragmoplasts. Significant differences (** $p<0.01$, one-way ANOVA, post-hoc Turkey HSD) are indicated. P-values for PPBs versus phragmoplast of the same genotype were non-significant; Col-0 PPB versus phragmoplast P = 0.31; *phgap1 phgap2* PPB versus phragmoplast P = 0.41; *pPHGAP2:GFP-PHGAP2 phgap1 phgap2* PPB versus phragmoplast P = 0.21.

(k and l) Frequencies of different PPB and phragmoplast orientations. Col-0 (white, *phgap1 phgap2* (pink); rescue line *pPHGAP2:GFP-PHGAP2 phgap1 phgap2* (green). Distributions in Col-0 and *phgap1 phgap2* and distributions in *phgap1 phgap2* and rescue line are significantly different (Mann-Whitney U test, $p<0.01$). Col-0 and rescue are non-significant ($p = 0.28$ for PPBs, $p = 0.11$ for phragmoplasts).

References

1 Yang, Z. Cell polarity signaling in Arabidopsis. *Annu Rev Cell Dev Biol* **24**, 551-575, doi:10.1146/annurev.cellbio.23.090506.123233 (2008).

2 Walker, K. L., Muller, S., Moss, D., Ehrhardt, D. W. & Smith, L. G. Arabidopsis TANGLED identifies the division plane throughout mitosis and cytokinesis. *Curr Biol* **17**, 1827-1836, doi:S0960-9822(07)02078-7 [pii]10.1016/j.cub.2007.09.063 (2007).

3 Xu, X. M. *et al.* RanGAP1 is a continuous marker of the Arabidopsis cell division plane. *Proc Natl Acad Sci U S A* **105**, 18637-18642, doi:0806157105 [pii]10.1073/pnas.0806157105 (2008).

4 Lipka, E. *et al.* The Phragmoplast-Orienting Kinesin-12 Class Proteins Translate the Positional Information of the Preprophase Band to Establish the Cortical Division Zone in Arabidopsis thaliana. *Plant Cell* **26**, 2617-2632, doi:10.1105/tpc.114.124933 (2014).

5 Cherfils, J. & Zeghouf, M. Regulation of Small GTPases by GEFs, GAPs, and GDIs. *Physiological Reviews* **93**, 269-309, doi:10.1152/physrev.00003.2012 (2013).

6 Craddock, C., Lavagi, I. & Yang, Z. New insights into Rho signaling from plant ROP/Rac GTPases. *Trends in Cell Biology* **22**, 492-501, doi:http://dx.doi.org/10.1016/j.tcb.2012.05.002 (2012).

7 Oda, Y. & Fukuda, H. Initiation of cell wall pattern by a Rho- and microtubule-driven symmetry breaking. *Science* **337**, 1333-1336, doi:10.1126/science.1222597 (2012).

8 Oda, Y. & Fukuda, H. Rho of plant GTPase signaling regulates the behavior of Arabidopsis kinesin-13A to establish secondary cell wall patterns. *Plant Cell* **25**, 4439-4450, doi:10.1105/tpc.113.117853 (2013).

9 Facette, M. R. *et al.* The SCAR/WAVE complex polarizes PAN receptors and promotes division asymmetry in maize. *Nature Plants* **1**, 14024, doi:10.1038/nplants.2014.24 (2015).

10 Guilluy, C., Garcia-Mata, R. & Burridge, K. Rho protein crosstalk: another social network? *Trends in Cell Biology* **21**, 718-726, doi:http://dx.doi.org/10.1016/j.tcb.2011.08.002 (2011).

11 Zuo, Y., Oh, W. & Frost, J. A. Controlling the switches: Rho GTPase regulation during animal cell mitosis. *Cellular signalling* **26**, 2998-3006, doi:http://dx.doi.org/10.1016/j.cellsig.2014.09.022 (2014).

12 Hwang, J. U., Vernoud, V., Szumlanski, A., Nielsen, E. & Yang, Z. A tip-localized RhoGAP controls cell polarity by globally inhibiting Rho GTPase at the cell apex. *Curr Biol* **18**, 1907-1916, doi:10.1016/j.cub.2008.11.057 (2008).

13 Karnik, R. *et al.* Binding of SEC11 Indicates Its Role in SNARE Recycling after Vesicle Fusion and Identifies Two Pathways for Vesicular Traffic to the Plasma Membrane. *The Plant Cell* **27**, 675-694, doi:10.1105/tpc.114.134429 (2015).

14 Muller, S., Han, S. & Smith, L. G. Two kinesins are involved in the spatial control of cytokinesis in Arabidopsis thaliana. *Curr Biol* **16**, 888-894, doi:S0960-9822(06)01331-5 [pii] 10.1016/j.cub.2006.03.034 (2006).

15 Grefen, C. & Blatt, M. R. A 2in1 cloning system enables ratiometric bimolecular fluorescence complementation (rBiFC). *Biotechniques* **53**, 311-314, doi:Doi 10.2144/000113941 (2012).

16 Yoshida, S. *et al.* Genetic control of plant development by overriding a geometric division rule. *Dev Cell* **29**, 75-87, doi:10.1016/j.devcel.2014.02.002 (2014).

17 Schaefer, A., Miertzschke, M., Berken, A. & Wittinghofer, A. Dimeric Plant RhoGAPs Are Regulated by Its CRIB Effector Motif to Stimulate a Sequential GTP Hydrolysis. *Journal of Molecular Biology* **411**, 808-822, doi:10.1016/j.jmb.2011.06.033 (2011).

18 Mucha, E., Fricke, I., Schaefer, A., Wittinghofer, A. & Berken, A. Rho proteins of plants – Functional cycle and regulation of cytoskeletal dynamics. *European Journal of Cell Biology* **90**, 934-943, doi:10.1016/j.ejcb.2010.11.009 (2011).

19 Hwang, J. U. *et al.* Pollen-tube tip growth requires a balance of lateral propagation and global inhibition of Rho-family GTPase activity. *J Cell Sci* **123**, 340-350, doi:10.1242/jcs.039180 (2010).

20 Huang, J. B. *et al.* ROP3 GTPase Contributes to Polar Auxin Transport and Auxin Responses and Is Important for Embryogenesis and Seedling Growth in Arabidopsis. *Plant Cell* **26**, 3501-3518, doi:10.1105/tpc.114.127902 (2014).

Figure 1

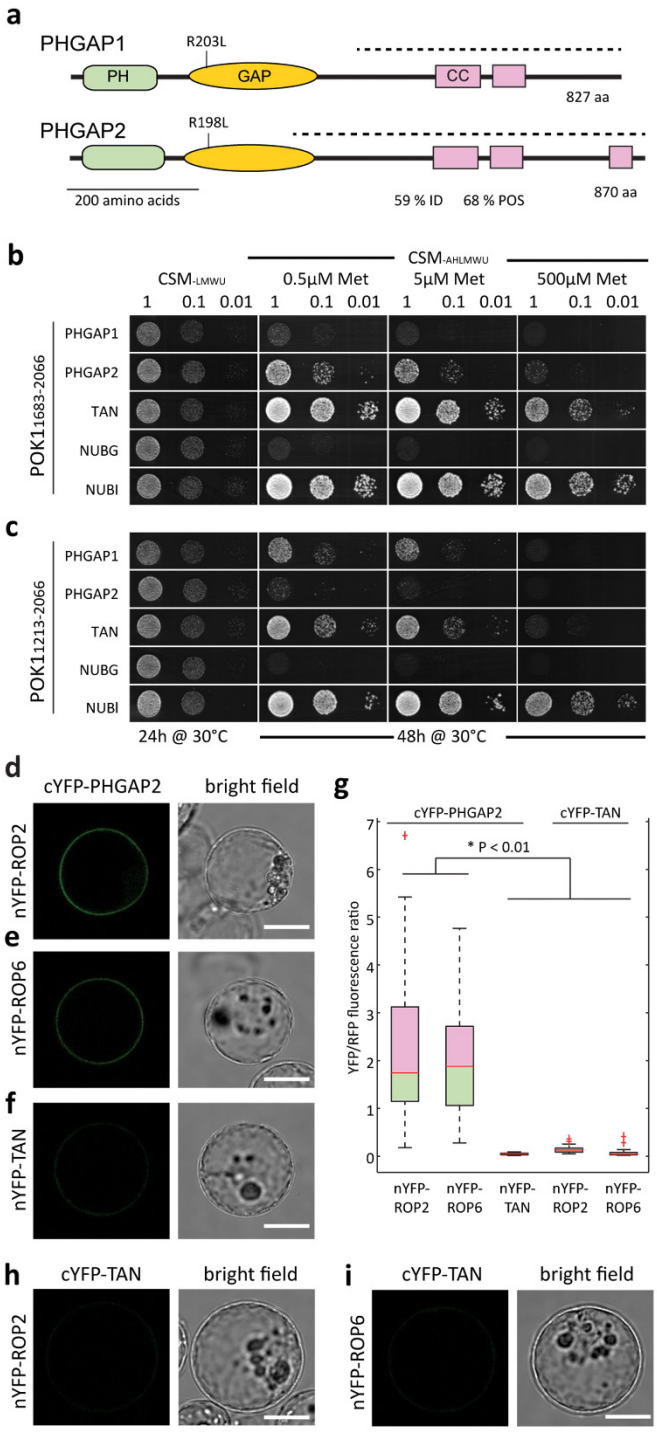
a
PHGAP1
R203L
PH
GAP
CC
827 aa
PHGAP2
R198L
200 amino acids
59 % ID
68 % POS
870 aa
b
CSM-LMWU
CSM-AHLMWU
0.5µM Met
5µM Met
500µM Met
1 0.1 0.01
POK1 11683-2066
PHGAP1
PHGAP2
TAN
NUBG
NUBI
c
POK1 11213-2066
24h @ 30°C
48h @ 30°C
d
cYFP-PHGAP2
bright field
nYFP-ROP2
e
nYFP-ROP6
f
nYFP-TAN
g
cYFP-PHGAP2
cYFP-TAN
* P < 0.01
YFP/RFP fluorescence ratio
nYFP-ROP2
nYFP-ROP6
nYFP-TAN
h
cYFP-TAN
bright field
nYFP-ROP2
i
cYFP-TAN
bright field
nYFP-ROP6

Figure 2

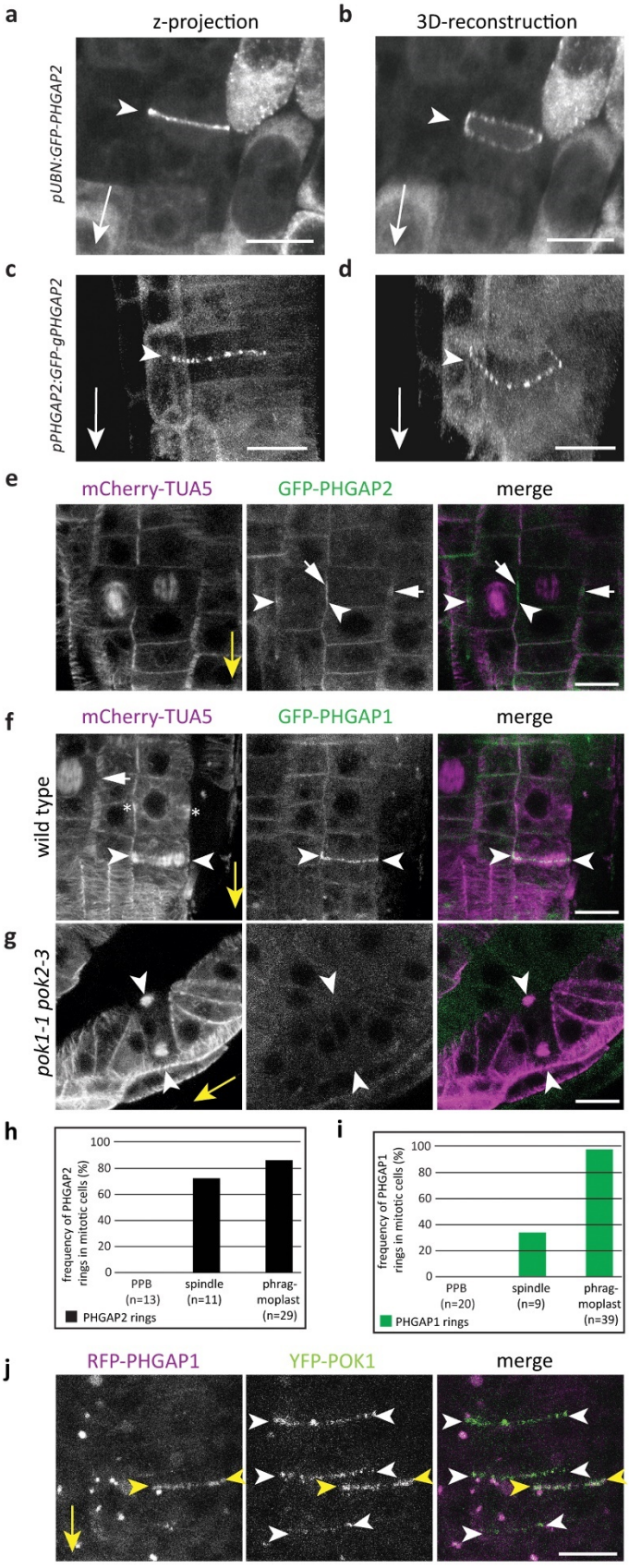
a
z-projection
b
3D-reconstruction
pUBN:GFP-PHGAP2
c
d
pPHGAP2:GFP-gPHGAP2
e
mCherry-TUA5
GFP-PHGAP2
merge
f
mCherry-TUA5
GFP-PHGAP1
merge
wild type
g
pok1-1 pok2-3
h
frequency of PHGAP2 rings in mitotic cells (%)
100
80
60
40
20
0
PPB (n=13)
spindle (n=11)
phrag-moplast (n=29)
PHGAP2 rings
i
frequency of PHGAP1 rings in mitotic cells (%)
100
80
60
40
20
0
PPB (n=20)
spindle (n=9)
phrag-moplast (n=39)
PHGAP1 rings
j
RFP-PHGAP1
YFP-POK1
merge

Figure 3

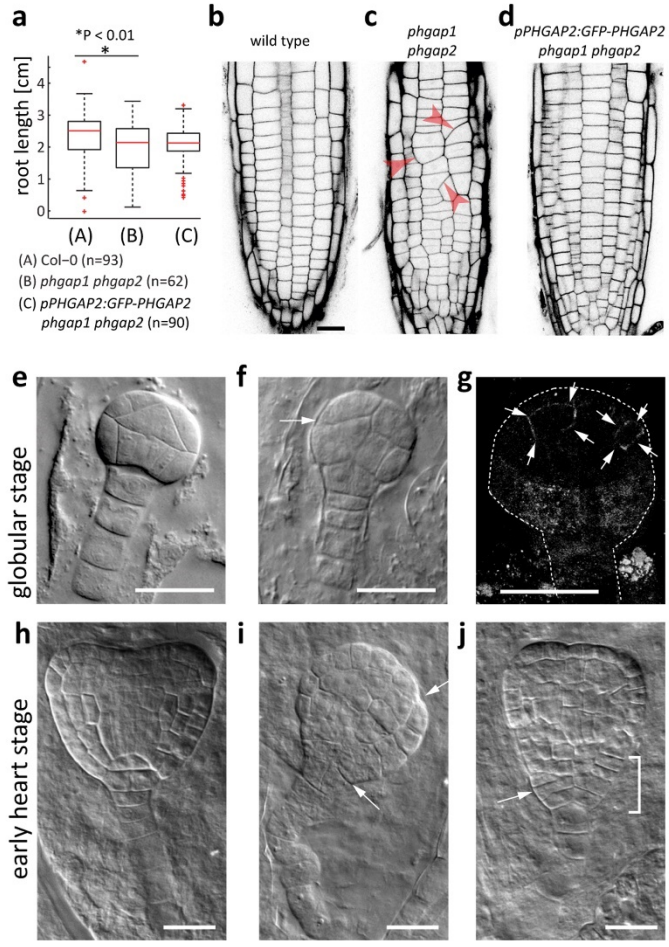
a
*P < 0.01
*
root length [cm]
0
1
2
3
4
(A) (B) (C)
(A) Col–0 (n=93)
(B) phgap1 phgap2 (n=62)
(C) pPHGAP2:GFP-PHGAP2 phgap1 phgap2 (n=90)
b
wild type
c
phgap1 phgap2
d
pPHGAP2:GFP-PHGAP2 phgap1 phgap2
e
f
g
globular stage
h
i
j
early heart stage

Figure 4

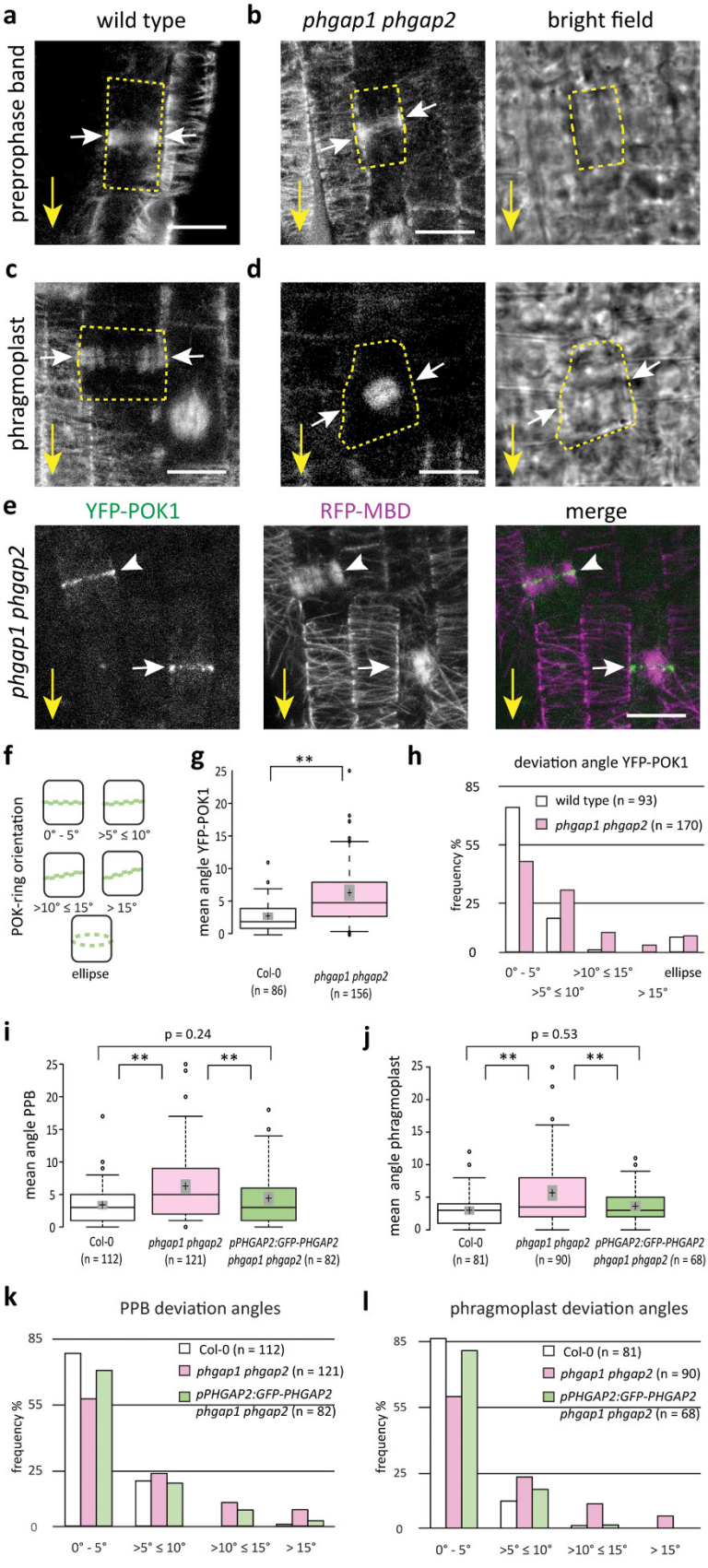
a
wild type
b
phgap1 phgap2
bright field
preprophase band
c
d
phragmoplast
e
YFP-POK1
RFP-MBD
merge
phgap1 phgap2
f
POK-ring orientation
0° - 5°
>5° ≤ 10°
>10° ≤ 15°
> 15°
ellipse
g
mean angle YFP-POK1
**
Col-0 (n = 86)
phgap1 phgap2 (n = 156)
h
deviation angle YFP-POK1
wild type (n = 93)
phgap1 phgap2 (n = 170)
frequency %
i
p = 0.24
mean angle PPB
Col-0 (n = 112)
phgap1 phgap2 (n = 121)
pPHGAP2:GFP-PHGAP2 phgap1 phgap2 (n = 82)
j
p = 0.53
mean angle phragmoplast
Col-0 (n = 81)
phgap1 phgap2 (n = 90)
pPHGAP2:GFP-PHGAP2 phgap1 phgap2 (n = 68)
k
PPB deviation angles
l
phragmoplast deviation angles

Plant Growth

For analysis of mutant phenotypes, localization studies, crosses and reproduction, seeds were surface sterilized and placed on ½ MS medium (Murashige and Skoog medium) followed by stratification at 4°C in the dark for at least two days. Then plants were grown in growth chambers under long day conditions (cycling 16 h light / 8 h dark) at 19°C to 22°C. For further experimentation and propagation two to three week old seedlings were transferred to soil.

In this study *Arabidopsis thaliana* plants, ecotype Columbia (Col-0, wild type) were used. For mutant analysis of *PHGAP* genes, T-DNA insertion lines *phgap1-1* (WiscDsLoxHs135_04D) and *phgap2-1* (SALK_083351) were obtained from the Arabidopsis biological resource center (ABRC, Ohio, US) and Nottingham Arabidopsis stock center (NASC, Nottingham, UK) [5]. All other transgenic lines in this study were created by *Agrobacterium tumefaciens* (*A. tumefaciens*) mediated transformation of respective plasmids into Col-0 [6].

For examination of the microtubule cytoskeleton the previously described microtubule reporter line *p35S:GFP-MBD* [7] was used.

Generation of fluorescent fusion proteins

For localization studies cDNA of *PHGAP1* and *PHGAP2* was reverse transcribed from RNA isolated from seedlings or flower buds and cloned into Gateway® compatible pENTR vectors. In addition, for *PHGAP2* a pENTR clone (G21877) was obtained from the ABRC [8]. *pENTR-PHGAP1* and *pENTR-PHGAP2* were subsequently recombined with destination vectors *pUBN:GFP* and *pUBN:RFP* [9] using LR clonase. Stable plant transformation was mediated by the *A. tumefaciens* strain GV3101. Transformants were selected on nutrient agar plates containing 0.05% phosphinotricin (Duchefa) or by spraying plants with 0.1% Basta (Bayer) respectively. Three independent *pUBN:GFP-PHGAP1* and ten independent *pUBN:GFP-PHGAP2* T1 lines were selected and propagated for further analysis. Analysis of localization patterns was performed using confocal microscopy in the T2 generation. All lines showed comparable localization pattern and fluorescence intensity. For co-localization studies selected lines expressing RFP-PHGAP1 were crossed with YFP-POK1 lines previously characterized in [1].

Investigation of the respective GAP domains in PHGAP1 and PHGAP2 was carried out by substitution of a highly conserved catalytic arginine residue within the GAP domain by leucin. As previously shown a conserved arginine in the GAP-domain is essential for GAP activity [10] . The respective residues in PHGAP1 (R203L) and PHGAP2 (R198L) were mutated to leucine by site directed mutagenesis using miss-match primers (Table S2) in a rolling cycle PCR reaction and *pENTR cPHGAP1* and *pENTR cPHGAP2* as respective templates. (Table S2). Resulting mutants *pENTR cPHGAP1*^{R203L} and *pENTR cPHGAP2*^{R198L} were recombined to obtain *pUBN:GFP-PHGAP1* ^{R203L} (five independent T1 lines) and *pUBN:GFP-PHGAP2* ^{R198L} (seven independent T1 lines).

Interaction studies using ratiometric Bimolecular Fluorescence Complementation (rBiFC)

The Gateway compatible 2 in 1 system [11] was used to test putative interactions of PHGAP2 and POK1$_{1683-2066}$ as well as PHGAP2 and selected ROPs. Negative controls are indicated in figure legends. In brief, potential interaction partners were fused to either nYFP or cYFP on the same plasmid, each expressed und the control of a 35S promoter. In addition the plasmid include an internal expression control (p35S:RFP). Interaction strength was determined by the YFP/RFP ratio. Amplicons (primers listed in table 1) with appropriate recombination sites were cloned into either pDONOR221-P3P2 or pDONOR221-P1P4 by BP clonase, also described previously in [1]. Subsequent LR clonase reaction was performed with the pBiFCt-2in1-NN destination vector.

Polyethylene glycol (PEG) mediated transfections of plasmids into *A. thaliana* root cell protoplasts were carried out by the transformation unit of the ZMBP as described previously [1].

Mating-Based Cyto-SUS Assays

POK1$_{1213-2066}$ and POK1$_{1683-2066}$ coding sequences without stop codon were amplified from entry clones described by [1] and cloned into pENTR2B via BamHI/XhoI and into pENTR3C via EcoRI/XhoI. In a single Gateway LR reaction each ENTR clone was cloned into the OST-Cub destination vector [12], whereas cTAN [1], cGAP1 and cGAP2 with stop codon were cloned into the pNX35-Dest Destination vector [13]. The haploid yeast strains THY.AP4 and THY.AP5) [14] were transformed according to [15] and plated on selective media (CSM-Leu, Met (LM) for THY.AP4 and CSM-Met, Tyr, Ura (MTU) for THY.AP5. For liquid cultures 10 to 15 yeast colonies were selected and inoculated for overnight growth at 180 rpm and 28°C. Yeast mating was performed in sterile PCR tubes after harvesting and re-suspending of liquid cultures in YPD medium. Equal aliquots of cultures containing either OST-POK1$_{1213-2066}$-Cub or OST-POK1$_{1683-2066}$-Cub in THY.AP4 with the appropriate NubG-X in THY.AP5 were mixed. Aliquots of 5 µL from each mixture were dropped on YPD plates and incubated at 28°C for at least 6h. Then colonies were transferred from YPD on CSM- Leu, Met, Trp, Ura (LMWU) plates and incubated at 28°C overnight. After 16h colonies were inoculated in 2 ml of liquid CSM-LMWU media and grown at 180 rpm and 28°C overnight. 100µl of each mating combination were harvested and re-suspended in sterile water. Serial dilutions of 7µl per spot at OD600 1.0, 0.1 and 0.01 were dropped on CSM- Ade, His, Leu, Met, Trp, Ura (AHLMWU) plates with added methionine in increasing concentrations (0.5, 5, 50 and 500 µM) and on a CSM– LMWU control plate to confirm mating efficiency. Plates were incubated at 28°C and images were taken after 24h for CSM – LMWU control plate and 48h for CSM-AHLMWU plates.

Immuno-localization

Immunofluorescence staining was essentially performed as previously described [16]. In brief, seven-day-old seedlings were fixed in 4% paraformaldehyde/microtubule-stabilizing buffer (MTSB, 50 mM Pipes, 5 mM EGTA, 5 mM MgSO4, pH 7.0) and washed three times in water. Seedlings were subsequently placed on charged slides (Thermo Scientific), protected with coverslips dipped in liquid nitrogen. Coverslips were removed and samples dried overnight. Seedlings were rehydrated in MTSB for 5 min before cell walls were partially digested with 2% driselase (Sigma-Aldrich) in MTSB for 1 h at 37°C. After three times of washing with phosphate buffered saline (PBS, 137 mM NaCl, 2.7 mM KCl, 10 mM Na2HPO4, 2 mM KH2PO4, pH 7.4), the

plasma membrane was permeabilized with 3% Nonident P40 in 10% DMSO-MTSB for 1 h at 37°C followed again by washing six times with PBS. Samples were blocked in 5% bovine serum albumin (Sigma)/PBS overnight at 4° C Primary antibodies rat-anti-tubulin 1:600 (YL1/2, Abcam, 1:600) and rabbit-anti-GFP (Invitrogen, 1:1000) and secondary antibodies goat-anti-rabbit Alexa 488 (Invitrogen, 1:600) and goat-anti-rat Cy3 (Dianova, 1:600) in 5% BSA/PBS, were used. Primary and secondary antibodies were incubated at 37°C for 3h each and subsequently washed 3 times with PBS. DNA was stained with 4',6-diamidino-2-phenylindole (DAPI; 1:1000) for 15 min at room temperature. Samples were mounted in Citifluor (Amersham). Imaging was performed on Leica TCS SP8 with appropriate settings.

Table S1: Oligonucleotides used for cloning

cDNA cloning	
PH-GAP1 ATG_F	GGTACCATGGAGGCTTCTCTAGCTGTTA
PH-GAP1 Stop_R	GCGGCCGCCTAATTCCATGGTGGAGAAGA
PH-GAP2-ATG_F	GGATCCATGGAGGCTTCTTTAGCGGCTTT
PH-GAP2 Stop_R	GCGGCCGCTTAGTTCCAAGGTGGAGATGAT
promotor cloning	
PH-GAP1 1.5 kb pro_F	CTGCAGAGAGACGGAAGTGAGTTGCTGACTT
PH-GAP1 1.5 kb pro_R	CTGCAGTGCAGAAGTACACACTTAATC
proPHGAP2_Not_R	GCGGCCGCTGCCTCAACAGCATAATCTCCAGAT
proPHGAP2-2R	CTGCAGAAAGAAGCCTCCATTGCCTCAACA
GAP mutation	
PHGAP1 R198L_F	AGGGATATTACTGCAGTCTGCTGAT
PHGAP1 R198L_R	ATCAGCAGACTGCAGTAATATCCCT
PHGAP2 R203L_F	AGGAATTTTACTGCAGTCTGCAGATGT
PHGAP2 R203L_R	ACATCTGCAGACTGCAGTAAAATTCCT
rBiFC cloning	
attB3 POK1C-short _F	GGGGACAACTTTGTATAATAAAGTTGTAATGGATGAAGAAGT AAAAAGGCATCGT
attB2 POK1C-short_R	GGGGACCACTTTGTACAAGAAAGCTGGGTTTTACCGATATCT TGTACCAGAGCT
attB3 TAN1_F	GGGGACAACTTTGTATAATAAAGTTGTAATGGTTGCAAGAAC CCCACAGAAGCA
attB2 TAN1_R	GGGGACCACTTTGTACAAGAAAGCTGGGTTCTACACTTTCCT GCTCTTCATTGGA
attB1 PHGAP2_F	GGGGACAAGTTTGTACAAAAAAGCAGGCTTAATGGAGGCTTC TTTAGCGGCTTT
attB4 PHGAP2_R	GGGGACAACTTTGTATAGAAAAGTTGGGTGTTAGTTCCAAGG TGGAGATGATG
attB4 TAN_r	GGGG AC AAC TTT GTA TAG AAA AGT TGG GTG CTACACTTTCCTGCTCTTCATTGGA
attB1 TAN	GGGG ACA AGT TTG TAC AAA AAA GCA GGC TTA ATGGTTGCAAGAACCCCACAGAAGCA
attB3 ROP4	GGGG ACA ACT TTG TAT AAT AAA GTT GTA ATGAGTGCTTCGAGGTTTATAAAGTGT

attB2 ROP4 r	GGGG AC CAC TTT GTA CAA GAA AGC TGG GTT TCACAAGAACACGCAGCGGTTCTT
attB3 ROP2	GGGG ACA ACT TTG TAT AAT AAA GTT GTA ATGGCGTCAAGGTTTATAAAGTGT
attB2 ROP2 r	GGGG AC CAC TTT GTA CAA GAA AGC TGG GTT TCACAAGAACGCGCAACGGTTCTT
attB3 ROP6	GGGG ACA ACT TTG TAT AAT AAA GTT GTA ATGAGTGCTTCAAGGTTTATCAAGT
attB2 ROP6 r	GGGG AC CAC TTT GTA CAA GAA AGC TGG GTT TCAGAGTATAGAACAACCTTTCTG
ROP1_attB2_R	GGGGACCACTTTGTACAAGAAAGCTGGGTTTCATAGAATGGA GCATGCCTTCT
ROP1_attB3_F	GGGG ACA ACT TTG TAT AAT AAA GTT GTAATGAGCGCTTCGAGGTTCGTAA
Split-Ubiquitin	
pAD-POK1-5047 EcoRI	GAATTCACCATGGATGAAGAAGTAAAAAGGCATCGTA
POK1C w/o STOP_XhoI	TACTCGAGTACCGATATCTTGTACCAGAGCTCT
genotyping	
PHGAP1_EcoRI-R	TCTTCAGGACTGAATTCTGTCTT
L4	TGATCCATGTAGATTTCCCGGACATGAAG
PHGAP2_ATG_F	GGATCCATGGAGGCTTCTTTAGCGGCTTT
PHGAP2_03R,	GGATCCATGGAGGCTTCTTTAGCGGCTTT
LBa1	TGGTTCACGTAGTGGGCCATCG
PH-GAP1_EcoR1-F	AGGCAAGACAGAATTCAGTCCTGAA
PH-GAP1 1506_R	TACTGGGAGTAACTGAGGGTATA
LBDs-Lox	AACGTCCGCAATGTGTTATTAAGTTGTC
PHGAP2 02_R	ATCTGCTCTCCAGCTTGTTGAT
PHGAP-g4913_F	TGCTGAAGCTGATGTCGCAAGGT
PHGAP1-01_R	ATACAGAGGCTCGAGCACATG
PHGPAP1-p954_F	ACTCTTATGTACACTACATCTA

References

1 Lipka, E. *et al.* The Phragmoplast-Orienting Kinesin-12 Class Proteins Translate the Positional Information of the Preprophase Band to Establish the Cortical Division Zone in Arabidopsis thaliana. *Plant Cell* **26**, 2617-2632, doi:10.1105/tpc.114.124933 (2014).

2 Muller, S., Han, S. & Smith, L. G. Two kinesins are involved in the spatial control of cytokinesis in Arabidopsis thaliana. *Curr Biol* **16**, 888-894, doi:S0960-9822(06)01331-5 [pii] 10.1016/j.cub.2006.03.034 (2006).

3 Blazquez, M. A., Soowal, L. N., Lee, I. & Weigel, D. LEAFY expression and flower initiation in Arabidopsis. *Development* **124**, 3835-3844 (1997).

4 Hauser, M. T. & Bauer, E. Histochemical analysis of root meristem activity in Arabidopsis thaliana using a cyclin : GUS (beta-glucuronidase) marker line. *Plant Soil* **226**, 1-10, doi:Doi 10.1023/A:1026421417979 (2000).

5 Alonso, J. M. *et al.* Genome-Wide Insertional Mutagenesis of Arabidopsis thaliana. *Science* **301**, 653-657, doi:10.1126/science.1086391 (2003).

6 Clough, S. J. & Bent, A. F. Floral dip: a simplified method forAgrobacterium-mediated transformation ofArabidopsis thaliana. *The Plant Journal* **16**, 735-743, doi:10.1046/j.1365-313x.1998.00343.x (1998).

7 Marc, J. *et al.* A GFP-MAP4 reporter gene for visualizing cortical microtubule rearrangements in living epidermal cells. *Plant Cell* **10**, 1927-1940 (1998).

8 Yamada, K. *et al.* Empirical Analysis of Transcriptional Activity in the Arabidopsis Genome. *Science* **302**, 842-846, doi:10.1126/science.1088305 (2003).

9 Grefen, C. *et al.* A ubiquitin-10 promoter-based vector set for fluorescent protein tagging facilitates temporal stability and native protein distribution in transient and stable expression studies. *Plant J* **64**, 355-365, doi:10.1111/j.1365-313X.2010.04322.x (2010).

10 Sermon, B. A., Lowe, P. N., Strom, M. & Eccleston, J. F. The Importance of Two Conserved Arginine Residues for Catalysis by the Ras GTPase-activating Protein, Neurofibromin. Journal of Biological Chemistry **273**, 9480-9485, doi:10.1074/jbc.273.16.9480 (1998).

11 Grefen, C. & Blatt, M. R. A 2in1 cloning system enables ratiometric bimolecular fluorescence complementation (rBiFC). *Biotechniques* **53**, 311-314, doi:Doi 10.2144/000113941 (2012).

12 Karnik, R. *et al.* Binding of SEC11 Indicates Its Role in SNARE Recycling after Vesicle Fusion and Identifies Two Pathways for Vesicular Traffic to the Plasma Membrane. *The Plant Cell* **27**, 675-694, doi:10.1105/tpc.114.134429 (2015).

13 Grefen, C. & Blatt, M. R. Do Calcineurin B-Like Proteins Interact Independently of the Serine Threonine Kinase CIPK23 with the K+ Channel AKT1? Lessons Learned from a Ménage à Trois. *Plant Physiology* **159**, 915-919, doi:10.1104/pp.112.198051 (2012).

14 Obrdlik, P. *et al.* K(+) channel interactions detected by a genetic system optimized for systematic studies of membrane protein interactions. *Proceedings of the National Academy of Sciences of the United States of America* **101**, 12242-12247, doi:10.1073/pnas.0404467101 (2004).

15 Grefen, C., Obrdlik, P. & Harter, K. in *Plant Signal Transduction* Vol. 479 *Methods in Molecular Biology* (ed Thomas Pfannschmidt) Ch. 14, 217-233 (Humana Press, 2009).

16 Lauber, M. H. *et al.* The Arabidopsis KNOLLE Protein Is a Cytokinesis-specific Syntaxin. *The Journal of Cell Biology* **139**, 1485-1493, doi:10.1083/jcb.139.6.1485 (1997).

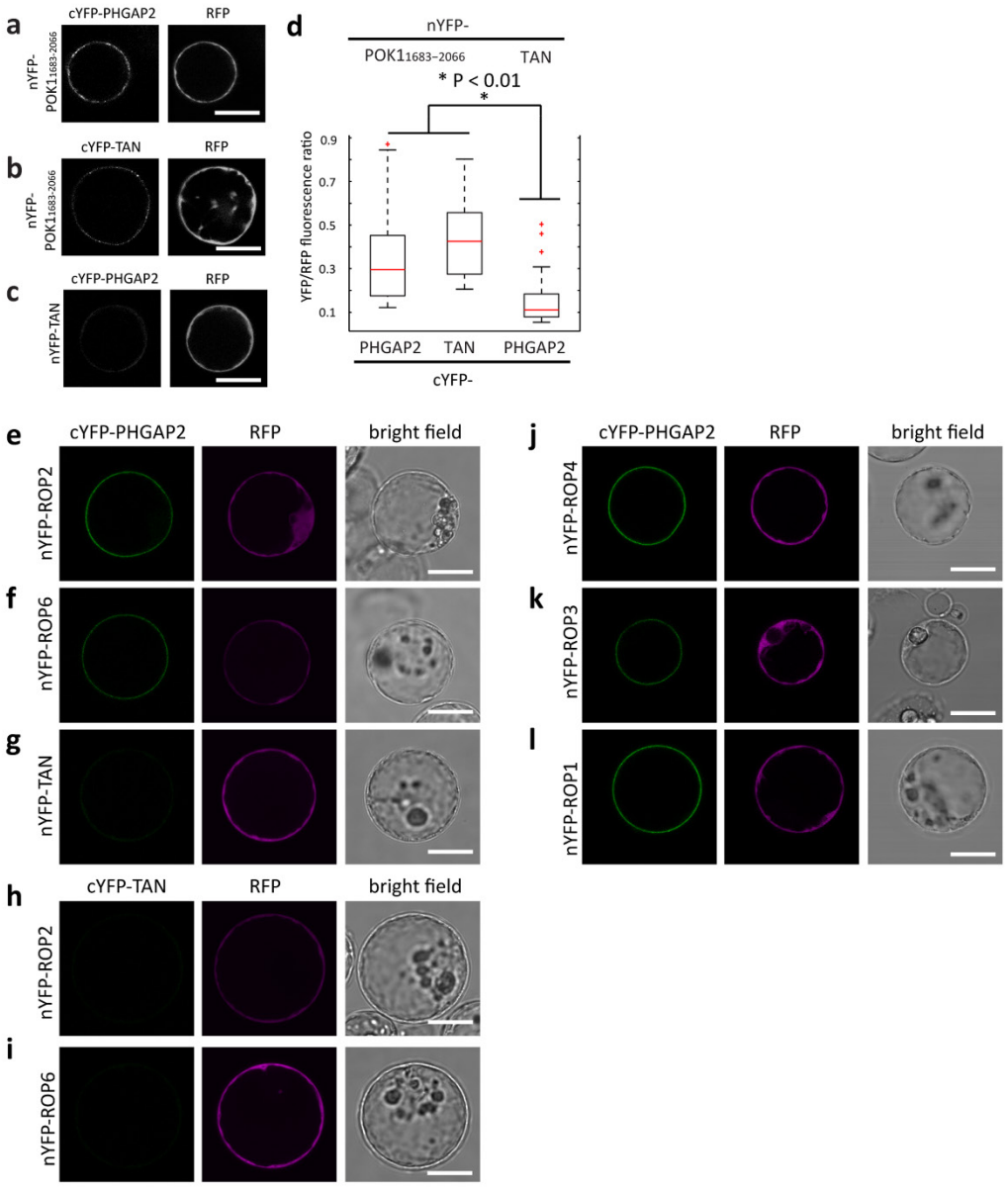
a
cYFP-PHGAP2
RFP
nYFP-POK1 1683-2066
b
cYFP-TAN
RFP
nYFP-POK1 1683-2066
c
cYFP-PHGAP2
RFP
nYFP-TAN
d
nYFP-
POK1 1683–2066
TAN
* P < 0.01
*
YFP/RFP fluorescence ratio
0.9
0.7
0.5
0.3
0.1
PHGAP2
TAN
PHGAP2
cYFP-
e
cYFP-PHGAP2
RFP
bright field
nYFP-ROP2
f
nYFP-ROP6
g
nYFP-TAN
h
cYFP-TAN
RFP
bright field
nYFP-ROP2
i
nYFP-ROP6
j
cYFP-PHGAP2
RFP
bright field
nYFP-ROP4
k
nYFP-ROP3
l
nYFP-ROP1

Supplemental Figure S1: Interaction assays. (a to c) Ratiometric bimolecular fluorescence complementation (rBiFC) analysis in *Arabidopsis thaliana* protoplasts assaying the interaction between (a) POK1$_{1683-2066}$ and PHGAP2, as well as (b) POK1$_{1683-2066}$ and its *bona fide* interactor TANGLED (TAN). (c) No n/cYFP complementation is observed between TAN and PHGAP2, serving as a biological negative control. Images in left panels show single optical sections of n/cYFP fluorescence. Right panels show cytoplasmic RFP fluorescence, co-expressed from the same plasmid like nYFP and cYFP-fusion proteins. (d) Boxplot of mean YFP fluorescence intensities ratioed against mean RFP fluorescence intensities (YFP/RFP fluorescence intensity). Boxplot depicts mean YFP/RFP fluorescence intensity ratio between POK1$_{1683-2066}$ and PHGAP2 (n = 27), POK1$_{1683-2066}$ and TAN (n = 30) and between PHGAP2 and TAN (n = 41). Significant differences (*P<0.01) between mean fluorescence intensity ratios were determined by One Way Anova. (e to i) Images correspond to samples in Figure 1d, 1e, 1f, 1h, 1i, but include the respective RFP images. Image acquisition and quantification was performed as previously described[1]. (j to i) BiFC and corresponding RFP and bright field images of *Arabidopsis thaliana* protoplasts. n/cYFP fluorescence indicating interaction between (j) ROP4 and PHGAP2, (k) ROP3 and PHGAP2 and (i) ROP1 and PHGAP2. Scale bars indicate 20 µm. Each protoplast represents an independent transformation event. Boxplot was assembled in MATLAB.

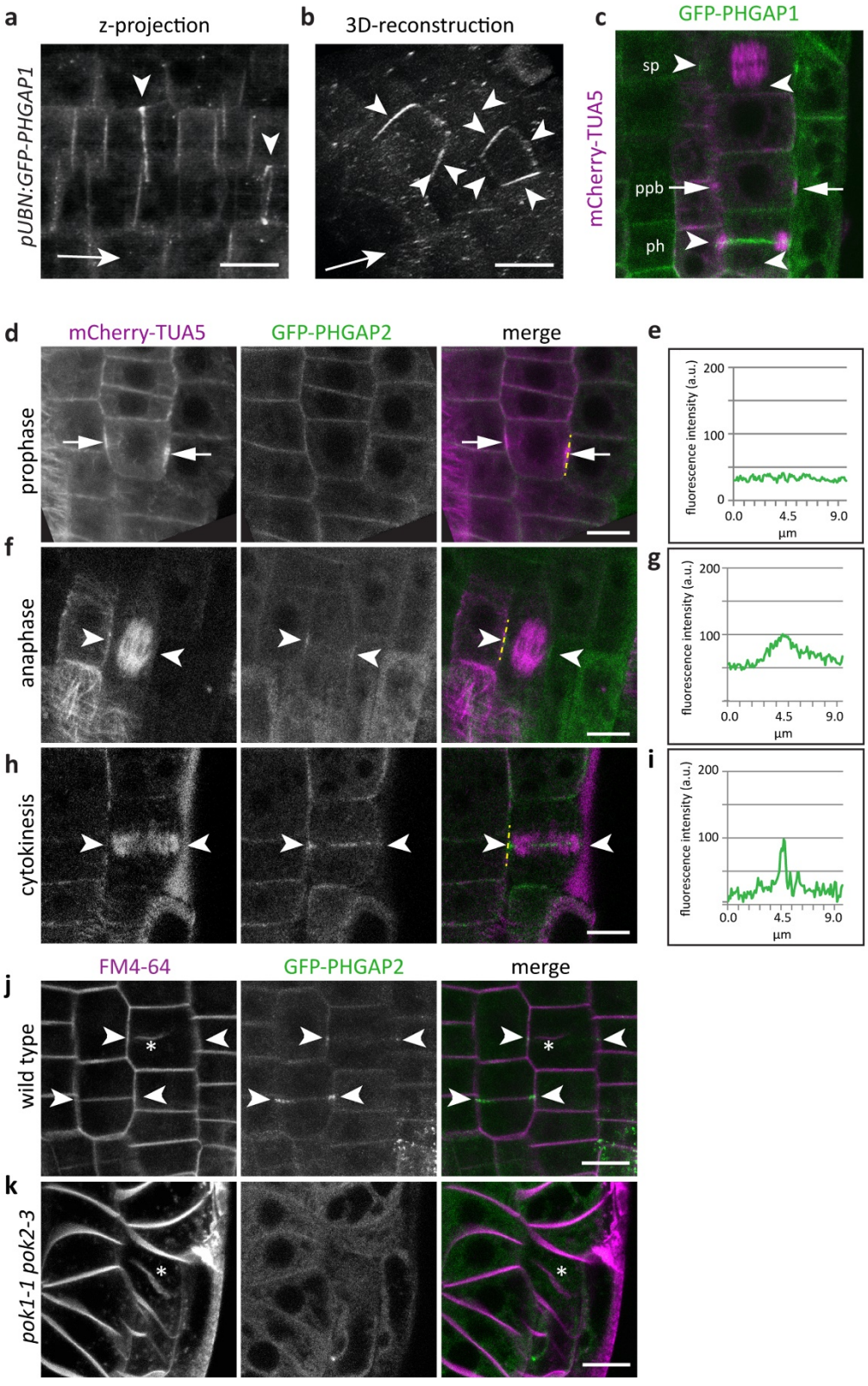
a
z-projection
pUBN:GFP-PHGAP1
b
3D-reconstruction
c
GFP-PHGAP1
mCherry-TUA5
sp
ppb
ph
d
mCherry-TUA5
GFP-PHGAP2
merge
prophase
e
fluorescence intensity (a.u.)
200
100
0
0.0
4.5
9.0
µm
f
anaphase
g
h
cytokinesis
i
FM4-64
GFP-PHGAP2
merge
j
wild type
k
pok1-1 pok2-3

Supplemental Figure S2: PHGAP localization and POK-dependency. (a, b) Root meristem cells expressing *pUBN:GFP-PHGAP1.* (a) GFP-PHGAP1 is present in the cytoplasm, associates with the plasma membrane and (b) accumulates in a continuous ring-like pattern (3D-reconstruction, arrows point out ring-shape. (c) Root meristem cells co-expressing *pUBN:GFP-PHGAP1* and the microtubule reporter construct *35S:mCherry-TUA5.* Mitotic figures are indicated. Note that only PPB is not associated with GFP-PHGAP1, while cells with spindle and phragmoplast display GFP-PHGAP1. (d,f,h) Root meristem cells co-expressing *pUBN:GFP-PHGAP2* and the microtubule reporter construct *35S:mCherry-TUA5*. (e) Plot profile of GFP-PHGAP2 intensity along dashed, yellow line in (d, merge). Note the uniform GFP-PHGAP2 intensity. (f) PHGAP2 accumulation (arrow heads) in cell with spindle. (g) Plot profile of PHGAP2 corresponding to yellow line in merge panel of (f). Note the shallow arch of GFP-PHGAP2 fluorescence intensity. (h) PHGAP2 accumulation (arrow head) in cytokinetic cell displaying phragmoplast. (i) Plot profile of PHGAP2 corresponding to yellow line in merge panel of (h). Note the GFP-PHGAP2 intensity peak. U and k) Root meristem cells expressing *pUBN:GFP-PHGAP2,* stained with the endocytic sterol dye FM4-64 (Molecular Probes) to visualize cell walls and cell plates. U) GFP-PHGAP2 accumulates at the cortical division site (arrow heads) in cytokinesis. Asterisk indicates the developing cell plate. (k) GFP-PHGAP2 localizes to cytoplasm and plasma membrane but does not accumulate in a ring-pattern in a cytokinetic cell forming a new cell plate (asterisk). Scale bars indicate 10 µm. Relates to Figure 2

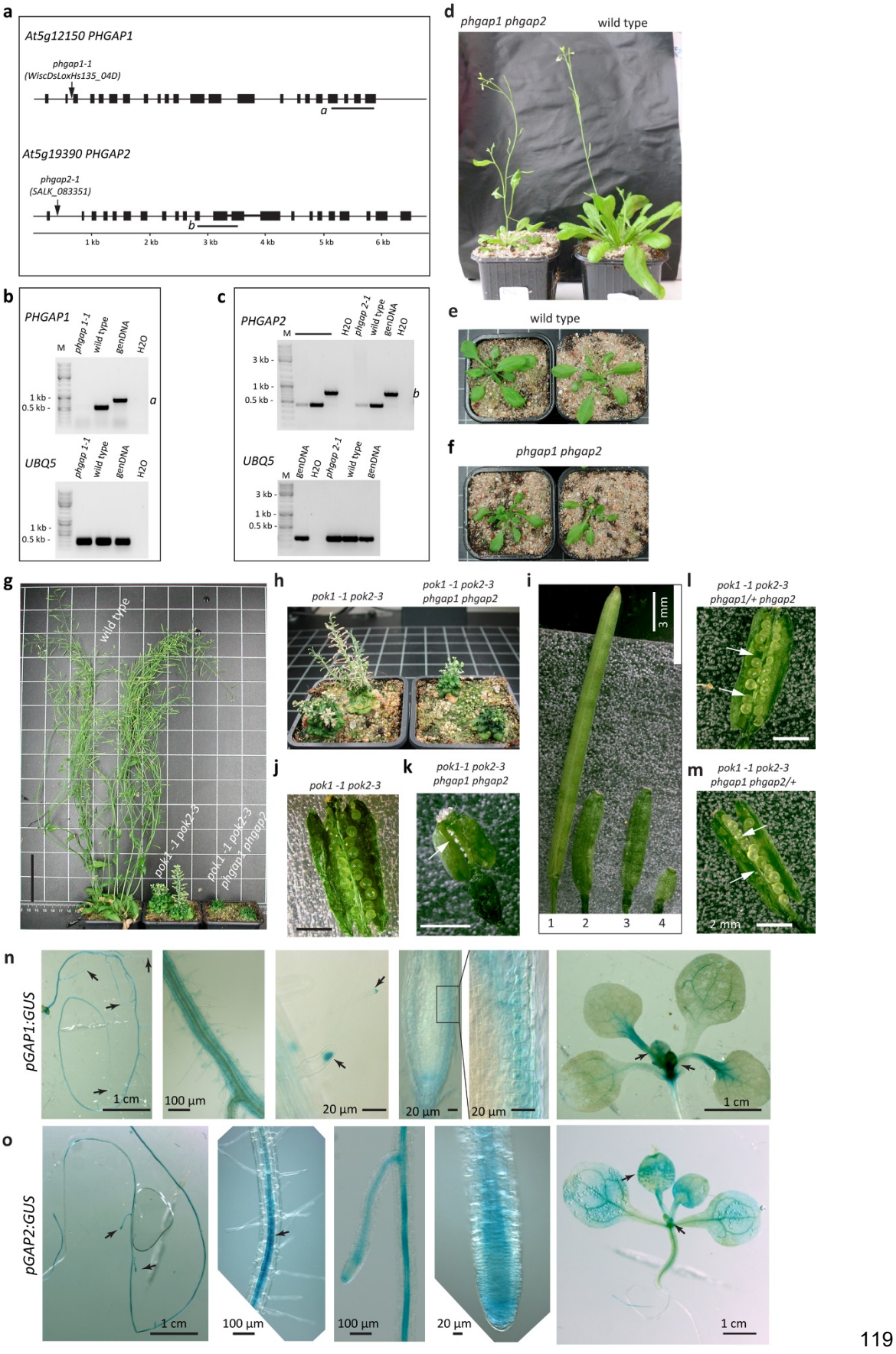
a
At5g12150 PHGAP1
phgap1-1
(WiscDsLoxHs135_04D)
a
At5g19390 PHGAP2
phgap2-1
(SALK_083351)
b
1 kb
2 kb
3 kb
4 kb
5 kb
6 kb
b
PHGAP1
M
phgap 1-1
wild type
genDNA
H2O
1 kb -
0.5 kb -
a
UBQ5
c
PHGAP2
M
H2O
phgap 2-1
wild type
genDNA
H2O
3 kb -
1 kb -
0.5 kb -
b
UBQ5
d
phgap1 phgap2
wild type
e
wild type
f
phgap1 phgap2
g
wild type
pok1 -1 pok2-3
pok1 -1 pok2-3
phgap1 phgap2
h
pok1 -1 pok2-3
pok1 -1 pok2-3
phgap1 phgap2
i
3 mm
1
2
3
4
l
pok1 -1 pok2-3
phgap1/+ phgap2
j
pok1 -1 pok2-3
k
pok1-1 pok2-3
phgap1 phgap2
m
pok1 -1 pok2-3
phgap1 phgap2/+
2 mm
n
pGAP1:GUS
1 cm
100 µm
20 µm
20 µm
20 µm
1 cm
o
pGAP2:GUS
1 cm
100 µm
100 µm
20 µm
1 cm

Supplemental Figure S3: Schematic representation of gene organization and position of T-DNA insertion sites. *PHGAP1* (At5g12150) and *PHGAP2* (At5g19390) gene organization is depicted and exons are indicated by bars. Respective positions of T-DNA insertions are specified by arrows. (b and c) Gel electrophoresis images of semi- quantitative RT-PCR comparing transcript levels of *phgap* mutant alleles and wild type. (b) For transcript amplification of *PHGAP1,* primer combinations (a), indicated in (a) were utilized. (c) *PHGAP2* amplification was accomplished using primers PHGAP2 01F and PHGAP2 01R (b), indicated in (a). Note that *PHGAP2* transcript was greatly reduced but not abolished. Genomic DNA (genDNA) and H20 served as positive and no-template control for the PCR reactions, respectively. Amplification of *UB/QU/TIN* (UBQ) *5* gene using primers NUBQ and CUBQ[2] served as loading control. cDNA synthesis was performed as described previously[2]. (g) Overview of wild type plants, *pok1-1 pok2-3* double mutant plants and *pok1-1 pok2-3 phgap1 phgap2* quadruple mutant plants at the same age. (h) Adult *pok1-1 pok2-3* double and *pok1-1 pok2-3 gap1 gap2* quadruple mutants. (i) Comparison of silique size (1) wild type, (2) *pok1-1 pok2-3* mutant, (3) *pok1-1 pok2-3 phgap1 phgap2/+* sesqui-mutant and (4) *pok1-1 pok2-3 phgap1 phgap2* quadruple mutant. (j to m) Comparison of the seed set in siliques. (j) *pok1-1 pok2- 3* double mutant displays abnormally round, fertilized ovules. (k) Non-fertilized ovules (arrow) in silique of infertile *pok1-1 pok2-3 phgap1 phgap2* quadruple mutant. (i) *pok1-1 pok2-3 phgap1/+ phgap2* and (m) *pok1-1 pok2-3 phgap1 phgap2/+* sesqui-mutants. Arrows point out gaps in seed set, indicative of aborted ovules. Scale bars indicate 6 cm in (g), 2 mm in (j. k, I, m). (n and o) Analysis of gene expression patterns in lines expressing *PHGAP* promoter:/3-Glucuronidase (GUS). (n) *PHGAP1* gene expression: GUS reporter gene expression was observed in elongated primary and lateral roots and in root hairs. In root meristems *PHGAP1:GUS* expression was predominant in the (e) epidermal and cortex cell files (zoom in of boxed area). In addition, GUS expression was evident in young leaf tissues and in the leaf vasculature. (o) *pPHGAP2:GUS* expression. In *pPHGAP2:GUS* lines, GUS reporter gene expression was evident in the root meristem and along the entire root system. Above the root meristem, expression becomes restricted to the vasculature in elongated and meristematic tissue. GUS expression was also prominent in young leaf tissues and in the leaf vasculature. While three hours of substrate incubation sufficed for strong staining in case of *pPHGAP2:GUS,* the samples expressing *pPHGAP1 :GUS* were incubated for three days resulting in faint staining. Cloning into pWD137 and analysis was performed as previously described[2-4]. Images were taken at a Zeiss Axiophot

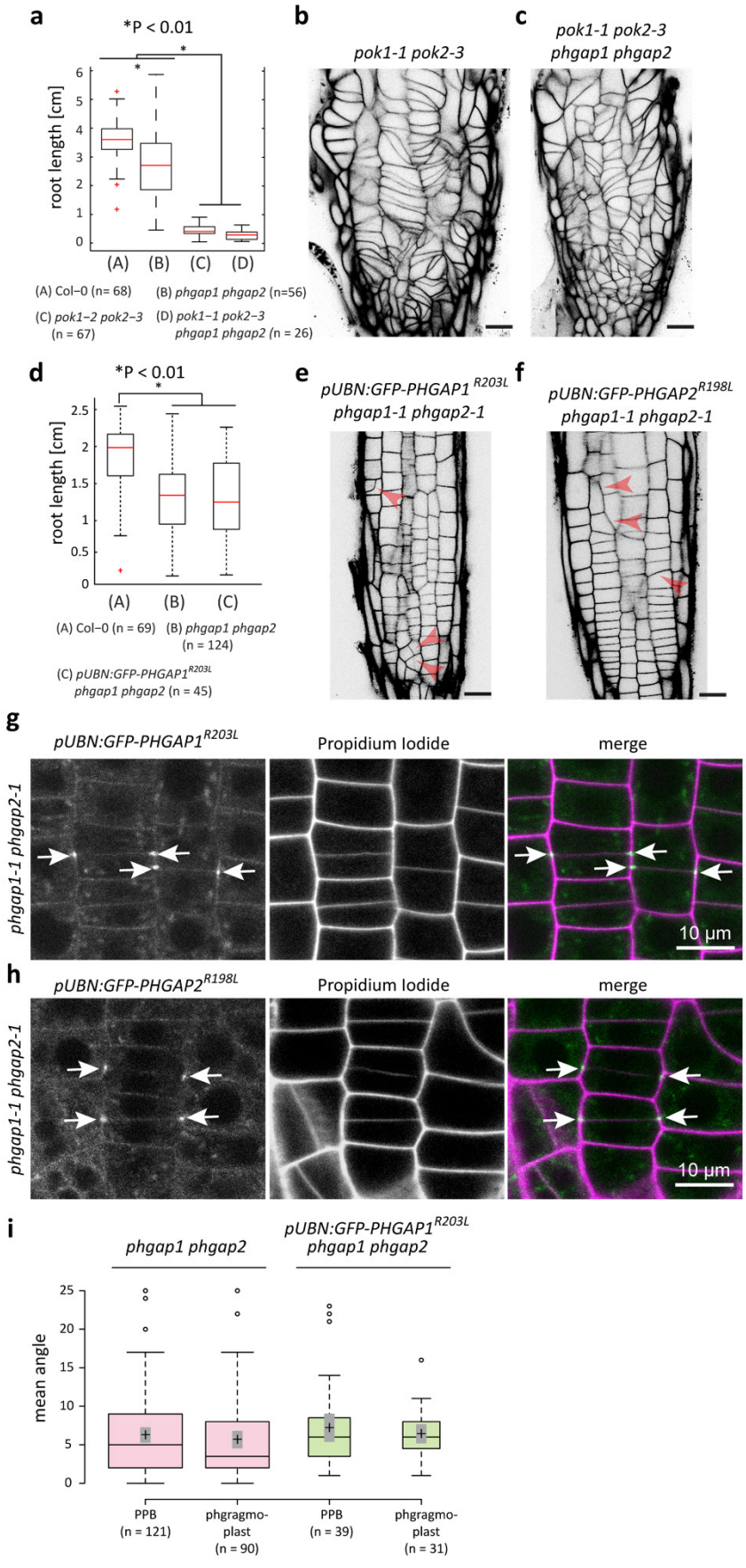
a
*P < 0.01
root length [cm]
(A) (B) (C) (D)
(A) Col–0 (n= 68)
(B) phgap1 phgap2 (n=56)
(C) pok1–2 pok2–3 (n = 67)
(D) pok1–1 pok2–3 phgap1 phgap2 (n = 26)
b
pok1-1 pok2-3
c
pok1-1 pok2-3 phgap1 phgap2
d
*P < 0.01
root length [cm]
(A) (B) (C)
(A) Col–0 (n = 69)
(B) phgap1 phgap2 (n = 124)
(C) pUBN:GFP-PHGAP1R203L phgap1 phgap2 (n = 45)
e
pUBN:GFP-PHGAP1 R203L phgap1-1 phgap2-1
f
pUBN:GFP-PHGAP2R198L phgap1-1 phgap2-1
g
pUBN:GFP-PHGAP1R203L
Propidium Iodide
merge
phgap1-1 phgap2-1
10 µm
h
pUBN:GFP-PHGAP2R198L
Propidium Iodide
merge
phgap1-1 phgap2-1
10 µm
i
phgap1 phgap2
pUBN:GFP-PHGAP1R203L phgap1 phgap2
mean angle
PPB (n = 121)
phgragmo-plast (n = 90)
PPB (n = 39)
phgragmo-plast (n = 31)

Supplemental Figure 54: Phenotype comparison. (a) Boxplot of primary root growth (10 day old seedlings) as indicated. Wild type (Col-0, A, mean 3.6 cm ± 0.7 STD) and *phgap1 phgap2* (B, mean 2.6 cm ± 1.2 STD) double mutants differ significantly in their root length (*P<0.01) and both, Col-0 and *phgap1 phgap2* are significantly (*P<0.01) different from *pok1-1 pok2-3* (C, mean 0.4 cm ± 0.2 STD) and *pok2-1 pok2-3 phgap1 phgap2* (D, mean 0.3 cm ± 0.2 STD) quadruple mutants.Significance was determined using One Way ANOVA. (b) Cell wall pattern of *pok1-1 pok2-3* root meristem. (c) Cell wall pattern of *pok2-1 pok2-3 phgap1* phgap2 quadruple mutant. (d) Boxplot of root growth of 7 day old seedlings as indicated. Wild type (A, mean 1.9 cm ± 0.4 STD) differs significantly (*P<0.01) from *phgap1 phgap2* (B, mean 1.3 cm ± 0.5 STD) and *pUBN:GFP-PHGAP1^{R203L}; phgap1 phgap2* (C, mean 1.3 cm ± 0.5 STD). Significance was determined using One Way ANOVA. (e and f) Cell wall pattern of root meristems expressing either (e) *pUBN:GFP-PHGAP1^{R203L}* or (f) *pUBN:GFP-PHGAP2^{R198L}* in *phgap 1phgap2* double mutant. Arrow heads indicate examples of cell wall miss-positioning. (g and h) Root meristem cells expressing either (g) *pUBN:GFP-PHGAP1^{R203L}* or (h) *pUBN:GFP-PHGAP2^{R198L}* in *phgap1 phgap2* double mutant. Note that GFP-PHGAP1^{R203L} and GFP-PHGAP2^{R198L} still locate to the cortical division site (CDS) in *phgap1 phgap2* mutants. (i) Mean deviation angle of PPBs and phragmoplast in *phgap1 phgap2* (corresponds to data shown in Figure 4i and 4j) and *GFP-PHGAP1^{R203L} phgap1 phgap2* are not significantly different. One Way Anova, post-hoc Turkey HSD P 0.39-0.9. Boxplots were assembled in MATLAB and BoxPlotR (http://boxplot.tyerslab.com/).

9.3 Herrmann et al. 2018

Dual localized kinesin-12 POK2 plays multiple roles during cell division and interacts with MAP65-3.

Arvid Herrmann, Pantelis Livanos, Elisabeth Lipka, Astrid Gadeyne, Daniel Van Damme, Marie-Theres Hauser and Sabine Müller

Embo Reports

Dual localized kinesin-12 POK2 plays multiple roles during cell division and interacts with MAP65-3

Arvid Herrmann[1‡], Pantelis Livanos[1‡], Elisabeth Lipka[1], Astrid Gadeyne[2], Marie-Theres Hauser[3], Daniël Van Damme[2], Sabine Müller[1*]

[1] Center for Plant Molecular Biology - Developmental Genetics; University of Tübingen; Tübingen, 72076; Germany

[2] Department of Plant Systems Biology; VIB; 9052 Ghent; Belgium

[3] Department of Applied Genetics and Cell Biology, University of Natural Resources and Life Sciences; 1190 Vienna, Austria

[*]Corresponding author: Sabine Müller

Developmental Genetics

ZMBP - Center for Plant Molecular Biology

University of Tübingen

Auf der Morgenstelle 32

72076 Tübingen

Germany

‡ these authors contributed equally

Summary

Kinesins are versatile nano-machines that utilize variable non-motor domains to tune specific motor-microtubule encounters. During plant cytokinesis, the kinesin-12 orthologs PHRAGMOPLAST ORIENTING KINESIN (POK)1 and POK2, are essential for rapid centrifugal expansion of the cytokinetic apparatus, the phragmoplast, towards a pre-selected cell plate fusion site at the cell cortex. Here, we report on the spatio-temporal localization pattern of POK2, mediated by distinct protein domains. Functional dissection of POK2 domains revealed the association of POK2 with the site of the future cell division plane and with the phragmoplast during cytokinesis. Accumulation of POK2 at the phragmoplast midzone depends on its functional POK2 motor domain and is fine-tuned by its carboxy-terminal region that also directs POK2 to the division site. Furthermore, POK2 likely stabilizes the phragmoplast midzone via interaction with the conserved microtubule associated protein MAP65-3/PLEIADE, a well-established microtubule cross-linker. Collectively, our results suggest that dual localized POK2 plays multiple roles during plant cell division.

Cell division, kinesin, cytokinesis, division site, division plane, MAP65, microtubule, cytoskeleton, phragmoplast, preprophase band, mitosis

Introduction

During cytokinesis, the physical partitioning of all cellular content, plant cells separate by an inward-to-outward directed division mode of centrifugal cell plate assembly, as opposed to a centripetal furrowing predominant in metazoan cytokinesis [1-3]. The plant cytokinetic apparatus, called phragmoplast, aids in cell plate biosynthesis. Here, we adopt the current nomenclature of plant cytokinesis structures and functions [4]. The phragmoplast is a bipolar array of highly dynamic microtubules, actin filaments and endomembranes that coordinates the delivery of cell plate biosynthetic vesicles for subsequent fusion within the plane of cell division [4, 5]. The majority of microtubules are organized antiparallel with their minus ends pointing towards the daughter nuclei (distal phragmoplast) and their plus ends adjoining the plane of cell division (phragmoplast midzone). This overall, bipolar organization guides secretory vesicle trafficking towards the division plane from both daughter cells [6, 7].

The conserved microtubule cross-linkers MAP65 are integral components of the phragmoplast. Their homologs in yeast, Ase1 and human, PRC1, maintain antiparallel microtubule overlap regions in the spindle and the midbody, the animal analog of the phragmoplast [8-10]. In plants, the microtubule cross- linking function of MAP65-3/PLEIADE (PLE), member of a protein family of nine in *Arabidopsis*, is in particular required for phragmoplast integrity and efficient cell plate formation [11-15]. Loss of MAP65- 3/PLE results in a functionally compromised phragmoplast due to a wider midzone than wild type, causing incomplete cell plate formation featuring stubs and gaps [11, 12]. Several other members of the MAP65 family, act redundantly with MAP65-3/PLE and localize at the entire phragmoplast or its midzone [15-18]. Spatial confinement to the phragmoplast midzone and MAP65 activity during cytokinesis is regulated by phosphorylation [19, 20]. Aurora kinase and mitogen activated protein kinases (MAPK) deactivate MAP65 and release the antiparallel microtubule overlap [18, 19, 21].

Subsequently, microtubules depolymerize in the central zone of the phragmoplast, where cell plate assembly initiated, while new microtubules polymerize at the phragmoplast leading zone, promoting its centrifugal expansion [4, 6]. Phragmoplast expansion is tightly coordinated with cell plate growth by the addition of newly arriving vesicles at its margins [22, 23]. The initial disk phragmoplast turns into a ring that expands radially, concurrent with the centrifugally evolving cell plate [24, 25]. Finally, the fusion of the cell plate with the parental plasma membrane terminates cytokinesis, but the subcellular location of cell plate fusion is not random.

A poorly understood guidance mechanism directs the radial expansion of the phragmoplast towards a pre-determined division site that is marked in prophase by the plant specific cytoskeletal preprophase band [26, 27]. Essentially, the preprophase band delineates the periphery of the division plane at the cell cortex and facilitates the recruitment of proteins that remain at the cell cortex, serving as fiducial markers of the division plane throughout cell division [4, 24, 28-32]. Perturbations of the division site or the guidance mechanism that ensures centrifugal phragmoplast expansion towards this site, lead to oblique cell plate insertions with dramatic consequences on growth performance [30, 31, 33-35].

Previous work established a closely related pair of *Arabidopsis* kinesin-12 motor proteins, PHRAGMOPLAST ORIENTING KINESIN (POK) 1 and its homolog POK2 as essential contributors of cytokinesis [31]. Based on the persistent presence of POK1 at the division site and the requirement

for both *POK1* and its homolog *POK2* to retain division site resident proteins beyond prophase, these kinesins are regarded as pivotal factors to identify and maintain the division site [28, 29, 31, 36]. In *pok1 pok2* double mutants, the distinct subcellular localization of division site resident proteins is lost from the division site upon metaphase, suggesting a scaffolding function for POKs at the division site [29, 31]. In these mutants, co-alignment of preprophase band, phragmoplast and cell plate fusion site, is disrupted, due to a notable slant of the phragmoplast [31, 34]. Furthermore, in *pok1 pok2* cytokinetic cells the rate of phragmoplast expansion is slower compared to wild type [31], implicating an additional function of POKs in phragmoplast dynamics. Here, we report a novel spatio-temporal localization pattern of POK2 that requires distinct protein domains. In addition to its anticipated localization at the cortical division zone the unexpected accumulation of POK2 at the phragmoplast midzone accounts for the phragmoplast expansion delay observed in the *pok1 pok2* double mutant. POK2 localization at the phragmoplast midzone requires motility and the microtubule cross-linker MAP65-3/PLE. Surprisingly, two separate POK2 regions bind to MAP65 proteins with distinct specificities. We propose that POK2 interaction further enhances MAP65-3 mediated stability of the midzone allowing rapid centrifugal expansion of phragmoplast.

Results

POK2 facilitates timely phragmoplast expansion

Previously, we reported on the cellular phenotype of *pok1 pok2* double mutants. Phragmoplast guidance is compromised, slowing down cytokinesis and causing oblique insertion of cell plates at high frequency, consequently affecting meristem organization and growth (Figure 1A-C) [31]. However, POK1 localizes exclusively at the division site, supporting its role in division site maintenance, but this localization pattern does not offer an immediate explanation for the puzzling reduction in the phragmoplast expansion rate that we observed in the *pok1 pok2* double mutant [31]. We suspected that the uncharacterized POK1 ortholog, POK2 performs non-redundant functions in phragmoplast expansion. Therefore, we investigated the expansion rate in *pok2-1* single mutants using kymograph analysis [37]. Phragmoplasts of *pok2-1* mutants, expand at a mean velocity (0.16 µm/min ± 0.04) similar to the *pok1 pok2* double mutant (0.15 µm/min ± 0.02), while wild type phragmoplasts expand about twice as fast (0.32 µm/min ± 0.07), consistent with our hypothesis that POK2 is involved in phragmoplast dynamics (Figure 1D-F) [31].

Dual localization of POK2 at the division site and the phragmoplast midzone

To investigate POK2 involvement in phragmoplast expansion further, we generated transgenic plant lines expressing a Green Fluorescent Protein (GFP)-POK2 fusion protein (Figure 2A, EV1A). Our attempts to propagate full length cDNA or full genomic clones and in *Agrobacterium* failed. However, we

succeeded to generate a full-length clone consisting of POK2 cDNA and genomic DNA (see Materials and Methods) driven by the *p35S* promoter. Polymerase chain reaction of wild type, transgenic and rescue line cDNA yielded identical fragments sizes, indicating correct splicing of the transgene (Figure EV1B). Introgression of *p35S:GFP-POK2* into the *pok1 pok2* mutant restored the phenotypic defects, confirming the functionality of GFP-POK2 transgene (Figure 2B, Appendix Figure S1A-G). Subsequently, we determined the cell cycle-specific, subcellular localization of GFP-POK2 in plant lines that co-express the microtubule reporter RFP-MBD (Figure 2C, EV1C, EV1D). We observed that POK2 displays a dual localization pattern. Consistent with our expectation and reminiscent of POK1 localization [31], GFP-POK2 marks the division site throughout cell division, forming a continuous equatorial ring at the plasma membrane (Figure 2C-F, Movie EV1, Movie EV2). This circular GFP-POK2 assembly accumulates at the preprophase band and remains associated with the underlying plasma membrane region, designated cortical division zone, beyond the disassembly of the preprophase band (Figure 2C, EV1C) [4]. The initially broad GFP-POK2 rings narrow during cytokinesis, resembling the narrowing of POK1, TAN and RanGAP1 at the cell plate fusion site (Figure 2E) [4, 28, 29, 31]. However, in addition to POK2 at the cortical division zone and cell plate fusion site, we observe GFP-POK2 at the midzone of the early disk phragmoplast, where it remains present throughout radial phragmoplast expansion (ring phragmoplast) (Figure 2E, 2F, EV1D, Table 1). Ultimately, the phragmoplast resident POK2 population merge with the division site resident POK2 as the phragmoplast leading edge approaches the division site upon cell plate fusion. The merge does not occur simultaneously at all sites but is particularly lagging behind only in cell corners (Figure 2F). The association of GFP-POK2 with the phragmoplast midzone strongly supports the requirement for POK2 in phragmoplast expansion. We cannot exclude that the reported localization pattern deviates from the endogenous POK2. However, the fusion-protein is regulated in a cell cycle dependent manner and shows the anticipated localization pattern and dynamics, based on POK2 functional analysis.

To determine whether POK2 localization depends on microtubules, we treated seedlings with the microtubule depolymerizing drug oryzalin. GFP-POK2 persists at the cortical division zone, even after the complete depolymerization of microtubules, similar to POK1 [31]. In contrast, GFP-POK2 at the phragmoplast vanished upon microtubule depolymerization (Figure EV1E). Consequently, once POK2 tethers to the division site, it is independent of microtubules, while its association with the phragmoplast midzone depends on the intact microtubule cytoskeleton, indicating that distinct mechanisms mediate division site and phragmoplast association of POK2.

To examine how individual protein domains, contribute to and establish the dual localization pattern and function of POK2, we decided to analyze the localization of POK2-domain deletion mutants. POK2 carboxy-terminal domain is sufficient to mark the division site. First, we determined the localization of the POK2 C-terminal region that corresponds to the respective POK1 region responsible for division site targeting (Figure 3A, EV2A) [31, 34]. GFP-POK2(2083-2771) decorates filaments, reminiscent of cortical microtubules and puncta or clusters close to the plasma membrane in interphase (Figure 3B). In mitotic cells, GFP-POK2(2083-2771) co-localizes with the preprophase band and disperses on spindle and phragmoplast, but it distinctly decorates the division site throughout mitosis and cytokinesis, demonstrating that the C-terminal region is sufficient for division site targeting (Figure 3C-3E, Table 1). De-polymerization of microtubules using 10 µM oryzalin abolishes filamentous GFP-POK2(2083-

2771), indicating its dependency on the microtubule cytoskeleton, but GFP-POK2(2083-2771) that is already present at the division site, persists throughout the treatment, revealing POK2 microtubule independent maintenance at the division site (Figure EV1F). To exclude a contribution of endogenous POK2 to the observed localization pattern, we examined GFP-POK2(2083-2771) distribution in the *pok1 pok2* double mutant (Figure EV2B-D). Compared to wild type mitotic cells that display intact GFP-POK2(2083-2771) rings, in *pok1 pok2* mutants about 30% of GFP-POK2(2083- 2771) rings are discontinuous, unveiling a reduction in the efficacy of cortical division zone targeting or retention (Figure 3E, 3F,3G, 3H, Table 1). However, the majority of *pok1-1 pok2-1* double mutant cells forms continuous rings at the position imposed by the preprophase band [34]. Yet, the expanding phragmoplasts disregard the spatial information provided by the cortical GFP-POK2 (2083-2771) rings resulting in inappropriate cell plate positioning (Figure 3E, 3F, EV2C, EV2D). Therefore, demarcation of the division site by GFP-POK2(2083-2771) alone is not sufficient to guide the phragmoplast.

In *Arabidopsis* interphase protoplasts, transiently expressed GFP-POK2(2083-2771) forms punctate clusters similar to the ones recorded in plants, but lack the microtubule association (Figure EV2G), suggesting that a cell cycle specific binding partner facilitates microtubule interaction *in planta*. Hence, *in planta* the POK2 C-terminal domain associates with microtubules either directly, and/or through interaction partners. Since POK2 C-terminal domain is sufficient to identify the division site, but fails to complement the mutant phenotype, these observations denote a critical contribution of POK2 motor domain for POK function at the division site.

The motor domain targets POK2 to the phragmoplast midzone

Next, we investigated the localization of the N-terminal POK2 motor domain by expression of GFP-POK2(1-589). This fusion protein contains the first coiled-coil domain of POK2 to facilitate anticipated dimerization (Figure 4A). As expected for a kinesin motor, GFP-POK2(1-589) associates with cortical microtubules in *Arabidopsis* interphase protoplasts (Figure EV2H). However, in *Arabidopsis* seedlings, we rarely observe GFP-POK2(1-589) association with cortical microtubules in interphase cells and only one fifth of preprophase bands are decorated with GFP-POK2(1-589) before it disappears upon preprophase band disassembly, in contrast to the C-terminal domain POK2(2083-2771) (Table 1, Appendix Figure S2A). In meta- and anaphase, GFP-POK2(1-589) remains cytosolic but, as the cells proceed to telophase, GFP-POK2(1-589) progressively associates with the midzone of the evolving phragmoplast and subsequently persists at the phragmoplast midzone until completion of cytokinesis (Figure 4B, Movie EV3). In *pok1 pok2* mutants, we observe the same topology, confirming that the N-terminal motor domain directs POK2 towards the phragmoplast midzone, but this is not sufficient to rescue the mutant phenotype (Figure 4C). Moreover, GFP-POK2(1-589) association with the phragmoplast disappears upon microtubule de-polymerization with oryzalin, demonstrating its microtubule-dependency (Figure EV1G). Taken together these results show that POK2 N-terminal domain mediates the interaction with microtubules. However, the distinct localization of GFP-POK2(1-589) at the preprophase band and the phragmoplast midzone, together with its absence from the spindle, support the existence of a regulatory mechanism underlying its cell cycle stage-specific accumulation.

ATP-hydrolysis is a prerequisite for POK2 phragmoplast midzone targeting

The exclusive localization of GFP-POK2(1-589) at the phragmoplast midzone where the majority of microtubule plus ends convene, suggests microtubule plus end directed motility, consistent with the prediction for N-terminal motor domains [38]. Consequently, we asked whether motility is a requirement for phragmoplast midzone association of GFP-POK2(1-589). Since ATP-hydrolysis is essential for motor motility, we generated a hydrolysis-deficient mutant GFP-POK2(1-589)^{T281N} by replacing the conserved threonine with asparagine at position 281 of the ATP-binding site within the motor domain (Figure 4A). Such rigor mutants bind microtubules tightly but are incapable of stepping along microtubules [39]. Contrary to GFP-POK2(1-589), the rigor mutant GFP-POK2(1-589)^{T281N} indeed associates with the entire length of microtubules, and lacks the distinct accumulation at the phragmoplast midzone (Figure 4D-4F, Appendix Figure S2B). In support of POK2 motility, GFP-POK2(1-589) traces linear trajectories with a mean velocity of 4.19 ± 1.03 µm/min (Appendix Figure S2I) in interphase cells of the root meristem (Appendix Figure S2C-E, Movie EV4). When co-expressed with RFP- End Binding (EB) 1b, a *bona fide* microtubule plus end tracking protein, their co-localization strongly supports the view that the POK2 motor domain is motile and moves towards microtubule plus ends (Appendix Figure S2F-H, Movie EV5). Collectively, these data suggest that microtubule plus end directed motility is a prerequisite for POK2 phragmoplast midzone targeting.

POK2 midzone association requires fine-tuning

Comparing the signal distribution with GFP-POK2, we noticed that the signal of GFP-POK2(1-589) at the phragmoplast midzone appeared wider (Figure 4G, Figure EV1E, EV1G, Appendix Figure S2A). Therefore, we quantified the average full width half maximum (FWHM) [40] of both signals at the midzone and confirmed that the distribution of GFP-POK2(1-589) is considerably broader than GFP-POK2, while the phragmoplast size remains equal (Figure 4H, 4I). This implies that POK2 restriction to the midzone is fine-tuned by POK2 domains that are absent from GFP-POK2(1-589).

In contrast to the C-terminal POK2(2083-2771), the N-terminal GFP-POK2(1-589) does not localize to the division site but is responsible for POK2 association with the phragmoplast midzone. Thus, the distinct dual localization pattern of POK2 at the division site and at the phragmoplast midzone is mediated independently, utilizing distinct protein domains and is regulated in a cell cycle dependent manner, likely by specific binding partners, by post-translational protein-modifications and/or by intramolecular inhibition. While POK2 at the plasma membrane marks/maintains the division site together with POK1, POK2 at the phragmoplast assists its timely expansion towards the division site. During the final stages of cytokinesis, the seemingly separate populations merge at the division site (Figure 2F).

Investigation of the POK2 central domain, lacking motor- and C-terminal domain, was hampered by our unsuccessful cloning attempts. Deletion of the central domain in GFP-POK2(Δ590-2082) did not interfere with microtubule association (Figure EV2I) or its localization pattern during mitosis, although it appears

less abundant compared to POK2(1-2771) (Figure EV2J-K, Table 1). This indicates that the central domain is dispensable for POK2 localization, but it might contribute to protein stability.

MAP65-3/PLE retains POK2 at the phragmoplast midzone

The striking localization of POK2 at the phragmoplast midzone is reminiscent of MAP65-3/PLE, an effective microtubule cross-linker of anti-parallel microtubules that is essential for phragmoplast integrity [11, 13]. Impairment of MAP65-3/PLE function causes a widening of the phragmoplast at the midzone that is hampering efficient cell plate assembly, featuring multinucleate cells, cell plate stubs and gaps (Figure 5, Appendix Figure S3) [11, 12]. The similarity of POK2 and MAP65-3/PLE localization in the phragmoplast midzone prompted us to investigate the potential interaction between the two proteins. We examined the phragmoplast midzone localization of GFP-POK2 in the MAP65-3/PLE mutant *pleiade (ple)-2* (Figure 5) [23, 41]. While GFP-POK2 signal at the division site is readily detectable, abundance of GFP-POK2 is diminished at the midzone of *ple-2* mutants compared to wild type (Figure 5A, 5B). Furthermore, in *ple-2* cytokinetic cells, the motor domain GFP-POK2(1-589) lacks the confinement to the phragmoplast midzone; instead, GFP-POK2(1-589) frequently decorates the entire length of phragmoplast microtubules, revealing the involvement of MAP65-3/PLE in restricting POK2 to the phragmoplast midzone (Figure 5C, Appendix S3B). As for the localization of the C-terminal domain POK2(2083-2771) we did not observe an altered localization in *ple-2* mutants. Like in wild type, GFP- POK2(2083-2771) localizes to the division site and scarcely decorates phragmoplast microtubules (Figure 5D, Appendix Figure S3A, S3C, S3D). In contrast to the GFP-POK2(1-589) motors that move towards the microtubule plus end-enriched midzone where they are retained by MAP65-3/PLE, the C-terminal GFP- POK2(2083-2771) does not even reach the midzone due to the lack of motility, however it might bind to other interaction partners along the phragmoplast.
Next, we investigated whether loss of *POK1* and *POK2* interferes with the localization pattern of MAP65-3/PLE in root meristematic cells [42]. In *pok1 pok2* mutants, as in wild type, GFP-MAP65-3/PLE is directed to the phragmoplast midzone, indicating that POK2 functions downstream of MAP65-3/PLE (Figure 5E, 5F, Appendix Figure S3E, S3F). However, the phragmoplast midzone in *pok1 pok2* mutants displays pronounced undulations hinting to a lack of stability (Figure 5E, 5F, Appendix Figure S3E, S3F), consistent with the reduction in phragmoplast expansion rate due to the loss of *pok2*. Taking these data together, we conclude that MAP65-3/PLE acts upstream of POK2.

POK2 interacts with MAP65-3/PLE via two distinct binding sites

The genetic interaction between POK2 and MAP65 might be indirect. Therefore, we investigated the interaction between POK2 and MAP65-3/PLE further by transient co-expression of GFP-POK2 domains and MAP65-3/PLE-RFP in tobacco leaves (Figure 6A). Notably, in tobacco, there is no expression of a MAP65-3 homolog [17]. Co-expression of the N-terminal GFP-POK2(1-589) with MAP65-3 showed the anticipated co-localization along microtubules, as each protein when expressed alone decorates microtubules (Figure 6B, 6C, 6D). However, MAP65-3/PLE, which specifically

cross-links anti-parallel microtubules labelled fewer microtubules than GFP-POK2(1-589). Since the motor domain POK2(1-589) is mis-localized in the *ple-2* mutants (Figure 5C, Appendix S3B), we wondered whether the disordered region upstream of the motor-domain might be responsible for interaction with MAP65-3/PLE. So, we removed the motor domain and created GFP-POK2(1-189). This fusion protein does not bind to microtubules in tobacco pavement cells, but remains cytosolic (Figure 6E). However, when co-expressed with MAP65-3/PLE, we observe co-localization of the short fragment GFP-POK2(1-189) with MAP65- 3/PLE (Figure 6F), but not with MAP65-5 which also localizes to the phragmoplast midzone (Figure EV3F, EV3G) [17], suggesting that this disordered POK2 domain is sufficient to facilitate interaction with the midzone resident MAP65-3/PLE.

Considering that the C-terminal domain POK2(2083-2771) might fine-tune POK2 localization at the midzone, we also investigated the interaction between POK2(2083-2771) and MAP65-3/PLE. In tobacco pavement cells, GFP-POK2(2083-2771) accumulates in punctate clusters, similar to the pattern observed in *Arabidopsis* interphase protoplasts (Figure 6G, Figure EV2G). When we co-expressed with MAP65- 3/PLE-RFP, we observe substantial overlap of GFP-POK2(2083-2771) and MAP65-3/PLE-RFP signal suggesting MAP65-3/PLE recruits the POK2 C-terminal domain to microtubules (Figure 6H). A mating-based split-ubiquitin assay in yeast, further corroborates direct interaction between both, the N-terminal GFP-POK2(1-189) (Figure 7A-C) and the C-terminal POK2(2083-2771) (Figure 7C) with MAP65-3/PLE. Expression of interactors was confirmed by immuno-blotting (Figure 7D, 7E, 7F, 7G). Together, these observations suggest that POK2 uses two distinct domains to interact with MAP65-3/PLE. We wondered about the specificity of the observed interactions and tested additional MAP65 family members, reported to associate with the phragmoplast, for co-localization with C-terminal POK2(2083-2771) in tobacco transient expression. In addition to MAP65-3/PLE, POK2 C-terminal domain co-localized with MAP65-1 and MAP65-5 (Figure EV3B, EV3C, EV3H, EV3G), indicating that the POK2 C-terminal binding site was not specific for MAP65-3/PLE. Interestingly, GFP-POK2(2083-2771) only co-localizes with MAP65-1-RFP along microtubules, but it is not recruited to the cytosol by MAP65-1(9D) mutant that fails to bind microtubules in tobacco (Figure EV3D, EV3E) [21], suggesting that interaction of POK2 and MAP65 requires the presence of microtubules. Along these lines, upon treatment with oryzalin, C- terminal POK2(2083-2771) reforms clusters close to the plasma membrane while MAP65-5 diffuses into the cytosol (Figure EV3I). Together the results support the view that POK2 interacts with microtubule bound-MAP65 isoforms.

In summary we show that two distinct protein domains are responsible for the dual localization of POK2 during cell division. The C-terminal domain is required for accurate localization at the division site, and the motor domain directs POK2 towards the phragmoplast midzone, where it contributes to phragmoplast stability in a MAP65-3/PLE dependent manner. ATP-dependent motor motility ensures microtubule plus end-directed translocation of POK2 toward phragmoplast midzone, where it is retained by MAP65-3/PLE through its interaction with the intrinsically disordered N-terminus of POK2 and further fine-tuned by the C-terminal POK2 domain.

Discussion

In this study, we clarified the cause of the phragmoplast expansion phenotype in the *pok1 pok2* double mutant phenotype. We investigated the role of the kinesin-12 POK2 in phragmoplast expansion and identified its dual localization pattern. POK2 resides at the division site aiding in its maintenance whereas the unexpected association with the phragmoplast assists radial expansion. Furthermore, we identified two potential MAP65-3/PLE binding sites in POK2 that likely differ in their specificity for MAP65 binding.

POK2 acts redundantly with POK1 in division site maintenance

Our previous work determined the homologous genes *POK1* and *POK2* as essential for division plane maintenance. Their joint effort identifies and preserves the division site by retaining division site resident proteins [29, 31, 36]. Reminiscent of POK1 localization [31], also POK2 tethers to the division site and displays comparable cell cycle and microtubule dependencies, suggesting redundancy of POK1 and POK2 activities. Of the six kinesin-12 in *Arabidopsis*, so far, only POK1 and POK2 are present to the division site [43-45]. Beyond their function in division site maintenance, we previously proposed POKs active involvement in phragmoplast guidance during late cytokinesis, mediated by peripheral microtubules that emanate from the phragmoplast leading zone [31]. In tobacco bright yellow (BY)-2 cells, peripheral microtubules of opposing phragmoplast halves polymerize from extant microtubules at shallow angles, some being cross-linked in the midzone by MAP65 [46]. In this study, in addition to its anticipated localization at the division site, we report POK2 at the phragmoplast midzone. Thus, POK2 localizes to these entities that merge upon cell plate fusion. This novel finding promotes POK2 as realistic candidate for interaction with peripheral microtubules, bridging the phragmoplast and the division site. Strikingly, in the moss *Physcomitrella patens*, the actin dependent motor protein MYOSIN (MYO) 8A, moves towards the phragmoplast midzone along peripheral microtubules and localizes to the division site [47]. Genetic impairment of all five moss *MYO8* genes causes disorganized cell wall insertion [47], together, pointing to possible mechanistic analogies between MYO8 and POK2 in *Physcomitrella* and *Arabidopsis* respectively. Nonetheless, how the expanding phragmoplast and the division site at the cell cortex communicate exactly, is still unresolved.

Regarding the exact mode of POK2 function at the division site and at the phragmoplast midzone only hypotheses can be made. Evidence concerning how kinesin-12 interact with microtubules from plants is still missing. However, in metazoan, kinesin-12 displays microtubule bundling and sliding activity. HsKif15 regulates spindle dynamics although the exact mechanism is currently debated [48-51]. *In vitro*, dimeric HsKif15 promotes microtubule sliding of higher order microtubules utilizing a motile motor in concert with a non-motor microtubule binding domain [50]. Other *in vitro* studies report tetrameric HsKif15 switching between microtubule tracks and HsKif15 motor collectives that display processive movement at steady velocity [52]. Recently, formation of tetrameric HsKif15 was reported also *in vivo* [53]. Whether POK2 form di- or tetramers and how they interact with microtubules requires further scrutiny and the dual localization of POK2 might complicate matters. POK2, at the division site, tethered by its C-terminal domain is likely dimeric and independent of microtubules. On the other hand, POK2 at the phragmoplast midzone depends on motility along microtubules and might be capable of

forming tetramers. Therefore, the mode of interaction of POK2 with microtubules might vary depending on its subcellular localization. Given the enormous size of POK2 and the different subcellular activities, intramolecular inactivation must be deemed likely and might be regulated post-translationally.

POK2 phragmoplast midzone targeting requires motility and accelerates phragmoplast expansion

The specific localization of POK2 at the phragmoplast midzone indicates a site-specific function. In *pok2* single and *pok1 pok2* double mutants alike, the mean phragmoplast expansion velocity is significantly slower than wild type, indicating POK2 is a major contributor to the timely expansion of the phragmoplast. Nevertheless, neither does the slower expansion rate interfere with the phragmoplast guidance mechanism towards the division site, since *pok2* single mutants do not show division plane defects [34], nor is the rapid phragmoplast expansion required for cell plate biosynthesis, as cell wall stubs, gaps and multi-nucleate cells, characteristics of failing cell plate biosynthesis, are absent from *pok2* single and *pok1 pok2* double mutants [31, 34]. In contrast, another pair of kinesin-1 in *Arabidopsis*, KINESIN12A and KINESIN12B exclusively localize to the phragmoplast in a MAP65-3/PLE- dependent manner and together these kinesins are essential for proper cell plate biosynthesis during male gametogenesis [13, 43, 54, 55]. Unless unknown redundancies are unresolved, rapid phragmoplast expansion is not compulsory for successful phragmoplast guidance or for normal cell plate biosynthesis. Our results suggest that motility is the prerequisite for POK2 midzone accumulation. The N-terminal region of POK2, containing the motor domain, localizes to the phragmoplast midzone in a microtubule dependent manner, demonstrating that this region is sufficient for POK2 midzone targeting. However, compared to full length POK2 at the midzone, the accumulation of the motor domain is slightly wider, suggesting a fine-tuning mechanism that involves additional regions of POK2. In contrast, the catalytically-inactive, motility-impaired mutant POK2(1-589)^{T281N} fails to localize to the midzone. This finding implies that POK2 moves towards microtubule plus ends to reach the division plane, where it likely contributes to microtubule plus end stabilization, as observed for high concentrations of tetrameric hKif15 which disables catastrophe at microtubule plus ends *in vitro* [51]. Consistent with the notion that POK2 might serve auxiliary function in microtubules plus-end stabilization, phragmoplasts are often twisted and bend in *pok1 pok2* mutants.

Kinesin-12 at the phragmoplast interact with MAP65

Although their roles in cytokinesis apparently differ, POK2 and kinesin-12A/B share the specific localization at the phragmoplast midzone, suggesting they utilize a similar targeting and/or retention mechanism possibly via conserved interactions with a specific binding partner, such as the phragmoplast specific MAP65-3/PLE. MAP65 proteins were proposed to serve as local platforms for the recruitment of kinesins [56, 57]. Indeed, kinesin12-A/B are completely abolished in the MAP65-3/PLE mutant *dyc283,* while PAKRP2 kinesin becomes evenly distributed along phragmoplast microtubules [12], similar to the N-terminal GFP-POK2(1-589) in the *ple-2* allele. On the other hand, MAP65-3/PLE localization is not impaired in *pok1 pok2* mutants, placing POK2 function downstream of MAP65-3/PLE.

Together with the genetic data, our co-localization and interaction assays demonstrate that MAP65-3/PLE may interact directly with both, POK2 motor-domain and C-terminal domain, recruiting them to microtubules. This provides compelling evidence for interaction of POK2 and MAP65 at the phragmoplast midzone. In tobacco, the N-terminal binding site in POK2(1-189), interacts specifically with MAP65-3, but not with phragmoplast midzone resident MAP65-5, while the C-terminal binding site in POK2(2083-2771) interacts with all MAP65 isoforms examined. This result suggests that the POK2 C- terminal domain may also associate with other paralogs of MAP65-3/PLE at the phragmoplast, such as MAP65-1/2, MAP65-5 and MAP65-4 [15, 17, 18]. While MAP65-1 decorates the entire phragmoplast, MAP65-5 is restricted to the midzone, similar to MAP65-3/PLE [16]. We propose that the interaction of the C-terminal GFP-POK2(2083-2771) with MAP65-3/PLE might reflect a general affinity of POK2 to MAP65 proteins, which also explains why POK2 recruitment to the midzone is not prohibited, but it is less efficient in *ple-2* mutants. Hence, microtubule association of POK2 C-terminal domain with the phragmoplast and cortical microtubules, which has never been observed in the case of POK1 C-terminal domain, when constitutively expressed [31], is likely mediated by MAP65 proteins.

We summarized the possible mechanism regarding potential POK2 functions in cytokinesis in a schematic model (Figure EV4). We show that motile POK2 moves towards microtubule plus ends and arrives at the midzone utilizing its motor-domain (Figure EV4). Both, the motor- and the C-terminal domain bind MAP65-3/PLE at anti-parallel microtubule overlaps, thereby sequestering POK2 at the phragmoplast midzone. We hypothesize that, in analogy to hKif15, POK2 might interact with microtubules, in the immediate vicinity of MAP65-3/PLE, which in turn might increase the affinity of POK2 C-terminal domain for microtubule interaction. Potentially, like HsKif15, POK2 motor collectives impede microtubule plus end catastrophe, thereby conferring further stability to the expanding phragmoplast. Besides, at the division site, tethered POK2 motors might stabilize microtubule plus ends of peripheral phragmoplast microtubules [31, 46], forming stable, transient connections at final stages of cytokinesis.

The dual localization of POK2 essentially represents the intersection of known plant kinesin-12 localization patterns. Its closest relative POK1 resides exclusively at the division site, although we must not categorically dismiss POK1 abundance at the phragmoplast below the detection limit of our imaging system [31]. The more distant relatives kinesin-12A and kinesin-12B exclusively localize to the phragmoplast midzone [54]. Animal kinesin-12 serve in spindle assembly, suggesting that microtubule sliding, bundling and stabilizing activity is its core function that might contribute to phragmoplast midzone stability in concert with MAP65 mediated phragmoplast organization. Therefore, POK localization at the division site is likely a derived plant specific function, while function at the phragmoplast might reflect an ancestral function. Thorough phylogenetic analysis and domain swap experiments might clarify whether POK2 incarnates an evolutionary intermediate between kinesin12A/B and POK1.

Materials and Methods

Plant material

In the present study, wild type, transgenic and mutant plants of the *Arabidopsis thaliana* accession Columbia (Col-0) were utilized. Mutants *pok1 pok2* and *pleiade-2* and GFP-MAP65-3/PLE were described previously [23, 31, 41, 42]. The allele combination *pok1-1 pok2-3* was used throughout the study.

Growth conditions

Arabidopsis seeds were surface sterilized with 6 % (v/v) sodium hypochlorite (Roth, Cat. 9062.3) and sown on plates containing ½ x Murashige and Skoog medium (Duchefa-Biochemie, MO221.0005) in 1 % (w/v) agar (Serva, 11396.03). Seeds were stratified for at least 24 hours at 4 °C in darkness. Subsequently, seedlings were grown at standard conditions (22 °C, 16 h light/8 h darkness cycle). For crossing or reproduction, two-week-old seedlings were transferred to soil and grown in a plant growth chamber under the above listed conditions.

Imaging

Imaging of seedlings was performed using either a Leica TCS-SP8, or a Zeiss LSM 880, both equipped with Argon/Krypton mixed gas laser source, proper filters and detectors and water immersion objective lens 40x or 63x with a numerical aperture of 1.10 or 1.20, respectively. Fluorescence signal in both microscopes was detected either with conventional photomultipliers or using Leica hybrid detectors and Zeiss GaAsP or the Airyscan detectors. GFP was exited with a 488 nm laser line whereas the detection wavelength range was 500-550 nm. For excitation of RFP, Propidium iodide and FM4-64, a 561 solid state laser line was used and the detection wavelength range was adjusted (570-650 nm and 570-720, respectively). Imaging was performed at constant room temperature of 22 °Celsius.

Localization patterns of POK2 fusion proteins

Dividing cells from seedlings co-expressing either of the fusion proteins along with the microtubule reporter RFP-MBD [31] were classified into individual cell cycle stages, based on mitotic microtubule array organization. For determining the presence or absence of GFP signal at a distinct subcellular location, only cells exhibiting RFP-MBD were taken into consideration.

Full width half maximum (FWHM) analysis

In ImageJ, single image planes of midzone/phragmoplasts were rotated (bicubic interpolation) to align the midzone with the y-axis. A plot profile of a rectangular selection of the phragmoplast was generated for each channel and the FWHM of the resulting plot profiles were determined in Excel. Measurements were averaged and Box plots were created using BoxPlotR (http://boxplot.tyerslab.com/). The Tukey-

whiskers extend to data points that are less than 1.5 x IQR away from 1st/3rd quartile. The significance values *P* were determined using one-way ANOVA with the post hoc Tukey HSD.

Treatment with oryzalin

Young seedlings, co-expressing either of the GFP fusion proteins and RFP-MBD, were treated with 10 µM oryzalin (Supelco, PS-410). Confocal images of the same root meristem region were obtained before and after treatment. An aqueous solution of 10 µM oryzalin was added at one edge of the microscope slide and simultaneously the mounting medium was removed from the other edge using filter paper. During treatment, z-stacks were taken at 3-5 min intervals. Depolymerization of microtubules was confirmed by the disappearance of RFP signal.

Image processing

Raw images were processed by ImageJ/Fiji [58], http://rsb.info.nih.gov/ij/. To correct for drift of single-channel and multichannel stacks were appropriate, the ‘‘StackReg’’ plugin was applied. Time laps movies were processed in ImageJ v1.51k. To reduce noise “Subtract Background” was performed with using Rolling Ball Radius 100.0. Kymographs were created in ImageJ v1.51k, using “Multiple Kymograph” plugin. Color merges were carried out with ImageJ v.1.48s, ImageJ v1.51k or Adobe Photoshop CS5 v12.0.4 (Adobe Systems). Only linear adjustments were applied. Figures were assembled in Adobe Illustrator CS5 v15.0.2.

Generating cDNA, amplification of PCR products and ligation

cDNA was essentially generated as described previously [34], using Superscript Reverse Transcriptase II (Invitrogen, 18064-022). PCR products for cloning purposes were amplified with Phusion DNA Polymerase (New England Biolabs, M0530L) (Appendix Table S2). Standard cloning was performed using Quick Ligation Kit (New England Biolabs, M2200L).

Generating entry clones

pENTR:POK2(2083-2771): The corresponding coding sequence was amplified from flower cDNA, digested with BamHI/XbaI and ligated with pENTR3C, digested with BamHI/XbaI.

pDONR:POK2(2083-2771): Coding sequence was amplified from pENTR:POK2(2083-2771) using primers flanked with minimal attB sites (Appendix Table S1). The PCR product was amplified with full-length attB1F and attB2R (Appendix Table S1) and cloned into pDONR221 via a Gateway BP reaction (Invitrogen, 11789-020).

pENTR:POK2(1-589): Corresponding coding sequence was amplified from flower cDNA and inserted into pOCC10 sub-cloning vector via NotI/AscI. Subsequently the insert, digested with AscI, blunted and digested with BamHI. Simultaneously, pENTR3C was digested with BamHI/EcoRV. Subsequently fragments were ligated .

pENTR:POK2(1-589)^{T281N}: Point mutations in the AT binding site (T281N) was introduced by amplification from pENTR3C_POK2(1-589) using mismatch primers (Appendix Table S1). The two overlapping amplicons were fused via extension PCR. The resulting fragment was cloned into the pENTR:POK2(1-589) via NotI/BstEII digest to replace the respective wild type fragment.

pENTR:POK2(1-189) and pENTR:POK2(183-589): PCR products corresponding to fragments POK2 (1-189) or POK2(183-589) were amplified with appropriate primers (Appendix Table S1), digested with NotI/XbaI and ligated into NotI/XbaI sites of pENTR:POK2(1-589).

pENTR:POK2(Δ590-2082): POK2(1-589) and POK2(2083-2771) were amplified from respective pENTR clones and subsequently combined by fusion PCR introducing a short linker sequence (Appendix Table S1). The PCR product and pENTR:POK2(1-589) were digested with NcoI/XbaI and ligated, resulting in pENTR3C:POK2(Δ590-2082).

pENTR:POK2(1-2771): The pENTR:POK2(Δ590-2082) vector and PCR product PCRI (Appendix Table S1) were digested with BstEII/XhoI and ligated. The resulting vector was linearized with BstEII and a 3654 bp BstEII fragment, resulting from a digest of PCR product PCRII (Appendix Table S1), was inserted. The final full length clone represents a hybrid of cDNA and genomic DNA.

pENTR:MAP65-3/PLE: The coding sequence, without stop codon was amplified (Appendix Table S1) from seedling cDNA and cloned into pENTR3C via KpnI/NotI.

pENTR:EB1b: The coding sequence of EB1b was amplified from seedling cDNA and cloned in to the pGEM T-easy vector (Promega, A1360). From there, it was cloned into pENTR2B via EcoRI/XhoI digest and subsequent ligation.

Generating XFP-expression clones

GFP-POK2(2083-2771): pDONR221: POK2(2083-2771) was used in a Gateway LR reaction (Invitrogen, 11791-020) with pK7WGF2 to create the N-terminal GFP-fusion protein [59].

GFP-POK2(1-589): Subcloning vector pOCC10:POK2(1-589) was sequentially digested with SgsI, blunted and digested with XbaI. Simultaneously binary vector pFK241 pGreenIIS was sequentially digested with BsrgI, blunted and digested with XbaI. The resulting fragments were ligated.

GFP-POK2(1-2771): pENTR:POK2(1-2771) was recombined with pFK241 pGreenIIS in a Gateway LR reaction.

MAP65-X-RFP: pENTR:MAP65-3/PLE, pDONR207: MAP65-1 [16], pDONR207: MAP65-1-(9D) [21] and pDONR207: MAP65-5 [16] were used in a Gateway LR reaction (Invitrogen, 11791-020) with pB7RWG2 to create the C-terminal RFP-fusion protein [59].

Plant transformation

Transgene integration into the plant genome was accomplished by the *Agrobacterium tumefaciens* transformation [60], using strain GV3101. Screening for resistant transformants was performed on appropriate selective medium.

Rescue lines

To examine the rescue ability of GFP-POK2(1-2771), a selected transgenic T2 line was crossed with the *pok1-1 pok2-3* double mutant. F2 plants were examined for the presence of the GFP-POK2(1-2771) transgene (resistance to Kanamycin) and the *pok1-1 pok2-3* mutant phenotypes, which was reduced to 9% (n = 137) compared to the expected 20% usually obtained for *pok1-1 pok2-3* mutant [31]. F2 plants were genotyped for the presence of the T-DNA insertion in *pok1-1 pok2-3* [31]. Phenotypes of selected F3 plants (87> n < 102) homozygous for both were further examined. Phenotypic defects, characteristic of *pok1-1 pok2-3* double mutant (number of cotyledons and angle between them, reduced seed germination) and root development are repressed in the F3 lines compared to *pok1-1 pok2-3* mutants and GFP-POK2(1-2771) transgenic line, implying that GFP-POK2(1-2771) is sufficient to rescue the mutant phenotype. All F3 plants were genotyped and confirmed to be *pok1-1 pok2-3.*

Staining with fluorescent dyes

To visualize cell plate formation and the root architecture, 4 to 6 day old seedlings were mounted in aqueous solution of either FM4-64 (1:1000; Invitrogen Cat. F34653) or propidium iodide (10 µg/ml; Sigma-Aldrich, 1002395778). FM4-64 stains the plasma membrane as well as the developing cell plate, and propidium iodide labels the cell walls of living plant cells.

Mating-Based Cyto-SUS Assays

The Mating Based Cyto-SUS Assay was performed as described previously [36]. In single Gateway LR reactions, pENTR:MAP65-3/PLE was cloned into the OST-Cub destination vector, whereas pENTR:POK2(1-189), pENTR:POK2(183-589), pENTR:POK2(1-589) and pENTR:POK2(2083-2771) were cloned into the pNX35-Dest destination vector [61, 62]. Expression clones were transformed into yeast, mated and dropped on selection plates. To confirm fusion protein expression, yeast cells were harvested before mating and proteins were extracted. To detect fusion proteins, we performed Western Blot analyses using anti-HA antibody coupled with Peroxidase (1:10000; Roche, Cat. 12013819001) for detection of NubG-2xHA-X fusion proteins and for detection of OST-MAP65-3/PLE-LexA fused to Cub, anti-VP16 (1:1000; GeneTex, Cat. GTX30776) antibody was used as a first antibody and anti-rabbit-POD (1:10000; Merck-Millipore, Cat. AP307P) for detection (BM Chemiluminescence Blotting Substrate POD, Roche 11500708001).

Transient Expression of fusion proteins in *Tobacco* leaves

Wild-type tobacco (*Nicotiana benthamiana*) plants were grown in soil at 26°C on standard day and night conditions (16-h-day/8-h-night cycle). Up to three fully expanded leaves of four to five-week-old tobacco seedling were infiltrated with 2 ml of *Agrobacterium tumefaciens* GV3101 culture carrying respective plasmids. Before infiltration, cultures, grown to OD_{600} 1.0, were pelleted and washed twice in dH2O,

then adjusted to OD_{600} 0.8. For co-expression of fusion proteins, *Agrobacterium* cultures carrying different plasmids were mixed before infiltration.

Bioinformatic analyses

Motor domain prediction was extracted from Uniprot (http://www.uniprot.org/uniprot/A0A178VJB1) [63]. Coiled-coil domains were predicted by Pair Coil (http://cb.csail.mit.edu/cb/paircoil2/)[64].

Data availability

Sequence data from this article can be found in the Arabidopsis Genome Initiative or GenBank/EMBL databases under the following accession numbers: POK2 (AT3G19050), MAP65-3/PLEIADE (AT5G51600), MAP65-1 (AT5G55230), MAP65-5 (AT2G38720), EB1b (AT5G62500).

Acknowledgements

We acknowledge the ABRC and NASC for distribution of seed used in this study. We appreciate the help of Bettina Alber, Jens Reich, Leander Rohr, Steffi Zimmermann and Luise Zühl with data collection. We thank Frank Küttner for sharing the plasmid pFK241 pGreenIIS. We gratefully acknowledge support from the University of Tübingen and funding from the Deutsche Forschungsgemeinschaft to SM (MU 3133/1-1 and MU 3133/5-1).

Author Contributions

E.L., A.H., P.L. performed experiments and analyzed data. A.G., D.V.D. and M.-T.H. provided material. S.M. analyzed data, conceptualized research, wrote the initial manuscript, all authors contributed to editing of the final manuscript.

Conflict of interest

The authors declare no conflict of interest.

References

1. Rappaport R (1986) Establishment of the mechanism of cytokinesis in animal cells. *Int Rev Cytol* **105**: 245-81

2. Jurgens G (2005) Cytokinesis in higher plants. *Annu Rev Plant Biol* **56**: 281-99

3. Lipka E, Herrmann A, Mueller S (2015) Mechanisms of plant cell division. *WIREs Dev Biol* **4**: 391– 405

4. Smertenko A, Assaad, F., Baluska, F., Bezanilla, M., Buschmann, H., Van Damme, D, Drakakaki, G, Hauser, M.-T., Janson, M., Mineyuki, Y., Moore, I., Müller, S., Murata, T., Otegui, M.S., Panteris, E., Rasmussen, C., Schmit, A.-C., Šamaj, J, Samuels, L., Staehelin, A., Wasteneys, G., Žárský, V., (2017) Plant cytokinesis: terminology for structures and processes. *Trends Cell Biol* **27**: 885-894

5. Park M, Touihri S, Muller I, Mayer U, Jurgens G (2012) Sec1/Munc18 protein stabilizes fusioncompetent syntaxin for membrane fusion in Arabidopsis cytokinesis. *Developmental cell* **22**: 989-1000

6. Smertenko AP, Piette B, Hussey PJ (2011) The Origin of Phragmoplast Asymmetry. *Curr Biol* **22**: 1924-1930

7. Richter S, Kientz M, Brumm S, Nielsen ME, Park M, Gavidia R, Krause C, Voss U, Beckmann H, Mayer U*, et al.* (2014) Delivery of endocytosed proteins to the cell-division plane requires change of pathway from recycling to secretion. *eLife* **3**: e02131

8. Otegui MS, Verbrugghe KJ, Skop AR (2005) Midbodies and phragmoplasts: analogous structures involved in cytokinesis. *Trends in Cell Biology* **15**: 404-413 26

9. Yamashita A, Sato M, Fujita A, Yamamoto M, Toda T (2005) The Roles of Fission Yeast Ase1 in Mitotic Cell Division, Meiotic Nuclear Oscillation, and Cytokinesis Checkpoint Signaling. *Molecular Biology of the Cell* **16**: 1378-1395

10. Subramanian R, Wilson-Kubalek EM, Arthur CP, Bick MJ, Campbell EA, Darst SA, Milligan RA, Kapoor TM (2010) Insights into antiparallel microtubule crosslinking by PRC1, a conserved nonmotor microtubule binding protein. *Cell* **142**: 433-443

11. Müller S, Smertenko A, Wagner V, Heinrich M, Hussey PJ, Hauser MT (2004) The plant microtubule-associated protein AtMAP65-3/PLE is essential for cytokinetic phragmoplast function. *Curr Biol* **14**: 412-7

12. Ho C-MK, Hotta T, Guo F, Roberson RW, Lee Y-RJ, Liu B (2011) Interaction of antiparallel microtubules in the phragmoplast is mediated by the microtubule-associated protein MAP65-3 in *Arabidopsis*. *Plant Cell* **23**: 2909-2923

13. Ho C-MK, Lee Y-RJ, Kiyama LD, Dinesh-Kumar SP, Liu B (2012) Arabidopsis Microtubule-Associated Protein MAP65-3 Cross-Links Antiparallel Microtubules toward Their Plus Ends in the Phragmoplast via Its Distinct C-Terminal Microtubule Binding Domain. *The Plant Cell Online* **24**: 2071-2085

14. Kosetsu K, de Keijzer J, Janson ME, Goshima G (2013) MICROTUBULE-ASSOCIATED PROTEIN65 Is Essential for Maintenance of Phragmoplast Bipolarity and Formation of the Cell Plate in Physcomitrella patens. *The Plant Cell Online* **25**: 4479-4492

15. Li H, Sun B, Sasabe M, Deng X, Machida Y, Lin H, Julie Lee YR, Liu B (2017) Arabidopsis MAP65-4 plays a role in phragmoplast microtubule organization and marks the cortical cell division site. *New Phytologist* **215**: 187-201

16. Van Damme D, Van Poucke K, Boutant E, Ritzenthaler C, Inzé D, Geelen D (2004) In Vivo Dynamics and Differential Microtubule-Binding Activities of MAP65 Proteins. *Plant Physiology* **136**: 3956- 3967

17. Smertenko AP, Kaloriti D, Chang H-Y, Fiserova J, Opatrny Z, Hussey PJ (2008) The C-Terminal Variable Region Specifies the Dynamic Properties of Arabidopsis Microtubule-Associated Protein MAP65 Isotypes. *The Plant Cell* **20**: 3346-3358

18. Sasabe M, Kosetsu K, Hidaka M, Murase A, Machida Y (2011) Arabidopsis thaliana MAP65-1 and MAP65-2 function redundantly with MAP65-3/PLEIADE in cytokinesis downstream of MPK4. *Plant signaling & behavior* **6**: 743-7

19. Sasabe M, Machida Y (2006) MAP65: a bridge linking a MAP kinase to microtubule turnover. *Current opinion in plant biology* **9**: 563-70

20. Sasabe M, Soyano T, Takahashi Y, Sonobe S, Igarashi H, Itoh TJ, Hidaka M, Machida Y (2006) Phosphorylation of NtMAP65-1 by a MAP kinase down-regulates its activity of microtubule bundling and stimulates progression of cytokinesis of tobacco cells. *Genes & Development* **20**: 1004-1014 27

21. Boruc J, Weimer AK, Stoppin-Mellet V, Mylle E, Kosetsu K, Cedeño C, Jaquinod M, Njo M, De Milde L, Tompa P*, et al.* (2017) Phosphorylation of MAP65-1 by Arabidopsis Aurora Kinases Is Required for Efficient Cell Cycle Progression. *Plant Physiology* **173**: 582

22. Boruc J, Van Damme D (2015) Endomembrane trafficking overarching cell plate formation. *Current opinion in plant biology* **28**: 92-98

23. Steiner A, Rybak K, Altmann M, McFarlane HE, Klaeger S, Nguyen N, Facher E, Ivakov A, Wanner G, Kuster B*, et al.* (2016) Cell cycle-regulated PLEIADE/AtMAP65-3 links membrane and microtubule dynamics during plant cytokinesis. *Plant J* **88**: 531-541

24. Müller S, Jürgens G (2016) Plant cytokinesis—No ring, no constriction but centrifugal construction of the partitioning membrane. *Seminars in Cell & Developmental Biology* **53**: 10-18

25. Smertenko A, Hewitt SL, Jacques CN, Kacprzyk R, Liu Y, Marcec MJ, Moyo L, Ogden A, Oung HM, Schmidt S*, et al.* (2018) Phragmoplast microtubule dynamics - a game of zones. *J Cell Sci* **131**

26. Wick SM, Duniec J (1983) Immunofluorescence microscopy of tubulin and microtubule arrays in plant cells. I. Preprophase band development and concomitant appearance of nuclear envelopeassociated tubulin. *The Journal of cell biology* **97**: 235-43

27. Mineyuki Y (1999) *The Preprophase Band of Microtubules: Its Function as a Cytokinetic Apparatus in Higher Plants*. In International Review of Cytology, Kwang WJ (ed) pp 1-49. Academic Press

28. Walker KL, Muller S, Moss D, Ehrhardt DW, Smith LG (2007) Arabidopsis TANGLED identifies the division plane throughout mitosis and cytokinesis. *Curr Biol* **17**: 1827-36

29. Xu XM, Zhao Q, Rodrigo-Peiris T, Brkljacic J, He CS, Muller S, Meier I (2008) RanGAP1 is a continuous marker of the Arabidopsis cell division plane. *Proc Natl Acad Sci U S A* **105**: 18637-42

30. Martinez P, Luo A, Sylvester A, Rasmussen CG (2017) Proper division plane orientation and mitotic progression together allow normal growth of maize. *Proc Natl Acad Sci U S A* **114**: 2759-2764

31. Lipka E, Gadeyne A, Stöckle D, Zimmermann S, De Jaeger G, Ehrhardt DW, Kirik V, Van Damme D, Müller S (2014) The Phragmoplast-Orienting Kinesin-12 Class Proteins Translate the Positional Information of the Preprophase Band to Establish the Cortical Division Zone in Arabidopsis thaliana. *Plant Cell* **26**: 2617-2632

32. Buschmann H, Dols J, Kopischke S, Peña EJ, Andrade-Navarro MA, Heinlein M, Szymanski DB, Zachgo S, Doonan JH, Lloyd CW (2015) Arabidopsis KCBP interacts with AIR9 but stays in the cortical division zone throughout mitosis via its MyTH4-FERM domain. *Journal of Cell Science* **128**: 2033-2046

33. Smith LG, Hake S, Sylvester AW (1996) The tangled-1 mutation alters cell division orientations throughout maize leaf development without altering leaf shape. *Development* **122**: 481-9

34. Müller S, Han S, Smith LG (2006) Two kinesins are involved in the spatial control of cytokinesis in Arabidopsis thaliana. *Curr Biol* **16**: 888-94

35. Mir R, Morris VH, Buschmann H, Rasmussen CG (2018) Division Plane Orientation Defects Revealed by a Synthetic Double Mutant Phenotype. *Plant Physiology* **176**: 418-431 28

36. Stöckle D, Herrmann A, Lipka E, Lauster T, Gavidia R, Zimmermann S, Müller S (2016) Putative RopGAPs impact division plane selection and interact with kinesin-12 POK1. *Nature Plants* **2**: 16120

37. Livanos P, Chugh M, Müller S (2017) *Analysis of Phragmoplast Kinetics During Plant Cytokinesis*. In Plant Protein Secretion: Methods and Protocols, Jiang L (ed) pp 137-150. New York, NY: Springer New York

38. Endow SA, Kull FJ, Liu H (2010) Kinesins at a glance. *Journal of Cell Science* **123**: 3420-3424

39. Nakata TH, Nobutaka (1995) Point mutation of adenosine triphosphate-binding motif generated rigor kinesin that selectively blocks anterograde lysosome membrane transport. *The Journal of cell biology* **131**: 1039-1053

40. de Keijzer J, Kieft H, Ketelaar T, Goshima G, Janson ME (2017) Shortening of Microtubule Overlap Regions Defines Membrane Delivery Sites during Plant Cytokinesis. *Current Biology* **27**: 514-520

41. Müller S, Fuchs E, Ovecka M, Wysocka-Diller J, Benfey PN, Hauser MT (2002) Two new loci, PLEIADE and HYADE, implicate organ-specific regulation of cytokinesis in Arabidopsis. *Plant Physiol* **130**: 312-24

42. Steiner A, Muller L, Rybak K, Vodermaier V, Facher E, Thellmann M, Ravikumar R, Wanner G,Hauser MT, Assaad FF (2016) The Membrane-Associated Sec1/Munc18 KEULE is Required for Phragmoplast Microtubule Reorganization During Cytokinesis in Arabidopsis. *Mol Plant* **9**: 528-40

43. Lee YR, Li Y, Liu B (2007) Two Arabidopsis phragmoplast-associated kinesins play a critical role incytokinesis during male gametogenesis. *Plant Cell* **19**: 2595-605

44. Lipka E, Müller S (2012) Potential roles for Kinesins at the cortical division site. *Frontiers in plantscience* **3**: 158

45. Zhu C, Dixit R (2012) Functions of the Arabidopsis kinesin superfamily of microtubule-based motor proteins. *Protoplasma* **249**: 887-99

46. Murata T, Sano T, Sasabe M, Nonaka S, Higashiyama T, Hasezawa S, Machida Y, Hasebe M (2013) Mechanism of microtubule array expansion in the cytokinetic phragmoplast. *Nat Commun* **4:** doi:10.1038/ncomms2967

47. Wu S-Z, Bezanilla M (2014) Myosin VIII associates with microtubule ends and together with actin plays a role in guiding plant cell division. *eLife* **3:**e03498

48. Boleti H, Karsenti E, Vernos I (1996) Xklp2, a Novel Xenopus Centrosomal Kinesin-like Protein Required for Centrosome Separation during Mitosis. *Cell* **84**: 49-59

49. Hancock William O (2014) Mitotic Kinesins: A Reason to Delve into Kinesin-12. *Current Biology* **24**: R968-R970

50. Sturgill Emma G, Das Dibyendu K, Takizawa Y, Shin Y, Collier Scott E, Ohi Melanie D, Hwang W, Lang Matthew J, Ohi R (2014) Kinesin-12 Kif15 Targets Kinetochore Fibers through an Intrinsic Two-Step Mechanism. *Current Biology* **24**: 2307-2313 29

51. Drechsler H, McAinsh AD (2016) Kinesin-12 motors cooperate to suppress microtubule catastrophes and drive the formation of parallel microtubule bundles. *Proceedings of the National Academy of Sciences* **113**: E1635-E1644

52. Drechsler H, McHugh T, Singleton MR, Carter NJ, McAinsh AD (2014) The Kinesin-12 Kif15 is a processive track-switching tetramer. *eLife* **3**: e01724

53. Mann BJ, Balchand SK, Wadsworth P (2017) Regulation of Kif15 localization and motility by the Cterminus

of TPX2 and microtubule dynamics. *Molecular Biology of the Cell* **28**: 65-75

54. Lee YR, Liu B (2000) Identification of a phragmoplast-associated kinesin-related protein in higher plants. *Curr Biol* **10**: 797-800

55. Pan R, Lee YR, Liu B (2004) Localization of two homologous Arabidopsis kinesin-related proteins in the phragmoplast. *Planta* **220**: 156-64

56. Lee Y-RJ, Liu B (2013) The rise and fall of the phragmoplast microtubule array. *Current opinion in plant biology* **16**: 757-763

57. Walczak CE, Shaw SL (2010) A MAP for Bundling Microtubules. *Cell* **142**: 364-367

58. Rasband WS (1997-2014) ImageJ. *(Bethesda, Maryland: US National Institutes of Health)*

59. Karimi M, Inzé D, Depicker A (2002) GATEWAY™ vectors for Agrobacterium-mediated plant transformation. *Trends in Plant Science* **7**: 193-195

60. Clough SJ, Bent AF (1998) Floral dip: a simplified method forAgrobacterium-mediated transformation of Arabidopsis thaliana. *The Plant Journal* **16**: 735-743

61. Grefen C, Blatt MR (2012) Do Calcineurin B-Like Proteins Interact Independently of the Serine Threonine Kinase CIPK23 with the K+ Channel AKT1? Lessons Learned from a Ménage à Trois. *Plant Physiology* **159**: 915-919

62. Karnik R, Zhang B, Waghmare S, Aderhold C, Grefen C, Blatt MR (2015) Binding of SEC11 Indicates Its Role in SNARE Recycling after Vesicle Fusion and Identifies Two Pathways for Vesicular Traffic to the Plasma Membrane. *The Plant Cell* **27**: 675-694

63. Consortium TU (2017) UniProt: the universal protein knowledgebase. *Nucleic Acids Research* **45**: D158-D169

64. McDonnell AV, Jiang T, Keating AE, Berger B (2006) Paircoil2: improved prediction of coiled coils from sequence. *Bioinformatics* **22**: 356-358

Figure and Table Legends

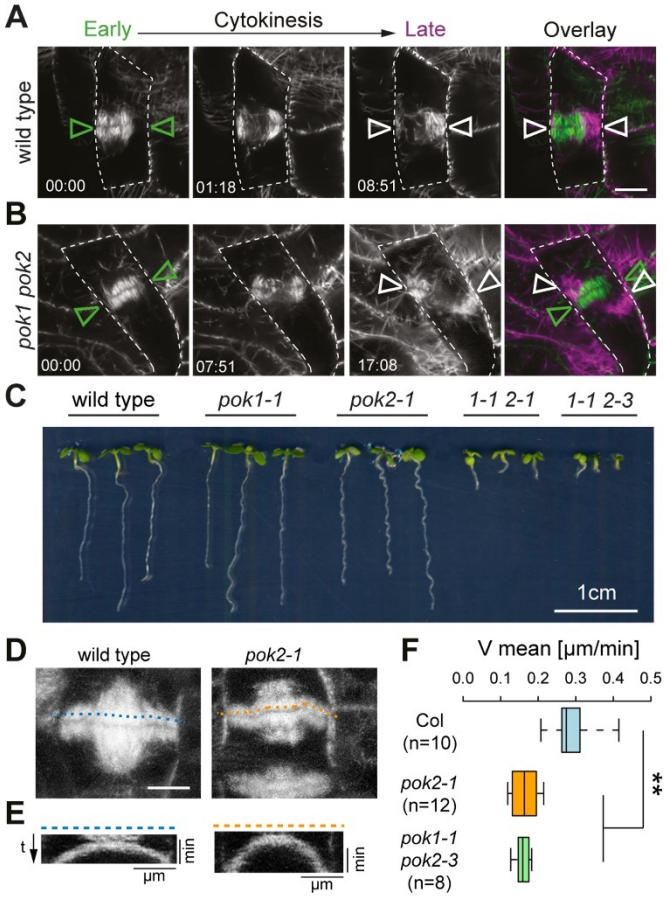

Figure 1

Figure 1: Comparative analysis of phragmoplast expansion.

(A, B) Three representative time points (in min) of phragmoplast expansion in (A) wild type and (B) *pok1 pok2* double mutant are depicted. Microtubules are visualized with fluorescent reporters. (A) In wild type, the principal orientation of the phragmoplast does not alter between early (green triangles) and late cytokinesis (white triangles). (B) *pok1 pok2* double mutant, note the mis-alignment of phragmoplast orientation in early (green triangles) and late cytokinesis (white triangles). Overlays show merges of early and late cytokinesis time points. Dashed line traces cell outlines. Scale bar indicates 5 µm. Images were taken on Zeiss LSM880 with the Airyscan detector. (C) Comparison of growth of six day old seedlings from different genetic background. (D) Time projection of cell division in wild type (Col-0) and *pok2-1* single mutants. Scale bar indicates 5 µm. (E) Kymographs of the microtubule reporter signal, using line selections corresponding to the dashed lines in (D). (F) Box plot depicting velocities of phragmoplast expansion deduced from kymograph analysis. Wild type (Col-0) phragmoplasts expand faster (0.32 µm/min ± 0.07, mean ± STDV) than *pok2-1* single (0.16 µm/min ± 0.04, mean ± STDV, ** p = 0.001) and *pok1 pok2* double mutants (0.15 µm/min ± 0.02, mean ± STDV, ** p = 0.001)., Box ranges represent median and 25th and 75th percentiles, respectively. Whiskers extend to minimum and maximum values. (n) indicates the number of phragmoplasts analyzed. Significance value (**p) was determined using One-way Anova with Tukey HSD post hoc test.

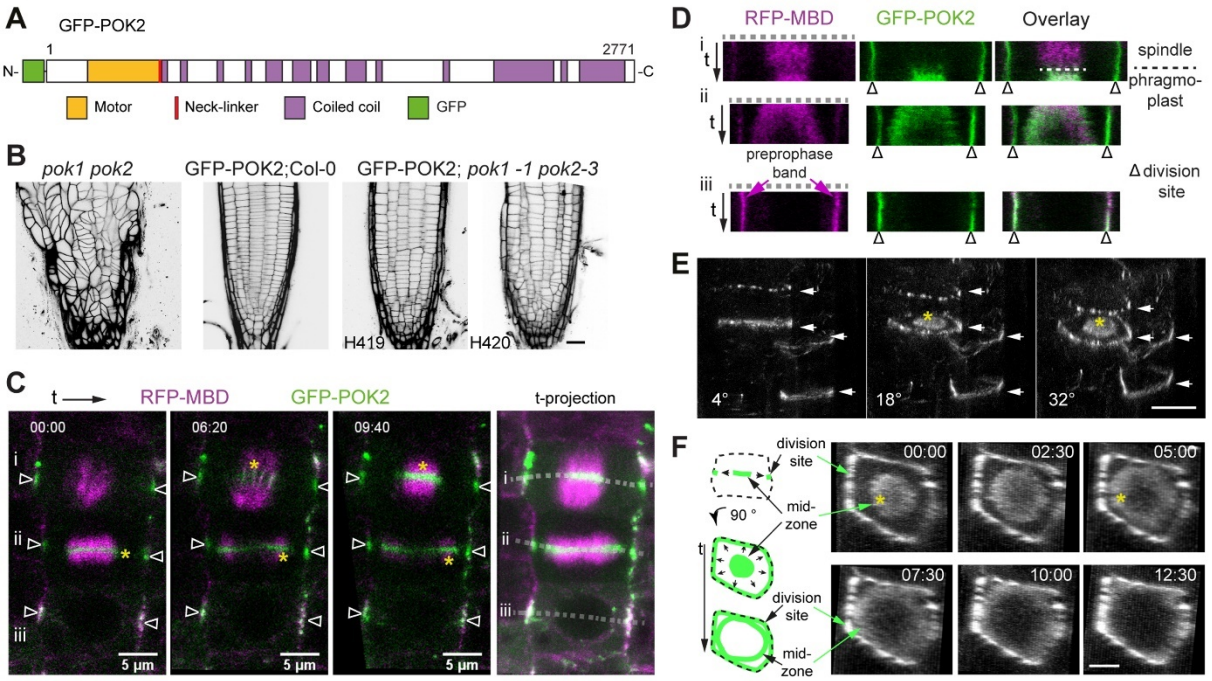

Figure 2

Figure 2: GFP-POK2 localization depends on the cell cycle stage.

(A) Protein domain organization of POK2. (B) Propidium iodide stained root meristems of *pok1 pok2* double mutant, wild type (Col-0) expressing *p35S:GFP-POK2* (GFP-POK2) and two examples (H419, H420) of rescue lines expressing *p35S:GFP-POK2* (GFP-POK2) in *pok1 pok2* (inverted grey scale). Scale bar indicates 20 µm. (C) Three time points of a time series showing GFP-POK2 and microtubules (RFP-MBD) during cell division. Three cells, at different cell cycle stages (i anaphase, ii early cytokinesis, iii prophase) were recorded. Triangles indicate the division site. Yellow asterisks indicate the enrichment of GFP-POK2 at the phragmoplast midzone. Dotted lines in each stage indicate line selection used for kymographs (space-time plots) depicted in (D). (D) Single channel images and overlay of kymographs along line selection (dashed line) in (C). Note the differences in GFP and RFP signal distribution. Triangles indicate the division site. Relates to Appendix Figure S1 and Movie EV1. (E) Rotational views (angle is indicated) of 3-D reconstructed GFP-POK2 localization patterns, displaying rings (arrows) and a disk-like distribution at the phragmoplast midzone (asterisk). Note the variety of ring morphologies (filamentous, diffuse and pearl-string). Scale bar indicates 10 µm. (F) Top view (90° rotation) and a graphical representation of a cytokinetic cell displaying GFP-POK2 at the phragmoplast midzone (disk) and at the division site (ring). Asterisk in time point 00:00 min indicates GFP-POK2 association with disk-phragmoplast and at 05:00 min with ring-phragmoplast. At 12:30, the merge of midzone GFP-POK2 and POK2 at division site is almost completed. Scale bar indicates 5 µm.

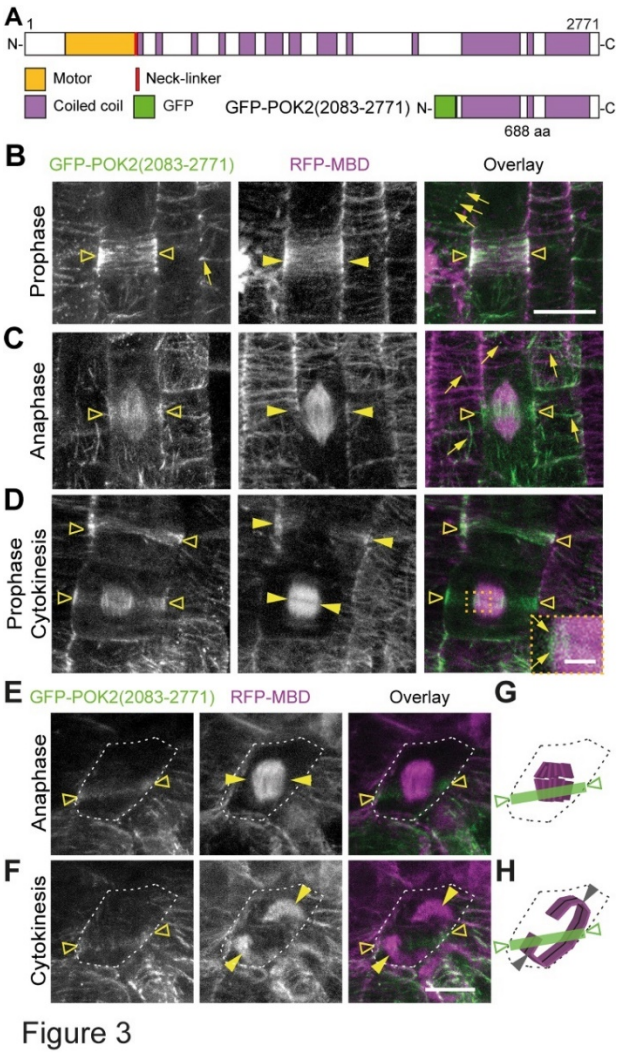

Figure 3

Figure 3: The carboxy-terminal domain POK2(2083-2771) localizes to the division site in mitosis. (A) Protein domain organization of POK2 and GFP-POK2(2083-2771). (B to D) POK2(2083-2771) localizes to the cortical division zone (triangles) throughout mitosis. (B) POK2(2083-2771) (triangles) co-localizes with preprophase band (arrow heads). (C) Anaphase cell exhibiting GFP-POK2 signal (triangles) at the cortical division zone and the spindle and (D) prophase and cytokinetic cell displaying preprophase band and phragmoplast (arrow heads) and GFP-POK2(2083-2771) (triangles) at the preprophase band, phragmoplast and cortical division zone. Inset shows magnification of boxed area; arrows point to GFP-POK2(2083-2771) at the phragmoplast leading zone. Examples of GFP-POK2(2083-2771) labelled interphase microtubules are indicated by arrows in (B) and (C). (E and F) Cell of *pok1 pok2* double mutant with intact GFP-POK2(2083-2771) cortical division zone localization (triangle). (E) Upper and (F) lower panels show the same cell (cell shape is indicated by dashed line in ana- and telophase. Note the mismatch between the GFP-POK2(2083-2771) cortical division zone signal at the plasma membrane (triangles) and direction of the phragmoplast expansion (arrow heads). Microtubules are visualized by RFP-MBD (magenta). (G and H) Illustration of cell outlines (dashed line), microtubules (magenta) and GFP-POK2(2083-2771) signal distribution (green) of cell depicted in (E and F).

Data information: Scale bars indicate 10 µm, except for (D) indicating 2.5 µm. Relates to Figure EV2.

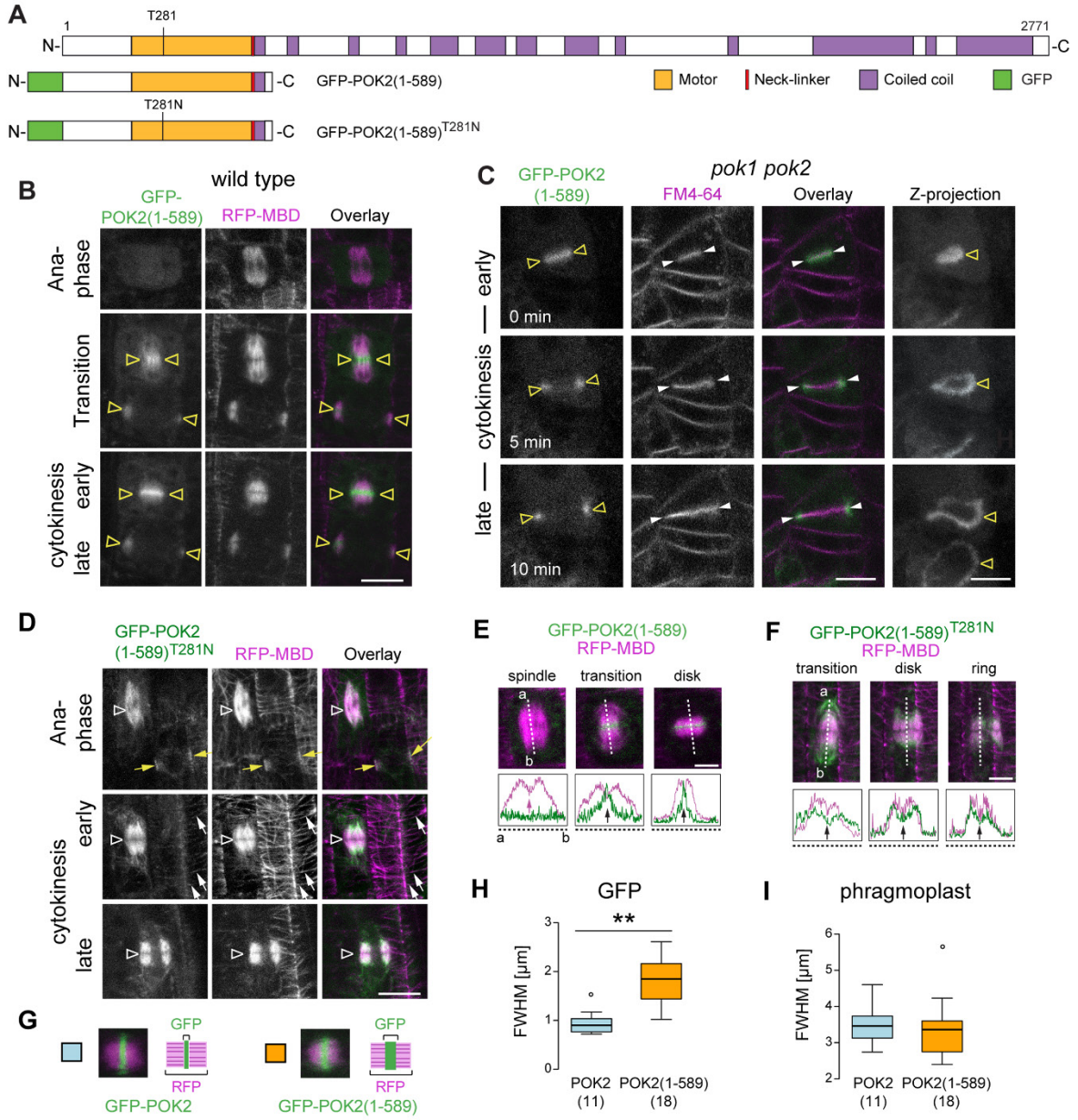

Figure 4

Figure 4: POK2 motor domain, POK2(1-589) is sufficient for phragmoplast midzone targeting during cytokinesis.

(A) Domain organization and overview of fusion proteins. N-terminal domain POK2(1-589) including predicted disordered regions (white) motor domain (yellow), neck-linker (red) and coiled coil. The position of conserved threonine (T) 281 in the ATP-binding site and mutation of T281 to asparagine (N) in GFP-POK2(1-589)^{T281N} rigor mutant is indicated. (B) GFP-POK2(1-589) accumulates at the phragmoplast midzone (triangles) during the transition from ana-to telophase and remains restricted to the midzone. (C) Single plane images of a time series during cytokinesis in the *pok1 pok2* double mutant. GFP-POK2(1-589) co-localizes with the early cell plate (triangles), stained with FM4-64 (arrow heads) and associates with the cell plate margins throughout cytokinesis. Z-projections illustrates the ring-shaped localization of GFP-POK2(1-589). Note that the POK2 motor domain does not localize to the division site and does not rescue the *pok1 pok2* mutant phenotype. (D) The rigor mutant GFP-POK2(1-

589)^{T281N} localizes to mitotic and cortical microtubules (white arrows). Yellow arrows indicate a preprophase band in the upper panel, triangles indicate the phragmoplast midzone region. (E and F) Individual images of a time series, showing (E) GFP-POK2(1-589) and (GFP-POK2(1-589)^{T281N} signal in cytokinesis. Plot profiles illustrate GFP (green) and RFP (magenta) signal distribution along the dashed lines in the respective figure panels above. Arrows in plot profiles point to intensity maxima (peaks) or local minima (valleys). (G-I) Comparison between signal width of GFP-POK2 and GFP-POK2(1-589) in cytokinesis. (H and I) Full width at half maximum (FWHM) of (H) GFP-POK2 (blue, 0.94 ± 0.25 µm, mean ± STDV, n = 11) and GFP- POK2(1-589) (yellow, 1.81 ±0.47 µm, mean ± STDV, n = 18) differ significantly (** p = 0.001, One-way Anova and Tukey HSD) while FWHMs of (I) phragmoplast are comparable (3.45 ± 0.52 µm, mean ± STDV, n = 11 and 3.37 ±0.80 µm, mean ± STDV, n = 18 respectively). Box ranges represent median and 25th and 75th percentiles, respectively. Tukey-whiskers extend to data points that are less than 1.5 x IQR away from 25th/75th quartile, outlier is indicated by circles.

Data information: Scale bars indicate 10 µm (B-D) and 5 µm (E, F). Relates to Figure EV2, Movie EV3.

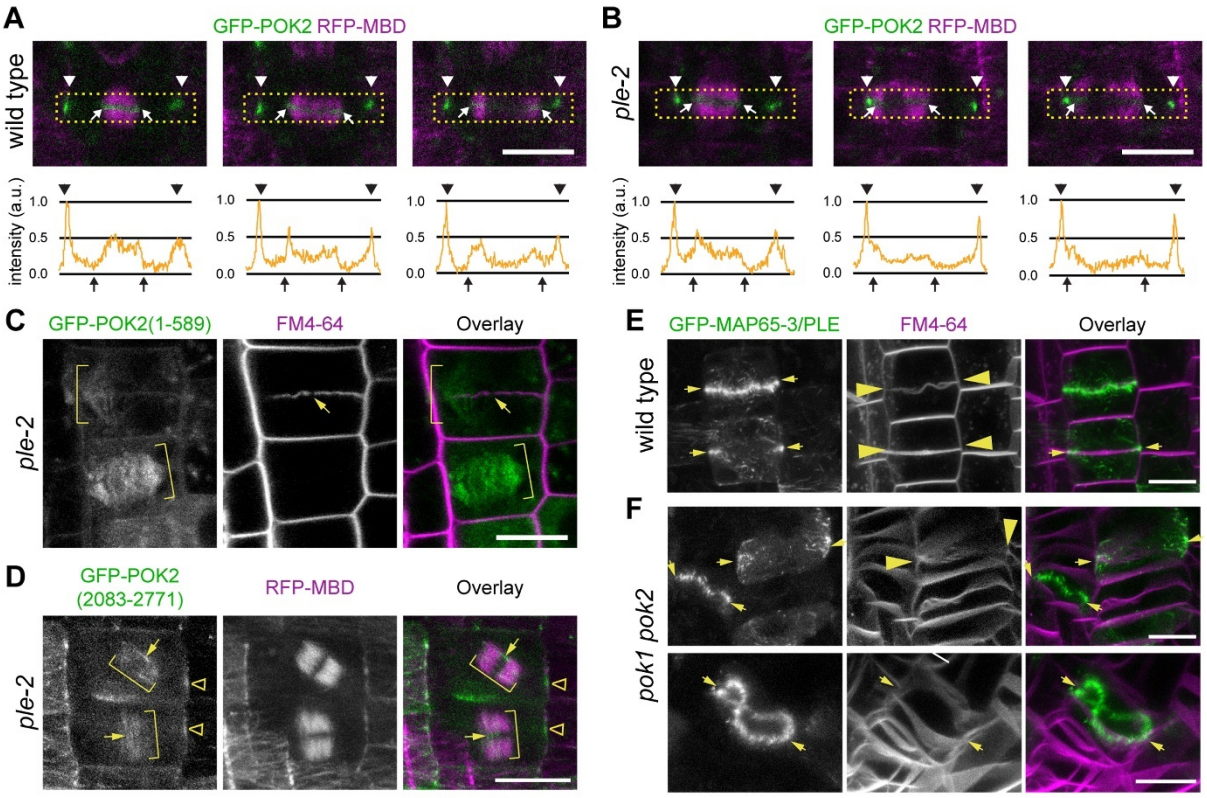

Figure 5

Figure 5: POK2 MAP65-3/PLEIADE interaction at the phragmoplast midzone requires an N-terminal binding site .

(A and B) Comparison of GFP-POK2 localization in (A) wild type and (B) *pleiade* (*ple*)-2 mutant at three consecutive stages of cytokinesis. Arrow heads indicate the division site. Arrows point to the midzone margins. Lower panels show intensity profile plots of GFP-POK2 in the rectangular selection indicated in the corresponding confocal image above. Images are single confocal sections depicting median planes recorded with identical settings. Normalized intensities are shown in arbitrary units (a.u.). (C) Localization of GFP-POK2. Localization of GFP-POK2(1-589) motor domain along phragmoplast microtubules (brackets) in the *ple-2* mutant. Note that GFP-POK2(1-589) in wild type localizes to the phragmoplast midzone (Figure 4). Plasma membranes are stained with FM4-64. Arrow indicates a characteristic gap in the incomplete cell plate.(D) Co-expression of GFP-POK2(2083-2771) and microtubule reporter (RFP-MBD) in *ple-2* mutant. Note the increased phragmoplast size (brackets) and the wider than normal midzone. GFP-POK2(2083-2771) faintly decorates phragmoplast microtubules, also across the midzone (arrows) and accumulates at the cortical division zone (triangles). Note that the localization is not altered compared to wild type (Figure 3). (E and F) GFP-MAP65-3/PLE localizes at the midzone (arrows) in (E) wild type and (F) *pok1 pok2* mutant cytokinetic cells. FM4-64 staining visualizes the plasma membranes. Arrows indicate cell plate fusion sites. Images are maximum Z-projections. Note the extreme midzone undulations in *pok1 pok2* mutants (lower panel).

Data information: Scale bars indicate 10 µm.

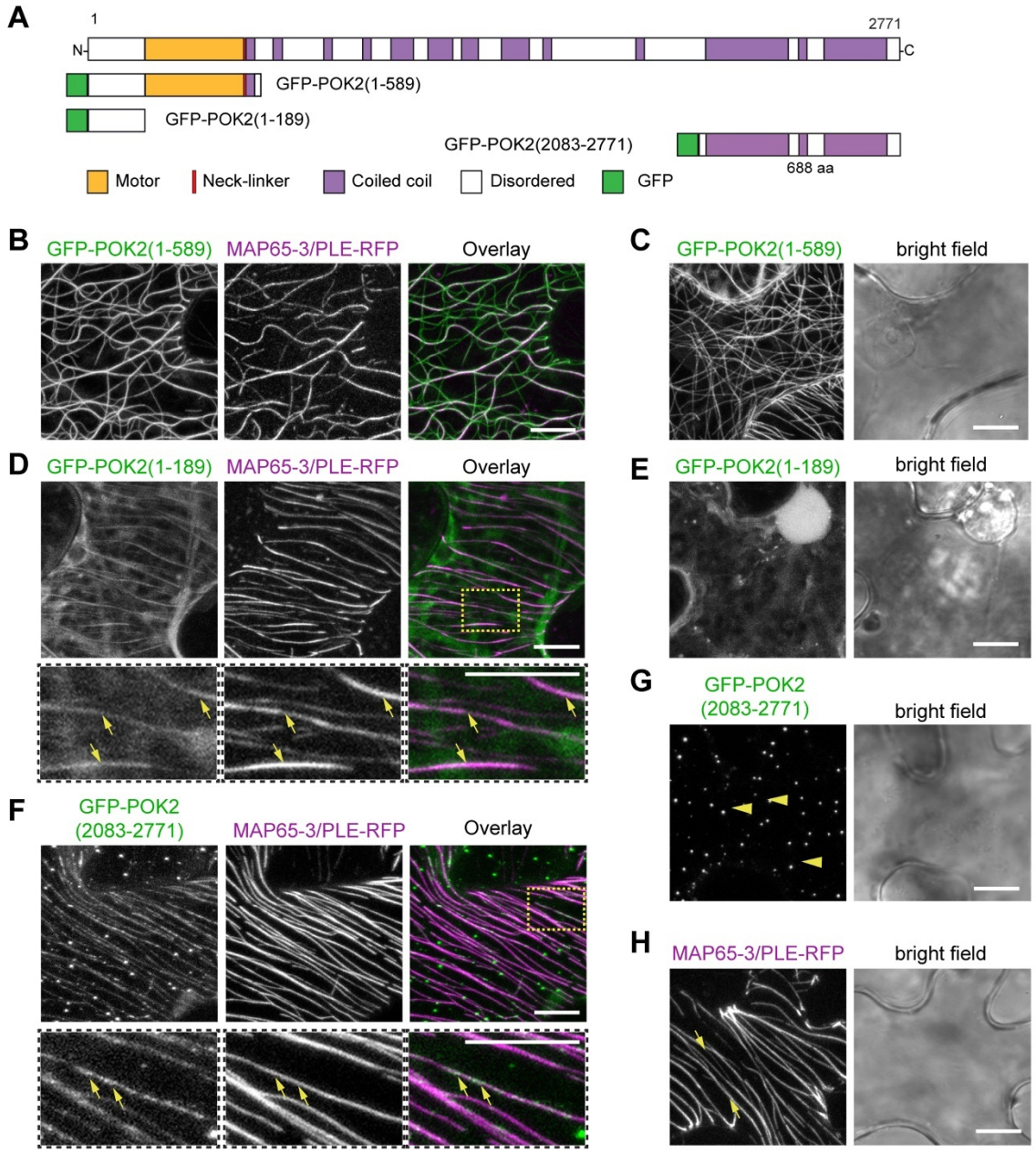

Figure 6

Figure 6: Tobacco abaxial leaf epidermal cells transiently expressing fusion proteins.

(A) Domain organization and overview of fusion proteins. (B) Single expression of GFP-POK2(1-589). Note the association with microtubules. (C) MAP65-3/PLE-RFP labels microtubules, individual examples indicated by arrows. (D) Co-expression of GFP-POK2(1-589) and MAP65-3/PLE-RFP. Overlay shows partial co-localization of GFP-POK2(1-589) and MAP65-3/PLE-RFP. (E) Single expression of GFP-POK2(1-189). Note the cytosolic distribution. (F) Co-expression of GFP- POK2(1-189) and MAP65-3/PLE-RFP. Overlay shows partial co-localization of GFP-POK2(1-189) and MAP65-3/PLE-RFP (individual examples indicated by arrows). Lower panels show three-fold magnification of boxed area in (F overlay). (G) Single expression of GFP-POK2(2083-2771). Note that GFP-POK2(2083-2771) alone does not associate with microtubules but forms punctate clusters (examples indicated by arrow heads). (H) Co- expression of GFP-POK2(2083-2771) and MAP65-3/PLE-RFP. Overlay shows partial

co-localization of GFP- POK2(2083-2771) and MAP65-3/PLE-RFP. Lower panels show three-fold magnification of boxed area in (H overlay). Arrows indicate GFP-POK2(2083-2771) along MAP65-3/PLE-RFP labelled microtubules.

Data information: All images were obtained in sequential mode. Scale bars indicate 10 μm. Relates to Figure EV3.

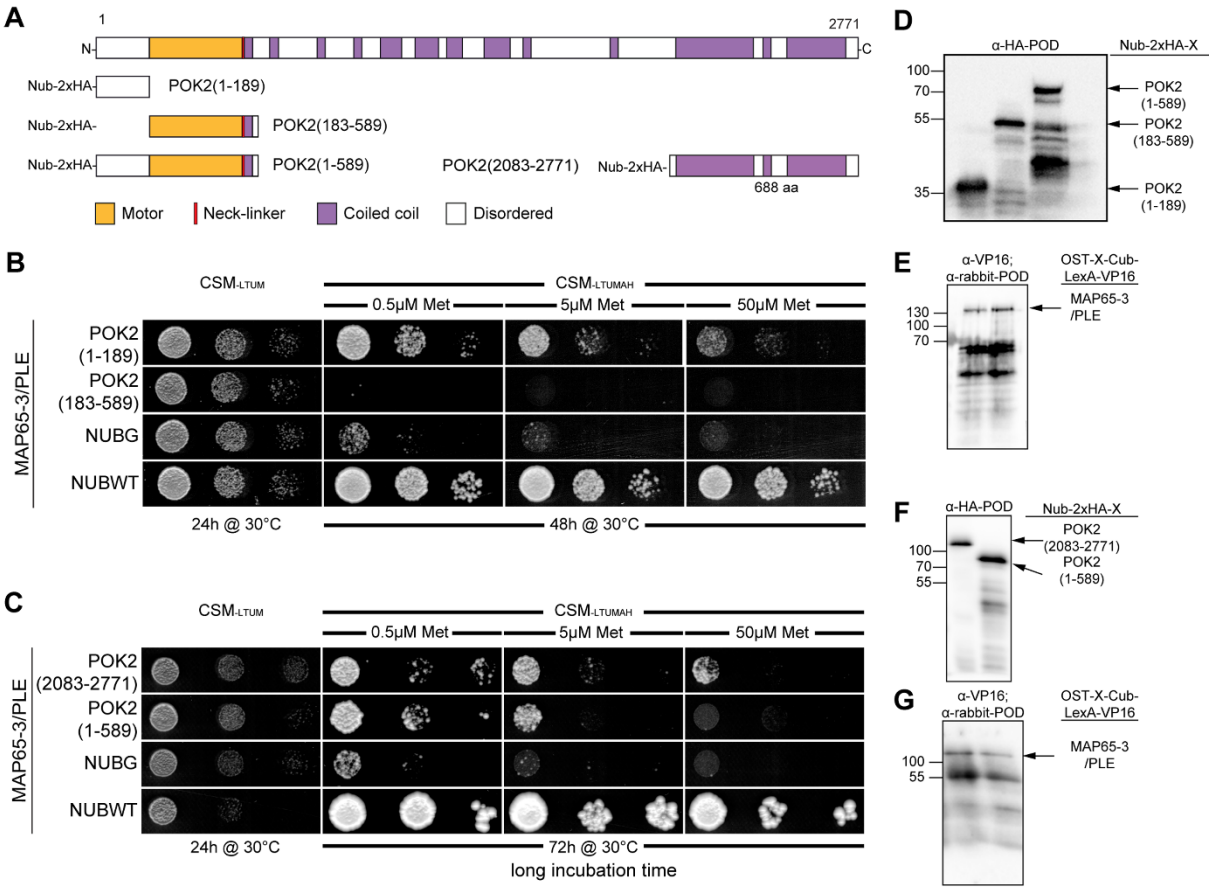

Figure 7

Figure 7: The yeast mating-based Split-Ubiquitin Cyto-SUS interaction assay.

(A) Domain organization and overview of fusion proteins. (B, C) Interaction of OST-MAP65-3/PLE-Cub and NubG–POK2x fusion as indicated, with controls (NubG, negative; NubWT (wild type), positive). Yeast diploids were spotted (from left to right, dropped at 1.0, 0.1 and 0.01 *A600* in each case) on CSM-Leu-, Met-, Trp-, Ura- (CSM-LMWU) medium to verify mating, and on CSM-Ade-, His-, Leu-, Met-, Trp-, Ura- (CSM-AHLMWU) with the addition of different methionine concentrations to assay for interaction. (D-G) Immunoblot-detection of fusion proteins expressed in yeast. (D) Nub-2xHA-POK2(1-189) (31 kDa) and Nub-2xHA-POK2(183-589) (57 kDa), corresponding to (B), and (F) Nub-2xHA-POK2(1-589) (75 kDa) and Nub-2xHA-POK2(2083-2771) (91 kDa) corresponding to (C), using an anti-HA antibody conjugated with peroxidase (POD). (E, G) Immunoblot-detection of MAP65-3/PLE-Cub-VP16 (137 kDa) in yeast protein extracts, using an anti-VPS16 as a primary antibody and anti-rabbit-POD as a secondary antibody. (E) corresponds to (B), (G) corresponds to (C). Relates to Figure 6.

Table 1

	Prophase	Meta-/Anaphase	Cytokinesis		
	PPB	Spindle / CDZ	Phragmoplast midzone only	Phragmoplast midzone / CDZ	Cell plate fusion site only
POK2 (1-2771) (n=12 seedlings)	98 % (n=49)	100 % (n=14)	4 %	96 % (n = 79)	0 %
POK2 (2083-2771) (n=34 seedlings)	100 % (n=120)	89 % (n=37)	8 %	64 % (n = 78)	21 %
POK2 (1-589) (n=28 seedlings)	16 % (n=55)	9 % (n=13)	99 %	0 % (n=104)	0 %
POK2 (Δ589-2771)	100 % (n=36)	2% (n=4)	9 %	59 % (n= 22)	32 %

Table 1: Differential subcellular distribution of POK2 fusion proteins during cell division. Subcellular distribution and frequency of different Green fluorescent protein (GFP) fusion proteins was scored throughout cell division. Preprophase band (PPB), cortical division zone (CDZ). Total number or cells (n) scored in each cell cycle stage is given. Relates to Figure 1, Figure 2 and Figure 3.

Table 2: Signal distribution of GFP-POK2 fusion proteins before and after microtubule depolymerization with oryzalin. Green fluorescent protein (GFP) and Red fluorescent protein (microtubule reporter, MT) signal distribution was examined before treatment with oryzalin, and after depolymerization of microtubules. Cell cycle stages are indicated, according to mitotic microtubule arrays. We scored cells for presence of GFP signal at PPB, cortical division zone, phragmoplast midzone and cell plate fusion site. Relates to Figure EV1.

Table 2

	Prophase		Meta-/Anaphase		Cytokinesis			
	PPB		Spindle / cortical division zone		Phragmoplast midzone		Cell plate fusion site	
POK2(1-2771) (n = 6 roots)	GFP	MT	GFP	MT	GFP	MT	GFP	MT
Before oryzalin	16	16	6	6	25	27	27	0
After oryzalin	4	0	5	0	0	0	25*	0
POK2(2083-2771) (n = 6 roots)	GFP	MT	GFP	MT	GFP	MT	GFP	MT
Before oryzalin	21	21	3	3	6	10	10	0
After oryzalin	8	0	3	0	0	0	7**	0
POK2(1-589) (n = 6 roots)	GFP	MT	GFP	MT	GFP	MT	GFP	MT
Before oryzalin	1	13	2	5	30	31	0	0
After oryzalin	0	0	0	0	0	0	0	0

*(n=2) Cells without GFP signal after treatment due to completion of cytokinesis during

*(n=3) incubation with oryzalin

Expanded View Figure Legends

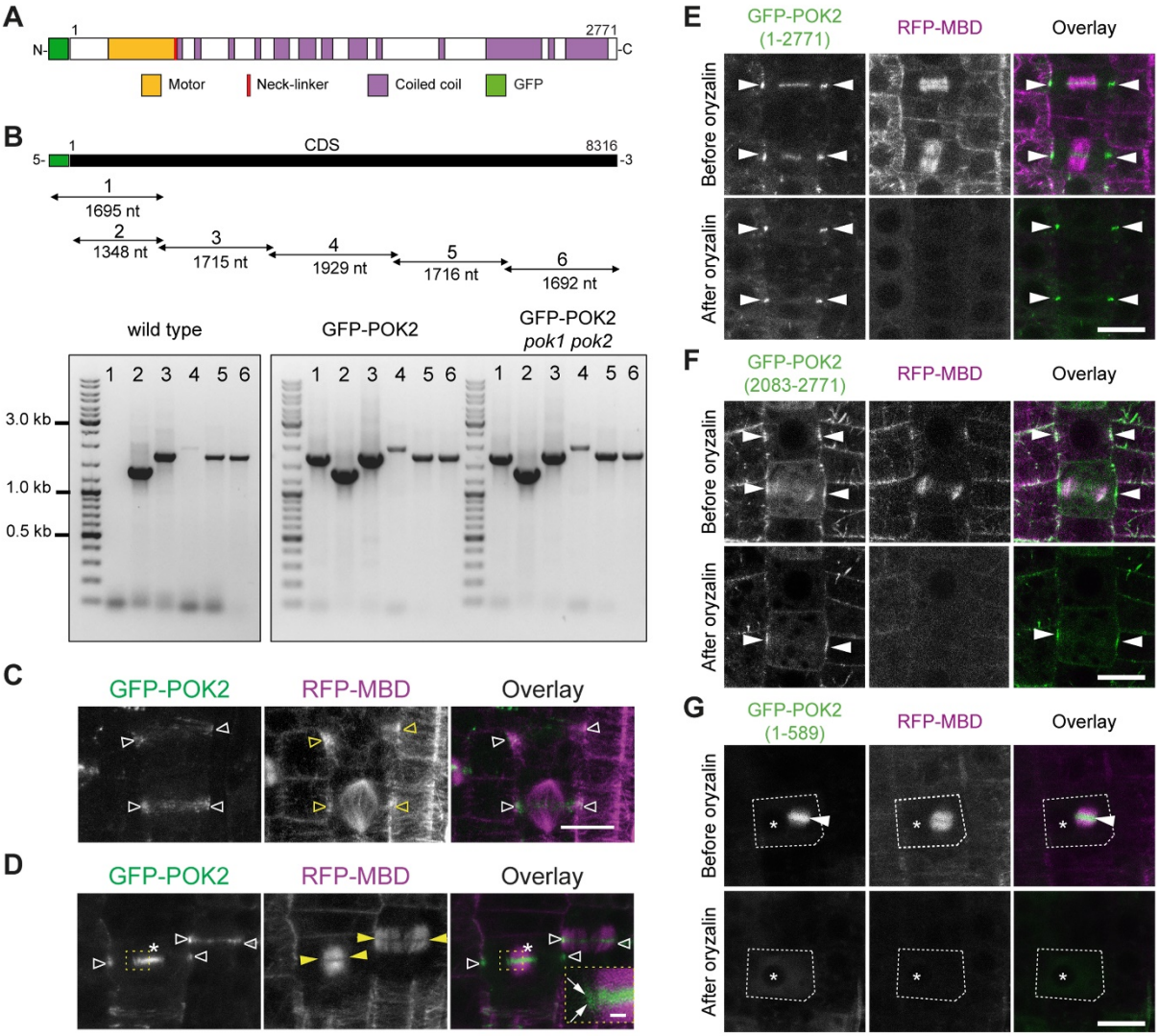

Figure EV1

Figure EV1: Microtubule dependencies of POK2 protein domains.

(A) GFP-POK2 protein organization. (B) graphical representation of transgene coding sequence (CDS) and relative position of PCR fragments (consecutive numbers and fragment sizes are indicated) amplified from cDNA derived from wild type, transgenic line (GFP-POK2) and rescue line (GFP-POK2 *pok1 pok2*). Primer combinations are given in Supplemental Appendix Table S2. (C and D) Co-localization of GFP-POK2 and microtubule marker RFP-MBD. (C) Prophase cells displaying preprophase bands and pro-spindle (yellow triangles), respectively and filamentous GFP-POK2 (white triangles). (D) Telophase cells displaying phragmoplasts (yellow arrowheads) and GFP-POK2 at the division site (white triangles) and at the phragmoplast midzone (asterisk). The inset shows the leading edge of the phragmoplast (arrows) at a higher magnification. Images are Z-projections. Scale bar 10 µm. Relates to Figure 1 and Movie EV1, EV2. (E to G) Root meristem cells expressing (E) GFP-POK2(1-2771), (F) GFP-POK2(2083-2771), or (G) GFP- POK2(1-589) along with the microtubule marker RFP-MBD are shown before (upper row) and after (lower row) treatment with 10 µM oryzalin. Images of the same cells are shown in each case. Arrow heads point to GFP signal at the

division site (E and F) and to the phragmoplast midzone (G, dashed line indicates cell outline). The asterisks mark a conspicuous vacuole present before and after treatment. Note the persistence of GFP signal at the division site in (E) and (F), despite the depolymerization of phragmoplast microtubules and cytosolic GFP in (G). Images are maximum Z-projections. Scale bars indicate 10 µm. Relates to Figure 1, Figure 2, Figure 3.

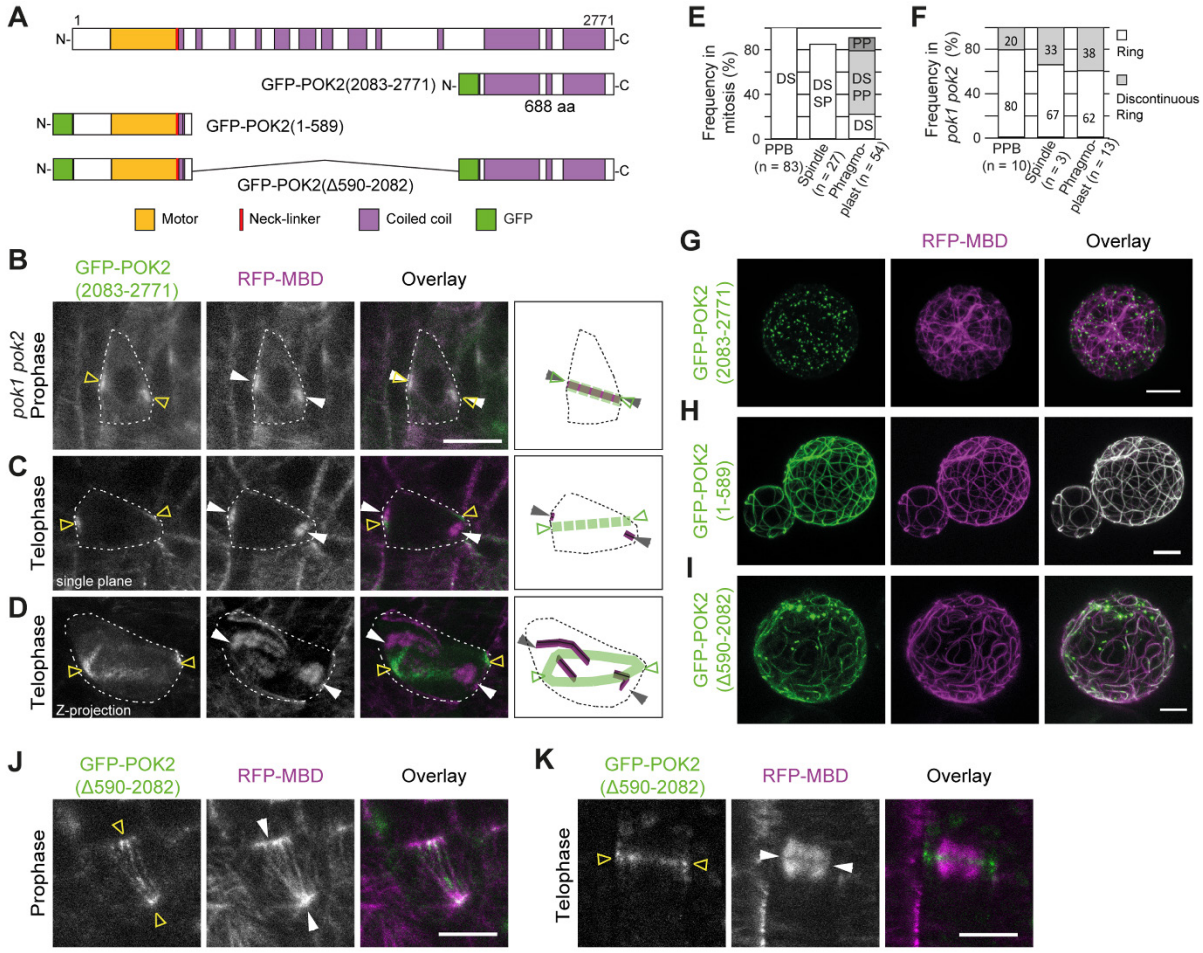

Figure EV2

Figure EV2: The carboxy-terminal domain POK2(2083-2771) localizes to the division site in *pok1 pok2* double mutants, transient expression of POK2 domains and their microtubule dependency.

(A) Graphical representation of protein domain organization of POK2, GFP-POK2(2083-2771) and GFP- POK2(1-589). (B-D) (B) GFP-POK2(2083-2771) co-localizes with the preprophase band (arrow heads) (C and D) Mis- alignment of GFP-POK2(2083-2771) (triangles) and phragmoplasts (arrow heads). (B and C) are single plane images. (D) shows a maximum Z-projection. Cartoons illustrate microtubule (magenta) and GFP- POK2(2083-2771) subcellular distribution in cells, outlined by dashed lines. (E) Frequency (%) of mitotic cells displaying GFP-POK2(2083-2771) in wild type. Numbers indicate the percentage of cells that showed GFP-POK2(2083-2771) association with preprophase band (PPB), spindle (SP), phragmoplast (PP) and division site (DS). (F) Frequency (%) of complete and discontinuous rings at the division site of *pok1 pok2* mutants during cell division. (G-I) Transient co-expression of (G) GFP-POK2(2083-2771), (H) GFP-POK2(1-589) and (I) GFP-POK2(Δ590-2082) with the microtubule reporter RFP-MBD in *Arabidopsis* protoplasts. Note the complete co- localization of GFP-POK2(1-589) and microtubules. (J and K) Localization of GFP-POK2(Δ590-2082) (triangles) in (J) prophase cell with preprophase band (arrow heads) and (K) telophase cell with phragmoplast (arrow heads).

Data information: Scale bars indicate 10µm.

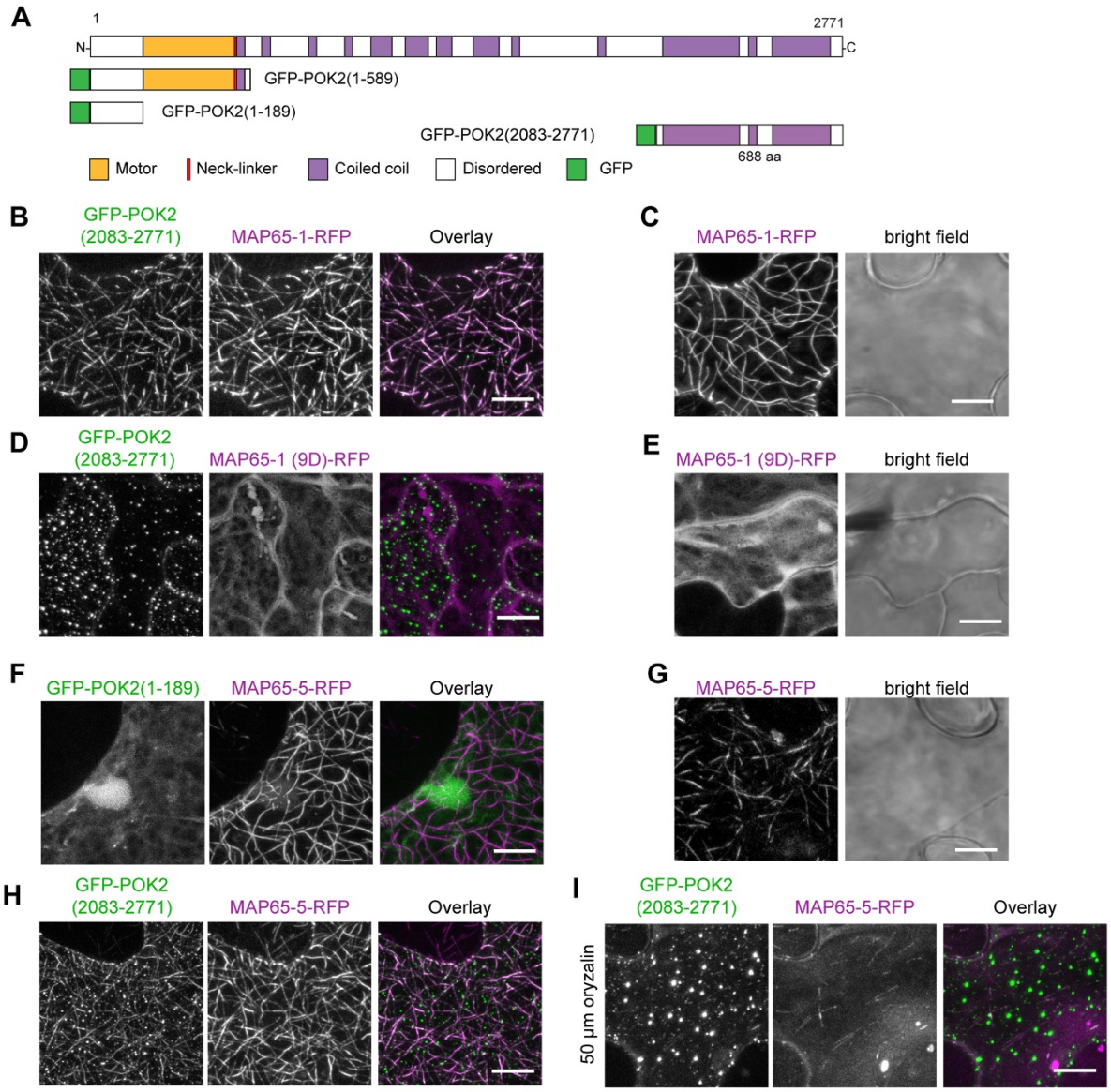

Figure EV3

Figure EV3: Transient Co-expression of fusion proteins in tobacco abaxial leaf epidermal cells.

(A) Domain organization and overview of fusion proteins. (B-I) Transient co-expression of GFP-POK2(2083-2771) and (B) MAP65-1-RFP, (D) MAP65-1(9D)-RFP, (H and I) MAP65-5-RFP in tobacco abaxial leaf epidermal cells. Note that microtubules are labeled by both fusion proteins in cells co-expressing GFP-POK2(2083-2771) and MAP65-1-RFP, and MAP65-5-RFP. In cells expressing MAP65-1(9D), which does not bind microtubules and MAP65-5-RFP treated with oryzalin to depolymerize microtubules, GFP-POK2(2083-2771) displays punctate clusters, similar to the pattern observed when expressed alone (Figure 6G). Single expression of (C) MAP65-1-RFP, (E) MAP65-1(9D)-RFP and (G) MAP65-5-RFP. Note that MAP65-1(9D)-RFP is cytosolic. (F) Co-expression of GFP-POK2(1-189) with MAP65-5 RFP. Scale bar indicates 10 µm.

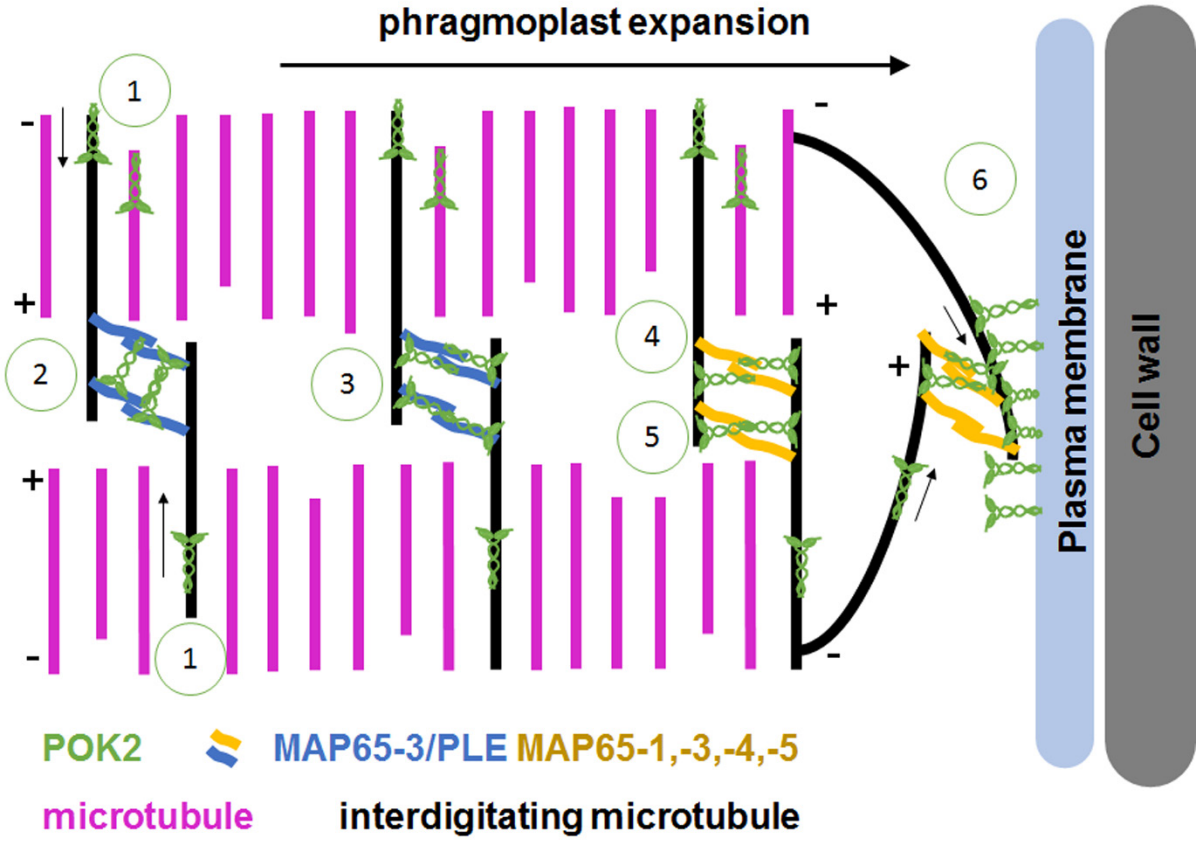

Figure EV4: Putative model for POK2 activities in cytokinesis.

Schematic representation of phragmoplast expansion during cytokinesis. Based on our data and available literature we propose the following scenarios for POK2 activities during centrifugal phragmoplast expansion: (1) POK2 moves towards the phragmoplast midzone where it associates with MAP65/PLE and other MAP65 dimers. In accordance with HsKif15-microtubule encounters, POK2 forms dimers and/or tetramers and potentially prevent microtubule plus-end catastrophe. POK2 interacts with MAP65 isoforms via distinct protein domains. Interaction with MAP65-3/PLE (2, 3) is mediated by both, the disordered region (1-189) and the C-terminal domain (2083-2771). POK2 might bind between two MAP65-3/PLE dimers (2) or parallel to the axis of one MAP65-3 dimer (3). For interaction with other MAP65 isoforms dimeric (4) or tetrameric (5) POK2 solely utilizes the C-terminal region. POK2 at the division site (6) is likely dimeric, due to the tethering via its C-terminal region. With their motor domains, POKs might interact with peripheral microtubules directly. Microtubule plus-ends (+), microtubule minus ends (-). Arrows indicate direction of POK2 motility.

Herrmann et al Appendix Content

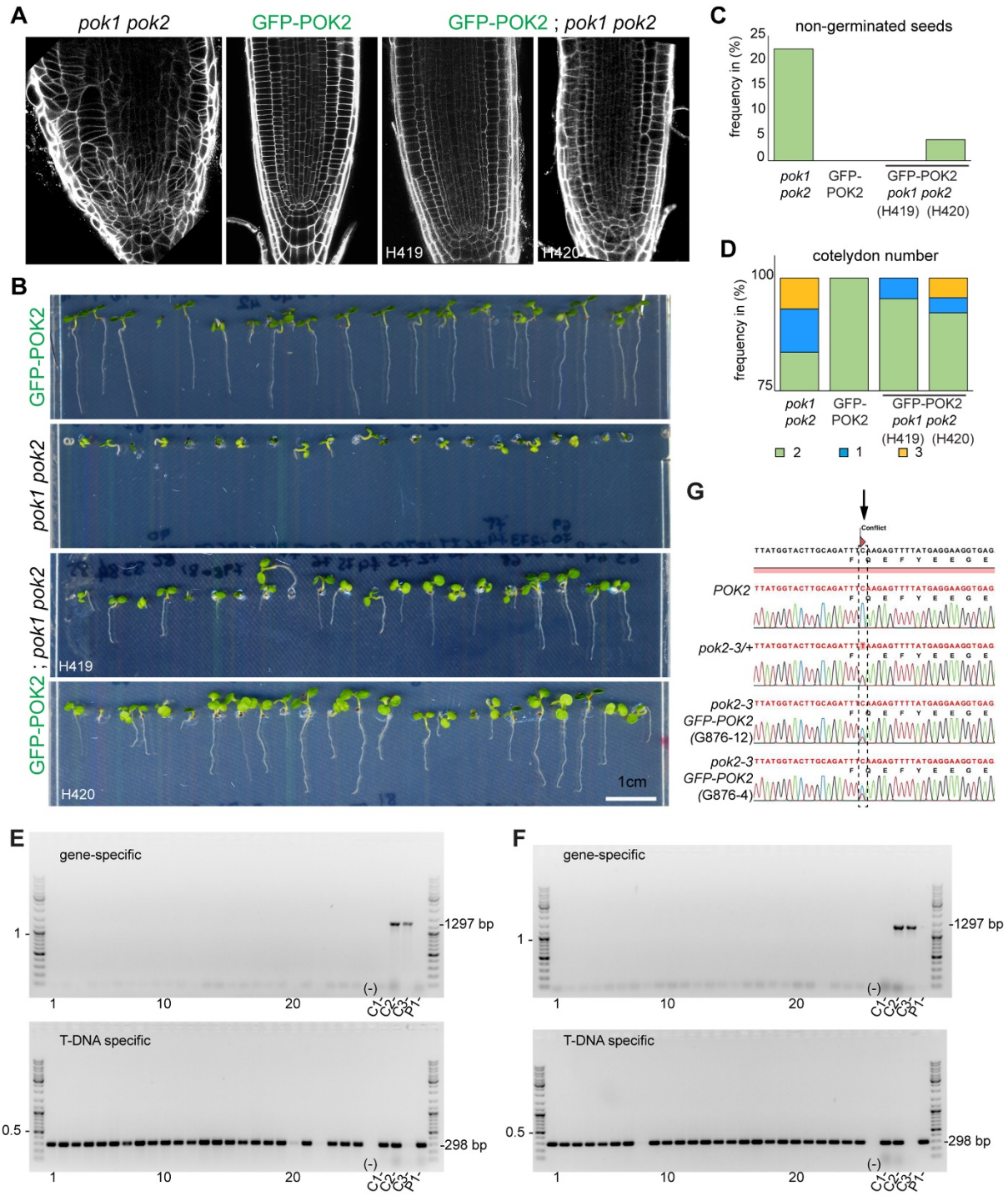

Appendix Figure S1

Appendix Figure S1: Phenotype rescue and localization of GFP-POK2. (A) Single images showing a median plane in roots of *pok1 pok2* seedlings as well as of seedlings expressing GFP-POK2 in wild type and double mutant background (GFP-POK2; *pok1 pok2*, rescue lines) after staining with propidium iodide. Note the restoration of phenotypically wild type cellular organization in the rescue lines (H419, H420). (B) Images of seedlings corresponding to the above mentioned transgenic plant lines. Note the restoration of root growth. (C and D) Quantification of phenotypic abnormalities in *pok1 pok2* mutants, transgenic line expressing *GFP-POK2* (GFP-POK2) and two rescue lines GFP-POK2; *pok1 pok2* (H419, n = 87; H420, n = 95). (C) Frequency (%) of non-germinating seeds. (D)

Frequency (%) of seedlings with two (2), one (1) or three (3) cotyledons. (E and F) Representative gel electrophoresis of polymerase chain reaction (PCR) products from 25 randomly selected individuals of (E) H419 and (F) H420 rescue lines. (E) The 298 bp PCR fragment amplified with POK1-Nru/Xba-F and LBb1.3 (Appendix Table S2) indicates the presence of the T-DNA-specific insertion in the POK1 locus. (F) The 1297 bp PCR fragment amplifies from genomic POK1 using POK1-Nru/Xba-F and POK1-Spe-R (Appendix Table S2). For all samples, except for #20 and 22 in (E) and #8 in (F), which were of low quality, T-DNA-specific, but not gene-specific PCR fragments were amplified, indicating that the *pok1-1* T-DNA allele was homozygous in the rescue line. C1-C3 indicate controls. C1 *pok1 pok2*, C2 *pok1/+ pok2/+*, C3 Col-0. (-) indicates negative (no DNA) control. P1 is parent G876-4 in (E) and parent P2 G876-12 in (F). *POK1* and *POK2* are closely linked. Therefore, homozygosity of *pok1-1* implies homozygosity of *pok2-3*. (G) The parent plants P1 G876-4 (parent of H419) and P2 G876-12 (parent H420) were sequenced and simultaneous presence of the *pok2-3* mutation and GFP-POK2 transgene were confirmed by the double peaks (dashed box) in the histogram. Thymine (T) indicates *pok2-3* mutation and Guanine (G) indicates presence of *POK2* transgene (also confirmed by Kanamycin resistance). Sequences of wild type and *pok2-3/+* heterozygous plants are shown as well. Substitution of G by Thymine (T) leads to premature STOP codon (Lipka et al., 2014).

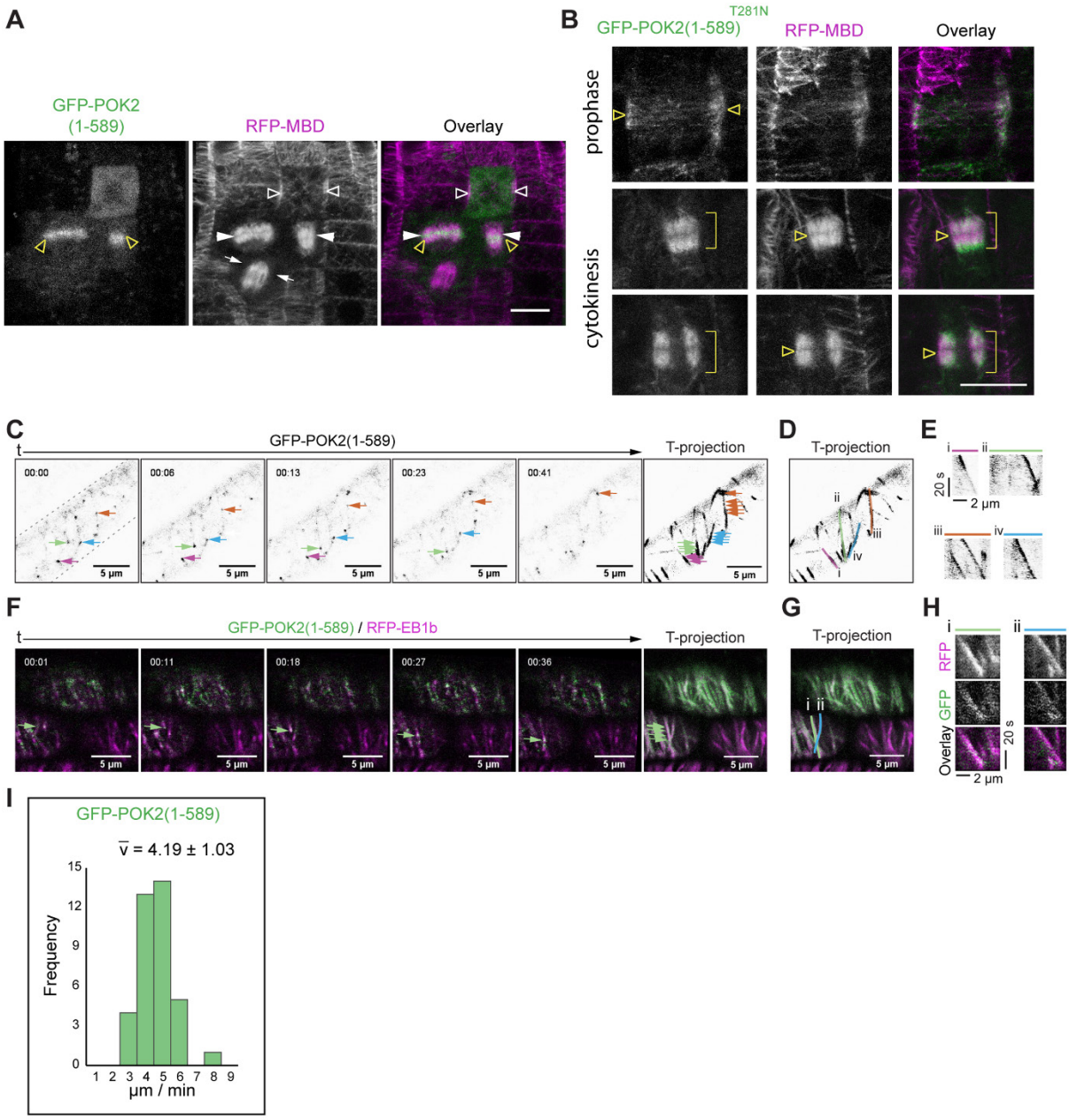

Appendix Figure S2

Appendix Figure S2: POK2 motor domain, POK2(1-589) localizes to the phragmoplast midzone. (A) Cells in cytokinesis (yellow triangles, white arrow heads) display GFP-POK2(1-589) signal at the midzone, while cells in prophase (white triangle) and anaphase (white arrows) show cytosolic GFP-POK2(1-589). (B) Co- localization of rigor mutant GFP-POK2 POK2(1-589)^{T281N} with mitotic micro-tubule arrays in prophase, early and late cytokinesis. The rigor mutant GFP-POK2(1-589)^{T281N} localizes to mitotic (brackets) and cortical microtubules (yellow triangles) point to the preprophase band but remains excluded from the phragmoplast midzone region (indicated by triangles). Scale bars indicate 10 µm. (C) Individual time points of time series depicting GFP-POK2(1-589) in interphase root cell. Colored arrows point to individual fluorescent dots. In the T-projection of the time series, arrows from individual frames are blotted. (D) T-projection as shown in (C) Tracks (i)-(iv) are indicated by color overlay. (E) Kymographs of tracks (i)-(iv) selected in (H), indicating continuous signal

displacement over time. (F) Selected images of a time series of root meristem cells, co-expressing GFP-POK2(1-589) and RFP-End Binding Protein (EB) 1b, arrows indicate GFP-POK2(1-589) signal along RFP-EB1b labelled microtubules. Time-projection (T-projection) shows maximum signal projection of all time frames. Arrows correspond to arrows in single time frames. (G) T-projection of time series in (F), green (i) and blue (ii) line indicate line selections, used for kymographs depicted in (H). (H) Single channels and overlay of kymographs along line selection indicated in (G). Note that the signal contrast edge of GFP-POK2(1-589) and RFP-EB1b co-align. (I) Frequency distribution of *in vivo* speeds of GFP-POK2(1-589) (n= 37, combined from five cells in four root meristems). Velocity 4.19±1.03 µm / min is presented as mean ± STDV. Relates to Figure 4 and Movie EV3, Movie EV4.

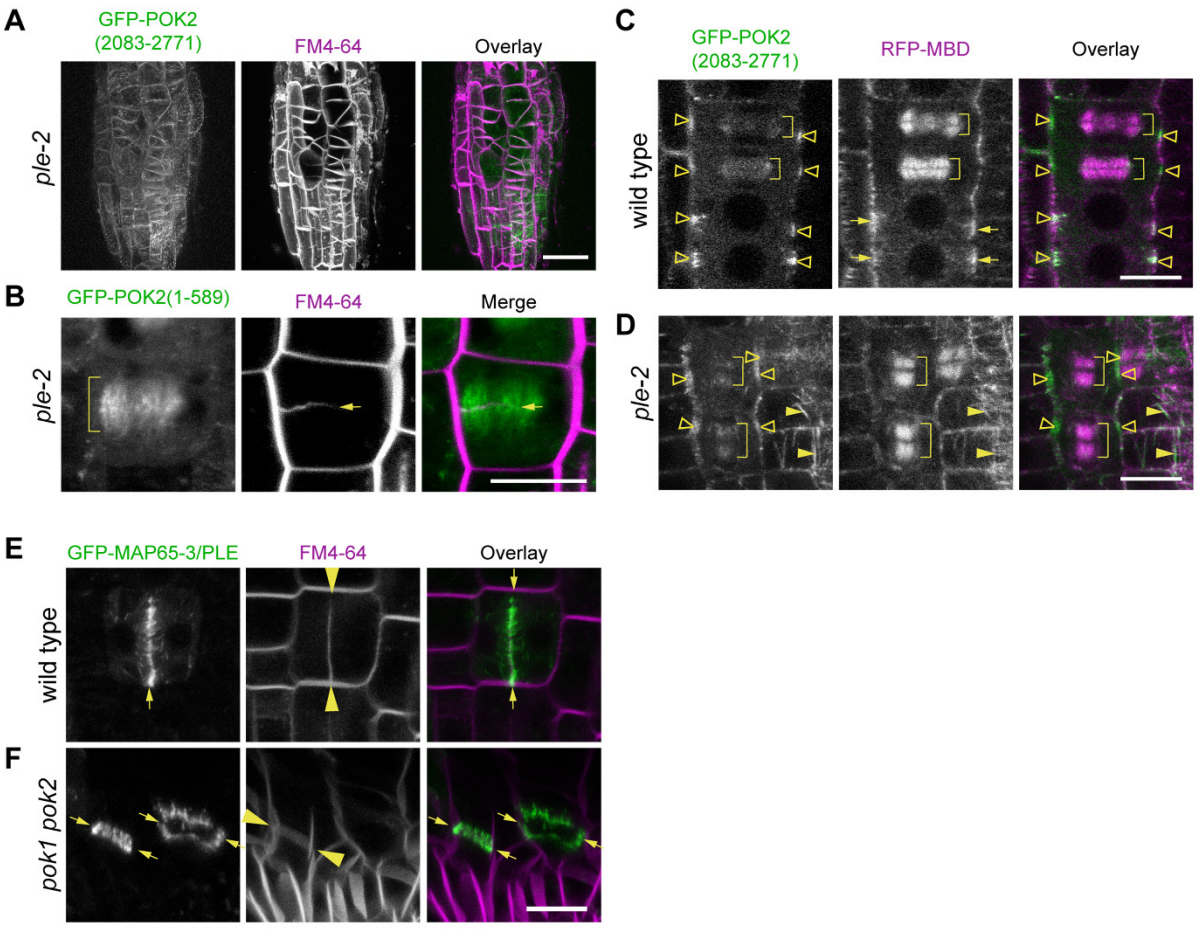

Appendix Figure S3

Appendix Figure S3: Genetic interaction of POK2 and MAP65-3/PLEIADE. (A) Root meristem of *pleiade* (*ple-2*) mutant expressing GFP-POK2(2083-2771). FM-64 staining allows visualization of the plasma membranes. Scale bar indicates 25 µm. (B) GFP-POK2(1-589) motor domain along phragmoplast microtubules (brackets) in the *pleiade* (*ple-2*) mutant. Arrow points to a cell wall stub, characteristic for *ple* mutants. Scale bar indicates 10 µm. (C and D) GFP-POK2(2083-2771) localization in (C) wild type and (D) *ple-2* mutant. GFP-POK2(2083-2771) co-localize with microtubules (brackets, arrows and arrowheads) and accumulates at the cortical division site (triangles). Scale bars 10 µm. (E and F) GFP-MAP65-3/PLE localizes at the midzone (arrows) in (E) wild type and (F) *pok1 pok2* mutant cytokinetic cells. Plasma membranes visualized by FM4-64 staining. Arrow heads indicate cell plate fusion sites. Images are maximum Z-projections. Scale bars indicate 10 µm.

Appendix Table S1: Oligonucleotides for Cloning

Cloning	Name	Oligos 5‘ – 3‘
MAP65-3/PLE	PLE_ATG_KPN_F	atggtaccATGGCAAGTGTTCAAAAAGAT
	PLE_w/o STOP_NOT_R	atgcggccgcttAACCAAACGACATTCAGACTGTA
pENTR:POK2 (1-189)	NotI_POK2_ATG_F	AATAATAACATGCGGCCGCaATGTCAAAGGAGACCAAGC TTTC
	POK2MD1-189aa_R	aaTCTAGAtcaCCAGAAAGATGGATCTTCCTT
pENTR:POK2MD(18 3-589)	NotI_POK2_549_F	AATAATAACATGCGGCCGCaATGGAAGATCCATCTTTCTG GATGGATCACAA
	Asc_POK2_1770 stop R	AATAATAACATGGCGCGCCtta*ACTTGATGGCGAATCGAC T*
pENTR:POK2(1-589)	NotI_POK2_ATG_F	AATAATAACATGCGGCCGCaATGTCAAAGGAGACCAAGC TTTC
	Asc_POK2_1770 stop R	AATAATAACATGGCGCGCCtta*ACTTGATGGCGAATCGAC T*
pENTR:POK2(1-589)T281N	POK2_T281N_F	AAGTGGAAAGaacTATACAATGCTT
	POK2_T281N_R	AAGCATTGTATAgttCTTTCCACTT
pDONR221:POK2(20 83-2771)	minB1F-POK2C	aaaaagcaggctccaccATGGACAAGAAAGATGAAATAAAGG AAATC
	minB2R-POK2C stop	agaaagctgggtcCTACCTGTCTAAAGAAGAGAAAAAAGGA AC
pENTR:POK2(2083-2771)	KAT2_BamHI_6250_F	ggatccGACAAGAAAGATGAAACAAAGGAAATC
	POK2_STOP_XbaI_R	ATtctagaTTtcacctgtctaaagaagagaaa
pENTR:POK2(Δ590-2082) and pENTR:POK2(1-2771)	POK2 MD linker C_F	aagttcctatactttctagagaataggaacttcAGGGACAAGAAAGA TGAAACAAA
	POK2 MD linker C_R	tcctattctctagaaagtataggaacttcccTACACTTGATGGCGAA TCGA
PCRI (6847 bp genomic fragment)	Kat2-BsrGI-F	ccgcggcatgctgtacaagagtgatatcg
	Kat2-68491R	gactctgactccatgatcttc
PCRII (5464 bp genomic fragment)	POK2-799 F	ATGGAGAGGAGTATAAATGGGTA
	Kat2-EcoRI-R	ctgtccttcactacagtgggctggag
	B1F	ggggacaagtttgtacaaaaaagcaggctccacc
	B2R	ggggaccactttgtacaagaaagctgggtc
pENTR:EB1b	EB1b ecoRI F	gaattcAAAAATGGCGACGAACATT
	EB1b xhoI R	ctcgagTTAAGTTTGGGTCTCTGCAGCA
Genotyping		
POK1-XbaI/NruI-F	*POK1/pok1-1*	gctctagatcgcgacagcattgacaagaatc
POK1SpeI-R	*POK1*	tcactagtgcacctctatcatag
LBb1.3	*pok1-1*	attttgccgatttcggaac

Appendix Table S2: Oligonucleotides for Transcript amplification

Fragment	Primer pair	Oligos 5‘–3‘
1	GFP-CDS 467_F	acaagcagaagaacggcatcaa
	POK2-BstEII_R	ttaggcggtcaccctcagcgc
2	NotI-POK2_ATG_F	aataataacatgcggccgcaatgtcaaaggagaccaagctttc
	POK2-BstEII_R	ttaggcggtcaccctcagcgc
3	POK2-BstEII_F	gcgctgagggtgaccgcctaa
	POK2-BsrGI_R	ccgcggcgatatcactcttgtacagcatg
4	POK2-BsrGI_F	ccgcggcatgctgtacaagagtgatatcg
	POK2-BspHI_R	actagtgagatagcacaatccttcatgat
5	POK2-BspHI_F	actagtatcatgaaggattgtgctatctc
	POK2-5084_R	cctctcatcgatggcatcat
6	POK2-5084_F	atgatgccatcgatgaga
	POK2-BamHI_Stop	ggatcctttcacctgtctaaagaagagaaa

Appendix References

Lipka, E., Gadeyne, A., Stöckle, D., Zimmermann, S., De Jaeger, G., Ehrhardt, D.W., Kirik, V., Van Damme, D., and Müller, S. (2014). The Phragmoplast-Orienting Kinesin-12 Class Proteins Translate the Positional Information of the Preprophase Band to Establish the Cortical Division Zone in Arabidopsis thaliana. Plant Cell 26, 2617-2632.

9.4 Chugh et al. 2018

Phragmoplast Orienting Kinesin 2 is a weak motor switching between processive and diffusive modes.

Mayank Chugh, Maja Reissner, Michael Bugiel, Elisabeth Lipka**, Arvid Herrmann**, Basudev Roy, Sabine Mueller and Erik Schaeffer

Biophysical Journal

Manuscript submitted to **Biophysical***Journal*
Article

Phragmoplast Orienting Kinesin 2 is a weak motor switching between processive and diffusive modes

Mayank Chugh[1], Maja Reißner[1], Michael Bugiel[1], Elisabeth Lipka[2], Arvid Herrmann[2], Basudev Roy[1,3], Sabine Müller[2], and Erik Schäffer[1,*]

[1]Cellular Nanoscience, Center for Plant Molecular Biology (ZMBP), University of Tübingen, Auf der Morgenstelle 32, 72076 Tübingen, Germany
[2]Developmental Genetics, Center for Plant Molecular Biology (ZMBP), University of Tübingen, Auf der Morgenstelle 32, 72076 Tübingen, Germany
[3]Current address: Department of Physics, Indian Institute of Technology, Madras 600036, India
[*]Correspondence: erik.schaeffer@uni-tuebingen.de

ABSTRACT Plant development and morphology relies on the accurate insertion of new cell walls during cytokinesis. However, how a plant cell correctly orients a new wall is poorly understood. Two kinesin class-12 members, Phragmoplast Orienting Kinesin 1 (POK1) and POK2, are involved in the process, but how these molecular machines work is not known. Here, we used *in vivo* and single-molecule *in vitro* measurements to determine how *Arabidopsis thaliana* POK2 motors function mechanically. We found that POK2 is a very weak, on average plus-end-directed, moderately fast kinesin. Interestingly, POK2 switches between processive and diffusive modes characterized by an exclusive-state–mean-squared-displacement analysis. Our results support a model that POK motors push against peripheral microtubules of the phragmoplast for its guidance. This pushing model may mechanically explain the conspicuous narrowing of the division site. Together, our findings provide mechanical insight into how active motors accurately position new cell walls in plants.

INTRODUCTION

Cytokinesis in plants is characterized by the insertion of a membranous cell plate in the center of a dividing parental cell. The assembly of the cell plate in the cell division plane is aided by a dynamic, plant-specific cytoskeletal scaffold structure called the phragmoplast (1). This phragmoplast apparatus arises from the mitotic spindle after chromosome segregation and consists of endoplasmic reticulum, filamentous (F)-actin and bipolar microtubules oriented perpendicular to the division plane (1). These microtubules serve as tracks for Golgi-derived vesicles translocating cell plate material towards the division plane where vesicle fusion results in cell plate formation. The phragmoplast expands centrifugally, by virtue of microtubule polymerization at the outer/leading zone and depolymerization at the inner/lagging zone where the cell plate assembly is achieved (1). The coordinated interplay of the phragmoplast dynamics and cell plate assembly ends by the fusion of the cell plate with the parental plasma membrane at the cell plate fusion site completing the new cell wall (2). In land plants, the cell plate fusion site is predicted by the cytoskeletal preprophase band during the G2/M transition (3). The cortical division zone, defined as the membrane region next to the preprophase band, remains at the cell cortex after the preprophase band disassembles. Memory of this region is kept throughout cell division and its location coincides with the later division site (2). Furthermore, the narrowing of this region from an initially broad zone to a definite cell plate fusion site during late cytokinesis occurs via a yet unknown mechanism (4–7). The kinesin-12 POK1, along with its dependents TANGLED (TAN) (5, 6) and RanGAP (8) localize to the division site throughout cell division (7). POK1 is functionally redundant with its homologue, POK2, as simultaneous impairment of both leads to loss of the TAN and RanGAP1 after preprophase band disassembly. Moreover, with the simultaneous impairment, newly formed cell plates position abnormally (7–9) presumably without proper guidance of the phragmoplast (7). Based on these findings, it was hypothesized that POKs might guide the phragmoplast by facilitating a mechanical communication between the division site at the cell cortex and microtubules of the phragmoplast leading edge (7).

Conventional kinesin-1 motors are dimers stepping in a rotary hand-over-hand mechanism along the microtubule lattice in an adenosine triphosphate (ATP)-dependent, directed manner (10). Dimerization facilitates processive motion—the ability to take many directed steps without dissociation (11). During this continuous, processive stepping behavior, the kinesin heads switch between strongly and weakly bound states before detaching from the microtubule lattice. Apart from processive, directed motion, some kinesins interact in a

diffusive manner with microtubules, such as human kinesin-13 MCAK (12) and kinesin-3 Kif1A (13). In addition, diffusive behavior has also been observed as an intermittent part of processive motion for *Drosophila* kinesin-14 Ncd using low-ionic-strength buffers (14, 15), for *Xenopus* kinesin-7 CENP-E (16), human kinesin-5 Eg5 (17), human kinesin-8 Kif18B (18) and human kinesin-12 Kif15 (19). During one-dimensional (1D) diffusive motion, both heads are thought to be in weakly bound states (20) and therefore exhibit random backwards and forwards motion on the microtubule lattice. Here, we asked how POKs mechanically interact with the peripheral microtubules of the expanding phragmoplast.

Outside of plants, the closest relative of POKs, the tetrameric human kinesin-12 hKif15, has recently attracted attention (19, 21–23). hKif15 is partially redundant to the tetrameric kinesin-5 Eg5 and is required during cell division for proper maintenance of spindle bipolarity by assisting formation of parallel microtubule bundles. While hKif15 is the sole member of the human kinesin-12 family, *Arabidopsis* has an extended family comprising six members (24). Thus, due to this increase and different cellular context, it is unclear whether the *Arabidopsis* kinesin-12 family members have similar molecular properties compared to hKif15. Here, we used *in vitro* single-molecule imaging and optical-tweezers-based force spectroscopy to characterize single POK2 motor proteins from *A. thaliana*. We found that POK2 motors exhibited both processive and diffusive motion and that individual motors frequently switched between the two modes. To quantify this switching behavior, we developed a mean-squared-displacement (MSD) analysis that accounts for the motor being exclusively either in the directed or diffusive state. This analysis can be robustly applied to a diverse range of other molecular machines. Additionally, to understand how POK2 would be able to guide the phragmoplast, we performed *in planta* imaging, visualizing the interaction of truncated POK2 motors with dynamic microtubules, the narrowing of the cortical division site, and the polarity of peripheral microtubules during late stages of cytokinesis. POK2 motors might pull on or push against these peripheral microtubules emanating from the expanding phragmoplast. Instead of intuitively pulling on the expanding phragmoplast for its guidance, our data supports the view that POK2 motors push against it.

MATERIALS AND METHODS

Protein expression and purification

Porcine brain tubulins were purified and labelled with tetramethylrhodamine (Invitrogen) according to standard protocols (25). 10% rhodamine-labelled taxol-stabilized microtubules were polymerized as described previously (26). $POK2_{1-589}$ GFP-His and $POK2_{183-589}$ GFP-His were expressed in SF9 insect cells (Expression Systems, Davis, CA, USA) using baculovirus expression (flashBAC, Oxford Expression Technologies, U.K. at Protein facility, MPI-CBG, Dresden). To pull on the tail domain of the kinesin in optical trapping experiments, the GFP was located at the C terminus. The protein was purified via sequential chromatography. Cation exchange chromatogrpahy (HiTrap SP HP 1 ml, GE Healthcare) followed by desalting (HiTrap desalting 1 ml, GE Healthcare) and subsequently affinity chromatography (HisTrap HP 1 ml, GE Healthcare). Cells were lysed in 50 mM HEPES, 150 mM NaCl, 5 % glycerol, 0.1 % Tween 20, 1.5 mM $MgCl_2$, 3 mM EGTA, 1 mM DTT, 0.5 mM ATP and protease inhibitors, at pH 7.5. The cation wash buffer consisted of 20 mM HEPES, 150 mM NaCl, 5 % glycerol, 1.5 mM $MgCl_2$, at pH 7.5. The cation elution buffer consisted of the same except the concentration of NaCl (600 mM) at pH 7.5. The desalting column was used to exchange the buffers to proceed towards metal affinity. The metal affinity wash buffer consisted of 50 mM phosphate buffer (pH 7.5), 300 mM NaCl, 10 mM imidazole, 10 % glycerol, 1 mM $MgCl_2$, 20 μM ATP, protease inhibitors, at pH 7.5. The metal affinity elution buffer consisted of the same except the concentration of imidazole (300 mM) at pH 7.5. Protein stability was confirmed from the SDS-PAGE and western blotting using anti-GFP antibody (mouse, Roche, Cat. 11814460001). The purified protein concentration was determined using a Bradford assay. Finally, the protein aliquots were snap frozen in liquid nitrogen and stored at −80 °C. The protein concentrations were measured using a NanoDrop. The concentration for the co-localization experiment were validated with the western blot.

Constructs

All the constructs used were amplified from the cDNA using standard PCR techniques. The whole RNA was extracted from col-o flower buds using RNeasy Plant Mini Kit (Qiagen, 74903) and cDNA was generated using Superscript Reverse Transcriptase II and oligo dT primers (Invitrogen, 18064-022) as described previously (9). All the constructs used were amplified from the cDNA using Phusion DNA Polymerase (New England Biolabs, M0530L) and standard PCR techniques. The cloning was performed using Quick Ligation Kit (New England Biolabs, M2200L). The used primers are mentioned in Table 1.

Microscopy assay and imaging conditions

The flow cell was constructed as described earlier (27), but the surface was rendered hydrophobic using chlorotrimethylsilane (Merck Millipore). The flow channels were washed 4–5 times with sterile filtered buffer BRB80 (80 mM PIPES, 1 mM $MgCl_2$, 1 mM EGTA, 100 mM KOH), pH 6.9. This was followed by incubation with anti-β tubulin (Sigma Aldrich, T7816) for 15–20 min at room temperature. Afterwards, the channels were washed once with BRB80 and blocked using 1 % Pluronic F-127 in BRB80 (Sigma-Aldrich, P2443) for 20–25 min. This step was followed by 5 times washing with BRB80 and incubation with 10% rhodamine-labelled, taxol-

TABLE 1 Used primers for all constructs.

Not $POK2_{1-589}$ F	AATAATAACATGCGGCCGCaATGTCAAAGGAGACCAAGCTTTC
NotI $POK2_{183-589}$ 549F	AATAATAACATGCGGCCGCaATGGAAGATCCATCTTTCTGGATGGATCACAA
AscI POK2 R	AATAATAACATGGCGCGCCttaACTTGATGGCGAATCGACT
EB1b EcoRI F	gaattcAAAAATGGCGACGAACATT
EB1b XhoI R	ctcgagTTAAGTTTGGGTCTCTGCAGCA

stabilized microtubules for 15 min. The assay buffer (BRB80, 0.08 mg/ml casein, 1 mM ATP, 20 mM D-glucose, 250 nM glucose oxidase, 134 nM catalase, 0.5 % BME) containing the protein was added after a quick wash of the channel. The samples were imaged at 25 °C on a custom built total-internal-reflection-fluorescence (TIRF) microscope combined with epifluorescence (28). The TIRF microscope is equipped with a sCMOS camera (Orca Flash 4.0, Hamamatsu Photonics) and an oil-immersion, TIRF objective (60×, 1.49 NA, Nikon). To visualize motor movement, 40 s long time-lapse videos were recorded at 10 fps using a continuous image acquisition mode at 100 ms exposure. The sample was excited using a 488-nm laser (Omicron, LuxX 488-100).

Polarity-marked microtubules

GMP-CPP-stabilized microtubule seeds were prepared using 2–3 μM unlabelled tubulin, 1 mM $MgCl_2$, 1 mM GMP-CPP (Jena Bioscience) and BRB80 and incubating them for one hour at 37 °C. Afterwards, microtubules were spun down and the pellet was re-suspended in the same constituents but with 1–2 μM of 10 % rhodamine-labelled tubulin. This reaction was incubated further for an hour at 37 °C. Then, 1–2 μM of 10 % rhodamine-labelled tubulin was added and incubated for another hour before they were spun down and re-suspended in BRB80.

Photobleaching assay

The photobleaching assay was conducted in the same manner as the rest of *in vitro* preparations, except for the assay buffer. The assay buffer consisted of 0.08 mg/ml casein, 1 mM AMP-PNP, 10 mM DTT and BRB80, pH 6.9. In the presence of AMP-PNP, motors are thought to bind with both heads in a strongly bound state. GMP-CPP stabilized microtubules were used. The data was acquired at the same conditions mentioned earlier using a higher excitation laser power. Post-acquisition, kymographs were generated and intensity values were extracted from them, followed by an analysis via a custom-written, MATLAB-based step-finding algorithm (20).

Microsphere preparation and force measurements

Microsphere functionalization and protein-microsphere coupling was performed as reported previously (29). The sample preparation and assay buffer for optical tweezers experiments were the same as mentioned above. All the measurements were performed on a custom-built, single-beam optical tweezers setup (30, 31). The setup has a millikelvin precision temperature control of the trapping objective, which was set to 29.200 °C. The experiments were conducted with a trap stiffness of 0.01 pN/nm and recorded with a sampling rate of 4 kHz. Calibration was performed by analysing the height-dependent power spectral density combined with a drag-force method as reported earlier (27, 32).

Single-molecule tracking and data analysis

Single molecules were tracked using FIESTA (33), which is based on 2D Gaussian model fitting. The resulting position coordinates were subjected to a rotation and projection on the microtubule axis, and subsequently MSD values were calculated. The same set of data was also subjected to a speed correlation index (SCI) analysis (34). All the *in vitro* data was analysed in MATLAB by using custom-written scripts. The kymographs were plotted using Fiji (http://fiji.sc) with a custom-written macro that auto-contrasts. *In vivo* images were analysed in Fiji.

Plant materials and growth conditions

Arabidopsis thaliana plants, *pok 1-1 pok 2-3* (7), microtubule marker line (7) were the base lines for this study. All other double-labelled transgenic lines were generated via crossing of single transgenic lines in accession Columbia (Col). All plants including seedlings were grown at 20–22 °C with 16 h-light/8 h-dark cycle. The seedlings used for the localization studies were grown on plates containing Murashige and Skoog medium (Sigma-Aldrich) and 1 % agarose, incubated at the aforementioned conditions.

Tobacco leaf infiltration

Nicotiana benthamiana leaves of 4-week-old plants were infiltrated with Agrobacterium suspension culture (OD_{600} 0.5) carrying respective plasmid DNA (GFP $POK2_{1-589}$). 48–72 h post infiltration, the leaf epidermis of transformed plants was imaged on a confocal microscope.

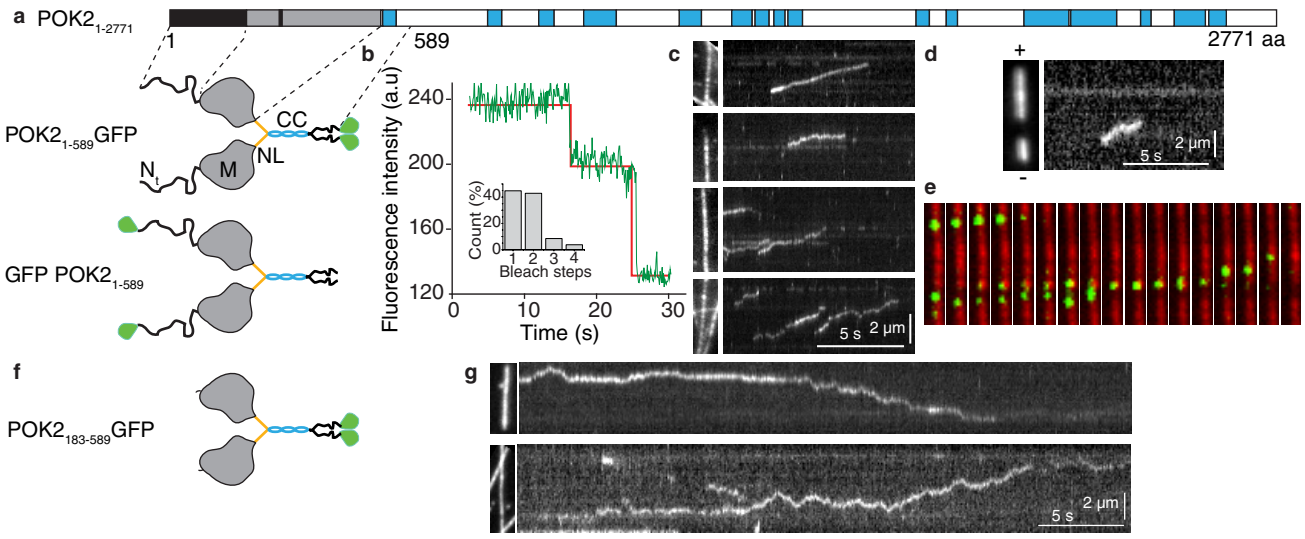

FIGURE 1 $POK2_{1-589}$ is a plus-end-directed dimeric motor. **(a)** Top: Full-length POK2 domain organization: motor domain (grey, M) with ATP binding site (black strip in M), coiled coil (cyan, CC) and intrinsically disordered N-terminus region (black, N_t). Bottom: Structural cartoon of the GFP-tagged truncated POK2 used in the *in vitro* (top) and *in vivo* (bottom) assays, where region N_t is followed by M, and a short neck linker (orange, NL) connecting M and CC. The domain organization and cartoon are based on a bioinformatics analysis (Fig. S1). **(b)** Example trace of the fluorescence intensity over time for a single $POK2_{1-589}$ bound to the microtubule in the presence of 1 mM AMP-PNP. The relative frequencies of bleaching steps are represented in the inset (N = 105). **(c)** Representative kymographs showing motile single $POK2_{1-589}$ and their typical behavior on the microtubule lattice. Left picture indicates respective microtubules. **(d)** Example kymograph for a single $POK2_{1-589}$ indicating its plus-end directionality. Left picture shows a polarity-marked microtubule. **(e)** Image sequence of single $POK2_{1-589}$ (green) interacting with a microtubule (red) corresponding to the third panel of **(c)**. Images are 4.75 μm high. The time between frames is 0.5 s. **(f)** Cartoon of the N-terminal truncation $POK2_{183-589}$-GFP construct. **(g)** Representative kymographs of $POK2_{183-589}$.

Cloning of pUBN:RFP-EB1b

EB1b was PCR-amplified from Arabidopsis cDNA accession Columbia using primers EB1b EcoRI F and EB1b XhoI R and cloned into pgem T-vector (Promega). Subsequently, the plasmid was digested with EcoRI and XhoI and Eb1b insert was ligated into the respective restriction sites in pENTR2B (Gateway). The resulting vector was recombined with destination vector pUBN:RFP (35) to obtain pUBN:RFP-EB1b. Transgenic lines were generated via Agrobacterium tumefaciens mediated transformation as described earlier (36).

Accession numbers

The full-length sequence of POK2 and EB1b can be found at Arabidopsis Genome Initiative or EMBL/GenBank databases using accession number At3g19050 and At5g62500, respectively.

Confocal microscopy

Localization imaging using a Leica SP8 confocal microscope equipped with a resonant scanner. Imaging was carried out at room temperature using 63× water immersion objective with an NA of 1.2. GFP and YFP were excited at 488 nm and 514 nm using an argon and krypton laser, respectively, and were detected using HyD detectors in the range of 500–550 nm and 520–550 nm, respectively. The excitation for RFP was done using a 561 nm laser line and the signal was detected by HyD detector in the range of 570-650 nm.

RESULTS

$POK2_{1-589}$ is a plus-end-directed dimeric motor that switches motility modes

To investigate the underlying molecular mechanism using reconstituted assays, we expressed and purified truncated and fluorescently tagged POK2 motors. POK2 is the largest identified kinesin to date with an extraordinary long and intrinsically disordered N-terminus (about 190 amino acids (aa) compared to 7 aa in conventional kinesin) preceding its motor domain (9). To focus on the motor functionality, we created a motor, $POK2_{1-589}$, truncated after the first predicted coiled coil and fused to a C-terminal green-fluorescent-protein (GFP) tag (Fig. 1a, Fig. S1). To test whether the coiled coil was sufficient for the dimerisation of the truncated motor, we performed photobleaching assays using a custom-built total-internal-reflection-fluorescence (TIRF) microscope (28). We immobilized taxol-stabilized and rhodamine-labelled microtubules at the cover glass surface and added purified $POK2_{1-589}$ molecules into the flow channel in the presence of adenosine 5'-[β,γ-imido]triphosphate (AMP-PNP) (Fig. S2, Fig. S3). This non-hydrolyzable ATP analogue, causes kinesin motors to interact with microtubules in a strongly bound, non-motile state. We recorded the fluorescence intensity of GFP-tagged motors that co-localized with microtubules as a

function of time and found that most GFP molecules bleached in one or two steps (Fig. 1b). For most of the single-step bleach events, the step amplitude was consistent with twice the amplitude of single-step bleach events suggesting that two GFP fluorophores bleached simultaneously. Together these data confirm that POK2$_{1-589}$ binds microtubules and is consistent with the notion that the first coiled coil region is sufficient for homodimer formation.

To characterize the motor functionality, we performed TIRF microscopy motility assays in the presence of ATP (1 mM). We found that POK2$_{1-589}$ is an active motor that robustly translocates on the microtubule lattice (Fig. 1c–e, Video S1). Using polarity-marked microtubules, POK2$_{1-589}$ showed on average plus-end-directed motility as expected for kinesins with an N-terminally located motor domain (Fig. 1d). We did not observe any preference for or extended dwells at microtubule ends. Interestingly, although the overall motion of POK2$_{1-589}$ molecules was towards the plus-end, we observed recurrent episodes of random, forwards and backwards motion (Fig. 1c–e) suggesting that POK2$_{1-589}$ motors switch between processive and diffusive modes while interacting with the microtubule lattice.

To test whether diffusion was due to the large N-terminal extension (Nte) of the motor (Fig. 1a), we truncated the N-terminus and repeated the same motility assay for the POK2$_{183-589}$ construct (Fig. 1f,g). Surprisingly, POK2$_{183-589}$ interacted with the microtubule lattice for a longer time of 11 ± 1 s (mean ± SEM, N = 38) compared to 1.9 ± 0.1 s for POK2$_{1-589}$ (Fig. 2a). Kymographs of POK2$_{183-589}$ showed more diffusive motion (Fig. 1g) suggesting that the Nte affected the processive mode. Furthermore, POK2$_{183-589}$ had a much lower affinity to microtubules (Fig. S4a). Therefore, we analyzed the Nte amino acid sequence and found a similarity to the ≈80 aa long Nte of BimC (Fig. S4b). BimC is the founding member of the kinesin-5 family and has a secondary microtubule-binding site in its Nte (37). Interestingly, loss of the Nte in BimC also reduced the affinity of BimC to microtubules; however, the structural mechanism is not understood. Together, these findings suggest that the Nte of the POK2 affects the motor-microtubule interaction strength and promotes the processive over the diffusive mode.

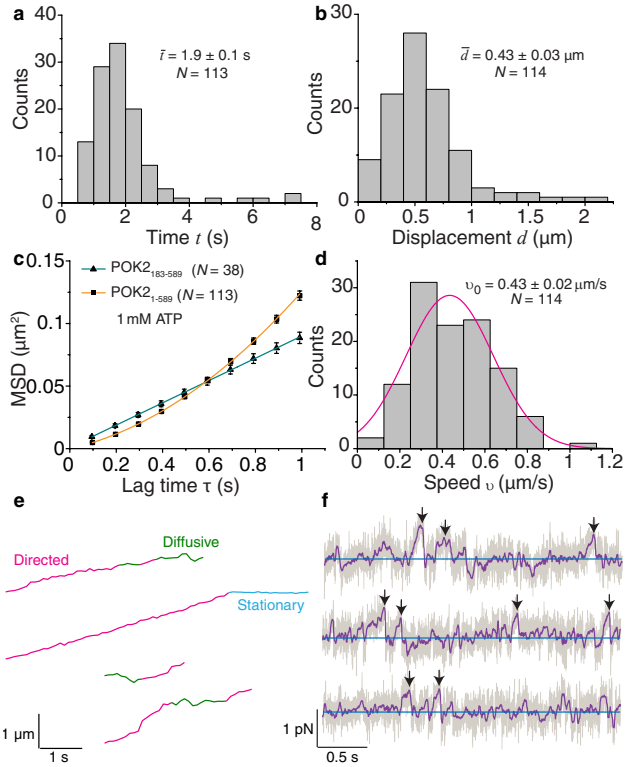

FIGURE 2 POK2$_{1-589}$ is a weak motor that switches between processive and diffusive modes. Distributions of total interaction time **(a)** and overall displacement **(b)** of POK2$_{1-589}$ on the microtubule lattice. Mean values, SEM, and total number of molecules are indicated. **(c)** Mean-squared displacement (MSD) of POK2$_{1-589}$ and POK2$_{183-589}$ in 1 mM ATP plotted against the lag time. The orange line is a fit of the Eq. (1) to the POK2$_{1-589}$ data while the green line is a linear fit to the POK2$_{183-589}$ data. Error bars are SEM of squared-displacement values. **(d)** Speed histogram of directed segments have a Gaussian distribution (magenta line). Mean speed, SEM and number of molecules are indicated. **(e)** Example trajectories of POK2$_{1-589}$ obtained via single-molecule tracking. Mode switches were detected using an SCI algorithm (Supplementary Information). Magenta, green, and cyan denotes directed, diffusive and stationary segments, respectively. Note that stationary segments were not at the microtubule end. **(f)** Representative traces depicting the force of single POK2$_{1-589}$ molecules as a function of time (grey line, running median filter over 500 data points: purple line). The blue line marks zero force. Maximum forces are marked by black arrows.

MSD for exclusive directed and diffusive states

To confirm the POK2$_{1-589}$ switching behavior, we tracked the motion of single POK2$_{1-589}$ motors on individual microtubules using an automated data analysis based on 2D-Gaussian models (33) (Fig. 1e). Histograms of the total microtubule interaction time and overall displacement of single motors show peaked distributions (Fig. 2a, b). Peaked distributions are indicative of multiple underlying processes, such as directed and diffusive modes. In contrast, exponential distributions are typical of a single, rate-limiting process (38). To quantify this behavior, we used a statistical approach to measure the spatial extent of motion over time: a MSD analysis. In our case, the MSD of a single POK2$_{1-589}$ motor as a function of lag time is best fitted by a parabola (orange line in Fig. 2c) with significant linear and parabolic coefficients. The presence of both terms confirms that POK2$_{1-589}$ indeed has two motility modes. While the linear term is related to diffusion, the quadratic term is due to directed motion (39, 40). Diffusion can occur simultaneously with directed motion, for example, when a particle is freely diffusing in 3D and subjected to a flow or drift. However, in our case, POK2$_{1-589}$ is exclusively either in the processive or the diffusive state. To the best of our knowledge, this scenario has not been addressed with respect to single molecular machines interacting with filaments in a one-dimensional diffusive system. Therefore,

we derived the expected MSD as a function of lag time τ for a motor being either in the diffusive or in the processive state (Appendix A)

$$\mathrm{MSD}(\tau) = \phi^2(\upsilon_0^2 + \sigma_\upsilon^2)\tau^2 + 2D(1-\phi)\tau + 2\varepsilon^2, \quad (1)$$

where ϕ is the fraction of the total interaction time the motor spends in the directed mode, υ_0 and σ_υ the mean speed and its standard deviation, respectively, D the diffusion coefficient, and ε an offset related to the tracking precision and image acquisition (41). Equation 1 accounts for the exclusive character of the states and the amount of time in the respective states avoiding an underestimation of both the speed and the diffusion coefficient (14, 18). Because five parameters enter Eq. 1, namely ϕ, υ_0, σ_υ, D, and ε, and a fit of Eq. 1 to the data only results in three independent coefficients of the parabola, the system is underdetermined. Thus, a MSD analysis alone cannot provide all the parameters. Therefore, in addition to the MSD, we used a speed correlation index (SCI) analysis. The SCI analysis is based on the temporal correlations of the speed of individual molecules, where high amount of correlation signifies directed motion and no correlation indicates purely Brownian motion (34). The SCI algorithm optimized to our POK2$_{1-589}$ dataset identified transient switches in the POK2$_{1-589}$ trajectories between directed, diffusive, and stationary states (Appendix B). However, because of limited spatio-temporal resolution of the TIRF measurements, our SCI algorithm could only reliably determine the speed in the directed mode of 430 ± 170 nm/s (mean ± SD, N = 114, Fig. 2d and 2e, Fig. S5). Using this speed υ_0 and its standard deviation σ_υ as an input for Eq. 1, i.e. we provide and fix two out of the five parameters for the fit, the best-fit diffusion coefficient is 0.056 ± 0.008 μm^2/s (mean ± SEM), the relative time spent in the directed mode is 62 ± 2 % (mean ± SEM; Fig. S6–S8), and the constant offset is ε = 32 ± 3 nm giving an estimate for the tracking precision. We also tracked single POK2$_{183-589}$ molecules. In contrast to POK2$_{1-589}$, their MSD was best fit by a line (green line in Fig. 2c) with no significant parabolic coefficient. Thus, the truncation of the Nte switched POK2 to a purely diffusive mode with a diffusion coefficient of 0.040 ± 0.001 μm^2/s not significantly different from the value for POK2$_{1-589}$. The value for the diffusion coefficient of POK2$_{1-589}$ is intermediate between reported values for other kinesins like Kip3 (26) and MCAK (12) of about 0.004 μm^2/s and 0.4 μm^2/s, respectively. Our MSD equation also quantitatively explains previous observations of motors switching between different states (18). Thus, with a combined SCI and MSD analysis approach, we could objectively quantify the two modes of the POK2$_{1-589}$ motor interaction with the microtubule lattice. Taken together, POK2$_{1-589}$ spends a large fraction, about two-thirds of its time in the processive state, walking in a directed manner along microtubules.

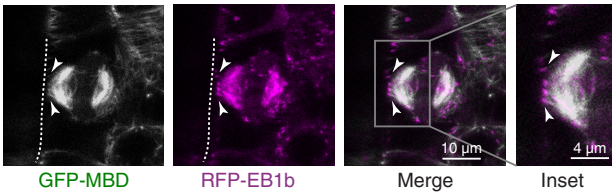

FIGURE 3 Directionality of the phragmoplast peripheral microtubules. *Arabidopsis* root meristem stably expressing 35S:GFP-MBD and pUBQ:RFP-EB1b during late cytokinesis. Plus-ends (RFP-EB1b) marked with arrow heads of peripheral microtubules (GFP-MBD) from the leading edge of the phragmoplast reach out towards the putative division site. The cell boundary is marked with a dashed line.

POK2$_{1-589}$ is a weak motor

To assess if POK2 motors are capable of generating force, we measured the maximum force that single machines could exert on artificial cargo using high-resolution optical tweezers (30, 42). As cargo we used microspheres coupled to POK2$_{1-589}$ via its GFP-tag ensuring functional activity of the motor (29) (Fig. S2). Using a stationary trap, single motors displaced microspheres from the trap centre with force increasing proportional to the displacement according to Hooke's law (Fig. 2f). Compared to conventional kinesin-1 and other kinesins (29), we observed that POK2$_{1-589}$ did not exhibit stalling behavior for extended periods. Instead, motor-coupled microspheres showed sudden and fast movements back to the trap centre consistent with a motor detachment from the microtubule or switching to a diffusive mode and slipping back on the microtubule (10, 43). We measured the maximum force before such events and found an average maximum force of 0.34 ± 0.02 pN (mean ± SEM, N = 67, Fig. 2f). Since POK2$_{183-589}$ did not show any directed motility, we did not use this motor for trapping experiments. Thus, for POK2$_{1-589}$, even though the motor spent most of its time in the directed mode when no loads were applied, single motors were unable to generate large forces. Forces exceeding 1 pN could be measured when multiple POK2$_{1-589}$ motors were pulling on trapped microspheres (Fig. S9).

The peripheral microtubule plus-ends point towards the putative cell plate fusion site

Having characterized the POK2$_{1-589}$ motor activity *in vitro*, we wanted to confirm the microtubule interaction, functionality, and speed of POK2$_{1-589}$ *in vivo*. Therefore, we transiently expressed GFP-POK2$_{1-589}$ (Fig. 1a) in *Nicotiana Benthamiana* leaves. We found that POK2$_{1-589}$ co-localizes with microtubules (Fig. S10). The microtubule decoration changed dynamically, consistent with motors keeping up with dynamic microtubule ends growing with a speed of 74 ± 3 nm/s (mean ± SEM, N = 41; Fig. S10) (44). However, the signal-to-noise ratio was insufficient to track the motility of single motors *in vivo* precluding direct measurements on peripheral microtubules emanating from the phragmoplast.

The polarity of peripheral microtubules at the phragmoplast leading zone approaching the cell cortex during late cytokinesis (7, 8) determine if motors pull on or push against such microtubules and thereby the phragmoplast itself. The majority of phragmoplast microtubules including the ones at the leading edge are oriented with their polymerizing, plus-ends towards the division plane (45) suggesting that peripheral microtubules are also oriented with their plus-ends towards the division site (46, 47). To confirm the polarity of the peripheral microtubules in *Arabidopsis*, we created an *Arabidopsis* transgenic line with GFP-labelled microtubules and red-fluorescent-protein (RFP)-labelled EB1b, a microtubule plus-end tracking protein. We imaged 4–5 day old seedlings using a confocal microscope and found that the leading edge of the phragmoplast indeed sends out peripheral microtubules with their plus-ends directed towards the putative division site (Fig. 3). However, the presence of microtubule plus ends at the division site, does not rule out that additional minus-end-directed microtubules are there as well. Yet, based on the overall structure and dynamics of the phragmoplast, we do not expect a high abundance of such microtubules. Suggested by the functional redundancy of POK1 and POK2, we assume that both POKs localize to the cortical division site (unpublished data by Sabine Müller confirm the assumption for POK2) and function alike. Thus, POK2 motors likely push against peripheral microtubules rather than pull on them.

DISCUSSION

Based on state-of-the-art single-molecule techniques and a combined MSD-SCI analysis, we have functionally characterized the plant kinesin-12 POK2 motor—without its long C-terminal tail—as a plus-end-directed, weak, and dimeric motor that switches between processive and diffusive modes. Because the long N-terminal extension before the motor domain appears to be required for the processive mode, this Nte domain seems to be involved in the switching process. As for BimC, the disordered region of the POK2 Nte might also have a microtubule-binding site that helps in the microtubule attachment explaining the low affinity of the construct lacking the Nte (Fig. S4). Once bound, the Nte interaction with the motor domain may promote processivity at the cost of total microtubule interaction time.

While MSD analyses are commonly applied to study mixed diffusive and directed motion, to the best of our knowledge, studies so far do not account for the mutually exclusive character of processive and diffusive states in case of molecular machines. Our novel MSD analysis (Eq. 1) not only accounts for this exclusive character of states, but also for the inherent speed distribution of motors. Not accounting for the exclusive character and distribution leads to systematic errors in the motility parameters.

Compared to conventional kinesin-1 with a stall force of about 5–6 pN (29), POK2$_{1-589}$ is one of the weakest kinesin motors across taxa. Reported weak motors belong to the kinesin-8 family with the members Kif18B, Kif18A, and Kip3 reaching maximum forces of about 0.6 pN, 0.8 pN and 1.1 pN, respectively (18, 43). For POK2$_{1-589}$, we attribute such low forces to the motor switching to a diffusive state similar to Kip3 that switches into a slip state (43). Since motors are weakly bound to the microtubules in the diffusive state, they can slide along the microtubule lattice with little resistance, but without detachment, when a force is applied (10, 20, 43). This sliding might enable the motor to dynamically link to microtubule plus ends in analogy to CENP-E (16, 48). CENP-E is almost as large as POK2 suggesting that a very long motor tail may enhance dynamic attachment to microtubules. Thus, we hypothesize that the function of the diffusive state and low force production is to provide a means of attachment to microtubules allowing for a relative sliding motion with little resistance. Based on this hypothesis and the intrinsic motor properties, how does POK2 guide the expanding phragmoplast during cytokinesis?

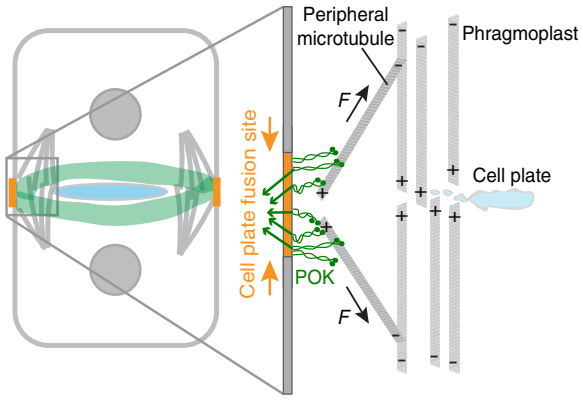

FIGURE 4 Proposed model for phragmoplast guidance. POK motors (green) localized at the division site push against the leading edge of the expanding phragmoplast by capturing the peripheral microtubules and walk towards their plus-ends pushing against the expanding phragmoplast. The black arrow marks the direction of the pushing force. This model also supports the narrowing of the division site (orange, Fig. S11) to the cell plate fusion site by a mechanical process. POK motors experience a counter force (green arrows). This force focusses the POKs to a precise spot, i.e., the cell plate fusion site.

Our combined *in vivo* and *in vitro* results support a phragmoplast guidance model in which POK2 motors push against peripheral microtubules (Fig. 4). We validated the POK2$_{1-589}$ interaction with microtubules *in planta* and the polarity of the peripheral microtubules that appear to connect the putative division site, where POK motors are located, with the phragmoplast. Peripheral microtubules are oriented with their plus-ends towards the putative cell plate fusion site and likely probe the cell cortex in a "search and capture" type mode (46). We propose that as the torus-shaped phragmoplast branches out plus-end-directed peripheral microtubules at the leading edge, POK2 full-length molecules at the division site (unpublished data, Sabine Müller) capture these microtubules and walk towards their plus-ends. Because the motor speed

(Fig. 2d) is faster compared to the phragmoplast expansion speed (7), we expect that motors catch up with the microtubule plus ends. If motors are attached to the cell boundary and since they walk towards the microtubule plus end, they counteract the microtubule expansion driven by the phragmoplast and, thus, push against the phragmoplast (Fig. 4). The POK2s' enormous size and contour length may enhance an effective capture of incoming microtubules in analogy to CENP-E. Pushing may seem counterintuitive for phragmoplast guidance but together with the unusual mechanics of these kinesin-12 motors provide insight into the guidance mechanism. As $POK2_{1-589}$ motors exert little force, forces of the expanding phragmoplast are expected to exceed the opposing pushing force of POK2 motors when they are in the processive state even when multiple motors interact simultaneously. Once the motors switch to the diffusive state, they can then slide along the microtubule lattice. The switching rate to the diffusive mode of the motors may even increase under load conditions as reported for the switching to the weakly-bound slip state of kinesin-8 (43). POK2 motors would, thus, guide the phragmoplast in a manner similar to the dynamic and diffusive attachment of microtubules to the kinetochore or chromosomes, for example, via the Ndc80 complex (49–51) or CENP-E (48), respectively. We believe that POK1 motors function in a similar manner as established by their functional redundancy with POK2 (7). If POK2 motors are regulated by importin-β during the cell cycle remains to be seen (52).

During cytokinesis, pushing forces by POKs have an important consequence. According to Newton's third law, there is a net force of equal magnitude and opposite direction acting on the anchoring points of the motors. Furthermore, due to the geometry of the connected peripheral microtubules, these opposing forces will focus the motors to a central spot, assuming that their membrane anchors are mobile within the lipid bilayer (Fig. 4). The small forces of a single-motor are sufficient to drag an anchoring point through a fluid membrane. Also, when multiple motors interact simultaneously with a microtubule, pushing forces of the expanding phragmoplast and counteracting motor forces are expected to be sufficient for moving the anchoring points in the membrane. This mechanical focusing could contribute to the poorly understood narrowing of POK1 and POK1-dependent components from the division site to a definite cell plate fusion site during late cytokinesis (5, 7, 8, 53) (Fig. S11). If POK motor motility itself is required for *in planta* guidance, if a diffusive tethering is sufficient, how motors switch to the diffusive state, and if and how much force is necessary for division site narrowing is unknown at the moment.

Interestingly, a few other microtubule-associated candidates occupy the division site such as minus-end-directed kinesin-14 KCBP (54, 55), TAN (6), and MAP65-4 (56). What possible role they play during the cell plate insertion process is also unclear at the moment. For example, forces generated by KCBP could accelerate phragmoplast guidance or MAP65-4 could contribute to cross-linking of peripheral microtubules.

CONCLUSION

In conclusion, our study offers first mechanistic insights into the operating behavior of single plant kinesin-12 POK2 motors. We quantified the motors motility by a novel MSD analysis that can be utilized for other diverse molecular machines. POK2 is the first kinesin-12 motor among five other members in *Arabidopis* to be characterized. The mechanical properties of POK2 provide a key step towards an active and dynamic understanding of the division site more than what can be inferred from localization studies alone. Moreover, the phragmoplast guidance-pushing model suggested here highlights the participation of active molecular machines needed for the accurate insertion of cell plates during plant cytokinesis and plausibly accounts for the narrowing of the division site to the cell plate fusion site. *In planta* experiments, ideally with single-molecule resolution, are required to test the proposed hypothesis involving pushing forces. In other cells, pushing forces are thought to provide a more precise centering mechanism compared to pulling forces, for example for centering of the mitotic spindle (57, 58). Here, pushing forces in combination with sliding of motors along microtubules dynamically attaching to their ends may lead to precise and accurate mechanical patterning and shaping of plant tissues.

APPENDIX A: MEAN-SQUARED DISPLACEMENT ANALYSIS

The average MSD was plotted against lag time and fitted with a parabola because the motor exhibited diffusive as well as directed motion. For *simultaneous* 1D diffusion and directed motion, the MSD as a function of lag time τ is given by the well-known equation:

$$\mathrm{MSD}(\tau) = \upsilon^2\tau^2 + 2D\tau + 2\sigma^2. \qquad (2)$$

The first term refers to the directed motion, where υ is the speed. The second term is the contribution by the diffusive motion, where D is the diffusion coefficient. The last term is a constant related to the tracking precision and image acquisition (41). Although this equation yields the parameters D and υ, the motion occurs simultaneously. An example for such simultaneous motion is a particle diffusing in a liquid with an applied flow. However, such simultaneous motion is impossible for a molecular motor taking discrete steps. Steps are exclusively either directed or random. Furthermore, for kinesins, the average stepping rate in the diffusive mode is typically much larger compared to the directed mode. For example, a kinesin moving with a directed speed of 400 nm/s takes about 50 steps per second. Assuming the motor takes 8 nm steps during diffusion (20) and has a diffusion coefficient of 0.032 $\mu m^2/s$, the diffusive stepping rate is $2D/\delta^2 = 1000$ steps per second ($\delta = 8$ nm), 20× higher compared to the

directed state. Thus, the motor has distinct and different properties in the two modes. To account for the switching behavior, a modification to the Eq. 2 is required. Therefore, the MSD equation that accounts for a motor being exclusively either in a diffusive or directed mode is derived in the following.

The motion of a motor that switches between the different modes is described by the Fokker-Planck equation

$$\frac{\partial p}{\partial t} + \eta(t)v\frac{\partial p}{\partial x} = [1-\eta(t)]\,D\frac{\partial^2 p}{\partial x^2}, \tag{3}$$

where $p(x,t)$ is the probability density of the motor being at a position x at time t. $\eta(t)$ is either 0 or 1, randomly switching between the two values as a function of time. The number indicates whether the particle is diffusing ($\eta = 0$) or translating ($\eta = 1$). Equation 3 is for one realisation of $\eta(t)$ and also assumes that the average switching rate is small compared to the stepping rate of the molecular motor, i.e. the time between switches is long compared to the time per step. The Fourier transform of Eq. 3 yields

$$\frac{\partial \tilde{p}}{\partial t} + ik\eta v\tilde{p} = -k^2(1-\eta)D\tilde{p}, \tag{4}$$

where $\tilde{p}$ is the Fourier transform of p, k is the spatial frequency corresponding to the Fourier transform of x, and i is the imaginary unit. Separating variables, Equation 4 can be written as

$$\frac{\partial \tilde{p}}{\tilde{p}} = -(k^2(1-\eta)D + ik\eta v)\partial t. \tag{5}$$

Integration of both sides of Eq. 5 yields

$$\ln\frac{\tilde{p}}{\tilde{p}_0} = -(k^2(1-\phi)D + ik\phi v)(t-t_0), \tag{6}$$

where $\tilde{p}_0$ is an integration constant, t_0 is the initial time and the time interval $t - t_0$ can be set to the time lag τ. The parameter ϕ is the time average of $\eta(t)$ over the time interval $t - t_0$ and, thus, represents the time fraction the motor spends in the directed state. For $\phi = 1$, the motor is purely in the directed mode and for $\phi = 0$ only diffusing. The equation holds for times large compared to the switching time, for which case the variance of ϕ is small. The last equation can be rewritten as

$$\tilde{p} = \tilde{p}_0 \exp\left[-(k^2(1-\phi)D + ik\phi v)\tau\right], \tag{7}$$

for which the inverse Fourier transform results in the probability density

$$p(x,\tau) = \frac{1}{\sqrt{4\pi(1-\phi)D\tau}}\exp\left[-\frac{(\phi v\tau + x)^2}{4(1-\phi)D\tau}\right]. \tag{8}$$

The mean-squared displacement is then defined by

$$\left\langle x^2(\tau)\right\rangle = \mathrm{MSD}(\tau) = \int_{-\infty}^{+\infty} p(x,\tau)x^2\mathrm{d}x, \tag{9}$$

which results in

$$\mathrm{MSD}(\tau) = (\phi v\tau)^2 + 2(1-\phi)D\tau, \tag{10}$$

where, as pointed out above, ϕ is the fraction of the time spent in the directed motion.

If the speed of an individual molecular motor is constant for an individual run but changes from molecule to molecule and run to run, then the average MSD of the indivdual MSDs of the individual runs differs from Eq. 10. The difference arises because of the non-linear, i.e. quadratic, contribution of the speed to the MSD. We assume that the speed is normally distributed with a mean speed v_0 and standard deviation σ_v. If we denote the various MSDs for different runs as $\langle x^2\rangle(\tau)_n$, where n is the index of the run, the expectation value of the average MSD for large n is calculated according to

$$\langle\langle x^2\rangle(\tau)\rangle_n = (1-\phi)2\langle D\rangle_n\tau + \phi^2\langle v^2\rangle_n\tau^2. \tag{11}$$

The second moment of the speed, i.e. the mean-squared speed, is $\left\langle v^2\right\rangle_n = v_0^2 + \sigma_v^2$ (note that the variance is $\sigma_v^2 = v_0^2 - \left\langle v^2\right\rangle$). If we denote the mean diffusion coefficient by $\langle D\rangle_n = D$ then the final result of the modified Eq. 10 is

$$\mathrm{MSD}(\tau) = \phi^2(v_0^2 + \sigma_v^2)\tau^2 + 2D(1-\phi)\tau + 2\sigma^2, \tag{12}$$

where we have added again the offset $2\sigma^2$ related to the tracking precision and image acquisition. Because the MSD has a linear dependence on the diffusion coefficient, a distribution in the diffusion coefficients does not affect the equation. For a small variance in speed relative to the mean, Equation 12 reduces to Eq. 10. Equation 12 corresponds to the MSD equation stated in the main text.

If the mean speed and standard deviation are known, the parameters D and ϕ can be calculated from a parabolic fit, $\mathrm{MSD} = A^2\tau^2 + B\tau + C$, to the overall MSD (Figure 2c in the main text) by the following relations

$$D = \frac{B/2}{1 - \frac{A}{\sqrt{v_0^2+\sigma_v^2}}} \tag{13}$$

and

$$\phi = \frac{A}{\sqrt{v_0^2 + \sigma_v^2}}. \tag{14}$$

APPENDIX B: SPEED CORRELATION INDEX (SCI) ANALYSIS

To determine the speed of the motor, we performed a speed correlation index (SCI) analysis (34). The SCI analysis relies on the temporal correlations of the speed of individual molecules. This correlation exists and persists for directed motion but disappears for Brownian motion. A MATLAB script was written to analyse the trajectories of each molecule. The SCI parameter is a normalized average over an optimal time window, which provides a local analysis whether speeds are correlated or not. In particular, the switch times between diffusive and directed segments were analysed by defining a threshold for temporal correlations. The SCI analysis cannot

distinguish between diffusive and stationary events. Thus, we identified the latter by comparing the root-mean-squared positional noise σ_x of the segments with that of stationary motors taken from immotile POK2 bound to microtubules. For a threshold of $\sigma_x < 32$ nm, segments were classified as being stationary. For our frame time of 0.1 s, we used a window size of 4 data points with an SCI threshold of 0.8. From 113 original POK2 trajectories, 95 traces were long enough for the SCI analysis. The algorithm found 65 diffusive, 114 directed, and 21 stationary segments. The relative time POK2 spent in the diffusive, directed, and stationary mode were 29 %, 63 % and 8 %, respectively. All diffusive and directed segments are shown in (Fig. S7). The mean duration of the diffusive and directed segments were 0.8 ± 0.1 s and 1.1 ± 0.1 s, respectively (Fig. S6). The mean speed and standard deviation of directed segments weighted by their number of data points was 430 ± 170 nm/s (Fig. 2e in the main text). A Shapiro-Wilk test confirmed a normal distribution of speeds. An MSD analysis of only the diffusive segments yielded a diffusion coefficient of 0.015 ± 0.001 μm^2/s (Fig. S5). However, the mean displacements of diffusive segments still showed a significant bias over time (Fig. S7). Such a bias is inconsistent with pure diffusion and indicates that the SCI analysis did not fully separate directed and diffusive segments. This bias remained for all tested combinations of SCI parameters, i.e. variations of window size and thresholds. Thus, our time resolution and tracking precision was not sufficient for the segmentation. Therefore, we conclude that POK2 sometimes switched between modes faster or on time scales comparable to the data acquisition time. An observation consistent with this conclusion is the lack of short diffusive segments due to the SCI algorithm when comparing the distribution to the expected exponential distribution (Fig. S6). Apart from the cut-off at short times, segments containing very short periods of directed and diffusive motion are identified as diffusive segments by the algorithm. As a consequence, the diffusion coefficient obtained from the MSD analysis of the diffusive segments is underestimated because during short directed periods, the motor takes far fewer steps compared to when it is in its diffusive mode (see Appendix A). Yet, we expect that long directed segments and their parameters are reliably detected. One indication for reliable directed parameters, it that the speed is normally distributed. The mean speed also corresponds to the mean speed that one obtains by manually analysing the slopes of the kymographs. Thus, Eqs. 13 and 14 can be used to determine diffusion constant D and relative time in the directed mode ϕ. The derivation of Eq. 12 did not account for the possibility of a stationary state. However, such a state only adds a constant to the MSD and is effectively adsorbed in our constant parameter. Thus, using Eq. 13, the diffusion constant was calculated to be 0.056 ± 0.008 μm^2/s and, using Eq. 14, the relative time in the directed state excluding stationary segments was determined to be 62 ± 2 %. To assess how the diffusion coefficient and speed depends on the relative time spent in the states, we plotted Eq. 13 as a function of the effective speed (Fig. S7). Not accounting for our standard deviation in speed of 170 nm/s, would change the time fraction to about 67 % with an increase in the diffusion coefficient of about 10 %. We expect to slightly underestimate the speed because the SCI algorithm misses short diffusive segments. In this case, ϕ-values might be higher and the diffusion coefficient lower. Because our parameters fall into the range of effective speeds, for which Eq. 13 flattens out, we do not expect a large difference in the true diffusion coefficient of the motor.

SUPPLEMENTARY MATERIAL

One movie and eight figures are available at http://www.biophysj.org/biophysj/supplemental/XXX

AUTHOR CONTRIBUTIONS

E.S., E.L., S.M., M.C. designed the research, M.C, M.R. performed *in vitro* experiments, M.B. assisted in force measurements and wrote MATLAB scripts, M.C., E.L., A.H., S.M. performed *in vivo* experiments, B.R. and E.S. derived the MSD equation, M.C., M.R., M.B., E.L., S.M., and E.S. analysed the data, and M.C., S.M. and E.S. wrote the manuscript.

ACKNOWLEDGMENTS

We thank Tobias Jachowski, Naghmeh Azadfar, and Mohammad Kazem Abdosamadi, Katharina Stuhrberg for technical assistance during the project and Suman De for building the TIRF microscope. We thank Pantelis Livanos and Christine Kiefer for comments on the manuscript and Martin Oettel for comments on the MSD equation. M.C. and M.B. acknowledge financial support from the IMPRS from Molecules to Organisms, Max Planck for Developmental Biology, Tübingen and the Rosa Luxemburg Foundation, respectively. This work was supported by the Deutsche Forchungsgemeinschaft (DFG) in terms of the Collaborative Research Center 1101 project A04 from S.M. and E.S. and the University of Tübingen.

REFERENCES

1. Smertenko, A., B. Piette, and P. Hussey, 2011. The Origin of Phragmoplast Asymmetry. *Curr. Biol.* 21:1924–1930.
2. Smertenko, A., F. Assaad, F. Baluška, M. Bezanilla, H. Buschmann, G. Drakakaki, M.-T. Hauser, M. Janson, Y. Mineyuki, I. Moore, S. Müller, T. Murata, M. S. Otegui, E. Panteris, C. Rasmussen, A.-C. Schmit, J. Šamaj, L. Samuels, L. A. Staehelin, D. Van Damme, G. Wasteneys, and V. Žárský, 2017. Plant Cytokinesis: Terminology for Structures and Processes. *Trends Cell Biol.* 27:885–894.
3. Buschmann, H., and S. Zachgo, 2016. The Evolution of Cell Division: From Streptophyte Algae to Land Plants. *Trends Plant Sci.* 21:872–883.
4. Gunning, B. E. S., and S. M. Wick, 1985. Preprophase Bands, Phragmoplasts, and Spatial Control of Cytokinesis. *J. Cell Sci.* 157–179.
5. Walker, K. L., S. Müller, D. Moss, D. W. Ehrhardt, and L. G. Smith, 2007. Arabidopsis TANGLED identifies the division plane throughout mitosis and cytokinesis. *Curr. Biol.* 17:1827–36.
6. Rasmussen, C. G., B. Sun, and L. G. Smith, 2011. Tangled localization

at the cortical division site of plant cells occurs by several mechanisms. *J. Cell. Sci.* 124:270–9.

7. Lipka, E., A. Gadeyne, D. Stöckle, S. Zimmermann, G. De Jaeger, D. W. Ehrhardt, V. Kirik, D. Van Damme, and S. Müller, 2014. The Phragmoplast-Orienting Kinesin-12 Class Proteins Translate the Positional Information of the Preprophase Band to Establish the Cortical Division Zone in Arabidopsis thaliana. *Plant Cell* 26:2617–2632.
8. Xu, X. M., Q. Zhao, T. Rodrigo-Peiris, J. Brkljacic, C. S. He, S. Müller, and I. Meier, 2008. RanGAP1 is a continuous marker of the Arabidopsis cell division plane. *Proc. Natl. Acad. Sci. U S A* 105:18637–42.
9. Müller, S., S. Han, and L. G. Smith, 2006. Two kinesins are involved in the spatial control of cytokinesis in Arabidopsis thaliana. *Curr. Biol.* 16:888–94.
10. Ramaiya, A., B. Roy, M. Bugiel, and E. Schäffer, 2017. Kinesin rotates unidirectionally and generates torque while walking on microtubules. *Proc. Natl. Acad. Sci. U.S.A.* 114:10894–10899.
11. Hancock, W. O., and J. Howard, 1998. Processivity of the motor protein kinesin requires two heads. *J. Cell Biol.* 140:1395–405.
12. Helenius, J., G. Brouhard, Y. Kalaidzidis, S. Diez, and J. Howard, 2006. The depolymerizing kinesin MCAK uses lattice diffusion to rapidly target microtubule ends. *Nature* 441:115–119.
13. Lu, H., M. Y. Ali, C. S. Bookwalter, D. M. Warshaw, and K. M. Trybus, 2009. Diffusive Movement of Processive Kinesin-1 on Microtubules. *Traffic* 10:1429–1438.
14. Furuta, K., and Y. Y. Toyoshima, 2008. Minus-End-Directed Motor Ncd Exhibits Processive Movement that Is Enhanced by Microtubule Bundling In Vitro. *Curr. Biol.* 18:152–157.
15. Fink, G., L. Hajdo, K. J. Skowronek, C. Reuther, A. A. Kasprzak, and S. Diez, 2009. The mitotic kinesin-14 Ncd drives directional microtubule–microtubule sliding. *Nat. Cell Biol.* 11:717.
16. Kim, Y., J. E. Heuser, C. M. Waterman, and D. W. Cleveland, 2008. CENP-E combines a slow, processive motor and a flexible coiled coil to produce an essential motile kinetochore tether. *J. Cell Biol.* 181:411–419.
17. Kwok, B. H., L. C. Kapitein, J. H. Kim, E. J. G. Peterman, C. F. Schmidt, and T. M. Kapoor, 2006. Allosteric inhibition of kinesin-5 modulates its processive directional motility. *Nat. Chem. Biol.* 2:480–485.
18. Shin, Y., Y. Du, S. E. Collier, M. D. Ohi, M. J. Lang, and R. Ohi, 2015. Biased Brownian motion as a mechanism to facilitate nanometer-scale exploration of the microtubule plus end by a kinesin-8. *Proce. Natl. Acad. Sci. U.S.A.* 112:E3826–E3835.
19. Drechsler, H., T. McHugh, M. R. Singleton, N. J. Carter, and A. D. McAinsh, 2014. The Kinesin-12 Kif15 is a processive track-switching tetramer. *eLife* 3:e01724.
20. Bormuth, V., V. Varga, J. Howard, and E. Schäffer, 2009. Protein Friction Limits Diffusive and Directed Movements of Kinesin Motors on Microtubules. *Science* 325:870–873.
21. Sturgill, E., D. Das, Y. Takizawa, Y. Shin, S. Collier, M. Ohi, W. Hwang, M. Lang, and R. Ohi, 2014. Kinesin-12 Kif15 Targets Kinetochore Fibers through an Intrinsic Two-Step Mechanism. *Curr. Biol.* 24:2307–2313.
22. Drechsler, H., and A. D. McAinsh, 2016. Kinesin-12 motors cooperate to suppress microtubule catastrophes and drive the formation of parallel microtubule bundles. *Proc. Natl. Acad. Sci. U.S.A.* 113:E1635–E1644.
23. Mann, B. J., S. K. Balchand, and P. Wadsworth, 2017. Regulation of Kif15 localization and motility by the C-terminus of TPX2 and microtubule dynamics. *Mol. Biol. Cell* 28:65–75.
24. Richardson, D. N., M. P. Simmons, and A. S. Reddy, 2006. Comprehensive comparative analysis of kinesins in photosynthetic eukaryotes. *BMC Genomics* 7:18.
25. Hunter, A. W., M. Caplow, D. L. Coy, W. O. Hancock, S. Diez, L. Wordeman, and J. Howard, 2003. The kinesin-related protein MCAK is a microtubule depolymerase that forms an ATP-hydrolyzing complex at microtubule ends. *Mol. cell* 11:445–457.
26. Bugiel, M., E. Böhl, and E. Schäffer, 2015. The Kinesin-8 Kip3 Switches Protofilaments in a Sideward Random Walk Asymmetrically Biased by Force. *Biophy. J.* 108:2019–2027.
27. Schäffer, E., S. F. Nørrelykke, and J. Howard, 2007. Surface forces and drag coefficients of microspheres near a plane surface measured with optical tweezers. *Langmuir* 23:3654–3665.
28. Schellhaus, A. K., D. Moreno-Andrés, M. Chugh, H. Yokoyama, A. Moschopoulou, S. De, F. Bono, K. Hipp, E. Schäffer, and W. Antonin, 2017. Developmentally Regulated GTP binding protein 1 (DRG1) controls microtubule dynamics. *Sci. Rep.* 7:9996.
29. Bugiel, M., H. Fantana, V. Bormuth, A. Trushko, F. Schiemann, J. Howard, E. Schäffer, and A. Jannasch, 2015. Versatile microsphere attachment of GFP-labeled motors and other tagged proteins with preserved functionality. *J. Biol. Methods* 2.4.
30. Mahamdeh, M., and E. Schäffer, 2009. Optical tweezers with millikelvin precision of temperature-controlled objectives and base-pair resolution. *Opt. Express* 17:17190–17199.
31. Mahamdeh, M., C. P. Campos, and E. Schäffer, 2011. Under-filling trapping objectives optimizes the use of the available laser power in optical tweezers. *Opt. Express* 19:11759–11768.
32. Tolić-Nørrelykke, S. F., E. Schäffer, J. Howard, F. S. Pavone, F. Jülicher, and H. Flyvbjerg, 2006. Calibration of optical tweezers with positional detection in the back focal plane. *Rev. Sci. Instrum.* 77:103101.
33. Ruhnow, F., D. Zwicker, and S. Diez, 2011. Tracking single particles and elongated filaments with nanometer precision. *Biophys. J.* 100:2820–2828.
34. Bouzigues, C., and M. Dahan, 2007. Transient directed motions of GABA A receptors in growth cones detected by a speed correlation index. *Biophys. J.* 92:654–660.
35. Grefen, C., N. Donald, K. Hashimoto, J. Kudla, K. Schumacher, and M. R. Blatt, 2010. A ubiquitin-10 promoter-based vector set for fluorescent protein tagging facilitates temporal stability and native protein distribution in transient and stable expression studies. *Plant J.* 64:355–365.
36. Clough, S. J., and A. F. Bent, 1998. Floral dip: a simplified method forAgrobacterium-mediated transformation of Arabidopsis thaliana. *Plant J.* 16:735–743.
37. Stock, M. F., J. Chu, and D. D. Hackney, 2003. The kinesin family member BimC contains a second microtubule binding region attached to the N terminus of the motor domain. *J. Biol. Chem.* 278:52315–52322.
38. Moffitt, J. R., Y. R. Chemla, and C. Bustamante, 2010. Chapter Ten-Methods in Statistical Kinetics. *Methods Enzymol.* 475:221–257.
39. Qian, H., M. P. Sheetz, and E. L. Elson, 1991. Single particle tracking. Analysis of diffusion and flow in two-dimensional systems. *Biophys. J.* 60:910–921.
40. Saxton, M. J., and K. Jacobson, 1997. SINGLE-PARTICLE TRACKING:Applications to Membrane Dynamics. *Annu. Rev. Biophys. Biomol. Struct.* 26:373–399.
41. Michalet, X., 2010. Mean square displacement analysis of single-particle trajectories with localization error: Brownian motion in an isotropic medium. *Phys. Rev. E.* 82:041914.
42. Bugiel, M., A. Jannasch, and E. Schäffer, 2017. Implementation and Tuning of an Optical Tweezers Force-Clamp Feedback System. *In* A. Gennerich, editor, Optical Tweezers: Methods and Protocols, Springer Press, New York, NY, chapter 5, 109–136.
43. Jannasch, A., V. Bormuth, M. Storch, J. Howard, and E. Schäffer, 2013. Kinesin-8 Is a Low-Force Motor Protein with a Weakly Bound Slip State. *Biophys. J.* 104:2456–2464.
44. Shaw, S. L., R. Kamyar, and D. W. Ehrhardt, 2003. Sustained microtubule treadmilling in Arabidopsis cortical arrays. *Science* 300:1715–8.
45. Murata, T., T. Sano, M. Sasabe, S. Nonaka, T. Higashiyama, S. Hasezawa, Y. Machida, and M. Hasebe, 2013. Mechanism of microtubule array expansion in the cytokinetic phragmoplast. *Nat. Commun.* 4.
46. Dhonukshe, P., J. Mathur, M. Hülskamp, and T. W. J. Gadella, 2005.

Microtubule plus-ends reveal essential links between intracellular polarization and localized modulation of endocytosis during division-plane establishment in plant cells. *BMC Biol.* 3:11.

47. Wu, S.-Z., and M. Bezanilla, 2014. Myosin VIII associates with microtubule ends and together with actin plays a role in guiding plant cell division. *eLife* 3:e03498.
48. Gudimchuk, N., B. Vitre, Y. Kim, A. Kiyatkin, D. W. Cleveland, F. I. Ataullakhanov, and E. L. Grishchuk, 2013. Kinetochore kinesin CENP-E is a processive bi-directional tracker of dynamic microtubule tips. *Nat. Cell Biol.* 15:1079.
49. Hill, T. L., 1985. Theoretical problems related to the attachment of microtubules to kinetochores. *Proc. Natl. Acad. Sci. U.S.A.* 82:4404–4408.
50. Powers, A. F., A. D. Franck, D. R. Gestaut, J. Cooper, B. Gracyzk, R. R. Wei, L. Wordeman, T. N. Davis, and C. L. Asbury, 2009. The Ndc80 kinetochore complex forms load-bearing attachments to dynamic microtubule tips via biased diffusion. *Cell* 136:865–875.
51. Sarangapani, K. K., and C. L. Asbury, 2014. Catch and release: how do kinetochores hook the right microtubules during mitosis? *Trends Genet.* 30:150–159.
52. Ganguly, A., L. DeMott, C. Zhu, D. D. McClosky, C. T. Anderson, and R. Dixit, 2018. Importin-β; Directly Regulates the Motor Activity and Turnover of a Kinesin-4. *Dev. Cell* 44:642–651.
53. Stöckle, D., A. Herrmann, E. Lipka, T. Lauster, R. Gavidia, S. Zimmermann, and S. Müller, 2016. Putative RopGAPs impact division plane selection and interact with kinesin-12 POK1. *Nat. Plants* 2:16120.
54. Buschmann, H., J. Dols, S. Kopischke, E. J. Peña, M. A. Andrade-Navarro, M. Heinlein, D. B. Szymanski, S. Zachgo, J. H. Doonan, and C. W. Lloyd, 2015. Arabidopsis KCBP interacts with AIR9 but stays in the cortical division zone throughout mitosis via its MyTH4-FERM domain. *J. Cell Sci.* 128:2033–2046.
55. Yamada, M., Y. Tanaka-Takiguchi, M. Hayashi, M. Nishina, and G. Goshima, 2017. Multiple kinesin-14 family members drive microtubule minus end–directed transport in plant cells. *J. Cell. Biol.* 216:1705–1714.
56. Li, H., B. Sun, M. Sasabe, X. Deng, Y. Machida, H. Lin, Y. Julie Lee, and B. Liu, 2017. Arabidopsis MAP65-4 plays a role in phragmoplast microtubule organization and marks the cortical cell division site. *New Phytol.* 215:187–201.
57. Tolić-Nørrelykke, I. M., 2008. Push-me-pull-you: how microtubules organize the cell interior. *Eur. Biophys. J.* 37:1271–1278.
58. Howard, J., and C. Garzon-Coral, 2017. Physical Limits on the Precision of Mitotic Spindle Positioning by Microtubule Pushing forces. *BioEssays* 39:1700122–n/a.

Biophysical *Journal*
Supporting Material

Phragmoplast Orienting Kinesin 2 is a weak motor switching between processive and diffusive modes

Mayank Chugh[1], Maja Reißner[1], Michael Bugiel[1], Elisabeth Lipka[2], Arvid Herrmann[2], Basudev Roy[1,3], Sabine Müller[2], and Erik Schäffer[1,*]

[1]Cellular Nanoscience, Center for Plant Molecular Biology (ZMBP), University of Tübingen, Auf der Morgenstelle 32, 72076 Tübingen, Germany
[2]Developmental Genetics, Center for Plant Molecular Biology (ZMBP), University of Tübingen, Auf der Morgenstelle 32, 72076 Tübingen, Germany
[3]Current address: Department of Physics, Indian Institute of Technology, Madras 600036, India
[*]Correspondence: erik.schaeffer@uni-tuebingen.de

CONTENTS

LIST OF FIGURES

S1 SUPPLEMENTARY VIDEOS

VIDEO S1 Motility of single $POK2_{1-589}$ on microtubules. Image sequence of single $POK2_{1-589}$ (green) interacting with a microtubule (red) corresponding to the third panel of Fig. 1c. Still images are displayed in Fig. 1e. The video is 11 μm wide and 17× real time.

S2 SUPPLEMENTARY FIGURES

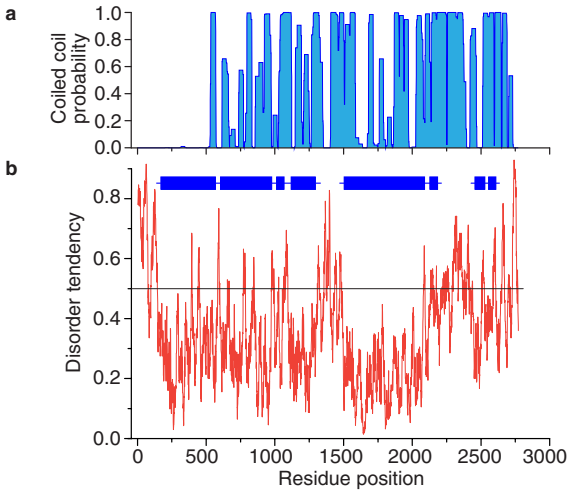

FIGURE S1 Protein domains of full-length POK2. **(a)** The coiled-coils prediction plot based on PCOILS (toolkit.tuebingen.mpg.de/#/tools/pcoils). Window size was 28. The predictions are consistent with MARCOILS (toolkit.tuebingen.mpg.de/#/tools/marcoil). **(b)** Disorder prediction plot based on IUPRED (iupred.enzim.hu). The blue bars indicate predicted globular/structured regions, while the red line represents disorder tendency estimated from pairwise amino acid energy content. The black line indicates the threshold.

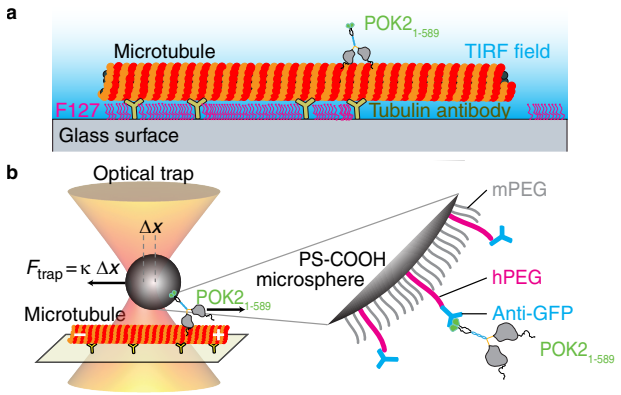

FIGURE S2 Schematic representation of *in vitro* assays. **(a)** Experimental setup for motility assays conducted using TIRF microscopy. $POK2_{1-589}$ specifically interacts with a microtubule bound via antibodies to a hydrophobic glass surface. **(b)** Illustration on an optical tweezers, $POK2_{1-589}$-microsphere coupling, and force measurement assays. In the presence of ATP, $POK2_{1-589}$ motors pull the microspheres out of the optical trap. The force is proportional to the displacement $F = \kappa\Delta x$, where κ is the trap stiffness and Δx the microsphere displacement from the stationary trap center. Pluoronic F127 is used in both assays to prevent unspecific interactions. GFP antibodies are covalently coupled via heterofunctional polyethylene glycol (hPEG), to carboxylated polystyrene microspheres (PS-COOH). Monofunctional PEG (mPEG) molecules prevent unspecific interactions.

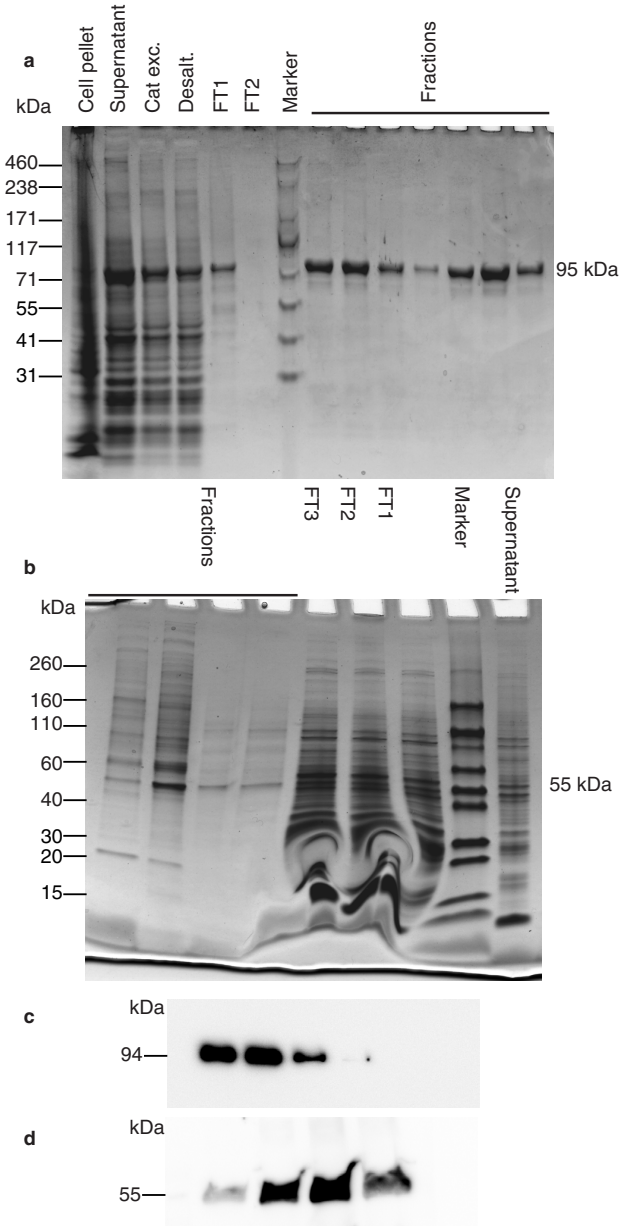

FIGURE S3 Quality control of $POK2_{1-589}$ and $POK2_{183-589}$ post-purification. **(a-b)** Coomassie-stained 4–20% Tris-Glycine SDS-PAGE gel showing purified protein fractions (95 kDa and 55 kDa) for $POK2_{1-589}$ and $POK2_{183-589}$ in **(a)** and **(b)**, respectively. Fractions denote collected protein eluates. (Cat exc.: cation exchange eluate, Desalt.: desalting eluate, FT: flow through). **(c-d)** Western blots against anti-GFP for the eluted proteins fractions of $POK2_{1-589}$ and $POK2_{183-589}$ in **(c)** and **(d)**, respectively.

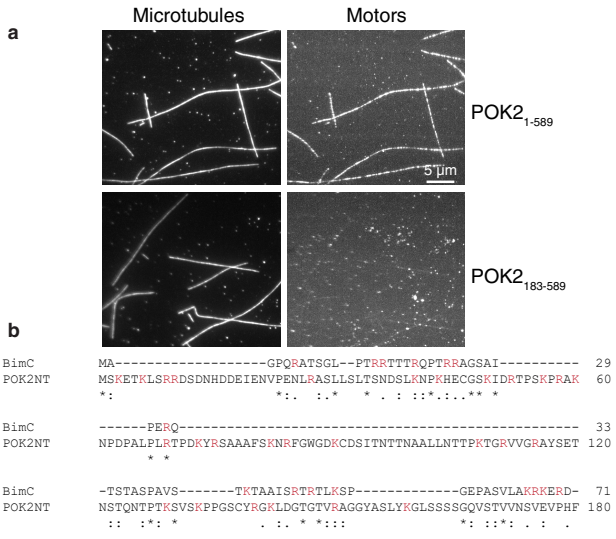

FIGURE S4 Reduced affinity of the POK2$_{183-589}$ towards the microtubule lattice. **(a)** Maximum projections representing the co-localization of motors onto the microtubule lattice in 1mM AMP-PNP. Images were acquired using TIRF microscopy under the same conditions and contrast. Even though the POK2$_{183-589}$ concentration was about twice that of POK2$_{1-589}$ based on the western blot and NanoDrop quantification, much less POK2$_{183-589}$ bound to the microtubules during the same amount of time. **(b)** Multiple sequence alignment (MSA) of the POK2 N-terminal extension (Nte) with BimC. The MSA was performed using Clustal Omega with default parameters (https://toolkit.tuebingen.mpg.de/#/tools/clustalo). Asterisks signify conserved residues, colons represent conservation among amino acids exhibiting strongly similar properties, and periods mark conservation among amino acids exhibiting weakly similar properties. Positively charged residues that may interact with the negatively charged tubulin e-hooks are indicated in red.

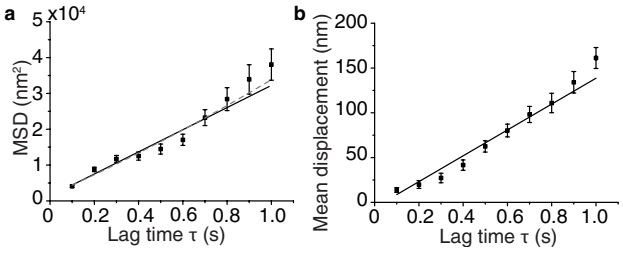

FIGURE S5 Diffusive segments exhibit bias. **(a)** Mean-squared displacement (MSD) and **(b)** mean displacement versus time lag τ for diffusive segments (mean ± SEM). A linear fit (black line) in **(a)** resulted in a diffusion coefficient of 0.015 ± 0.001 μm^2/s. A parabolic fit (grey dashed line) did not result in a significant speed. A linear fit (black line) in **(b)** resulted in a directed bias of 140 ± 10 nm/s. All fits were weighted by the error bars.

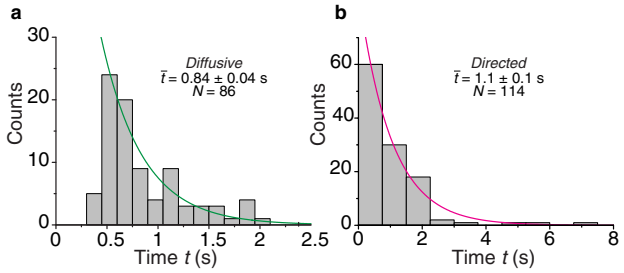

FIGURE S6 POK2$_{1-589}$–microtubule-interaction times of diffusive and directed segments. Time distributions for **(a)** diffusive and **(b)** directed segments (mean ± SEM and number of molecules are indicated, single exponentials are plotted as a guide to the eye).

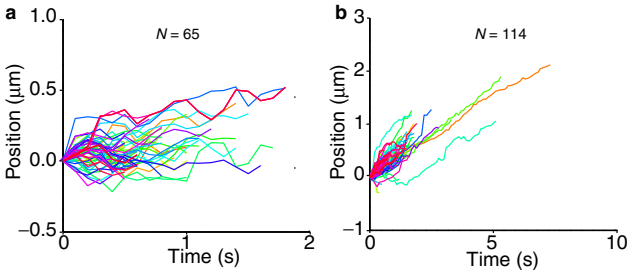

FIGURE S7 POK2$_{1-589}$ diffusive and directed segment trajectories. Trajectories of **(a)** all diffusive and **(b)** all directed segments from tracked single POK2$_{1-589}$ molecules. All segments are offset such that they start at zero.

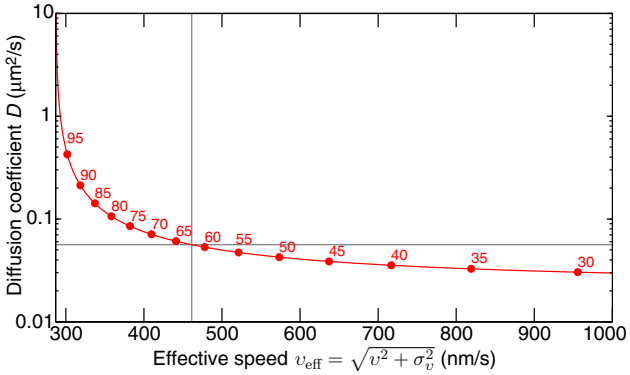

FIGURE S8 Relation between diffusion coefficient and effective speed. Dependence of the diffusion coefficient on the effective speed according to Eq. 12 (red line) for a set of fit parameters resulting from a parabolic fit to the MSD relation. Specific directed-mode time fractions ϕ (Eq. 13) are indicated by the red circles and numbers. Grey lines indicate the values for POK2$_{1-589}$.

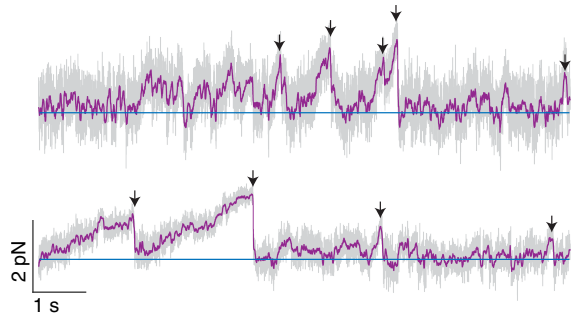

FIGURE S9 Multiple motors can exert higher force. Force traces of microspheres powered by multiple $POK2_{1-589}$ as a function of time. A 10× higher incubation concentration of $POK2_{1-589}$ with microspheres was used compared to the single-molecule assays resulting in the motility of 5 out of 6 microspheres. The blue line marks zero force. Arrow heads point to the maximum force prior to detachment events.

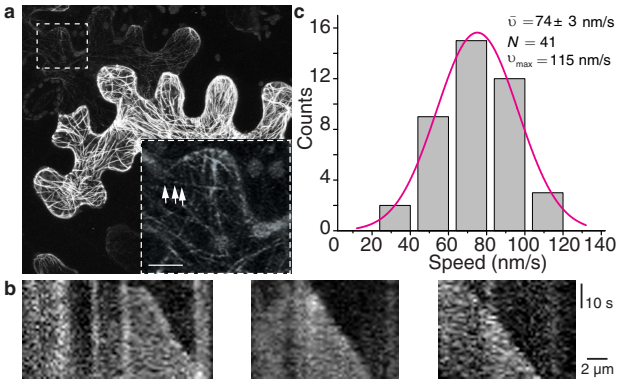

FIGURE S10 *In vivo* speeds of transiently expressed $POK2_{1-589}$ **(a)** Tobacco leaf epidermis show varying levels of 35S:GFP-$POK2_{1-589}$ expression. Cells with low and discontinuous GFP signal (boxed) were used for further *in vivo* analysis. Scale bar: 25 μm. Enlargement of the boxed region confirms low abundance of GFP-$POK2_{1-589}$. Scale bar: 8 μm. Arrow heads point towards the accumulations of GFP-$POK2_{1-589}$ along the linear trajectories. **(b)** Examples of kymographs. **(c)** Frequency distribution of *in vivo* speeds of GFP-$POK2_{1-589}$ (N = 41, combined from five cells from three different plants and two independent transformations).

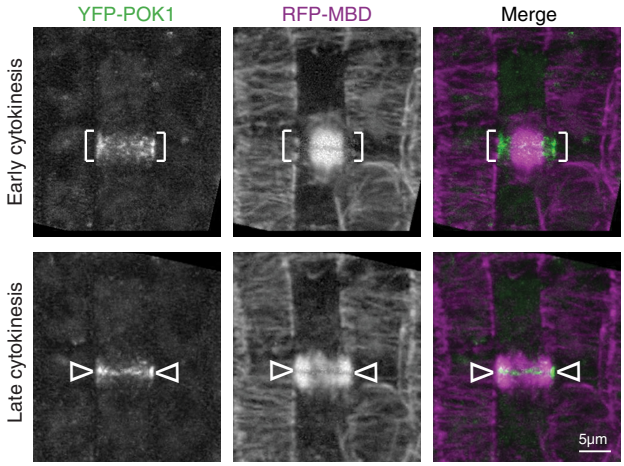

FIGURE S11 Narrowing of cortical division site. *Arabidopsis* root meristem expressing YFP-POK1 and RFP-MBD indicating narrowing of the division site from early cytokinesis to the presumably cell plate fusion site during late cytokinesis. For experimental details see reference (7) of the main text.

9.5 Lipka et al. 2015

Mechanisms of plant cell division.

Elisabeth Lipka, **Arvid Herrmann** and Sabine Müller (2015).

WIREs Dev Bio 4, 391-305.

WILEY
Interdisciplinary Reviews
DEVELOPMENTAL BIOLOGY

In partnership with Society for Developmental Biology

Article type: Advanced Review

Article title: Mechanisms of Plant Cell Division

Authors:

Full name and affiliation; email address if corresponding author; any conflicts of interest

First author Elisabeth Lipka, ZMBP – University of Tuebingen
Second author Arvid Herrmann, ZMBP – University of Tuebingen
Third author Sabine Mueller*, ZMBP – University of Tuebingen, sabine.mueller@zmbp.uni-tuebingen.de

The authors declare no conflict of interests.

Abstract

Plant cells are confined by a network of cellulosic walls which imposes rigid control over the selection of division plane orientations, crucial for morphogenesis and genetically regulated. While in animal cells and yeast, the actin cytoskeleton is instrumental in the execution of cytokinesis, in plant cells the microtubule cytoskeleton is taking the lead in spatially controlling and executing cytokinesis by the formation of two unique, plant specific arrays, the preprophase band and the phragmoplast. The formation of microtubule arrays in plant cells is contingent on acentrosomal microtubule nucleation. At the onset of mitosis the preprophase band defines the plane of cell division where the partitioning cell wall is later constructed by the cytokinetic phragmoplast, imposing a spatio-temporal relationship between the two processes. Current research progress in the field of plant cell division focuses on identifying and tying the links between early and late events in spatial control of cytokinesis and how microtubule array formation is regulated in plant cells.

Introduction

Cell division is a fundamentally important process, allocating cellular contents to two daughter cells. In eukaryotes, this task is in large accomplished by the highly dynamic cytoskeleton. While many cellular structures and molecular processes are conserved between eukaryotes, plant cells exhibit unique features that might be attributed to their mostly sedentary life style. Moreover, most plant cells are immobilized within the network of rigid polymeric cell walls. The microtubule cytoskeleton (Figure 1) is the main driver of cell division forming the chromosome segregating spindle which is the common mitotic feature shared by eukaryotes. However, plant cells accomplish this task by a self-organizing acentrosomal mechanism. In addition, two specialized cytoskeletal structures are instrumental in the selection and maintenance of the division plane and in the formation of the cell plate. The preprophase band (PPB) is a remarkable belt-like cortical formation of microtubules (Figure 1) and actin filaments assembling at the G2 to M transition, outlining the periphery of the future division plane. However, not all cell types (i.e. endosperm, meiocytes) utilize the PPB to determine the division site, proposing that alternative strategies exist. The other plant specific cytoskeletal array is the phragmoplast (Figure 1) that physical partitions daughter cell contents by synthesis of the cell plate. Motor and non-motor microtubule associated proteins (MAPs) reorganize microtubules by means of sliding, cross linking or severing into the characteristic functional arrays in accordance to cell cycle progression. Thus vigorous coordination of cellular signalling, cytoskeletal organization and cell cycle regulators is required for cell division. This review outlines the basic principles of plant cell division with a particular focus on recent advances on plant specific molecular mechanisms in the field of plant cell division.

DIVISION PLANE SELECTION AND ESTABLISHMENT

Regulation of division plane selection: who is to decide?

[Due to the fixed position of plant cells the site of cell division is of particular significance for plant morphology. While symmetric divisions are proliferative, producing daughter cells of identical fate and equal size, formative, asymmetric divisions give rise to unequally sized daughter cells that differ in cell fate thereby steering morphogenesis. Plant developmental programs such as embryo and root development as well as lateral root and stomata formation rely on asymmetric divisions, but the knowledge about their triggers is fragmentary.

Already in the 19th century botanists formulated rules of cell division placements succinctly summarized as the “shortest wall” rule, which implicate cell geometry as the determining factor (Rasmussen et al., 2013b). Recently the simple rule was extended by the stochastic component of several competing minimum area division planes, which best reflect the observed fluctuations in the 2D analysis of division site placement (Besson and Dumais, 2011). Thus, division planes approximating the “shortest wall” appear to be the geometry dependent default mechanism, likely employing the cytoskeleton as a tension sensor/generator (Flanders et al., 1990, Lloyd, 1991).

Although the geometric rule suffices to explain symmetric divisions, it fails to explain how formative divisions are controlled. However, a number of “polarizing events”, such as hormones signaling, nuclear

migration and polar protein distribution are implicated in division plane switching (Dong et al., 2009, Humphries et al., 2011, Facette and Smith, 2012, Rasmussen et al., 2011a, Wolters et al., 2011).

Recently, a 4D map of the invariant division pattern of early *Arabidopsis* embryos was constructed using high-resolution imaging and computational image analysis (Yoshida et al., 2014). (Figure 2A) (Yoshida et al., 2014). Compellingly, the 3D analysis revealed asymmetric division planes that were not detectable in 2D analysis. *Arabidopsis* auxin response mutants abandon certain asymmetric divisions in early embryo development, but conduct symmetric divisions instead (Mayer et al., 1991), suggesting that auxin triggers division plane switching in the early embryo. Suppression of transcriptional auxin response by a transgenic approach indeed provoked symmetric, minimal area divisions as seen in auxin response mutant embryos (Figure 2A) (Yoshida et al., 2014) and demonstrated that in embryo development, geometry based symmetric divisions are the default mechanism that is overridden by local auxin signaling (Figure 2A). Finally, a minimal set of empirically acquired geometric and volumetric rules allowed 3D computer simulations of the growing wild type embryo predicting realistic division planes and cell volumes (Yoshida et al., 2014). Effectors of auxin signaling that directly link it to the asymmetric division outcome still need to be identified.

In this respect, recent progress has been made in regulation of asymmetric division in the stomatal lineage. Symmetry breaking in the self-renewing stomatal stem cell lineage is regulated by the basic helix-loop-helix transcription factor SPEECHLESS (SPCH). *BASL,* which encodes a polarly localized protein, required for asymmetric cell divisions in stomatal meristemoid cells (Dong et al., 2009) is a direct target of SPCH (Lau et al., 2014). Moreover, the gene expression of the PPB localized kinesin ARK3KINUa is also regulated by SPCH. Cell type specific down-regulation of ARK/KINUa by expression of *SPCHpro:amiR-ark3* caused *basl* like phenotype linking SPCH directly to the regulation of asymmetric division in the stomatal lineage (Figure 2B). Future research should clarify how polar BASL and ARK3 interact to direct PPB positioning in asymmetric cell division.

These novel findings on the regulation of division symmetry further support the view that various “polarity cues” override the default, geometry-based division plane selection mechanism. Whether a common theme of asymmetric cell division plane selection will emerge remains to be seen. In this respect the *Arabidopsis aur1aur2* double mutant which displays specific defects in formative divisions in different developmental contexts (Van Damme et al., 2011), might become instrumental. However, the geometry-based mechanism may further be modulated without changes in cell fate. It was reported that mechanical forces generated by growth also direct division plane selection. Mutation in the p60 subunit of the microtubule severing protein KATANIN caused PPB mispositioning and failure to respond to mechanical forces (Uyttewaal et al., 2012), suggesting that KATANIN was required to translate cell geometry information into proper division planes.

Challenges for the future are the identification of the effectors that translate potentially variable positional cues into division planes.

Formation of the Preprophase band

[PPB formation at G2/M phase involves changes in microtubule dynamics and selective microtubule stabilization resulting in the gradual clearing of microtubules in apical and basal cell regions and concomitant formation of the belt-like sub-membranous PPB (Figure 1, Figure 3) (Vos et al., 2004, Dhonukshe and Gadella, 2003). Consistently, a number of microtubule associated proteins (MAPs) and components of microtubules nucleation complexes, including γ-tubulin co-localize with the PPB and aid in its organization and maintenance (reviewed in Rasmussen et al., 2013).

Microtubules structure, nucleation and dynamic behaviour

Dynamic instability is an intrinsic property of the polar microtubule. This behavior can be modulated by microtubule associated proteins (MAPs), which promote microtubule polymerization or depolymerization, regulate rescue and catastrophe rates, stabilize microtubule bundles by cross linking and sever microtubules. Microtubules nucleation *in vivo* occurs from acentrosomal nucleation complexes containing γ-tubulin and conserved GCP proteins forming a template for tube elongation by oriented addition of tubulin hetero-dimers. Additional microtubule assembly factors are GCP3-interacting proteins (GIPs) and NEDD1. All of these components play critical roles in microtubule nucleation and contribute to microtubule array patterning and mutation in either one or multiple of these genes lead to severe developmental defects in plants (Pastuglia et al., 2006, Janski et al., 2012). Microtubule nucleation complexes are dispersed throughout the cell cortex and associate with existing microtubules performing angle-dependent nucleation In addition, microtubule nucleation complexes colocalize with chromosomes. Little is known about the spatio-temporal specificity of microtubule –MAP interactions. Post-translational modifications are certainly involved in the regulation of MAP activity during the cell cycle. Post-translational tubulin modification such as reversible detyrosination, acetylation are suggested to provide a road map for MAPs and certain tubulin modification are predominantly associated with stable microtubules or during certain cell cycle stages. These layers of regulation add to the complexity of microtubule array organization in space and time.

These MAPs are likely targets of a protein phosphatase complex that is essential for PPB formation and consequently spatially controls cytokinesis (Figure 3, Figure 4). The heterotrimeric protein phosphatase 2 A (PP2A) consists of the regulatory B subunit FASS/TONNEAU (TON) 2 (Camilleri et al., 2002a) and variable catalytic C and scaffolding A subunits (Spinner et al., 2013a). Mutants in PP2A subunits lack PPBs and display random division planes (Torres-Ruiz and Jurgens, 1994, Yoshida et al., 2014, Traas et al., 1995a, Spinner et al., 2013a) similar to mutants lacking a pair of centrin homologous proteins, TON1a and TON1b. FASS interacts directly with TON1 and with variable TON1 RECRUITING MOTIF (TRM) proteins of a large plant specific family that targets the TTP complex (for TON1/TRM/PP2A, Figure 4 B) to the cytoskeleton (Drevensek et al., 2012a, Spinner et al., 2013a). Mutation in several MAPs including the polymerization promoting MAP MOR1 (Kawamura and Wasteneys, 2008) display mild PPB and cell wall positioning defects (Kawamura et al., 2006a). Furthermore, genetic evidence

identified MOR1 and TON1 as a potential target of FASS dependent phospho-regulation (Kirik et al., 2012a). Apparently, in cell cycle dependent manner, the phophatase complex is commisioned to spatially restrict common MAP activities allowing for the formation of the PPB.

Mutation in the CLIP170-associated protein CLASP1 causes improper placement of PPBs and subtle delays in development (Kirik et al., 2007a, Ambrose et al., 2007a). CLASP prevents edge-induced microtubule catastrophe at sharp cell edges (Ambrose et al., 2011) thereby maintaining the interphase cortical MT array. The putative transmembrane protein SABRE might direct CLASP activity towards the PPB region (Pietra et al., 2013b). Functional GFP-CLASP1 co-localized with misoriented PPB microtubules in *sab-5* mutants, suggesting SAB acts upstream of CLASP. In meristematic interphase cells SAB localizes to the apical and basal plasma membrane but flanks the PPB in prophase (Figure 4). This is an intriguing finding in support of the notion that not only the cortical microtubule cytoskeleton but also the membranous region underlying the PPB becomes differentially modified in order to establish the division plane. Whether SAB localization might actually be key to restrict CLASP to the PPB zone requires further investigation.

SPINDLE FORMATION

The establishment of spindle bipolarity and spindle function as the chromosome segregating entity requires the orchestrated force balancing between antagonistically acting cytoskeletal elements. A host of cytoskeletal proteins including motor and non-motor proteins aiding in maintaining antiparallel microtubule overlap in the spindle midzone have been identified that exhibit conserved functions across biological kingdoms. Furthermore, as in all microtubule arrays microtubule nucleation by γ-tubulin ring complexes (TuRC) contribute to spindle assembly. An exhaustive review on plant spindle formation is found in Masoud et al., 2013.

In plant cells bipolar spindles are formed by the spindle self-organizing pathway (Zhang and Dawe, 2011) also known to function in animal cells that lack centrosomes due to cell differentiation or as a consequence of genetic or laser inflicted disruptions. Here we focus on the involvement of the PPB in pro-spindle formation.

In late prophase, prospindle formation commences from the reorganization of perinuclear microtubules (Figure 1, Figure 5 A) (Masoud et al., 2013b). Mutants without PPBs or cells with multiple PPBs exhibit delayed bipolar prospindle formation or fail to form the prospindle (Chan et al., 2005, Camilleri et al., 2002a), suggesting a functional link between PPB and bipolar spindle formation. (Ambrose and Cyr, 2008). Indeed bridging microtubules are involved in the reorganization of the randomly oriented perinuclear microtubules into a bipolar prospindle oriented perpendicular to the PPB plane (Ambrose and Cyr, 2008), thereby communicating positional information from the PPB to the prospindl (Figure 5A).

Kinesin-14 proteins are involved in early spindle assembly. Mutation in *Arabidopsis thaliana* kinesin1 (ATK) or ATK5 impairs pro-spindle formation resulting in unfocused but fully functional spindles (Ambrose and Cyr, 2007, Marcus et al., 2003). ATK5 localization is mediated by its N-terminal tail

domain that tracks microtubule plus ends, and a central motor domain, which enabling microtubule minus end directed motility in *in vitro* gliding assay (Ambrose et al., 2005), consistent with a role in antiparallel microtubule sliding (Figure 5B) Sliding activity is well suited to account for the alignment of perinuclear microtubules into a prospindle.

Nucleation of prospindle microtubules seems to be mediated by the conserved spindle assembly factor targeting protein for XKLP2 (TPX2) (Vos et al., 2008) (Figure 5A). In animal cells, TPX2 modulates Aurora kinase activity and regulates binding of kinesin-5 and recruitment of kinesin-14 to microtubules (Masoud et al., 2013b). TPX2 inhibition by antibody injection in prophase cells delayed or arrested cell cycle progression, while later impairment had no effect, demonstrating the specific requirement of TPX2 for plant pro-spindle assembly. Plant TPX2 promotes nucleation of microtubule asters *in vitro* (Vos et al., 2008) and overexpression of TPX2 leads to the assembly of aster-like perinuclear and nuclear microtubules and a marked reduction of Ran and importin β signal in the nucleus, pointing towards Ran dependent regulation of TPX2 dependent microtubule nucleation (Petrovská et al., 2013). Furthermore, plant TPX2 co-immunoprecipitates with Aurora1 Ser/Thr kinase and with γ-tubulin in *Arabidopsis* protein extracts (Petrovská et al., 2012) and RNAi knock down of all three Aurora kinase homologs in Arabidopsis cause pleiotropic developmental defects including cell cycle arrest and ectopic re-initiation of cell division in mature tissues. These reports support a Ran GTPase dependent TPX2 mediated acentrosomal spindle assembly in plants. Whether this also includes interaction with kinesin-14 that are involve in pro-spindle formation will be interesting.

CORTICAL DIVISION SITE MAINTENANCE AND PHRAGMOPLAST GUIDANCE

Despite PPB disassembly at the end of prophase, the positional information of the preprophase band is preserved through mitosis, imposing the establishment of a molecular mechanism or structure, commonly referred to as the cortical division site (CDS) (Pickett-Heaps and Northcote, 1966). However, the identification of proteins or structures, qualifying for such a task remained challenging until genetic tagging and improved imaging systems allowed the fluorescence based detection of low abundance proteins at distinct sub-cellular localization.

Preprophase band, cortical division site and cortical division site

The preprophase band (PPB) roughly delineates the division plane at the cell cortex. The PPB also recruits a number of landmark proteins that remain in this cortical region, then referred to as the cortical division zone (CDZ). Upon cytokinesis the localization of CDZ resident proteins distinctly narrows and defines the cortical division site (CDS), where cell plate attachment takes place.

The highly basic, microtubule associated protein TANGLED (TAN) was initially characterized in maize (Smith et al., 2001). Mutations in *TAN* gave rise to stunted maize plants with narrow leave blades (Smith et al., 1996). In *tan* mitotic leave epidermis cells, phragmoplast and cell plate positions were oblique and

ortholog ATM1 is highly abundant in the phragmoplast midzone and the cell plate in mitosis and along F-actin filaments in protoplasts (Reichelt et al., 1999, Haraguchi et al., 2014). *In vitro*, ATM1 displayed rather sluggish kinetics, which suggests it might act as a tension sensor or generator rather than a transporter (Haraguchi et al., 2014). Taken together these observations suggest that plant myosin VIII might act in a tension sensing mechanism enabling phragmoplast expansion towards the CDS. How this actin-myosin based mechanism operates in the context of a CDZ is an interesting research question. Intriguingly, multiple POK like kinesin-12 homologs are present in moss but their functional significance is not fully characterized (Miki et al., 2014b). Investigation of the potential interplay between POK and Myo8 dependent pathways in moss and *Arabidopsis* should also provide insight into the evolution of phragmoplast guidance in the context of increasing tissue complexity.

PHRAGMOPLAST EXPANSION AND CELL PLATE SYNTHESIS

In telophase, the phragmoplast originates from overlapping non-kinetochore microtubules that are reorganized into a barrel shaped structure containing two antiparallel sets of bundled microtubules. Microtubule plus ends extending into the opposite array, creating a region of microtubule interdigitation that is accurately positioned at the division plane (Hiwatashi et al., 2008, Ho et al., 2011b) and likely fulfils a scaffolding function (Figure 7). Golgi-derived vesicles containing cell plate components arrive in the division plane along phragmoplast microtubules and build the laterally expanding cell plate by vesicle fusion. Although several kinesins were identified at the phragmoplast direct evidence for kinesin mediated vesicle trafficking from the Golgi to the division plane is not available. Nevertheless, cell plate synthesis occurs via a succession of characteristic, ultra-structurally discernable stages of cell plate consolidation (Samuels et al., 1995) and involves conserved and plant specific SNARE proteins and other components of the vesicle fusion machinery (Jurgens, 2005, McMichael and Bednarek, 2013). The lateral progression of cell plate synthesis a is coordinated with reiteration of microtubule nucleation and polymerization at the phragmoplast leading edge on the periphery and disassembly of phragmoplast microtubules at the trailing edge in the center, driving its lateral expansion towards the CDS (Figure 7).

Mutants impaired in either vesicle fusion or microtubule-based expansion of the phragmoplast display incomplete cell walls and multi-nucleate cells. Lateral phragmoplast expansion requires the disassembly of microtubules at the trailing edge of the phragmoplast and is necessary for cell plate maturation suggesting that feedback about the state of cell plate construction is sensed by the phragmoplast. Mutation in the kinesin-7 HINKEL (HIK)/NACK1, a key driver of trailing edge disassembly causes persistence of phragmoplast microtubules and incomplete cell plates (Strompen et al., 2002a). HIK controls a mitogen activated protein kinase (MAPK) pathway by binding to the respective MAPKKK and initiates the successive phosphorylation cascade (Sasabe and Machida, 2012). The timely initiation of the MAPK signaling pathway is controlled by transcriptional and post-translational regulation of HIK/NACK1 via cell cycle proteins (Ito, 2000, Ito et al., 1998a, Araki et al., 2004). Cyclin-dependent kinases phosphorylate both, NACK1 and NPK1 before metaphase and prevent their direct binding. Furthermore, expression of a phospho-mimic mutant of HIK/AtNACK1 did not rescue the *atnack1* mutant phenotype (Sasabe et al., 2011a). Thus timely cell cycle dependent phospho-regulation of NACK1 and

the MAPK is crucial for progression through cytokinesis. However, a relevant phosphatase that targets NACK1 and NPK1 has not been identified to date.

MAP65 proteins are the targets of the HIK/NACK1-MAPK signaling pathway and mutations in MAP65 proteins emulate HIK/NACK phenotypes. Loss of MAP65 widened the phragmoplast midzone, and compromised microtubule interdigitation (Muller et al., 2004, Ho et al., 2011b, Kosetsu et al., 2013b). Indeed *Arabidopsis* AtMAP65-3 cross-link antiparallel microtubules *in vitro* (Ho et al., 2011b) via its distinct C-terminal domain (Ho et al., 2012). Kinesin-12A is completely abolished from the phragmoplast midzone, while AtPAKRP2 becomes mis-localized to the entire phragmoplast (Ho et al., 2011b), indicating that MAP65 is required for proper targeting of these kinesins to the phragmoplast midzone. MAP65 microtubule cross-linking activity in cooperation with kinesin motors is a common theme to stabilize antiparallel microtubule overlaps in cell division throughout kingdoms (Walczak and Shaw, 2010).

Arabidopsis expression of a dominant-negative fragment of RUNKEL (RUK) FR5, a putative pseudo-kinase, caused mis-targeting of HIK to the entire phragmoplast and lead to incomplete cell plate formation (Krupnova et al., 2013) reminiscent of *ruk* mutant phenotypes (Krupnova et al., 2009). In *ruk* mutants the phragmoplast midzone increases in width, linking RUK to phragmoplast organization. However, there is no evidence for kinase function, rather expression of kinase-domain mutants RUK K33W and RUK D121A fully rescued embryonic *ruk* phenotypes and partially rescued post-embryonic phenotypes (Krupnova et al., 2009), suggesting that RUK function is not related to phosphorylation. Although the mutant phenotype places RUK in the HIK/MAPK pathway, it is entirely unclear how exactly RUK contributes to the pathway.

While regulation and mechanisms of phragmoplast trailing edge dynamics are under investigation for quite some time, little is known about the leading edge. A recent study in BY-2 cells suggested that γ-tubulin dependent nucleation along existing stable microtubules (Murata et al., 2013a). Nucleation events occurs at 40° angles from the template microtubule and nucleation complexes, visualized by γ-tubulin-GFP showed distal displacement away from the cell plate. GFP-MAP65 associated with both stable microtubule bundles as well as with dynamic microtubules, most likely cross-linking novel microtubule overlaps (Murata et al., 2013a). The authors proposed a model where new microtubules nucleate from existing microtubules at the leading edge subsequently translocation towards the minus end of the extant microtubule and are eventually cross-linked and stabilized. This hypothesis could also explain how the phragmoplast may maintain a constant width.

Conclusion

Recently, a number of reports have started to fill some of the gaps that we face in understanding plant cell division. Regulation of division plane selection is still poorly understood on a molecular level and it is yet too early to deduce whether asymmetric divisions are regulated by common mechanisms that operate in different tissue context or whether tissue specific polarity cues trigger asymmetry. Nevertheless, the available data suggest that once the division plane is defined, the universal molecular

deviated from expected positions based on the PPB orientations, predominantly affecting longitudinal divisions (Cleary and Smith, 1998). These observations implicated TAN in a phragmoplast guidance mechanism. Eventually, localization of TAN-YFP in dividing *Arabidopsis* root cells established TAN as a constituent of the cortical division zone CDZ (Figure 4). TAN-YFP co-localized with the PPB in a microtubule dependent manner and remained at the CDZ, independent of microtubules until completion of cytokinesis (Walker et al., 2007). The expression of different TAN protein domains in tobacco BY2- and *Arabidopsis* cells revealed that two distinct regions in the N-terminal half mediate TANs localization at the CDZ at different stages of cell cycle mitosis. While one region is responsible for TAN recruitment during prophase, recruitment during cytokinesis requires a second region, which also binds the formerly identified interaction partner kinesin-12 PHRAGMOPLAST ORIENTING KINESIN (POK) 1 (Rasmussen et al., 2011b, Muller et al., 2006). Like TAN, POK1 localizes to the PPB and CDZ/CDS. In prophase of *Arabidopsis* root meristem cells and in BY-2 cells, YFP-POK1 showed microtubule dependent and dynamic recruitment to the PPB, as determined in fluorescence recovery after photo-bleaching (FRAP) experiments. However, YFP-POK1 association with the CDZ in metaphase cells was neither dynamic nor microtubule dependent (Lipka et al., 2014), suggesting that POK1 becomes somehow tethered to the membrane in late prophase and likely act as a scaffold for CDS proteins, such as TAN. Indeed, *Arabidopsis* double mutants simultaneously mutated in *POK1* and its closest homolog *POK2* fail to retain TAN-YFP beyond metaphase (Lipka et al., 2014). In *pok1pok2* mutants, PPB and phragmoplast are misaligned due to tilting of the phragmoplast from its initial direction of expansion (Lipka et al., 2014) and consistent with defects in phragmoplast guidance and/or CDZ maintenance.

The protein RanGAP1, a regulatory protein in the Ran GTPase signaling pathway shows TAN-like localization and POK1-dependency at the CDS (Figure 4) (Xu et al., 2008a). However, immunolocalization experiments showed RanGAP1 at the nuclear envelope in interphase and association with kinetochores and the cell plate during mitosis. While induction of RNAi knock down of RanGAP1 and RanGAP2 results in oblique and incomplete cell plate formation (Xu et al., 2008a), double knock out RanGAP1/2 confers gametophyte lethality (Rodrigo-Peiris et al., 2011). These phenotypes might represent at least in part, misregulation of Ran and thus it is difficult to interpret how the loss of RanGAP1 at the CDZ affects cell division specifically. Currently, it is not resolved whether the *pok1pok2* phenotype merely reflects the loss of TAN and RanGAP1 at the CDZ, supporting a scaffolding function for POKs, or whether POKs actively contribute to phragmoplast guidance via interaction with phragmoplast derived microtubules, which would be in tune with molecular properties of kinesin motors.

Intriguingly, TAN, RanGAP1 and POK1, all undergo signal narrowing towards the end of cytokinesis precisely defining the cell plate insertion site (Figure 4), before they vanish upon completion of cytokinesis or shortly after. The mechanism of the narrowing is entirely unclear as well as whether it is functionally significant.

ROLE OF THE ACTIN CYTOSKELETON IN CELL DIVISION

The role of actin remains ambiguous. Mutations in actin or actin associated proteins do not inhibit plant cell division, but the treatment with actin depolymerizing drugs reliably results in misplacement of new

cross walls (Kojo et al., 2013). Although a component of the PPB, F-actin is conspicuously diminished from the CDS between prometaphase and anaphase, forming the actin depleted zone (ADZ), and therefore is regarded as a negative marker of the CDZ. Remarkably the ADZ is flanked by F-actin enrichments, termed actin twin peaks (Panteris, 2008a, Mineyuki and Palevitz, 1990, Sano et al., 2005a), though their visualization remains challenging in many cell types. It is likely that ADZ and CDZ occupy the same membrane region although experimental evidence is not available. The ADZ is first observed in late prophase and its establishment is potentially related to the accumulation of endocytic vesicles in the PPB region (Karahara et al., 2009). Reduction of F-actin in the ADZ might result in a gel-reduced cytoplasmic region that could limit protein dynamics. The cell cycle dependent differential protein dynamics of CDZ resident proteins TAN and POK1 certainly supports this view. Actin depolymerizing drugs might interfere with the establishment of the ADZ, which could then influence CDZ maintenance. Thus, investigation of the spatio-temporal relations between ADZ and CDZ are needed to further assess ADZ function.

The kinesin-14 KCA1 also becomes depleted from the CDZ, similar to the ADZ, but decorates the entire remaining cell cortex of BY-2 cells (Vanstraelen et al., 2006b). The depletion of KCA1 may be prevented by microtubule depolymerizing drugs, leading to cell plate misorientation. The functional significance of KCA1 depletion has not been unraveled, but it is also involved in actin dependent chloroplast movement in Arabidopsis (Suetsugu et al., 2010a), suggesting that KCA1 might interact with both the microtubule and actin cytoskeleton.

Recently an actin-myosin driven mechanism was implicated in phragmoplast guidance in moss. A quintuple knock out mutant of myoVIIIa-e in *Physcomitrella patens* displays mispositioned cell walls in branching protonemata cells (Wu and Bezanilla, 2014b). Expression of a moss myosinVIII motor protein (Myo8A-GFP) was sufficient to partially rescue the quintuple mutant phenotype. In prometaphase, Myo8A begins to accumulate at microtubule plus ends contingent on functional F-actin (Figure 6). In metaphase, additional Myo8A briefly surges at spindle poles but upon anaphase Myo8A-GFP is again restricted to microtubule plus ends in the spindle midzone. Concomitantly, Myo8A-GFP signal gathers in a cortical region (Wu and Bezanilla, 2014b) that is most likely the equivalent of the CDZ, although these cells divide without recognizable PPB formation. The plus end association of Myo8A on dynamic peripheral spindle microtubules that probe the space between spindle and cell cortex might actually serve as a mechanism to deliver Myo8 to the CDZ. During cytokinesis, Myo8A resides on phragmoplast microtubule plus ends of the leading edge and at the CDS. Live cell imaging revealed actin dependent centripetal mobility of microtubules with Myo8A-GFP decorated plus ends, suggesting that movement towards the phragmoplast occurred along F-actin via the Myo8 motors (Figure 6) (Wu and Bezanilla, 2014b). Reportedly, F-actin does bridge the phragmoplast midzone and CDS and actin nucleating formin2 (For2) localizes to the phragmoplast midzone (Wu and Bezanilla, 2014b). Thus Myo8A at peripheral MT plus ends uses actin bridges to trail back peripheral microtubules (Figure 6), in order to preserve phragmoplast integrity. Myo8A is conserved in land plants and Myo8A-GFP in BY-2 cells localized as a ring at the cell cortex in mitosis, as well as the phragmoplast midzone (Wu and Bezanilla, 2014b), showing that Myo8A recognizes a predetermined site, presumably the CDZ in different plant classes, although a conclusive experiment needs to be performed. Also the *Arabidopsis* myosin VIII

machinery is employed to progress through mitosis. Furthermore, the use of evolutionary distant plant models and even different cell types, demonstrates that divers strategies evolved in plant cells to achieve the accurate insertion of the new cell wall. For instance, it is yet to be determined whether actin-myosin and microtubule-kinesin based phragmoplast guidance mechanisms act entirely independently or whether they converge on the same pathway at some point. Further exciting challenges include how the acentrosomal microtubule cytoskeleton is organized into the plant specific mitotic arrays which might also bear relevant mechanistic insight for other biological kingdoms. The latest reports also show that plant cell division research is increasingly benefiting from recent advances in light microscopy and more is to be expected by application of the rapidly evolving plane illumination technology to continuously improve 3D and 4D resolution. Furthermore, computation allows taking a fresh look at longstanding hypothesis and puts them to the test.

References

[1. Rasmussen CG, Wright AJ, Müller S. The role of the cytoskeleton and associated proteins in plant cell division plane determination. *The Plant Journal* 2013,75: 258-269.

2. Besson S, Dumais J. Universal rule for the symmetric division of plant cells. *Proceedings of the National Academy of Sciences* 2011, 108:6294-6299.

3. Flanders DJ, Rawlins DJ, Shaw PJ, Lloyd CW. Nucleus-associated microtubules help determine the division plane of plant epidermal cells: avoidance of four-way junctions and the role of cell geometry. *J Cell Biol* 1990, 110:1111-1122.

4. Lloyd CW. How Does the Cytoskeleton Read the Laws of Geometry in Aligning the Division Plane of Plant-Cells. *Development* 1991:55-65.

5. Dong J, MacAlister CA, Bergmann DC. BASL Controls Asymmetric Cell Division in Arabidopsis. *Cell* 2009, 137:1320-1330.

6. Humphries JA, Vejlupkova Z, Luo A, Meeley RB, Sylvester AW, Fowler JE, Smith LG. ROP GTPases Act with the Receptor-Like Protein PAN1 to Polarize Asymmetric Cell Division in Maize. *The Plant Cell Online* 2011, 23:2273-2284.

7. Facette MR, Smith LG. Division polarity in developing stomata. *Curr Opin Plant Biol* 2012, 15:585-592.

8. Rasmussen CG, Humphries JA, Smith LG. Determination of symmetric and asymmetric division planes in plant cells. *Annu Rev Plant Biol* 2011, 62:387-409.

9. Wolters H, Anders N, Geldner N, Gavidia R, Jurgens G. Coordination of apical and basal embryo development revealed by tissue-specific GNOM functions. *Development* 2011, 138:117-126.

10. Yoshida S, Barbier de Reuille P, Lane B, Bassel GW, Prusinkiewicz P, Smith RS, Weijers D. Genetic control of plant development by overriding a geometric division rule. *Dev Cell* 2014, 29:75-87.

11. Mayer U, Ruiz RAT, Berleth T, Miseera S, Juurgens G. Mutations affecting body organization in the Arabidopsis embryo. *Nature* 1991, 353:402-407.

12. Lau OS, Davies KA, Chang J, Adrian J, Rowe MH, Ballenger CE, Bergmann DC. Direct roles of SPEECHLESS in the specification of stomatal self-renewing cells. *Science* 2014, 345:1605-1609.

13. Van Damme D, De Rybel B, Gudesblat G, Demidov D, Grunewald W, De Smet I, Houben A, Beeckman T, Russinova E. Arabidopsis α Aurora Kinases Function in Formative Cell Division Plane Orientation. *The Plant Cell Online* 2011, 23:4013-4024.

14. Uyttewaal M, Burian A, Alim K, Landrein B, Borowska-Wykret D, Dedieu A, Peaucelle A, Ludynia M, Traas J, Boudaoud A, et al. Mechanical stress acts via katanin to amplify differences in growth rate between adjacent cells in Arabidopsis. *Cell* 2012, 149:439-451.

15. Vos JW, Dogterom M, Emons AM. Microtubules become more dynamic but not shorter during preprophase band formation: a possible "search-and-capture" mechanism for microtubule translocation. *Cell Motil Cytoskeleton* 2004, 57:246-258.

16. Dhonukshe P, Gadella TW, Jr. Alteration of microtubule dynamic instability during preprophase band formation revealed by yellow fluorescent protein-CLIP170 microtubule plus-end labeling. *Plant Cell* 2003, 15:597-611.

17. Camilleri C, Azimzadeh J, Pastuglia M, Bellini C, Grandjean O, Bouchez D. The *Arabidopsis TONNEAU2* gene encodes a putative novel protein phosphatase 2A regulatory subunit essential for the control of the cortical cytoskeleton. *Plant Cell* 2002, 14:833-845.

18. Spinner L, Gadeyne A, Belcram K, Goussot M, Moison M, Duroc Y, Eeckhout D, De Winne N, Schaefer E, Van De Slijke E, et al. A protein phosphatase 2A complex spatially controls plant cell division. *Nat Commun* 2013, 4:1863.

19. Torres-Ruiz RA, Jurgens G. Mutations in the FASS gene uncouple pattern formation and morphogenesis in Arabidopsis development. *Development* 1994, 120:2967-2978.

20. Traas J, Bellini C, Nacry P, Kronenberger J, Bouchez D, Caboche M. Normal differentiation patterns in plants lacking microtubular preprophase bands. *Nature* 1995, 375:676-677.

21. Drevensek S, Goussot M, Duroc Y, Christodoulidou A, Steyaert S, Schaefer E, Duvernois E, Grandjean O, Vantard M, Bouchez D, et al. The *Arabidopsis* TRM1-TON1 interaction reveals a recruitment network common to plant cortical microtubule arrays and eukaryotic centrosomes. *Plant Cell* 2012, 24:178-191.

22. Kawamura E, Wasteneys GO. MOR1, the Arabidopsis thaliana homologue of Xenopus MAP215, promotes rapid growth and shrinkage, and suppresses the pausing of microtubules in vivo. *Journal of Cell Science* 2008, 121:4114-4123.

23. Kawamura E, Himmelspach R, Rashbrooke MC, Whittington AT, Gale KR, Collings DA, Wasteneys GO. MICROTUBULE ORGANIZATION 1 regulates structure and function of microtubule arrays during mitosis and cytokinesis in the Arabidopsis root. *Plant Physiol* 2006, 140:102-114.

24. Kirik A, Ehrhardt DW, Kirik V. TONNEAU2/FASS Regulates the Geometry of Microtubule Nucleation and Cortical Array Organization in Interphase Arabidopsis Cells. *The Plant Cell Online* 2012.

25. Kirik V, Herrmann U, Parupalli C, Sedbrook JC, Ehrhardt DW, Hulskamp M. CLASP localizes in two discrete patterns on cortical microtubules and is required for cell morphogenesis and cell division in Arabidopsis. *J Cell Sci* 2007, 120:4416-4425.

26. Ambrose JC, Shoji T, Kotzer AM, Pighin JA, Wasteneys GO. The Arabidopsis CLASP Gene Encodes a Microtubule-Associated Protein Involved in Cell Expansion and Division. *The Plant Cell Online* 2007, 19:2763-2775.

27. Pietra S, Gustavsson A, Kiefer C, Kalmbach L, Hörstedt P, Ikeda Y, Stepanova AN, Alonso JM, Grebe M. Arabidopsis SABRE and CLASP interact to stabilize cell division plane orientation and planar polarity. *Nat Commun* 2013, 4.

28. Zhang H, Dawe RK. Mechanisms of plant spindle formation. *Chromosome Research* 2011, 19:335-344.

29. Masoud K, Herzog E, Chaboute ME, Schmit AC. Microtubule nucleation and establishment of the mitotic spindle in vascular plant cells. *Plant J* 2013, 75:245-257.

30. Chan J, Calder G, Fox S, Lloyd C. Localization of the microtubule end binding protein EB1 reveals alternative pathways of spindle development in *Arabidopsis* suspension cells. *Plant Cell* 2005, 17:1737-1748.

31. Ambrose JC, Cyr R. Mitotic spindle organization by the preprophase band. *Mol Plant* 2008, 1:950-960.

32. Ambrose JC, Cyr R. The kinesin ATK5 functions in early spindle assembly in Arabidopsis. *Plant Cell* 2007, 19:226-236.

33. Marcus AI, Li W, Ma H, Cyr RJ. A kinesin mutant with an atypical bipolar spindle undergoes normal mitosis. *Mol Biol Cell* 2003, 14:1717-1726.

34. Ambrose JC, Li W, Marcus A, Ma H, Cyr R. A minus-end-directed kinesin with plus-end tracking protein activity is involved in spindle morphogenesis. *Mol Biol Cell* 2005, 16:1584-1592.

35. Vos JW, Pieuchot L, Evrard J-L, Janski N, Bergdoll M, de Ronde D, Perez LH, Sardon T, Vernos I, Schmit A-C. The Plant TPX2 Protein Regulates Prospindle Assembly before Nuclear Envelope Breakdown. *The Plant Cell Online* 2008, 20:2783-2797.

36. Petrovská B, Jeřábková H, Kohoutová L, Cenklová V, Pochylová Ž, Gelová Z, Kočárová G, Váchová L, Kurejová M, Tomaštíková E, et al. Overexpressed TPX2 causes ectopic formation of microtubular arrays in the nuclei of acentrosomal plant cells. *Journal of Experimental Botany* 2013.

37. Petrovská B, Cenklová V, Pochylová Ž, Kourová H, Doskočilová A, Plíhal O, Binarová L, Binarová P. Plant Aurora kinases play a role in maintenance of primary meristems and control of endoreduplication. *New Phytologist* 2012, 193:590-604.

38. Pickett-Heaps JD, Northcote DH. Cell division in the formation of the stomatal complex of the young leaves of wheat. *J Cell Sci* 1966, 1:121-128.

39. Smith LG, Gerttula SM, Han S, Levy J. Tangled1: a microtubule binding protein required for the spatial control of cytokinesis in maize. *J Cell Biol* 2001, 152:231-236.

40. Smith LG, Hake S, Sylvester AW. The tangled-1 mutation alters cell division orientations throughout maize leaf development without altering leaf shape. *Development* 1996, 122:481-489.

41. Cleary AL, Smith LG. The *Tangled1* gene is required for spatial control of cytoskeletal arrays associated with cell division during maize leaf development. *Plant Cell* 1998, 10:1875-1888.

42. Rasmussen CG, Sun B, Smith LG. Tangled localization at the cortical division site of plant cells occurs by several mechanisms. *J Cell Sci* 2011, 124:270-279.

43. Muller S, Han S, Smith LG. Two kinesins are involved in the spatial control of cytokinesis in Arabidopsis thaliana. *Curr Biol* 2006, 16:888-894.

44. Lipka E, Gadeyne A, Stockle D, Zimmermann S, De Jaeger G, Ehrhardt DW, Kirik V, Van Damme D, Muller S. The Phragmoplast-Orienting Kinesin-12 Class Proteins Translate the Positional Information of the Preprophase Band to Establish the Cortical Division Zone in Arabidopsis thaliana. *Plant Cell* 2014, 26:2617-2632.

45. Xu XM, Zhao Q, Rodrigo-Peiris T, Brkljacic J, He CS, Muller S, Meier I. RanGAP1 is a continuous marker of the Arabidopsis cell division plane. *Proc Natl Acad Sci U S A* 2008, 105:18637-18642.

46. Rodrigo-Peiris T, Xu XM, Zhao Q, Wang H-J, Meier I. RanGAP is required for post-meiotic mitosis in female gametophyte development in Arabidopsis thaliana. *Journal of Experimental Botany* 2011, 62:2705-2714.

47. Kojo KH, Higaki T, Kutsuna N, Yoshida Y, Yasuhara H, Hasezawa S. Roles of Cortical Actin Microfilament Patterning in Division Plane Orientation in Plants. *Plant and Cell Physiology* 2013, 54:1491-1503.

48. Panteris E. Cortical actin filaments at the division site of mitotic plant cells: a reconsideration of the 'actin-depleted zone'. *New Phytol* 2008, 179:334-341.

49. Mineyuki Y, Palevitz BA. Relationship between preprophase band organization, F-actin and the division site in *Allium. J Cell Sci* 1990, 97:283-295.

50. Sano T, Higaki T, Oda Y, Hayashi T, Hasezawa S. Appearance of actin microfilament 'twin peaks' in mitosis and their function in cell plate formation, as visualized in tobacco BY-2 cells expressing GFP-fimbrin. *Plant J* 2005, 44:595-605.

51. Karahara I, Suda J, Tahara H, Yokota E, Shimmen T, Misaki K, Yonemura S, Staehelin LA, Mineyuki Y. The preprophase band is a localized center of clathrin-mediated endocytosis in late prophase cells of the onion cotyledon epidermis. *Plant J* 2009, 57:819-831.

52. Vanstraelen M, Van Damme D, De Rycke R, Mylle E, Inze D, Geelen D. Cell cycle-dependent targeting of a kinesin at the plasma membrane demarcates the division site in plant cells. *Curr Biol* 2006, 16:308-314.

53. Suetsugu N, Yamada N, Kagawa T, Yonekura H, Uyeda TQ, Kadota A, Wada M. Two kinesin-like proteins mediate actin-based chloroplast movement in Arabidopsis thaliana. *Proc Natl Acad Sci U S A* 2010, 107:8860-8865.

54. Wu S-Z, Bezanilla M. *Myosin VIII associates with microtubule ends and together with actin plays a role in guiding plant cell division*. Vol. 3; 2014.

55. Reichelt S, Knight AE, Hodge TP, Baluska F, Samaj J, Volkmann D, Kendrick-Jones J. Characterization of the unconventional myosin VIII in plant cells and its localization at the post-cytokinetic cell wall. *The Plant Journal* 1999, 19:555-567.

56. Haraguchi T, Tominaga M, Matsumoto R, Sato K, Nakano A, Yamamoto K, Ito K. Molecular Characterization and Subcellular Localization of Arabidopsis Class VIII Myosin, ATM1. *Journal of Biological Chemistry* 2014, 289:12343-12355.

57. Miki T, Naito H, Nishina M, Goshima G. Endogenous localizome identifies 43 mitotic kinesins in a plant cell. *Proc Natl Acad Sci U S A* 2014, 111:E1053-1061.

58. Hiwatashi Y, Obara M, Sato Y, Fujita T, Murata T, Hasebe M. Kinesins are indispensable for interdigitation of phragmoplast microtubules in the moss *Physcomitrella patens. Plant Cell* 2008, 20:3094-3106.

59. Ho C-MK, Hotta T, Guo F, Roberson RW, Lee Y-RJ, Liu B. Interaction of antiparallel microtubules in the phragmoplast is mediated by the microtubule-associated protein MAP65-3 in *Arabidopsis. Plant Cell* 2011, 23:2909-2923.

60. Samuels AL, Giddings TH, Jr., Staehelin LA. Cytokinesis in tobacco BY-2 and root tip cells: a new model of cell plate formation in higher plants. *J Cell Biol* 1995, 130:1345-1357.

61. Jurgens G. Cytokinesis in higher plants. *Annu. Rev. Plant Biol.* 2005, 56:281-299.

62. McMichael CM, Bednarek SY. Cytoskeletal and membrane dynamics during higher plant cytokinesis. *New Phytologist* 2013, 197:1039-1057.

63. Strompen G, El Kasmi F, Richter S, Lukowitz W, Assaad FF, Jurgens G, Mayer U. The Arabidopsis HINKEL gene encodes a kinesin-related protein involved in cytokinesis and is expressed in a cell cycle-dependent manner. *Current Biology* 2002, 12:153-158.

64. Sasabe M, Machida Y. Regulation of organization and function of microtubules by the mitogen-activated protein kinase cascade during plant cytokinesis. *Cytoskeleton (Hoboken)* 2012, 69:913-918.

65. Ito M. Factors controlling cyclin B expression. *Plant Mol Biol* 2000, 43:677-690.

66. Ito M, Iwase M, Kodama H, Lavisse P, Komamine A, Nishihama R, Machida Y, Watanabe A. A novel cis-acting element in promoters of plant B-type cyclin genes activates M phase-specific transcription. *Plant Cell* 1998, 10:331-341.

67. Araki S, Ito M, Soyano T, Nishihama R, Machida Y. Mitotic cyclins stimulate the activity of c-Myb-like factors for transactivation of G2/M phase-specific genes in tobacco. *J Biol Chem* 2004, 279:32979-32988.

68. Sasabe M, Boudolf V, De Veylder L, Inzé D, Genschik P, Machida Y. Phosphorylation of a mitotic kinesin-like protein and a MAPKKK by cyclin-dependent kinases (CDKs) is involved in the transition to cytokinesis in plants. *Proceedings of the National Academy of Sciences* 2011, 108:17844-17849.

69. Muller S, Smertenko A, Wagner V, Heinrich M, Hussey PJ, Hauser MT. The plant microtubule-associated protein AtMAP65-3/PLE is essential for cytokinetic phragmoplast function. *Curr Biol* 2004, 14:412-417.

70. Kosetsu K, de Keijzer J, Janson ME, Goshima G. MICROTUBULE-ASSOCIATED PROTEIN65 Is Essential for Maintenance of Phragmoplast Bipolarity and Formation of the Cell Plate in Physcomitrella patens. *The Plant Cell Online* 2013, 25:4479-4492.

71. Ho C-MK, Lee Y-RJ, Kiyama LD, Dinesh-Kumar SP, Liu B. Arabidopsis Microtubule-Associated Protein MAP65-3 Cross-Links Antiparallel Microtubules toward Their Plus Ends in the Phragmoplast via Its Distinct C-Terminal Microtubule Binding Domain. *The Plant Cell Online* 2012, 24:2071-2085.

72. Walczak CE, Shaw SL. A MAP for Bundling Microtubules. *Cell* 2010, 142:364-367.

73. Krupnova T, Stierhof YD, Hiller U, Strompen G, Muller S. The microtubule-associated kinase-like protein RUNKEL functions in somatic and syncytial cytokinesis. *Plant J* 2013, 74:781-791.

74. Krupnova T, Sasabe M, Ghebreghiorghis L, Gruber CW, Hamada T, Dehmel V, Strompen G, Stierhof YD, Lukowitz W, Kemmerling B, et al. Microtubule-associated kinase-like protein RUNKEL needed [corrected] for cell plate expansion in Arabidopsis cytokinesis. *Curr Biol* 2009, 19:518-523.

75. Murata T, Sano T, Sasabe M, Nonaka S, Higashiyama T, Hasezawa S, Machida Y, Hasebe M. Mechanism of microtubule array expansion in the cytokinetic phragmoplast. *Nat Commun* 2013, 4.

76. Pastuglia M, Azimzadeh J, Goussot M, Camilleri C, Belcram K, Evrard J-L, Schmit A-C, Guerche P, Bouchez D. γ-Tubulin Is Essential for Microtubule Organization and Development in Arabidopsis. *The Plant Cell Online* 2006, 18:1412-1425.

77. Janski N, Masoud K, Batzenschlager M, Herzog E, Evrard JL, Houlne G, Bourge M, Chaboute ME, Schmit AC. The GCP3-interacting proteins GIP1 and GIP2 are required for gamma-tubulin complex protein localization, spindle integrity, and chromosomal stability. *Plant Cell* 2012, 24:1171-1187.]

Figure captions

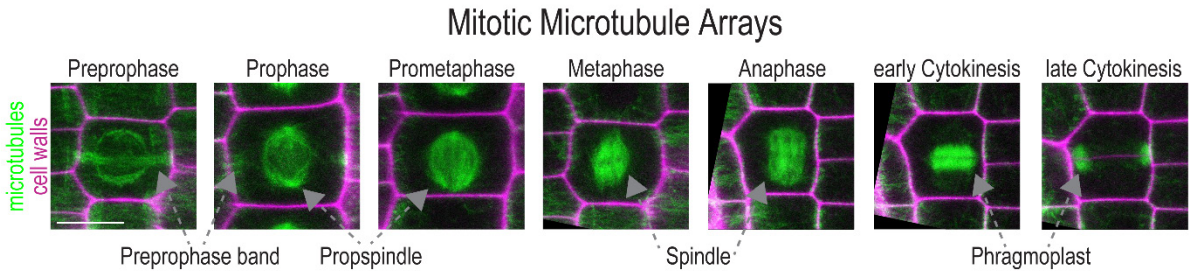

Figure 1: Micrographs of the microtubule arrays during plant cell division. Mitotic cell cycle stages are depicted in chronological order. Microtubules are visualized by GFP-MBD, depicted in green, cell walls are stained with propidium iodide (magenta). Maximum projections of GFP-MBD z-stacks are merged with a single propidium iodide image. In case were images were rotated non-imaged regions were filled with black background. Scale bar indicates 10 µm.

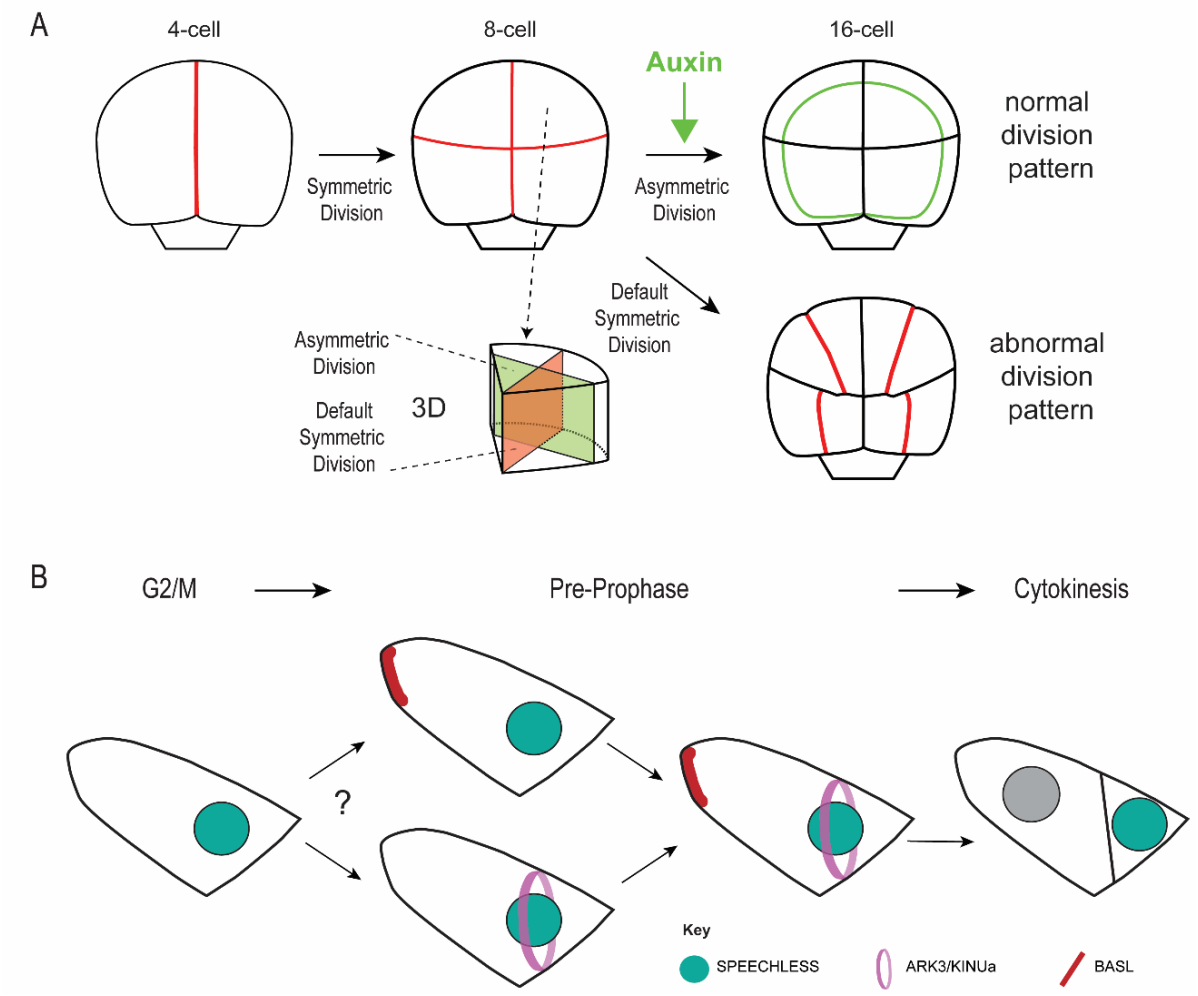

Figure 2: Regulation of division plane positioning in symmetric and asymmetric divisions. (A) Succession of divisions in the early *Arabidopsis* embryo. Chronologically invariant symmetric and asymmetric divisions contribute to normal development of globular stage embryos. Symmetric divisions give rise to the 8-cell embryo (indicated in red) obeying the geometric rule of minimal area division, while highly asymmetric divisions facilitate the separation of outer protoderm and inner cell types at the transition from 8- to 16-cell stage (indicated in green). Auxin signaling overrides default symmetric divisions, allowing asymmetric divisions. Changes in auxin response result in reversion to the geometry based symmetric default pathway. 3D reconstruction illustrates the default minimum rea division plane (red) in comparison to an asymmetric division plane (green) at the transition from 8-cell to 16-cell stage. (B) Model for the transcription factor regulated control of asymmetric division in the stomatal lineage. SPEECHLESS (SPCH, green) regulates both transcription of *BASL*and kinesin *ARK3/KINUa* in a meristemoide cell. SPCH precedes ARK3 (purple) localization at the PPB while BASL localizes at the plasma membrane opposing the imminent future division site, acting as a polarity cue. Presumably, *BASL* and *ARK3/KINUa*act in the same genetic pathway, yet the interdependency of their subcellular location needs to be clarified.

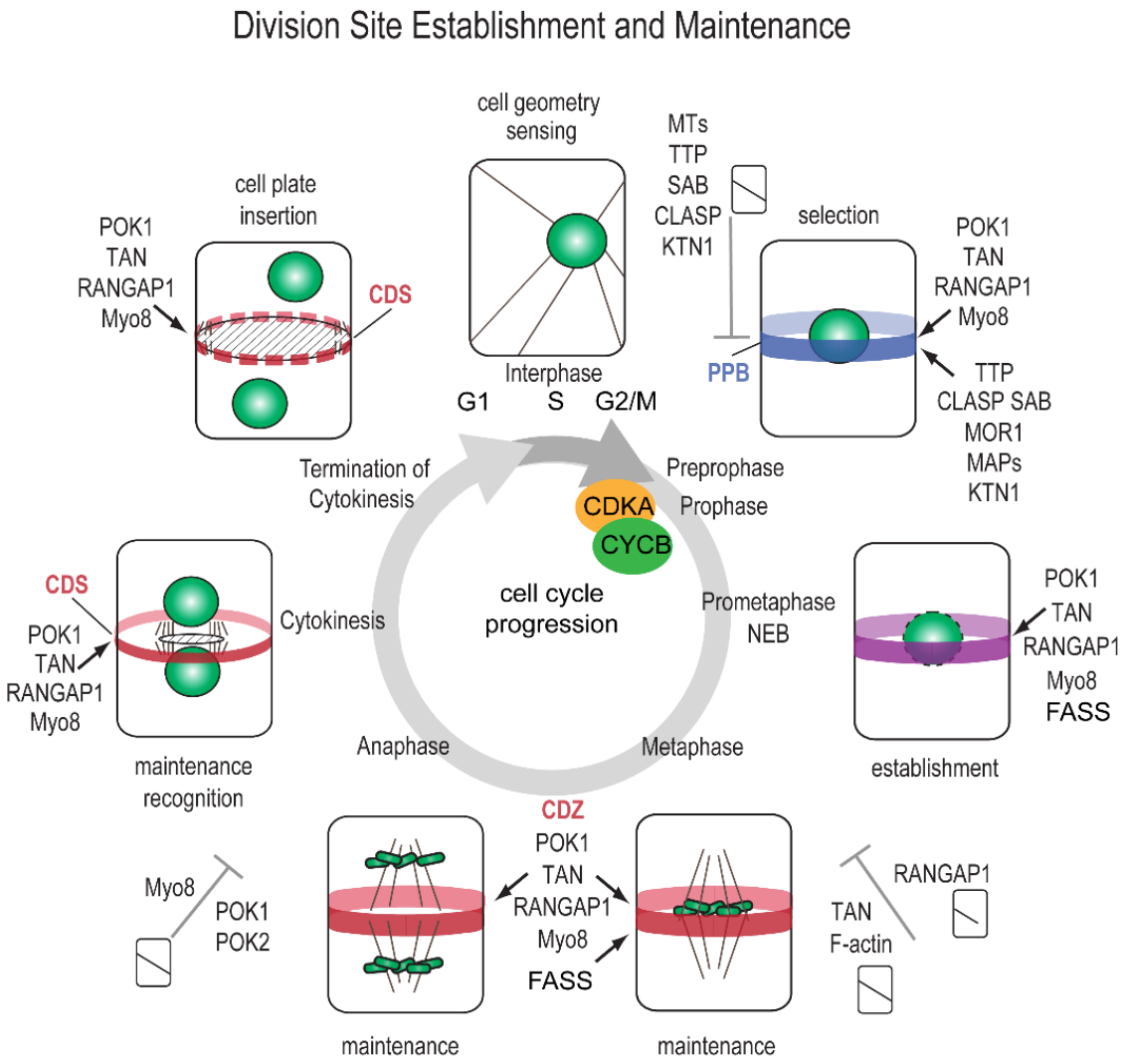

Figure 3: Overview of cortical division site establishment and maintenance. Entry into mitosis is under the control of the cell cycle. The transition from G2 phase to mitosis (M) is mediated by the CDKA;CYCB complex. The nucleus (green) gets centered as the cell enters mitosis and the preprophaseband (PPB, blue) subsequently assembles depending on TTP (TON1/TRM/PP2A) protein complex and phosphatase activity. A number of microtubule associated proteins (MAP), co-localize with the PPB and direct its position (SABRE, CLASP, MOR1, KTN1, MAPs). The PPB accurately predicts the future cell plate insertion site. Mutation of proteins involved in PPB assembly leads to loss of PPB formation and in consequence mispositioned cell walls. In the presence of PPB, TANGLED (TAN), RANGAP1and POK1 are recruited to the PPB during prophase establishing the cortical division zone (CDZ). The purple color indicates the co-localization of PPB microtubules and positive CDZ markers during prometaphase. Upon PPB disassembly the CDZ (red) preserves the positional information conveyed by the PPBPOK1 is required for the maintenance of TAN and RanGAP1 commencing in metaphase. The loss of POKs, TAN, F-actin and Myo8 leads to obliquely inserted cell walls, whereas knock down of RanGAP function causes incomplete cell walls. During cytokinesis the CDZ (including its residents) narrow to define cortical division site (CDS) as the precise cell plate insertion site POK1 and Myo8 are required for phragmoplast (PP) guidance towards the CDS. Upon completion of cell plate insertion CDS markers disappear.

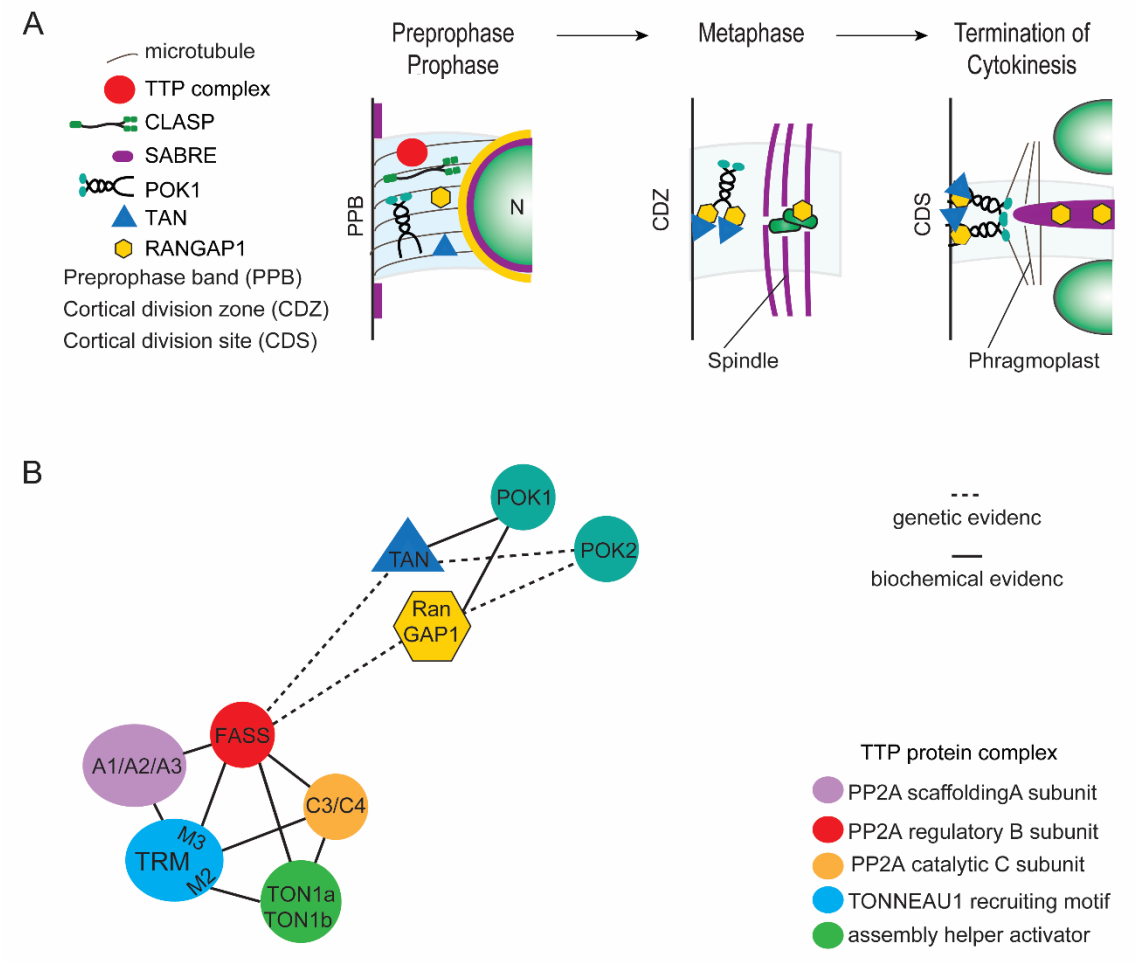

Figure 4: Protein dynamics at the cortical division site. A selection of proteins that are required for preprophase band (PPB) formation, positioning and cortical division zone (CDZ) establishment is depicted. Proteins of the TTP (TON1/TRM/PP2A, red) complex localize at the PPB and are required for its formation. CLASP (dark green) and SABRE (SAB, purple) genetically interact to position the PPB, although CLASP co-localizes with the PPB, SAB is located at its lateral boundaries. In prophase the proteins, POK1 (mint), TANGLED (TAN, blue) and RanGAP1 (yellow) are independently recruited to the PPB and remain at this cortical site beyond PPB disassembly. In metaphase POK1 is somehow tethered to the cortical division zone (CDZ) and retains TAN and RanGAP1 at this site throughout mitosis. In cytokinesis, the localization of POK1, TAN and RanGAP1 becomes narrow, most likely more accurately describing the site of cell plate fusion or cortical division site (CDS). Note that RanGAP1 also associates with the nuclear envelope in prophase and with kinetochores and the cell plate later in mitosis. (B) Interaction network of the above featured proteins at the PPB/CDZ as determined either by biochemical evidence (continuous line) or genetic evidence. The TPP complex consists Protein Phosphatase (PP) 2A variable scaffolding A subunit, the regulatory B subunit (FASS) and the variable catalytic C subunit as well as the assembly activator TONNEAU (TON) 1a/b and variable TONNEAU1 RECRUITING MOTIF (TRM) proteins. TRM interacts with FASS via the conserved M2 motif and Interaction of TON1 with TRM M3 motif mediates cytoskeletal targeting. Localization of TAN and RanGAP1 at the PPB depends on FASS.

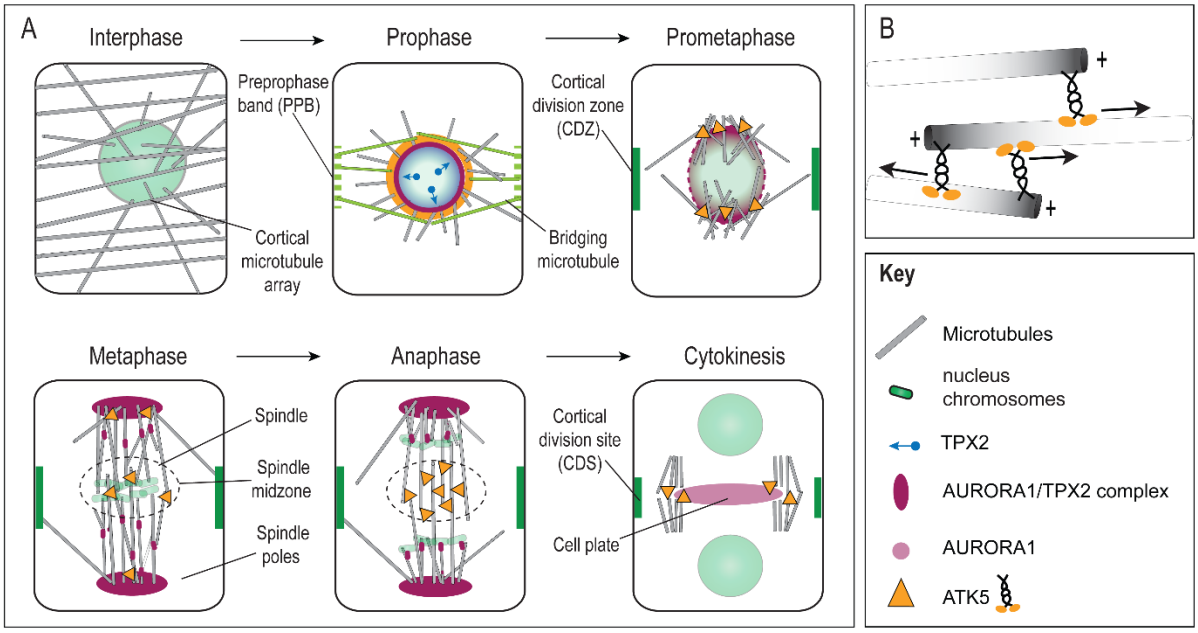

Figure 5: Schematic illustration of plant spindle formation. Cell cycle stages are illustrated as cell cross sections, while interphase is depicted as a projection. Perinuclear microtubules emanate from the nucleus and bridging microtubules (green) connect the nucleus and the preprophase band (PPB green dashed line) in late prophase. The microtubule associated protein TPX2, which accumulates in the nucleus during preprophase (blue gradient), is exported and associates with AURORA (AUR) 1 at the nuclear envelope (AUR1/TPX2 complex purple). During nuclear envelope breakdown (purple dashed line) the AUR1/TPX2 complex localizes to minus ends of perinuclear microtubules and subsequently co-localizes with spindle poles and accumulates at the spindle, presumable co-localizing with microtubule nucleation complexes. Note that the AUR1/TPX2 complex especially localizes at kinetochore microtubules during the transition from metaphase to anaphase. Whereas TPX2 rapidly disappears at the end of anaphase, AUR1 decorates the cell plate during cytokinesis (pink). Kinesin-14 ATK5 (yellow) co-localizes with perinuclear microtubules in preprophase/prophase and associates with anitparallel interpolar microtubules at the spindle midzone. During cytokinesis, ATK5 assembles at the phragmoplast midzone. (B) Microtubule plus end association of ATK5 is mediated through its C-terminal tail domain, while microtubule minus end directed mobility requires ATK5 motor domain.

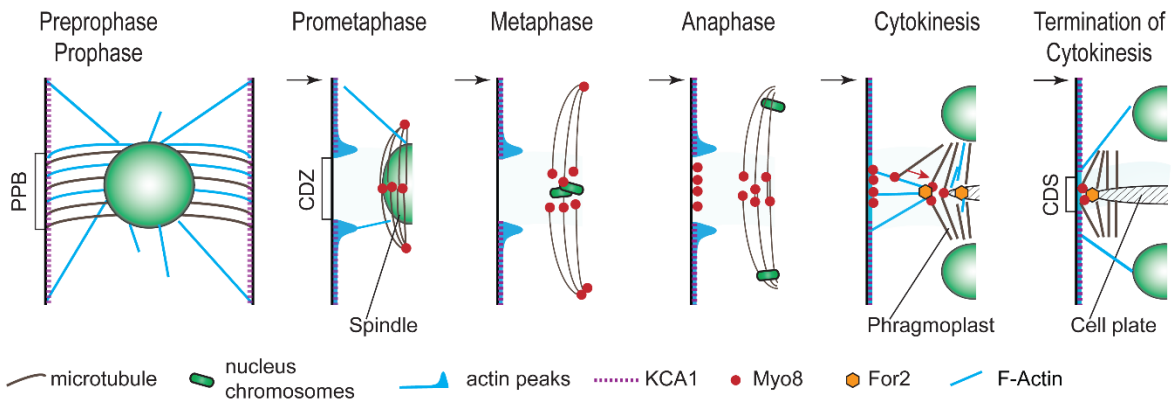

Figure 6: Illustration of the actin cytoskeleton and selected associated proteins in plant mitosis. F-actin (blue) is a component of the preprophase band (PPB) but not restricted to it. Actin-bundles span throughout the entire cell. Upon PPB disassembly in prometaphase the region of the cortical division zone remains almost devoid of F-actin, but is flanked by actin enrichments, also referred to as twin peaks. The kinesin-14 KCA1 (purple dashed line) decorates the cell cortex, but is depleted from the CDZ. Myo8 (red) associates with microtubules and localizes to the spindle poles and spindle midzone. During anaphase Myo8 locates exclusively to microtubule overlaps in the spindle midzone and also accumulates at the CDZ. During cytokinesis, Myo8 remains associated with dynamic phragmoplast microtubules at the leading edge and with peripheral microtubules that seem to contact the CDS. These peripheral microtubules move towards the leading phragmoplast edge. It is hypothesized that Myo8 might use actin filaments spanning the distance between the phragmoplast and the CDS for the relocation of the peripheral microtubules. F-actin is indeed present between the phragmoplast and the CDS and furthermore, actin nucleating formin For2a (orange) accumulates in the phragmoplast midzone, further supporting the notion that Myo8 acts in a mechanism to maintain phragmoplast integrity.

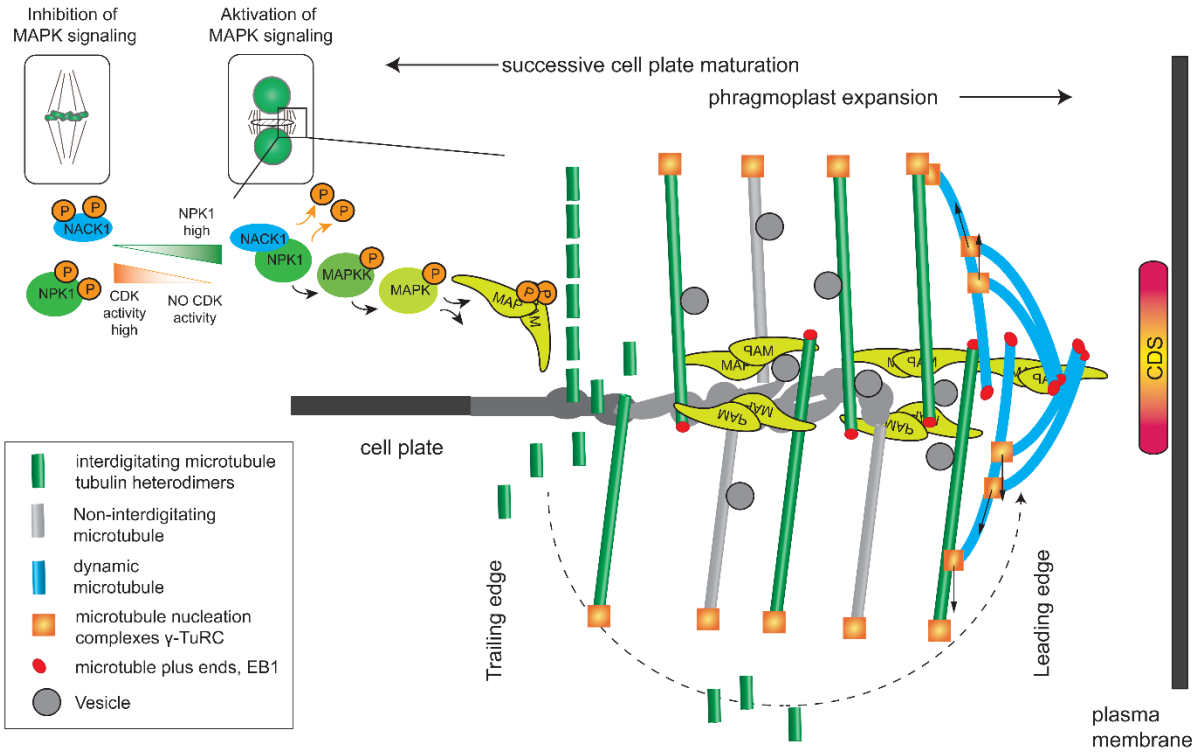

Figure 7: Regulation and mechanisms of phragmoplast expansion. HIK/NACK kinesin (blue) binding to a MAPKKK increases the kinase activity, to activate the NACK-PQR MAPK (green gradient) signaling cascade that targets MAP65 proteins. In metaphase, the NACK/HINKEL dependent mitogen activated protein kinase (MAPK) signaling cascade is inhibited by CDK dependent phosphorylation of the kinesin NACK1 and the MAPK kinase kinase NPK1 (dark green). During cell cycle progression CDK activity is switched off, allowing the accumulation of non-phosphorylated NPK1which eventually binds to non-phosphorylated NACK1 in the phragmoplast midzone regions. This complex formation triggers the kinase cascade, which targets MAP65 proteins at the trailing edge of the phragmoplast. Phosphorylation of MAP65 inhibits its cross-linking activity towards antiparallel microtubules. Consequently microtubules at the trailing edge become destabilized and disassemble, discharging tubulin heterodimers. At the leading edge of the phragmoplast, new, dynamic microtubules nucleate on existing microtubules at an angle around 40°. γ-tubulin containing nucleation sites move towards microtubule minus end as the new microtubules attached to them polymerize. Antiparallel dynamic microtubules are bundled by MAP65. Progressively the leading edge expands laterally allowing new vesicle fusion. At the trailing edge, where cell plate formation is completed, microtubules depolymerize.

Further Reading/Resources

http://www.els.net/WileyCDA/ElsArticle/refId-a0001686.html

http://www.els.net/WileyCDA/ElsArticle/refId-a0023760.html

http://www.els.net/WileyCDA/ElsArticle/refId-a0001685.html

Related Articles

Subtopic	**Article title**
Cell Biology of Plant Development	Cell division
Fertilization, Embryogenesis, and Seed Development	Patterning the embryo